



Generation and use of nanoparticles for selective organic transformation

Heba Alsharif

Thesis submitted in accordance with the regulations of the
University of Cardiff for the degree of
Doctor of Philosophy

2023

Supervisor:

Dr Meenakshisundaram Sankar and Stuart Taylor.

**Cardiff Catalysis Institute
School of Chemistry
Cardiff University**

Publication

1. The role of strong metal support interaction on the selective hydrogenation of furfural over Pt/TiO₂ catalyst. *Heba Alsharif, David J Morgan, Thomas E. Davies, Stuart H Taylor, Meenakshisundaram Sankar (to be submitted).*
2. The direct conversion of HMF to 1,6-hexanediol using a heterogeneous Pt/HAP catalyst. *Heba Alsharif, David J Morgan, Thomas E. Davies, Stuart H Taylor, Meenakshisundaram Sankar (to be submitted).*
3. Effect of support on the selective hydrogenation of furfural over supported Pt nanoparticles based catalysts. *Heba Alsharif, David J Morgan, Thomas E. Davies, Stuart H Taylor, Meenakshisundaram Sankar (to be submitted).*

Acknowledgements

All gratitude goes to Allah for His guidance and protection throughout this PhD program. My heartfelt gratitude goes to Dr. Sankar for his excellent advice and continuous support during my research. I appreciated Professor Taylor, my co-supervisor, who provided invaluable comments and guidance throughout my research.

Furthermore, I would like to thank Dr. Mark, Dr. Sam, Dr. Rich, and Dr. Greg for their advice and support. Furthermore, the experimental component of this thesis recognises the persons who took part in this research. Dr. Tom and David deserve special recognition for their XPS and TEM analyses.

I would like to acknowledge the contributions of the analytical services staff at the chemistry school who helped carry out this research. My sincere gratitude goes out to Simon for his efforts in completing this study successfully.

Also, I would like to express my sincere appreciation to Professor Graham Hutchings, whose leadership and dedication have helped establish the Cardiff Catalysis Institute as a leading research institute. Additionally, I would also want to thank the entire CCI community as well as members of Dr. Sankar's research group for their important assistance and experience. I will remember the lessons I learned from you all for many years to come.

I would like to express my sincere appreciation to everyone at Lab. 0.90, Lab. and 1.88, who have assisted me during my academic pursuits. In appreciation of Layla, Ahlam, Alba, Nomy, and Alex, I would like to thank them for making my time enjoyable. It has been a pleasure spending time in the UK with my friends Shekah, Rehab, and Noff.

I would want to express my gratitude to the Saudi Ministry of Higher Education for providing me with financial assistance. Because of this scholarship, my studies and knowledge have expanded.

Lastly, I would like to express my gratitude to my family for their unwavering support throughout this thesis journey. I consider their presence in my life to be the most significant. Their support and encouragement were crucial in helping me achieve my goals, and I would want to dedicate this thesis to them. As well as to my husband and

children, Tala and Gheina, who have been so loving, supporting, and patient with me throughout this journey. This journey would not have been possible without their support. Their self-sacrifice humbles me.

Abstract

Environmental pollution and global warming have become significant challenges for modern-day society because of our reliance on non-renewable resources. One of the obvious choices for renewable resources is plant biomass. Furfural and 5-hydroxymethylfurfural, which are platform chemicals derived from plant biomass, have become essential components in various chemical transformations and applications. It is remarkable how these building blocks can be used in many ways to achieve desired outcomes. Their source, versatility, and efficacy make them a popular choice among researchers and industries alike. The reactivity observed in Furfural and 5-hydroxymethylfurfural is attributed to the presence of various functionalities, including C=O, C=C, and C-O bonds. Hence, one of the objectives of this thesis is to design and synthesise new heterogeneous catalysts for the chemoselective hydrogenation of biomass-derived, furan-based, platform molecules. Furthermore, selective cleavage of the C-O bond to open the furan ring in 5-hydroxymethylfurfural in the presence of other functional groups is another objective we set out to achieve in this thesis.

In this study, the hydrogenation of furfural to furfuryl alcohol with high selectivity has been accomplished by using supported catalysts with enhanced active sites achieved via different post-synthesis thermal treatment protocols. The post-synthesis heat treatment protocols employed are calcination only (Calc), reduction only (Red) and calcination and reduction (Calc + Red). Interestingly, 97% conversion of furfural with 95% selectivity to 2-FFA was achieved on 0.6% Pt/TiO₂ with Calc + Red post-synthesis thermal treatment.

The first stage of this research screened the effect of different supports on the hydrogenation of furfural. Monometallic platinum nanoparticles (Pt-NPs) supported on different supports (TiO₂, Nb₂O₅, CeO₂, SiO₂ and C) were synthesised using the wet impregnation method and were later subjected to various post-synthesis heat treatment protocols. Catalysts screening were carried out at 30 °C under hydrogen (3-bar) in a Colaver glass reactor for 1-6 h. Pt/TiO₂ is the most promising catalyst with highest conversion and selectivity for furfuryl alcohol. Different Pt loadings were tested, and 0.6% Pt/TiO₂ (with Calc + Red post-synthesis thermal treatment) catalyst is the best with 97% conversion and 95% selectivity for furfuryl alcohol. We postulated that the catalyst's

activity and selectivity is due to the active site not being covered by the support material (TiO₂).

Detailed characterisation using XPS, TEM, and CO chemisorption techniques reveals the presence of nano-sized and highly distributed Pt⁰ species on the surface of the catalyst. The formation of Pt⁰ species, responsible for the high activity and selectivity observed, is influenced by post-synthesis heat treatment protocols. The Pt⁰ species improved selectivity to furfuryl alcohol by adsorbing the carbonyl group of furfural preferentially, rather than the alkene group on the surface of the catalyst.

Chapter 4 describes the liquid phase hydrogenation of furfural over monometallic catalysts (Au, Ru, Pd) and bimetallic nanoparticles (RuPt, RuPd, AuPt and PtPd) supported on TiO₂ and the results obtained are compared to that of monometallic platinum catalyst (0.6% Pt/TiO₂ Calc + Red). Pt/TiO₂ catalyst with Calc + Red post-synthesis heat treatment was used as a reference in this work owing to its high activity and selectivity in the hydrogenation of furfural. In order to improve the catalytic hydrogenation of furfural activity, these monometallic and bimetallic catalysts have been explored as alternative metals to platinum.

These catalysts have been prepared by the method described in chapter 2 and characterised by XPS, TEM and CO chemisorption. The hydrogenation of furfural over these catalysts exhibited different catalyst activity and product distributions. The results obtained show that bimetallic PtRu/TiO₂ catalyst with Calc + Red post-synthesis heat treatment is the best out of all the catalysts screened. However, the PtRu/TiO₂ Calc + Red catalyst presented poor stability and recyclability, with loss of activity after three cycles. Sintering of the NPs during the hydrogenation of FF was identified as the main reason for catalyst deactivation. In addition, the effect of the second metal on the catalyst's activity, selectivity and stability relative to Pt/TiO₂ Calc + Red was explored.

In chapter 5, direct transformation of 5-hydroxymethylfurfural to 1,6-hexanediol by a monometallic Pt-NPs and a series of bimetallic catalysts (PtPd, PtCo, PtRu and PtRe) on different support was investigated. The catalysts were prepared by wet impregnation method after which they were reduced in the furnace for 4 h at 450°C with 5 vol.% H₂/Ar. 5wt% PtRu/HAP catalyst exhibits the best activity in the direct conversion of 5-hydroxymethylfurfural to 1,6-hexanediol via hydrogenation/hydrogenolysis. The catalyst selectivity towards 1,6-hexanediol is found to be a function of the acid-base properties of

the hydroxyapatite support which is in line with what has been reported in literature. The effect of different reaction conditions was investigated by using different polar protic solvents, varying the temperature, H₂ pressure and reaction time. PtRu/HAP catalyst presented high stability after three cycles without loss of activity and the synergistic effect between the PtRu nanoparticles (NPs) and the acid-base properties of the hydroxyapatite support play a key in the catalyst activity and selectivity towards 1,6-HDO.

The overall conclusion of the thesis: the strong metal support interaction between Pt and reducible support (TiO₂) is significantly affected by the heat treatment protocol as effective for the formation of Pt⁰ on the catalyst surface, which is crucial for the selective hydrogenation of the carbonyl group in furfural to furfuryl alcohol under mild reaction conditions (30 °C, 3 bar of H₂ using Pt/TiO₂ cal + red catalyst). Also, this thesis has exhibited that the bimetallic catalyst PtRu/HAP is a more effective catalyst for the ring opening of HMF under mild reaction conditions compared to analogues monometallic catalysts.

Contents

Chapter 1: Introduction	1
1.1 Introduction	1
1.2 Biomass and platform molecules	1
1.3 Furfural and hydroxymethyl furfural as a platform molecule.....	3
1.4 Production of furfural.....	6
1.4.1 The mechanism of furfural production	7
1.5 The production of hydroxymethylfurfural from biomass	9
1.5.1 The mechanism of hydroxymethylfurfural formation from fructose.....	9
1.6 Hydrogenation of furfural and hydroxymethylfurfural.....	11
1.7 Hydrogenation of aldehyde group to alcohol in liquid and gas phases.....	14
1.7.1 Design the catalyst for the hydrogenation of furfural and hydroxymethylfurfural	15
1.8 Catalytic hydrogenation of carbonyl to alcohol.	23
1.8.1 Hydrogenation reactions using monometallic catalysts.....	23
1.8.1.1 Selective hydrogenation of furfural to 2- furfuryl alcohol using noble metal catalysts	23
1.8.1.2 Hydrogenation of furfural to 2- furfuryl alcohol using non-noble metal catalysts	23
1.8.2 Hydrogenation reactions using bimetallic catalysts.....	24
1.8.3 Tuning of the support sites.....	27
1.8.4 Strong metal support interactions	28
1.8.5 Effect of solvent on heterogeneous catalysis	29

1.9 Plausible mechanism of the chemoselective hydrogenation of the carbonyl group in furfural to 2-furfuryl alcohol over the catalyst surface	30
1.10 Catalytic hydrogenation of hydroxymethylfurfural to 2,5-dihydroxymethyl furan using noble metals.....	31
1.11 Ring opening of furan derivatives	32
1.11.1 Hydrogenolysis of furfural to pentanediol.....	32
1.11.1.1 The direct conversion of furfural to 1,2- pentanediol	33
1.11.1.2 Indirect conversion of 2-furfuryl alcohol to 1,2- pentanediol and 1,5-pentanediol.....	35
1.11.3 Direct conversion of furfural to 1.5- pentanediol.....	38
1.11.4 Hydrolysis of hydroxymethylfurfural	43
1.11.4.1 Hydroxymethylfurfural hydrogenation to produce 1,2,6-hexanetriol.....	43
1.11.4.2 Hydroxymethylfurfural hydrogenation to produce 1.6-hexandiol.....	46
1.11.4.3 Hydroxymethylfurfural hydrogenation to produce 1-hydroxy-2,5-hexane dione	49
1.11.4.4 Hydroxymethylfurfural hydrogenation to produce adipic acid.....	50
1.12 Why platinum metal was selected.....	51
1.13 Aim and objective of this thesis	52
1.14 Reference.....	54
Chapter 2: Experimental	71
2.1 Introduction	72
2.2 Materials	72
2.3 Hydrogenation of furfural and hydroxymethyl furfural.....	73

2.3.1 Preparation of monometallic and bimetallic catalysts for hydrogenation of furfural.....	73
2.3.1.1 Catalyst preparation.....	73
2.3.1.1.1 Wet-impregnation method.....	74
2.3.1.1.2 Sol-immobilisation method.....	77
2.3.2 Preparation of monometallic and bimetallic catalysts for hydrogenation of hydroxymethyl furfural	78
2.4 Catalytic testing.....	79
2.4.1 Colaver reactor	79
2.4.2 Autoclave reactor	79
2.5 Stability of the catalyst.....	81
2.5.1 Reusability of the catalyst	81
2.5.2 Determination of the quantity of metal(s) in a catalyst.....	82
2.5.2.1 Microwave plasma atomic emission spectroscopy).....	82
2.5.2.2 Inductively coupled plasma-mass spectrometry.....	83
2.6 Analysis techniques employed for the analysis reactions products	85
2.6.1 Gas chromatography.....	85
2.6.2 Gas Chromatography-mass spectrometry.....	90
2.7 Catalysts characterisation techniques.....	91
2.7.1 X-ray photoelectron spectroscopy.....	91
2.7.2 Transmission electron microscopy.....	93
2.7.3 Temperature-programmed reduction.....	95
2.7.4 CO chemisorption.....	96
2.8. References.....	98
Chapter 3: Chemoselective Hydrogenation of Furfural.....	100
3.1 Introduction.....	101

3.2 Objectives and aims	104
3.2.1 Objectives.....	104
3.2.2. Aims	104
3.3 Results and discussion	104
3.3.1 Reducible support Vs non-reducible support	104
3.4 Effect of post synthesis heat treatments on the catalysts' performance.....	117
3.5 Effect of different preparation techniques on catalytic activity and selectivity....	124
3.6 Reusability of catalyst	125
3.7 Catalyst characterisation	127
3.7.1 X-ray photoelectron spectroscopy characterisation.....	127
3.7.2 Transmission electron microscopic analysis	133
3.7.3 CO chemisorption:	137
3.7.4 Temperature programmed reduction	138
3.8 Conclusions	143
3.9 References:.....	145
Chapter 4:.....	149
Chemoselective Hydrogenation of Furfural over monometallic Pd, Ru, and Au, and bimetallic RuPt, RuPd, AuPt and PtPd catalysts supported on TiO ₂	149
4.1 Introduction	150
4.2 Results and discussion	152
4.2.1 Monometallic Vs bimetallic catalysts – catalyst testing:	152
4.2.2 Time-on-line studies	157
4.3 Catalyst stability.....	161

4.4	Catalyst characterisation	163
4.4.1	X-ray photoelectron spectroscopy	163
4.4.2	Transmission electron microscopy	167
4.5	Conclusion	171
4.6	References	173
Chapter 5: Hydrogenolysis of 5-hydroxymethyl furfural to 1,6-hexanediol		178
5.1	Introduction	179
5.2	Objective and aims	184
5.3	Results and discussion	184
5.3.1	Blank reaction.....	184
5.3.2	Effects of different polar protic solvents on conversion and selectivity	185
5.4	Influence of different reaction conditions on catalyst's performance.....	199
5.4.1	Influence of hydrogen gas pressure on catalyst's performance.....	200
5.4.2	Influence of reaction temperature on catalyst's performance	201
5.5	Recyclability of the catalyst.....	202
5.6	Catalyst characterisation	203
5.6.1	X-ray photoelectron spectroscopy analysis	203
5.6.2	Inductively coupled plasma atomic emission spectroscopy analysis.....	209
5.6.3	Transmission electron microscopy analysis	210
5.7	Proposed reaction mechanism.....	212
5.8	Conclusions	214
5.9	References	216
Chapter 6. Conclusions and Future Work.....		223

6.1	Conclusions	224
6.2	Future work	225
6.3	References	226

Chapter 1: Introduction

1.1 Introduction

Environmental pollution and global warming have become significant challenges for modern society because of nonrenewable resources.^{1, 2} A variety of chemicals we use daily are derived from crude oil, including polymers, pharmaceuticals, detergents, and food additives.^{2, 3} Therefore, to ensure the success of sustainability in chemical production, it is crucial to use alternative resources, particularly renewable ones.⁴ There are many renewable resources available, but biomass represents the most promising resource as a sustainable future energy system.^{2, 3} Biomass is an ideal alternative feedstock, as it is readily available, economical, and carbon-neutral polymer material.^{5, 6} Biomass consists of a variety of components, including carbohydrates, lignin, fatty acids, lipids, and proteins.

1.2 Biomass and platform molecules

Biomass is a polymeric material derived from plants that can be used for energy production.⁷⁻⁹ The sources of the lignocellulosic biomass include forest residues and agricultural waste to mention a few.⁹ Lignocellulosic biomass will be the most promising feedstock for the development of biorefineries and other bioproducts.⁹⁻¹¹ They are beneficial in a variety of applications because of their abundance, renewable nature, and ease of conversion into useful products.^{9, 12}

Lignocellulose includes three major constituents, which are hemicellulose, cellulose, and lignin. Hemicellulose (25–35%), is an amorphous carbohydrate biopolymer with diverse sugars mostly made up of C5 sugars and C6 sugars with definite composition and structure.¹³⁻¹⁸ Cellulose constitutes most of the lignocellulose fraction (40–50%). Cellulose is another carbohydrate polymer chain made up of C6 sugars and is the most abundant polysaccharide on earth. It is composed of unbranched D-glucose units connected by β -1,4-glycosidic bonds. These chains interact with each other via hydrogen bonding and van der Waals forces to protect hemicellulose and lignin.¹³⁻¹⁸ The third component, lignin (15–20%), which is a cross-linked polymer, provides mechanical strength and rigidity to the plant cell wall. It is a highly heterogeneous 3-dimensional amorphous polymer made up of three different methoxylated phenylpropane motif.¹³⁻¹⁶ Lignocellulosic biomass is made up of cellulose and lignin, linked by hemicellulose and its intricate structure is depicted below in Figure 1.1.

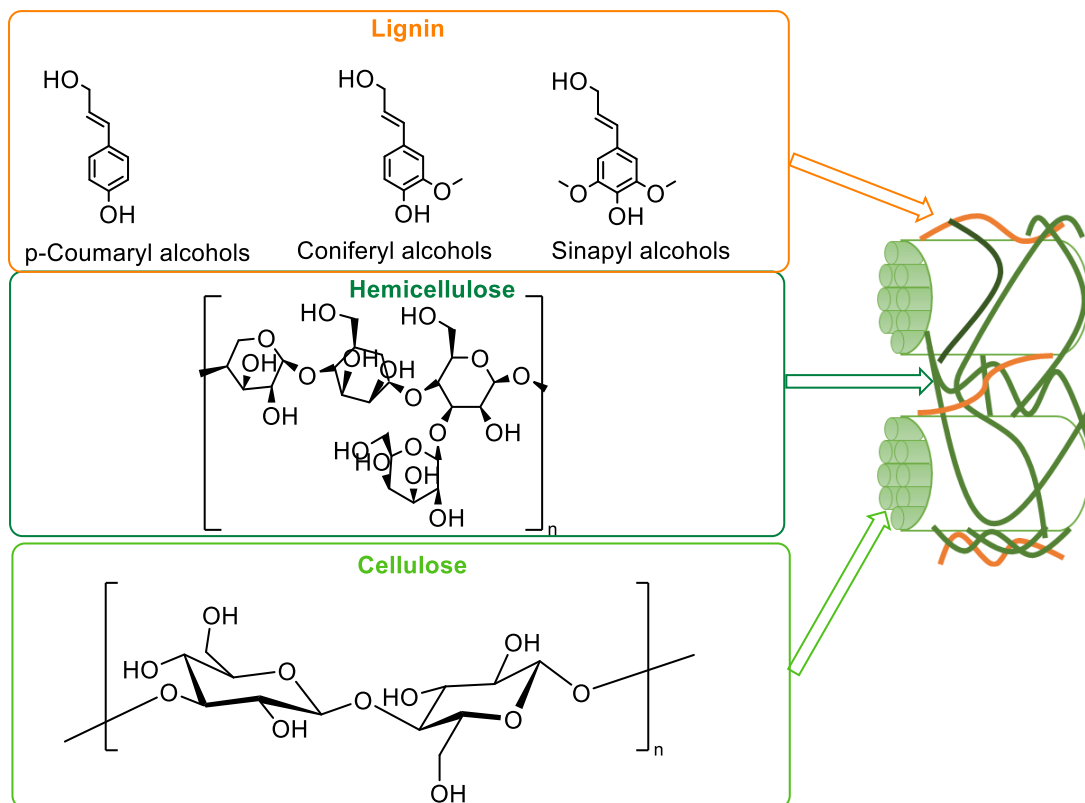
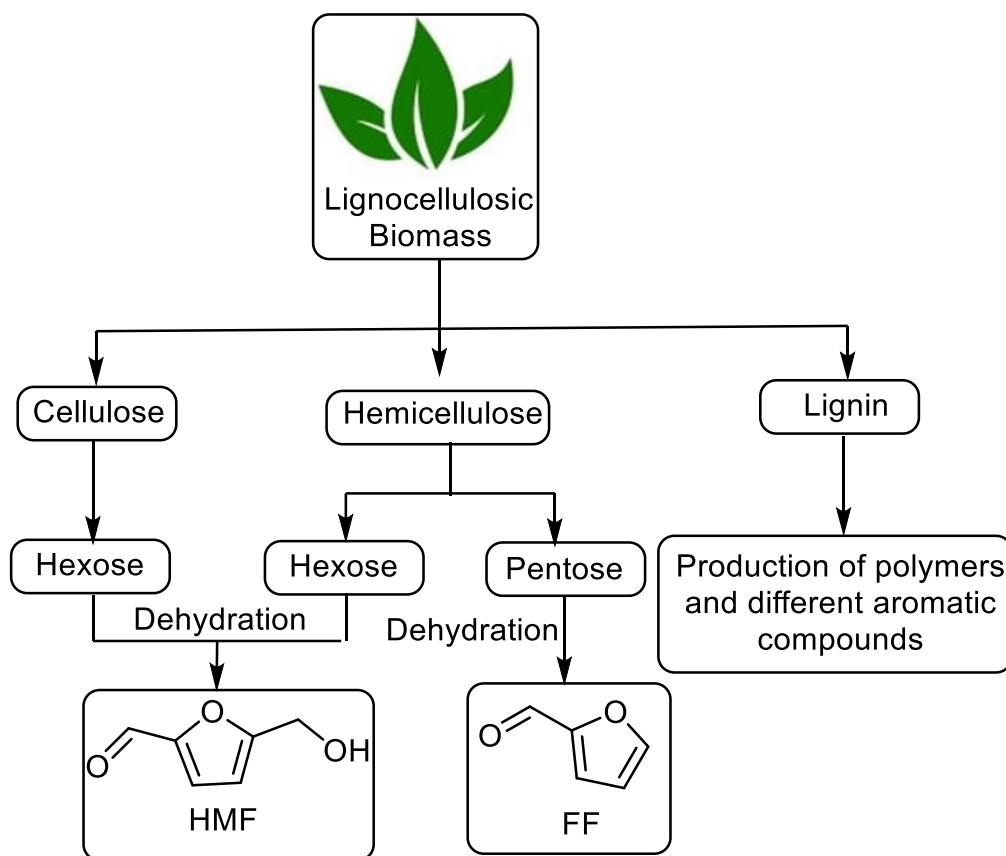


Figure 1.1: Lignocellulosic biomass depiction with schematic highlight of cellulose, hemicellulose, and lignin components. Adapted from Royal Society of Chemistry.¹⁹

Lignocellulosic materials are complex material, usually converted to small molecules called platform chemicals, such as Sugars (glucose, fructose, and xylose) which serves as building blocks for various applications.⁹ The process of breaking down lignin into its components is known as depolymerisation and can involve physical, chemical, or biological methods.⁹ These platform chemicals contain several functional groups, including alcohol, aldehyde, and furan ring groups, which could be converted into several high-value derivatives.²⁰ Scheme 1.1 shows the transformation of lignocellulosic materials into high-value materials²¹ Biomass materials are typically used to produce furfural (2-furdehyde, FF) and hydroxymethyl furfural (HMF).



Scheme 1.1: Schematic diagram of lignocellulosic transformation to platform molecules. Adapted from reference ¹⁸

1.3 Furfural and hydroxymethyl furfural as a platform molecule

Furfural (FF) and hydroxymethylfurfural (HMF) are two of the twelve important platform chemicals capable of being converted into alternative fuels, chemicals, and materials according to the US Department of Energy (DOE).²²⁻²⁴ Currently, the demand for FF is on the rise, estimated at around 550 million lbs/annum.^{3, 20, 25} FF and HMF have become essential components in various applications due to their high reactivity and it is remarkable how these building blocks are utilised in many ways to achieve desired outcomes. Their versatility and efficacy make them a popular choice among researchers and industries alike.^{26, 27} The reactivity observed in FF and HMF is attributed to the presence of various functional groups, including C=O, C=C, and C-O bonds.²⁰ Processes such as hydrogenation, hydrogenolysis, and oxidation could be used to transform these important platform chemicals into a wide range of high-value products.^{10, 20} Scheme 1.2 shows the conversion pathway of FF and HMF to high-value-added chemicals and the

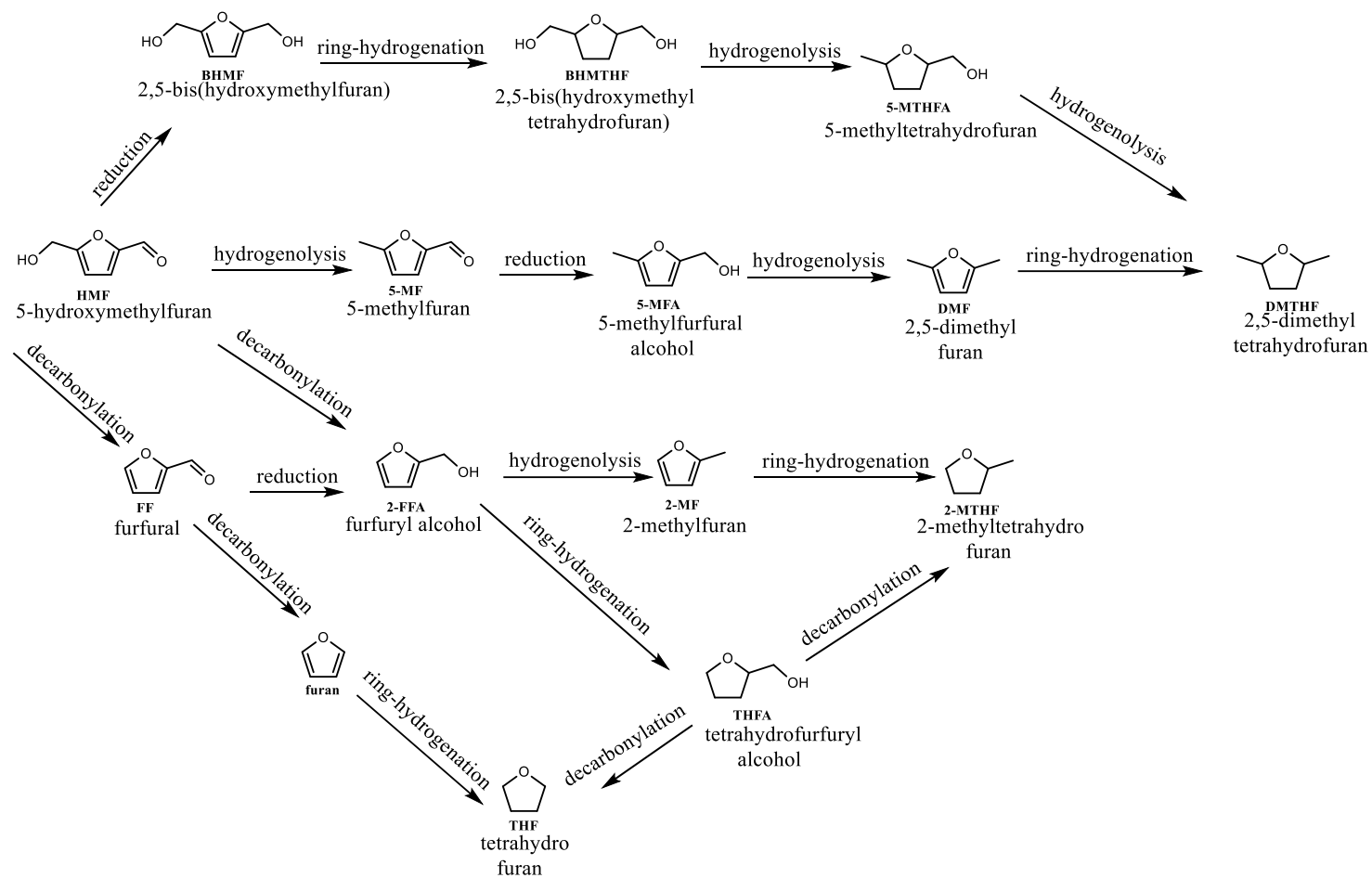
processes involved. Furthermore, selective hydrogenation or hydrogenolysis of one of the functional groups in FF and HMF could be crucial in the production of some high-value products.²⁰

FF and HMF derivatives have a broad range of important applications; for example, they are used in liquid biofuels, fuel additives, and the formation of crucial chemicals such as lubricants, adhesives, and medicinal products.^{3, 20, 25}

The hydrogenation of FF and HMF to 2-furfuryl alcohol (2-FFA) and 2,5-dihydroxy methyl furan (DHMF) respectively. To date, most research focuses on transforming FF to 2-FFA which is used in many industrial applications.²⁸ 2-FFA is widely used in diverse industrial applications. It provides resins, polymers, and adhesives that are important in different industrial fields and it is an intermediate in drug and crown ether production.²⁰ Furthermore, DHMF, which is a valuable chemical intermediate for the production of different chemicals, with applications in polyesters and medicine productions is obtained by the hydrogenation of the carbonyl group in HMF.^{20, 24}

Hydrogenolysis and other catalytic processes can be used to convert biomass-based furaldehydes into attractive biofuels, e.g., 2-methyl furan (2-MF) and 2,5-dimethylfuran (DMF) which are suitable fuel substitutes or additives due to their high energy density, boiling point, and octane number, as well as their low volatility. In addition, 2-MF has potential as a biofuel and in the production of speciality chemicals. It has a higher energy density than FF and can be used as a drop-in replacement for diesel fuel.²⁶ Equally, derivatives such as THFA, THF and 2-MTHF, are considered promising second-generation fuels can.²⁹

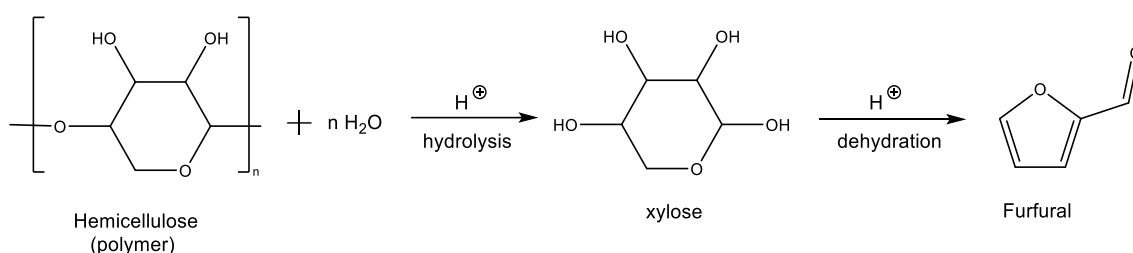
The oxidation of FF or HMF to 2-Furoic acid (FuA) and 2,5-furandicarboxylic acid (FDCA) could be used as polymer monomers. For instance, FDCA could serve as a replacement for terephthalic acid in the production of petroleum-derived polyethylene terephthalate, (PET).²⁰



Scheme 1.2: Schematic reaction pathway for transformation of biomass-based platform molecules to biofuels and chemicals.^{20, 30}

1.4 Production of furfural

The conversion of hemicellulose to FF involves hydrolysis of pentosan sugars in hemicellulose to form xylose, followed by dehydration to produce FF (Scheme 1.3).³¹ The second step in this process is very complex due to many side reactions between furfural itself called "resinification," or condensation (cross-polymerization) with intermediates of xylose-to-furfural, in addition to fragmentation reactions that cause a decrease in the FF yield.³¹ Furthermore, the numerous functional groups in pentosan are also a factor.



*Scheme 1.3: Reaction pathway for the production of furfural from hemicellulose.*³¹

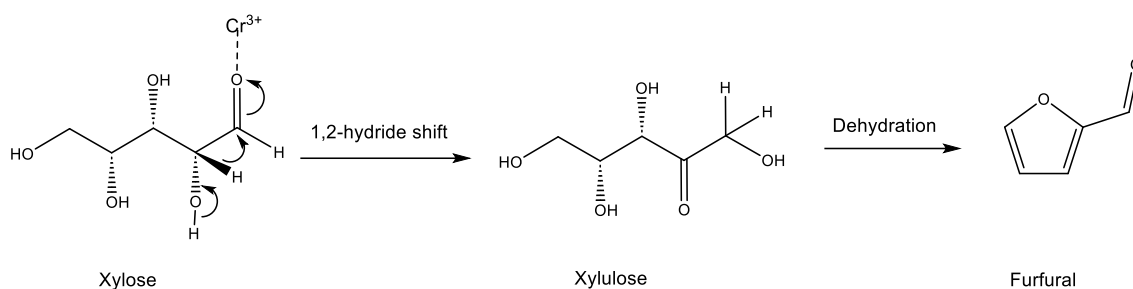
The most significant by-product is acetic acid, from the acetylation reaction of the acetyl group followed by formic acid, from the splitting of the formyl group, or the hydrolytic cleavage of the aldehyde group of FF and HMF. Besides, 2-furylmethylketone or 5-methylfurfural could be produced as a result of the dehydration of monomers of pentose with an additional methyl group in position 1 or 5.³¹

Currently, the production of FF and HMF in the industrial field is predominantly achieved through the dehydration of carbohydrates, primarily xylose and fructose, respectively. This process involves acid-catalysed hydrolysis, typically using either sulfuric acid or hydrochloric acid at high temperatures.^{27, 32} However, this process results in a low yield of FF and HMF due to the formation of numerous side dehydration products and polymeric side products. Additionally, the use of homogeneous acid catalysts results in high energy consumption.^{23, 32}

The production of FF by dehydration of xylose or hemicellulose has been modified, using for example, SnCl_4 ,³³ boron-doped biochar,³⁴ and protic Brønsted acidic ionic liquids,³⁵ as a catalyst respectively and in some instances imidazolium ionic liquids was used as a reaction medium.³⁶ Others include but are not limited to the use of a novel carbon-based solid acid catalyst,³⁷ a porous biochar catalyst and a butyrolactone-water medium.³⁸ All these investigations have led to efficient production of FF with high yields and selectivity.

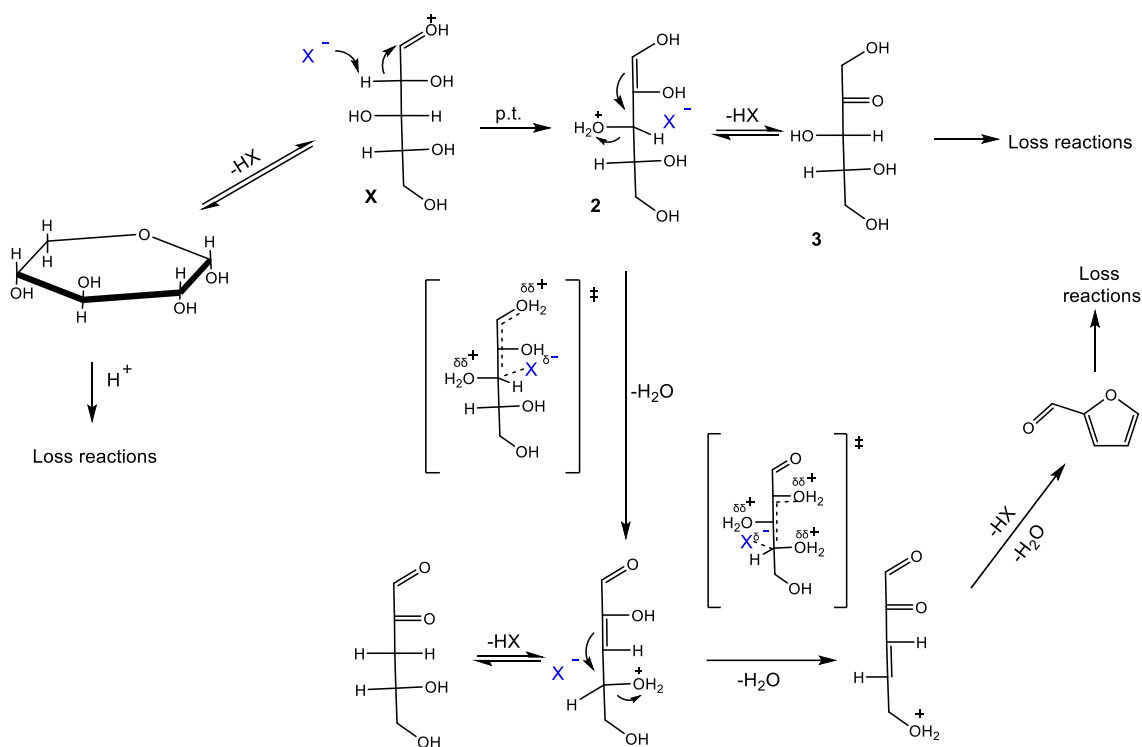
1.4.1 The mechanism of furfural production

Dissimilar reaction pathways have been proposed by different authors on the production of FF via dehydration of xylose. The proposed mechanisms can be delineated into the open chain and closed chain pathways. The open chain mechanism proposed by Binder et al., for the dehydration of xylose to FF is catalysed by $\text{CrCl}_3/\text{CrCl}_2$ going through xylulose intermediate. The coordination of Cr^{3+} to the carbonyl oxygen changes the formal charge of the carbonyl carbon atom, causing a 1,2-hydride shift and xylulose intermediate intermediate.³⁹ The xylulose is subsequently dehydrated to generate FF as shown in Scheme 1.4 below.



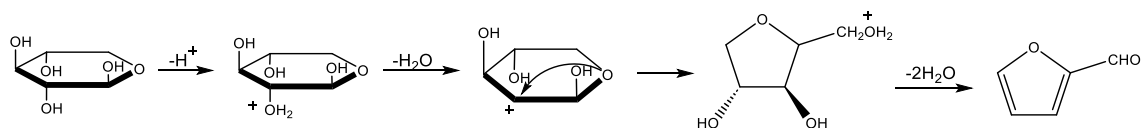
Scheme 1.4: Proposed open chain mechanism via 1,2-hydride shift and dehydration of xylose to FF catalysed by Lewis acid.³⁹

Marcotullo and de Jong in 2011 put forward a mechanism that involves starting the reactions with open-chain intermediates that is in equilibrium with 1,2-enediol (3), followed by dehydration to enolic (4) of a 3-deoxyglycosulose (5), which consequently dehydrates to structure (6) to produce the FF (7) (Scheme 1.5).⁴⁰



Scheme 1.5: Proposed open chain mechanism of xylose to FF in acidic medium by Marcotullo and de Jong. Adapted from Marcotullio et. al.⁴⁰

The closed chain pathway was proposed by Nimlos and coworkers in 2006.⁴¹ The reaction mechanism for FF formation started with the protonation of the hydroxyl group of xylose on the second carbon atom of the xylose molecule. Consequently, the formation of dehydrofuranose through dehydration and intramolecular rearrangement (ring contraction) then dehydration and hydride shift reactions on the dehydrofuranose to produce FF (Scheme 1.6).³⁹



Scheme 1.6: Proposed open chain mechanism of xylose to FF in acidic medium by Nimlos and coworkers.³⁹

1.5 The production of hydroxymethylfurfural from biomass

The first attempt to prepare HMF was published by Düll and Kiermayer in 1895 by heating inulin in an oxalic acid medium under pressure. Since then, research interest in the synthesis of HMF has grown considerably with fruitful results. HMF can be produced by the hydrolysis of cellulose followed by isomerization and dehydration.⁴² Dehydration of various derivatives of hexoses (glucose, sucrose, fructose, and inulin) produced HMF, however, the direct cyclic mechanism of fructose using an acid catalyst gave a relatively high yield of HMF.⁴³

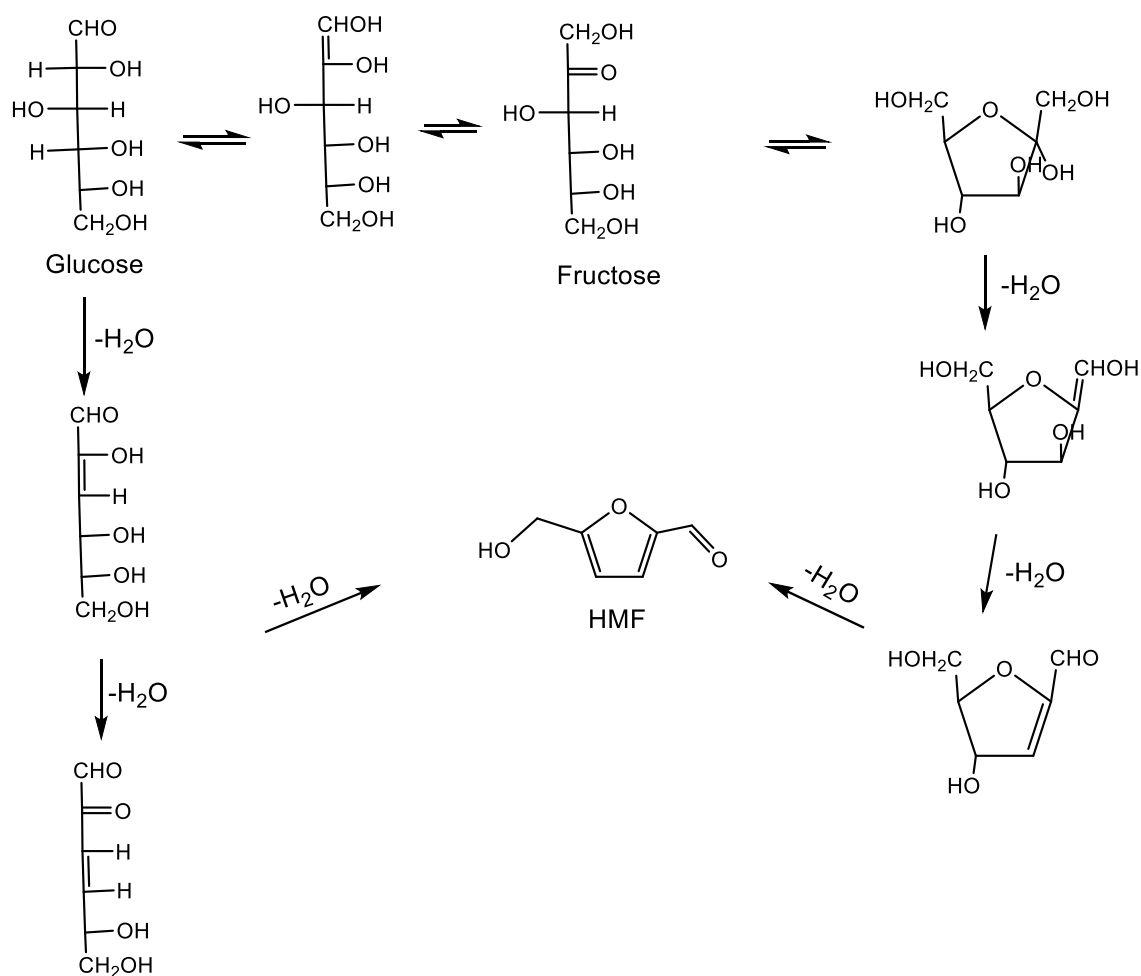
The mechanism for HMF production has been attempted based on fructose and sucrose respectively and studies conducted by researchers like Antal,⁴⁴ and Kuster,⁴⁵ have shown that the formation of HMF is a complex process that involves multiple chemical reactions beyond just dehydration. They also found that there are two possible pathways for the dehydration process to occur: one based on acyclic compounds and the other based on the transformation of ring systems. Additionally, it has been found that the yield of HMF is influenced by reactions such as isomerization, fragmentation, and condensation.

1.5.1 The mechanism of hydroxymethylfurfural formation from fructose

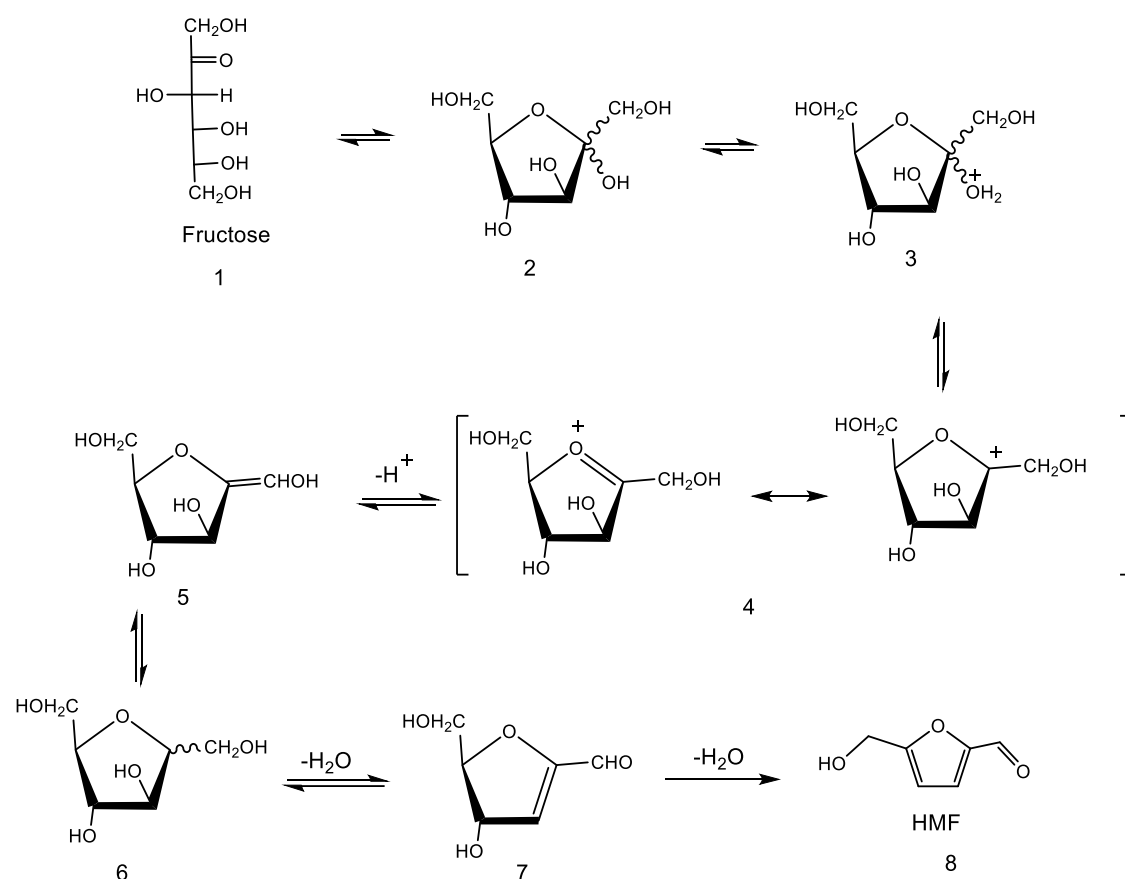
The mechanisms of HMF production from fructose and sucrose have been reported by many researchers, such as Antal and Mok⁴⁶. HMF could be produced via dehydration of fructose and glucose by a series of complex reactions comprising a variety of isomerization, condensation, fragmentation, and dehydration. The formation of HMF from hexoses is complex due to the formation of many side products during the dehydration process and its mechanism is as shown in Scheme 1.7. Under the same experimental conditions at pH ~0 (80-95°C in water for several hours), the yield of HMF is affected by isomerization, fragmentation, and condensation side products, while the dehydration of fructose is more effective and selective to produce HMF than that of glucose. The relative ease of formation of HMF from fructose has been attributed to the role of cationic fructofuranosyl intermediate, the low degree of enolization of glucose and the stability of the glucose ring structure (Scheme 1.8). At much higher temperatures (175-390°C), however, excellent yields of HMF is obtained from both fructose and glucose with lower concentration of mineral or Lewis acids. It is worth mentioning that there is another alternative mechanism-based base-catalysed β -elimination of the

hydroxyl group, which can form a 3-deoxyhexohexosulose from either fructose or glucose by an enediol intermediate.

Furthermore, oligosaccharides form due to the condensation of glucose, which can interact with HMF and cause cross-polymerization of materials. However, the low cost of glucose makes it more suitable as a feedstock for HMF formation.^{45, 47}



Scheme 1.7: Mechanism of formation of HMF from hexoses.⁴⁶



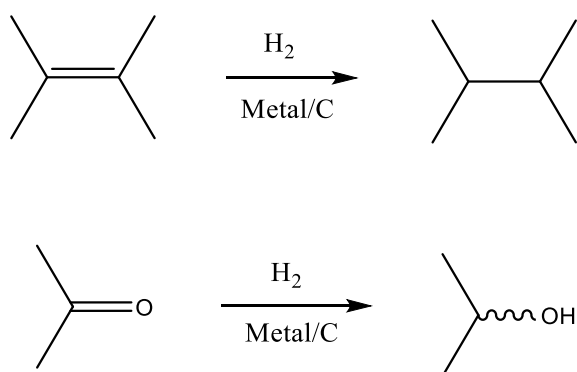
Scheme 1.8: Mechanism of formation of HMF from fructose.⁴⁶

1.6 Hydrogenation of furfural and hydroxymethylfurfural

Hydrogenation of FF and HMF is one of the most investigated topics for converting these compounds into useful products. Hydrogenation products are commonly used in fragrances, herbicides, pharmaceuticals, and other products.²⁰ FF and HMF contain a greater amount of oxygen (33 and 38 percent, respectively) relative to most petroleum products.⁴⁸ The oxygen content in FF and HMF is reduced by the hydrodeoxygenation process, which involves adding hydrogen to the C=O bond, and oxygen-containing molecules are eliminated by the hydrogenolysis process.²⁰ In biomass derivatives, hydrogenation or hydrogenolysis is used to increase the H/C and H/O ratios.⁴⁹ The hydrogenation process involves the addition of hydrogen atoms to an unsaturated bond using an external hydrogen source (Scheme 1.9).^{50, 51} the process could be carried out using molecules that could donate a proton such as fumaric acid (FA), alcohols (such as methanol, ethanol, glycerin or isopropanol) or hydrogen gas, in the presence of a heterogeneous or homogeneous catalyst. The catalyst accelerates the reaction rate and

increases the yield of desired products, and the product selectivity was found to be dependent on hydrogen sources applied in the reaction. Other factors such as the adsorption geometry of the substrate on the catalyst surface and acid-base properties on the catalyst surface equally play a role.⁵²

The hydrogenation of α , β -unsaturated aldehydes with high selectivity for a single product using a catalyst remains a challenging reaction. The critical problem in the hydrogenation of furan derivatives (HMF and FF) to alcohol derivatives (2-FFA and DHMFF) is the hydrogenation of C=O without further hydrolysis of C-O or hydrogenation of the C=C bond.⁵³ With heterogeneous metal catalysed processes, hydrogenation of the C=C group is more easily achieved than the hydrogenation of the C=O bond due to thermodynamics.^{54, 55} For this reason, the challenging reaction in biomass hydrogenation is the selective production of α , β unsaturated alcohols.⁵²



Scheme 1.9: Hydrogenation reaction with metal catalyst.^{50, 51}

The sources of hydrogen for the hydrogenation of the carbonyl group could be achieved by hydrogen gas or transfer hydrogenation using various protic polar solvents.^{24, 56} Transfer hydrogenation is a relatively benign hydrogenation technique which involves the use of protic polar solvents such as methanol, isopropanol, and butanol as hydrogen donors at high temperatures with metal catalysts. However, the majority of hydrogenation reactions employ molecular hydrogen gas (H_2) as the hydrogen source due to high yields and mild reaction conditions.^{24, 56}

Largely, it has been observed that catalyst activity and selectivity are affected by the nature, size, and dispersion of the nanoparticles on the support surface for the hydrogenation reaction. Hydrogen adsorption on transition metal surfaces is an important step in metal catalysed hydrogenation reaction and the extent of interaction is determined

by the relationship between the d-orbitals in metal surfaces and molecular hydrogen.⁵⁷ If the bonding is too strong, catalytic activity will be suppressed.^{58, 59} The activation and dissociation of molecular hydrogen is performed using different supported noble metals, for example, Rh, Pt, Pd, and Ru, or using supported non-noble metals such as Fe, Ir, Ni, Mo, Co, and Cu.^{60, 61} However, different metal catalysts have varying selectivity for hydrogenation of α,β -unsaturated aldehydes, because polarisation of C=O group differs on the surface of each metal. Sithisa and Resasco in 2011 established that product selectivity strongly depends on the metal catalyst employed. They explored three different catalysts, Cu, Pd, and Ni supported on silica and found that each metal interacts differently with the adsorbed FF resulting in different product distribution. Noble metal catalysts, such as Pt and Ru, have demonstrated good selectivity for unsaturated alcohols, with selectivity towards C=O hydrogenation in FF and HMF leading to high yields of 2-FFA and DHMF, respectively. On the other hand, Pd catalysts have been reported to exhibit moderate selectivity towards C=O hydrogenation and higher selectivity towards the hydrogenation of C=C bonds, which can lead to the formation of saturated hydrocarbons. However, Cu-based catalysts interact weakly with the C=C bond and adsorb carbonyl group almost preferentially with high selectivity towards 2-FFA.⁶² The metal centres are responsible for the adsorption and dissociation of H₂, after which the hydrogen is spilt over to the support where FF is adsorbed and activated for reduction.^{60, 63}

Furthermore, adsorption modes of FF on the active surface of the metals can adopt different modes that play a crucial role in the product's selectivity (Figure 1.2).⁶⁴ Nakagawa and co-workers reported an efficient Pd-Ir bimetallic catalyst supported on SiO₂ with complete hydrogenation of FF to 2-FFA at low reaction temperature.⁶⁵ This higher activity was hinged on the synergy between Pd and Ir and is due to a change of adsorption mode. The Ir atom on the surface strongly adsorbs C=O, facilitating strong interaction of the furan ring with the Pd surface.

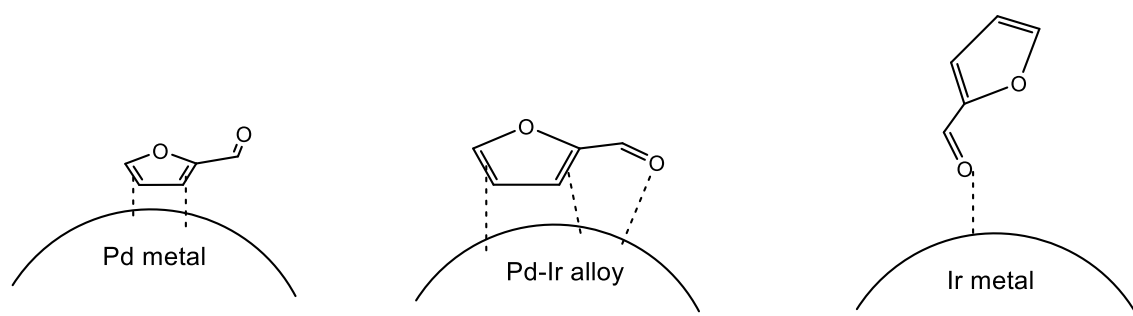


Figure 1.2: Suggested adsorption modes of furfural on Pd, Ir and Pd-Ir surface.⁶⁴

1.7 Hydrogenation of aldehyde group to alcohol in liquid and gas phases

The production of 2-FFA and DHMF from the hydrogenation of carbonyl bonds in furan derivatives, FF and HMF, has received much interest from both researchers and the industry during the past few years.^{28, 66} 2-FFA is recognised as the most significant product of the hydrogenation of FF, for instance, more than 65% of FF is currently used for 2-FFA production.⁶⁷⁻⁶⁹

The initial production of 2-FFA used sodium or sodium amalgam for the reduction of FF, but due to the adverse effects of working with mercury, research on catalytic reduction gained momentum. Researchers have exploited different metal catalysts for the reduction of FF to 2-FFA. Yan *et al.* reported a copper-catalyst-supported $\text{Na}_2\text{O} + x\text{SiO}_2$ system with 99% conversion of FF to 2-FFA in the gas-phase.^{70, 71} 2-FFA is one of the most promising intermediates with wide industrial applications, and presently, it is produced in the industry using a copper chromite catalyst at 200°C and 3 MPa of H_2 .⁷² It was found that the copper chromite catalyst ($\text{CuCr}_2\text{O}_4 \cdot \text{CuO}$) is the most efficient catalyst for the production of 2-FFA in liquid phase hydrogenation because Cu is more selective for hydrogenation of the C=O bond with little or no preference for the C=C bond in FF.^{30, 73, 74} However, copper-chromite catalyst is not economically attractive as it can only be operated in a batch process, it is toxic, harms the environment and is rapidly deactivated.⁷² For this reason, various chromium-free catalysts have been investigated to identify alternatives with selectivity towards 2-FFA. One of the objectives of this thesis is the hydrogenation of the carbonyl group in FF with high selectivity under mild reaction conditions using different kinds of metal catalysts and supports.

1.7.1 Design the catalyst for the hydrogenation of furfural and hydroxymethylfurfural

The hydrogenation of FF to 2-FFA can be achieved using a catalyst in either the liquid or gas phase.⁷⁵⁻⁷⁷ The hydrogenation of FF in the gas phase produces 2-FFA with high selectivity, however, gas phase reactions are energy intensive.^{76, 78, 79} Equally, the hydrogenation of FF and HMF can occur with both homogeneous and heterogeneous catalysts, however, heterogeneous catalysts with desired active sites are preferred over homogeneous catalysts for many reasons.⁸⁰ First, heterogeneous catalysts are in a different phase relative to the reactants and can be easily separated from the products by filtration or centrifugation.^{80, 81} In addition, heterogeneous catalysts could be used repeatedly with little or no loss of activity.⁸⁰ Moreover, heterogeneous catalysts are non-corrosive and typically require low reaction temperatures and pressures.^{80, 81} In contrast, homogeneous catalysts are in the same phase as the reactants and can provide high reactivity and selectivity with lower side products due to their proximity to the reactants.^{81, 82} However, these catalysts can be difficult to separate from the products, and they may also require high reaction temperatures and pressures.⁸¹

There have been many attempts to modify metal catalysts and optimize their reaction conditions for the hydrogenation of α,β -unsaturated aldehydes to improve their activity and selectivity towards α,β unsaturated alcohols.^{76, 79, 83, 84} The modification of the catalyst structure has been carried out by changing the particle sizes of the metal, adding a second metal, adjusting the catalyst using different heat treatment protocols, and using a variety of support materials. It was found that the metal-support interaction plays a crucial role in improving the catalyst's selectivity. For instance, the support increased the surface area of the catalyst with a low load of the metal, diluting the expensive metal and stabilising it.⁶¹ For this reason, the activity and stability of metal catalyst improve in the presence of the support. Moreover, using reducible oxide supports such as TiO_2 , CeO_2 , and Nb_2O_5 enhances the catalyst selectivity due to electronic interactions as a result of strong metal support interaction (SMSI).^{85, 86} Bimetallic catalysts improve the catalyst activity due to synergy, the geometry of the active sites, bi-functional effects and improves the stability of the catalyst.⁸⁷ Moreover, reaction conditions equally have a pronounced effect on catalysts activity and selectivity.⁸⁸⁻⁹⁰ For instance, the high pressure of hydrogen gas in some cases is essential to increase the catalyst activity and prevent catalyst deactivation via fouling and poisoning of the catalyst, and a low H_2 pressure could lead to strong

adsorption of the unsaturated organic compound on the catalyst surface.⁵¹ Furthermore, it is important to note that the hydrogen/furfural ratio would have an impact on the selectivity towards 2-FFA. Tables 1.1 and 1.2 highlight some monometallic and bimetallic catalyst compositions and their optimum reaction conditions for the hydrogenation of FF with selectivity towards 2-FFA in the liquid phase. Furthermore, Tables 1.3 and 1.4 presented some optimum reaction conditions for the gas-phase hydrogenation of FF to 2-FFA using monometallic and bimetallic materials, respectively

Table 1.1 Liquid phase hydrogenation of furfural using monometallic catalysts.

Entry	Catalyst	Cata. (mg)	FF (mmol)	Temp (°C)	Time (h)	Press. H ₂ (MPa)	Solvent	Conv. (%)	Sele (%)	Ref.
1	Pt/FHP(Ferric Hydroxyphosphate)	50	8	60	9	2	2-PrOH	97.3	100	88
2	Pt/MgO	20	0.002	50	7	0.1	MeOH	79	97	91
3	Pt/CeO ₂	20	0.002	50	7	0.1	MeOH	77	98	91
4	Pt/r-Al ₂ O ₃	20	0.002	50	7	0.1	MeOH	80	99	91
5	Pt/CeO ₂ /UIO	975	0.002	80	30	1	2-PrOH	100	99	92
6	Pt/Al ₂ O ₃	58	0.3	150	5	0.5	2-PrOH	95	98	93
7	Pt/MWNT	200	416	150	5	2	2-PrOH	94.4	79	94
8	Pt/TECN	50	4.16	100	5	1	water	99	99	95
9	Pt/HT	50	0.75	30	2	1.5	water	99.9	99	96
10	Pt/BN-U10-12	27	2.602	80	3	1	2-PrOH	94.2	96.3	97
11	Pt/C	100	10.40	175	0.5	8	n-BuOH	99.3	48.23	98
12	Pt/biochar	160	36	210	4	10.3	toluene	66.9	55.4	99
13	Pt/C	500	41	250	5	3.5	2-PrOH	89.3	58.9	100
14	Pt/SnNb ₂ O ₆	8	0.1	25	2	0.1	MeOH	99.9	99.9	101
15	Pt/TiO ₂	50	0.60	50	2	2	MeOH	85	61	102
16	Pt/C ₃ N ₄	29	2.62	70	2	1	2-PrOH	99	99	103
17	Pd/Al ₂ (SiO ₃) ₃	400	100	150	4	2	acetic acid + toluene	56.9	30.0	104
18	Ru/C	400	52.035g	165	6	2.5	MTHF	91	42.4	105
19	Ir/TiO ₂	500	1.25	90	5	0.62	Heptane/EtOH	30	30	106
20	Ir-ReO _x /SiO ₂	50	3.0	30	6	0.8	water	>99	>99	107

21	Cu ₄₀ -Mg-Al	200	12.07	150	8	-	2-PrOH as hydrogen donor	100	100	108
22	Ni/NAC-1-1073	20	0.2	138	5	4	2-PrOH	99.9	99.9	109
23	Co@NC-600-800	30	1	80	5	4	water	100	100	110

Table 1.2 Liquid phase hydrogenation of furfural using bimetallic catalysts

entry	Catalyst	Cata (mg)	FF (mmol)	Temp (°C)	Time (h)	Press. H ₂ (MPa)	Solvent	Conv. (%)	Sele (%)	Ref.
24	PtCo/C	78	3.642	100	5	1	2-PrOH	100	100	111
25	PtNi/C	100	2.08	100	1	1	2-PrOH	99	86	112
26	PtNi/HNFs	100	2.08	100	1	1	2-PrOH	99	99	112
27	Pt ₃ Fe/CeO ₂	20	4.41	100	4	2	2-PrOH	99	99	113
28	PtCo _{0.2} /TiO ₂	50	0.60	50	2	2	MeOH	100	98	102
29	FePt/AC	50	0.60	50	1	2	Water	100	74	114
30	Pt-Ni/MWNT	100	6.03	100	5	3	EtOH	96	80	115
31	Pt-Co/MWNT	100	6.03	100	5	3	EtOH	87	70	115
32	PtRe /TiO ₂ -ZrO ₂	200	10	130	8	5	EtOH	100	96	116
33	Pt-Sn _{0.3} /SiO ₂	250	0.002	100	4	1	2-PrOH	100	96	117
34	Ir-ReO _x /SiO ₂	50	3.0	30	6	0.8	water	>99	>99	107
35	Cu ₄₀ -Mg-Al	200	12.07	150	8	-	2-PrOH as hydrogen donor	100	100	108
36	Ni-Fe-B	1000	60	200	4	1	EtOH	100	~100	118
37	Cu _{11.2} Ni _{2.4} -MgAlO	1000	178	300	2	1	EtOH	90	87	119
38	Ni-Sn/TiO ₂	50	1.1	110	1.15	3	2-PrOH	>99	>99	120
39	NiCoCuZnFe/C-800	50	3	120	9	3	2-PrOH	100	100	121

Table 1.3 Gas phase hydrogenation of monometallic catalyst

entry	Catalyst	Temp (°C)	Time (h)	Press. H ₂ (MPa)	Conv. (%)	Sele (%)	Ref.
40	Pt/TiO ₂ /SiO ₂	150		0.1	68.3	64.1	122
41	Cu/SiO ₂	230	5min	H ₂ /Feed ratio=25, 1atm H ₂ ,	69	67.6	62
42	Cu/SiO ₂	170	4	H ₂ /furfural ratio=5, LHSV 0.5 h ⁻¹	98	97	123
43	Cu/SiO ₂	290	0.25	H ₂ /furfural ratio=25, WHSV 2.3 h ⁻¹	77	63	124
44	Cu/SiO ₂	140	10	H ₂ /furfural ratio=17 WHSV 0.5 h ⁻¹	98	73	125
45	Cu/SBA-15	170	1	H ₂ /furfural ratio=12 WHSV 1.5 h ⁻¹	92	85	126
46	Cu/MgO	180	5	H ₂ /furfural ratio=2.5 WHSV 4.8 h ⁻¹	98	96	127
47	Cu/ZnO	220	10	H ₂ /furfural ratio=17 WHSV 0.5 h ⁻¹	95	31	125
48	Cu-Ca/SiO ₂	130	20	0.1-H ₂ /furfural=5 LHSV 0.33 h ⁻¹	100	99	128
49	Ni/SiO ₂	220	-	H ₂ /furfural ratio=25, WHSV 10 h ⁻¹	84	31	129
50	Cu/CeO ₂	190	1	Feed flow = 2.3 mmol FF h ⁻¹).	83	35	130
51	Cu/ZnO	190	1	Feed flow = 2.3 mmol h ⁻¹ , H ₂ flow = 10 ml min ⁻¹).	95	75	131
52	Cu-kerolite	190	1	H ₂ flow=10 mL min ⁻¹ , feed flow=2.3 mmol FUR h ⁻¹	96	84	132

Table 1.4 Gas phase hydrogenation of bimetallic catalysts.

Entry	Catalyst	Temp (°C)	Time (h)	Press. H ₂ (MPa)	Conv. (%)	Sele (%)	Ref.
53	PtCo/C	100	5	1	100	100	111
54	Co–Cu/SiO ₂	200	12	H ₂ /Feed ratio=6 WHSV 3.1 h ⁻¹	65	64	133
55	Cu–La/MCM-41	140	-	0.1 H ₂ /furfural=5, GHSV 0.087 mol h ⁻¹ g catalyst ⁻¹	98	>97	134
56	Cu–Cr/TiO ₂	140	0.25	H ₂ /furfural=900, WHSV 1.2	90	79	78
57	CuCr ₂ O ₄ .CuO	200	-	0.1	96	77	135
58	CuCr ₂ O ₄ CuO)	200	4	6	94	83	72
59	Cu-Al oxide	220	2	H ₂ /FAL ratio = 3; atmospheric pressure.	87	74	136
60	CuOCeO ₂ /Al ₂ O ₃	175	3	0.5 aW/F = 60 gcat/molFALh	90	78	137
61	Ni ₂ P/SiO ₂	210	2	0.1	100	75	138

The heterogeneous catalysts used for the hydrogenation of HMF to DHMF were summarized in Table 1.5.

Table 1.5 Hydrogenation of HMF to DHMF using heterogeneous catalysts

entry	Catalyst	Cata. (mg)	HMF (mmol)	Temp (°C)	Time (h)	Press. H ₂ (MPa)	Solvent	Conv. (%)	Selc. (%)	Ref.
62	Ru/MSN-Zr	100	80	25	4	0.5	water	98.5	92	139
63	Pt/MCM-41	100	4	35	2	0.8	water	100	99	140
64	Cu _{0.59} Mg _{2.34} Al _{1.00}	100	4	100	3	5	EtOH	100	99	141
65	NiAl-300	100	11.9	180	4	1.2	1,4-dioxane	100	20	142
66	Cu-ZnO	500	11.9	100	20	1.5	1,4-dioxane	100	99	143
67	RANEY® Cu	140	0.08	90	1	9	water	94	91	144
68	Ni-Fe/CNTs	50	4	120	3	3	n-butanol	100	96	145
69	Cu/Al ₂ O ₃	5000	238	120	-	2	EtOH	99	99	146
70	CuNPs@ZIF-8	486.4	0.5	140	3	2	EtOH	100	99	147
71	Ru/C	0.15	10	50	4	3	water	100	93	148
72	Ru/Co ₃ O ₄	0.25	0.04	190	6	TH	2-PrOH	100	83	149

73	Ru/MnCO ₂ O ₄	400	8	80	16	6	MeOH	100	99	150
74	Ru/PM modified porous melamine	25	1.2	50	8	2	water	90	99	151

1.8 Catalytic hydrogenation of carbonyl to alcohol.

1.8.1 Hydrogenation reactions using monometallic catalysts

1.8.1.1 *Selective hydrogenation of furfural to 2-furfuryl alcohol using noble metal catalysts*

The selective reduction of FF to 2-FFA is an important hydrogenation reaction because 2-FFA is an important fine chemical for the polymer industry. This reaction has been attempted using both noble and non-noble metals by many researchers.^{82, 152-156}

Sivec and co-workers¹⁵⁷ used different metals supported on activated carbon (Cu/C, Ni/C, Pd/C, Pt/C, Re/C, Rh/C, and Ru/C) as catalyst for hydrotreatment of FF at 100, 150 and 200°C. Pt and Ru/C catalysts are more selective for hydrogenation of FF to 2-FFA, while Pd/C recorded the highest activity under all the reaction conditions tested albeit with poor selectivity. Kijenski and Winiarek¹²² observed that Pt catalyst deposited on monolayer TiO₂ showed good selectivity in the hydrogenation of α,β -unsaturated aldehyde (cinnamaldehyde) and this enhanced selectivity is attributed to the monolayer support.

1.8.1.2 *Hydrogenation of furfural to 2-furfuryl alcohol using non-noble metal catalysts*

The hydrogenation of FF to 2-FFA using non-noble metal catalysts such as Cu or Ni usually requires harsh reaction conditions.^{79,158} Moreover, Gong et al. in 2018 reported highly stable and recyclable Co encapsulated in N-doped carbon nanotube as excellent catalysts in aqueous phase hydrogenation of FF with high selectivity towards 2-FFA at 80°C.¹¹⁰

Nickel, copper and chromium catalysts on varying supports have equally been shown to be effective in the hydrogenation of FF to 2-FFA in the liquid¹⁰⁹ and gas phases.¹⁵⁹ Ni nanoparticles supported on an inert SiO₂ catalyst presented high activity but typically required higher hydrogen pressure and temperature compared to palladium and platinum catalysts. Nickel catalysts are prone to deactivation due to nickel sintering and coking. Coke species that form on the catalyst's surface due to Ni strongly adsorbing carbon¹⁶⁰ In addition, Cu/MgO catalyst system has been extensively studied for the hydrogenation of FF into 2-FFA because of its low cost, high activity, and selectivity for 2-FFA in the gas and liquid phases under harsh reaction conditions.^{126, 127, 159, 161-167}

1.8.2 Hydrogenation reactions using bimetallic catalysts

Chemoselective hydrogenation of FF using heterogeneous catalysts is faced with myriad of challenges due to so many competing reactions. Interestingly, the catalyst performance can be tuned by adding a second metal to monometallic catalysts to improve their activity, selectivity, and stability.^{87, 168} Catalysts can be tuned by adding a second metal due to alteration in composition, size, crystallinity, and electronic properties.²⁴ Bimetallic catalysts are characterised by a synergistic effect between the two metals in question and their properties are different from the constituent monometals,⁵⁰ and this synergy between two metals has been observed to influence catalyst performance in many ways. For instance, the formation of novel active sites with high dispersion, inhibition of migration and aggregation of nanoparticles on the catalyst surface are some of the critical features of bimetallic systems that improves the stability by reducing sintering processes.^{24, 87} Also, bimetallic catalysts improve the catalyst activity due the geometry of the active sites is altered, Bi-functional effects, where each metal species provides a different function in the reaction mechanism.⁸⁷ Catalysts can be tuned by adding a second metal due to alteration in composition, size, crystallinity, and electronic properties.^{24, 50} and this synergy between two metals has been observed to influence catalyst performance in many ways. For instance, the formation of novel active sites with high dispersion, inhibition of migration and aggregation of nanoparticles on the catalyst surface are some of the critical features of bimetallic systems that improves the stability by reducing sintering processes.^{24, 87} Also, bimetallic catalysts improve the catalyst activity due the geometry of the active sites is altered, Bi-functional effects, where each metal species provides a different function in the reaction mechanism.⁸⁷

Srivastava and co-workers prepared a NiCu/ γ -Al₂O₃ bimetallic catalyst by impregnation method and the catalyst was explored in hydrogenation of FF and HMF under mild operating conditions. This catalyst was found to be selective towards 2-FFA when employed for the hydrogenation of FF at low temperatures, and this result has been hinged on the strong interaction between copper oxide particles and nickel, which increased the copper dispersion on the catalyst surface, and the ratio of Cu:Ni.¹⁶⁹

Single metal catalysts have been found to be prone to leaching which leads to deactivation and poor activity, however, the addition of another metal can tune the electronic properties, crystallinity, size, and active centre composition which ultimately leads to

enhanced catalyst stability and activity.²⁴ For example, Zhao et al¹⁷⁰ fabricated a CuCo bimetallic catalyst supported on a nitrogen-doped carbon catalyst with high performance for hydrogenation of HMF to DHMF. The activity and selectivity exhibited by this catalyst have been attributed to the electronic interaction between copper and cobalt which leads to electron transfer from Cu to Co. This synergy between Cu and Co was confirmed with a reduction in the binding energy of Co by 1.1 eV and a corresponding 0.8 eV increase in that of Cu in the bimetallic catalyst compared to the individual monometallic catalyst respectively. The catalyst's stability is equally strengthened with HMF conversion ranging from 99.6 – 77.4% after nine consecutive reaction cycles. Wu et al. reported a co-impregnated PtNi catalyst for the hydrogenation of FF with high activity and selectivity towards THFA,¹⁷¹ while Lesiak and co-workers reported the influence of Cu on the activity and selectivity Pd–Cu/Al₂O₃ catalyst.¹⁷² The bimetallic catalyst exhibits high conversion of FF with selectivity for 2-FFA due to the synergistic effect between the two metals. Catalyst stability is one of the most important factors in the assessment of heterogeneous catalysts. These reports further highlight the roles of second metals in catalyst activity and stability.²⁴

Ferrando *et al.* classified the structures of the nanoalloy into four types depending on the mixing pattern of the nanoalloy. The first type is core–shell structures where one type of metal is in the centre of the nanoalloy as a core and is surrounded by the second metal as a shell. This is the most common structure of nanoalloy in the literature (Figure 1.3a).¹⁷³ The second type of pattern called segregated nanoalloys generated when the two metal components have a pseudo-planar interface between them (Figure 1.3b). This kind of nanoalloy is seldom reported in the literature. The third type of nanoalloy is a homogeneously mixed alloy where the two metals are intimately mixed in either an atomically ordered called ordered nanoalloys or a statically random manner which is called random nanoalloys (Figure 1.3c). The random nanoalloy is more common than the ordered one. The last type of nanoalloy is termed multi-shell nanoalloy which is generated when the core metal is encircled by concentric shells forming an “onion-like” structure and this was reported recently.

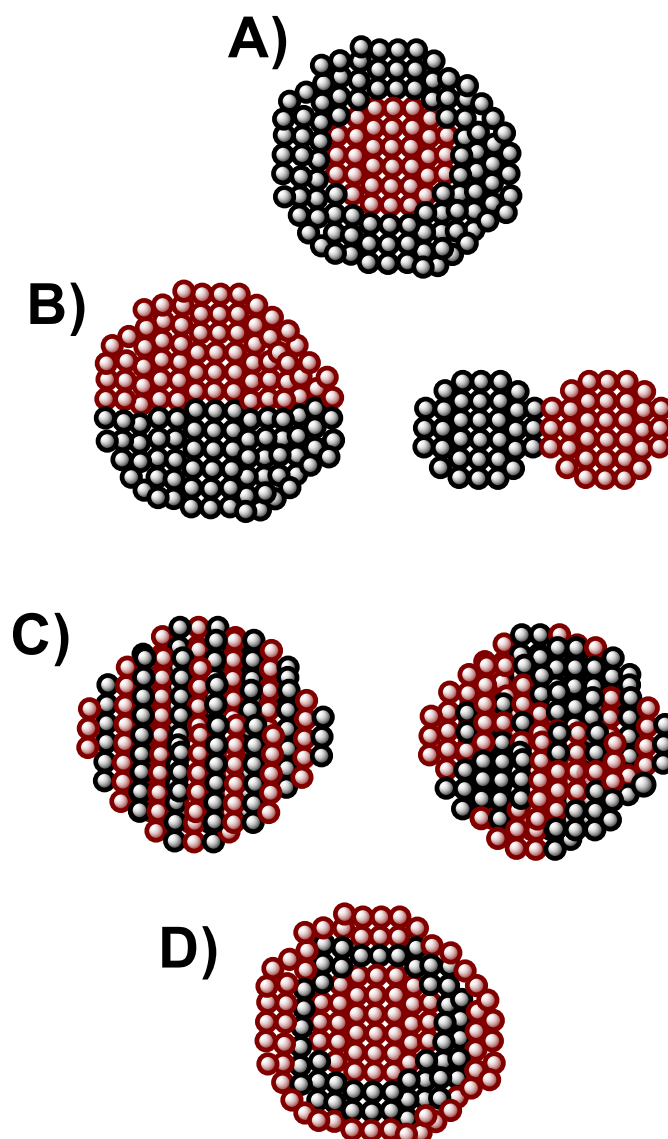


Figure 1.3: Schematic representation of some possible mixing patterns in bimetallic systems: (a) core–shell alloys, (b) sub-cluster segregated alloys, (c) ordered and random homogeneous alloys, and (d) multishell alloys. Adapted from Ferrando et. al.¹⁷³

The surface structure of the catalyst is affected by many factors such as bond strengths between metals, surface energies of the two metals, relative atomic sizes, charge transfer, binding strength to surface-active ligand and specific electronic/magnetic interaction that stabilizes a specific structure between two metals¹⁷³

It has been proposed that PtRu nanoalloy exhibits a core-shell arrangement where the Pt atoms are located on the surface (exterior shell) and the Ru atoms are located in the core.¹⁷⁴ The positioning of these metal atoms caused different electronic effects in the

bulk alloys, and the linked nanoparticles with two separate monometallic species are situated in very close proximity to one and other (Figure 1.4).

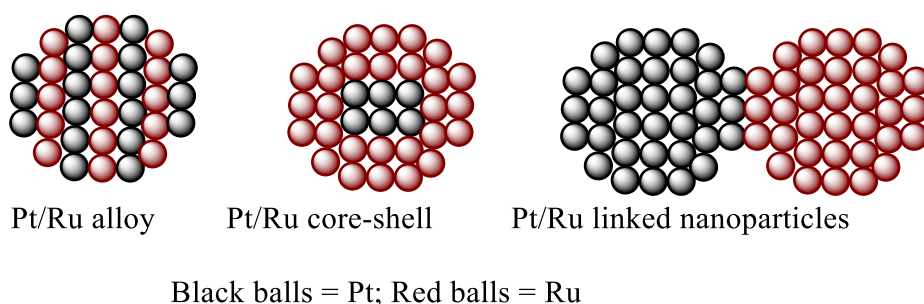


Figure 1.4: The difference in alloy structure for Pt/Ru depending on preparation methods. Adapted from Alayoglu *et. al.* ¹⁷⁴

1.8.3 Tuning of the support sites

Interactions between metals and supports have been reported to be of enormous importance to achieving good catalytic activity and selectivity and because of this, they are of fundamental interest in heterogeneous catalysis. Strong metal support interactions affect important parameters (electronic, geometry and bifunctional effects) which are responsible for catalysts' activity, selectivity, and stability. A perfect understanding of the interactions between metals and supports and the ability to tune this important parameter in order to achieve catalysts with enhanced activity, selectivity and stability are vital and research studies on metal-support interaction is progressing with modern surface analytical techniques.

Yang *et al.* observed that the small-sized micropores and organic ligands in metal-organic frameworks (MOFs) are the limiting factors affecting the use of MOFs as support in heterogeneous catalysis.¹⁷⁵ They fine-tuned the Ce-MOF support by a partial and full deligandation technique thereby generating active Pt/CeO₂ by partial/full decomposition of Ce-MOF at 270 and 600°C respectively, after which Pt nanoparticles were deposited on the supports by atomic layer deposition. Relatively, the Pt/CeO₂-270 obtained by partial deligandation showed excellent activity with 100% conversion for FF and high

selectivity (97.3%) of 2-FFA. This interesting result was attributed to the large surface area, extensive porous structure, abundant Ce³⁺ and oxygen vacancy, which stabilize the highly dispersed Pt nanoparticles and serve as electrophilic or Lewis acid sites for C=O adsorption, while residual organic ligands enhance furfural adsorption. Wang and co-workers also supported this notion in their seminal article that basic supports are essential for the carbonyl group hydrogenation in furan derivatives.¹⁷⁶

1.8.4 Strong metal support interactions

Strong metal support interaction (SMSI) was coined by Tauster *et al.* in 1978 to describe the metal-metal bonding observed between noble metals and titanium cations which led to decrease in the amount of H₂ and CO adsorb to near zero after the reduction of the noble metals supported on TiO₂ at 500°C.¹⁷⁷ SMSI generally refers to the interaction between noble metals and metal oxide supports that causes migration of the reducible metal oxide support to the metal surface at high-temperature reduction and forms interfacial bonds leading to loss of chemisorption sites.¹⁷⁸⁻¹⁸⁰ However, in some reactions for example CO oxidation,¹⁸¹ CO and CO₂ hydrogenation and dehydrogenation,^{178, 182, 183} products selectivity improve due to SMSI effect. SMSI could equally lead to changes in the electronic and geometric structures of metal catalysts, thereby, affecting their catalytic activity and selectivity due to the formation of O vacancies on oxide support surfaces and the reverse spillover of O atoms from oxide to the metal NPs.¹⁸⁴ The presence of oxide support on the catalyst can be observed in the XPS results with changes in the binding energies up to 0.5 eV.¹⁸⁴ Neyman and Kozlov suggest that the most important component of metal-support interactions is charge transfer and this is facilitated by the reducible nature of the oxide support and it is strongly dependent upon defects in the oxide and its nanostructuring.¹⁸⁴ Catalyst's performance can be tailored by incorporating strong metal support interactions,¹⁷⁶ For instance, the interaction between Pt NPs and TiO₂ reducible oxide support can lead to spillover of the hydrogen and formation of furfural-oxy intermediate over TiO₂, which has been shown to enhance the activity and selectivity of Pt-catalysts in various reactions.^{156, 180} Also, the migration of reduced species from the TiO₂ support is driven by the formation of metal-Ti bonds, which contributes to migration by providing the thermodynamic driving force. They are different from those in intermetallic compounds due to the presence of oxygen that makes the Ti and metal cationic.¹⁷⁹

Metal-support interaction can also affect the stability of the catalyst by preventing the sintering or agglomeration of metal particles during high-temperature reactions.¹⁸⁵ This is because the interaction between the metal and support can create a strong bond, which can prevent the metal particles from migrating or coalescing into larger particles. This interaction plays an important role in determining the performance of Group VIII metal catalysts supported on reducible oxides, and understanding the nature and strength of this interaction is crucial for designing and optimizing catalysts for various industrial applications. Recently, Zhang and co-workers reported that the catalyst selectivity of FF to 2-FFA using Ni/TiO₂ was enhanced by calcining the catalyst at high temperatures. The high calcined temperature enhanced the electronic interactions between the Ni NPs (NiO) and TiO₂ which are important for strong metal-support interaction. This interaction leads to electron transfer to fill the D-band of Ni⁰ to form Ni^{δ-} on the Ni/TiO₂ catalyst surface, which is the active site for the selective hydrogenation of FF to 2-FFA, and this happens due to the proximity of the formed oxygen vacancy (O_v) to Ni⁰.⁶⁹

1.8.5 Effect of solvent on heterogeneous catalysis

Solvent and solvent effects are some of the important parameters that are crucial in organic synthesis and hydrogenation reactions, and their effects in homogeneous catalysis have been well documented.¹⁸⁶ Many reports have equally reported the roles of solvents and their influence on supported metal heterogeneous catalysed reactions. In view of this, tuning heterogeneous catalysed reactions in the liquid phase for better activity and selectivity should include solvent and solvent effects alongside the need to control the atomic structure and electronic properties of the active sites. Water has been used as a solvent for some heterogeneously catalysed reactions because it is polar and can solubilize some polar organic materials, ubiquitous and regarded as a green solvent. It is usually preferred as a solvent because it is environmentally friendly, however, it is imperative to note that not all reactions can be conducted in water. Generally, solvents can be divided into three categories which are polar protic, polar aprotic and nonpolar solvents.

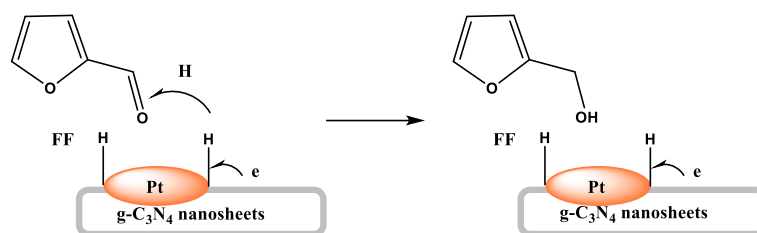
Recently, Wang and co-workers used DFT calculations to study the effect of solvent on FF hydrogenation over Pt(111) and observed that methanol could enhance the adsorption strength of FF and other oxygen containing species because of its strong polarity with improved activity and selectivity.¹⁸⁷ Besides, methanol was found to mitigate dehydrogenation of FF due to improved adsorption of FF on the catalyst surface, and for these

reasons, polar solvent is adjudged more efficient for 2-FFA selectivity.¹⁸⁷ Furthermore, Yoon et al. established that using water as a solvent in phenol hydrogenation reduces the activation energy effectively as a result of tautomerization of surface-bound enol intermediate.¹⁸⁸ Taylor and co-workers investigated the effects of different supports (SiO₂, ZnO, g-Al₂O₃, CeO₂ and MgO) and different solvents on the hydrogenation of FF. They found that the particle size and the solvent employed have a strong influence on the catalyst selectivity for the production of 2-FFA under mild reaction conditions.⁹¹ They assessed both polar and nonpolar solvents and found polar solvents to be more suitable for the hydrogenation of FF with selectivity towards 2-FFA.

1.9 Plausible mechanism of the chemoselective hydrogenation of the carbonyl group in furfural to 2-furfuryl alcohol over the catalyst surface

The chemoselective hydrogenation of FF to 2-FFA over the heterogeneous catalyst is an important process that furnishes the chemical industries with chemical intermediate used for the preparation of plasticizers, dispersing agents, lysine, and lubricants to mention a few. Typically, the hydrogenation of the C=C bond is favoured over that of C=O by about 35 kJ/mol, hence, tuning a catalyst and modifying other variables to achieve maximum selectivity towards C=O hydrogenation is a challenging process that has been studied extensively. Great efforts have been made over the years to gain insight into the mechanism of this chemoselective hydrogenation using state-of-the-art spectroscopic instruments and with many articles published on the different ways by which this process can be achieved, and they include introducing promoters or inhibitors, introducing a second metal component, tuning the particle sizes of the catalysts.¹⁸⁹

Chen and co-workers reported in 2016 the mechanism for the chemoselective hydrogenation of FF to 2-FFA using platinum nanoparticles supported over graphite carbon nitride nanosheets with complete conversion of FF and high selectivity of 2-FFA. This multi-step reaction was found to proceed via the adsorption of the C=O group in the FF onto the surface of the platinum catalyst. At the same time, the hydrogen molecule is adsorbed on the surface of the catalyst and split into atoms. Subsequently, the adsorbed hydrogen atom attacks the adsorbed C=O in a FF molecule to form C-OH functionality and the 2-FFA formed thereof is replaced by another FF to maintain the cycle on the surface of the catalyst.⁹⁵ This proposed chemoselective reduction is illustrated in Scheme 1.10.



Scheme 1.10: Plausible chemoselective hydrogenation mechanism. Adapted from Chen *et al.*⁹⁵

1.10 Catalytic hydrogenation of hydroxymethylfurfural to 2,5-dihydroxymethyl furan using noble metals

Catalytic hydrogenation using different noble metals and different reaction conditions has been widely studied due to their excellent activity and selectivity in the hydrogenation of HMF to DHMF. Relatively, Ru-based catalysts have been widely deployed due to their excellent activity and selectivity. Zhao *et al.* recently reported some developments and challenges of biomass derived HMF hydrogenation using noble metals with highlights on the catalytic performance of ruthenium-based supported catalysts.²⁴ They equally emphasized the crucial role of support in the selective hydrogenation of HMF. Alamillo and co-workers¹⁹⁰ found that using (basic) support such as CeOx, magnesia-zirconia Mg-Zr, and γ -alumina with high isoelectric point have an influential effect on the production of DHMF. They reported excellent yield and selectivity for the hydrogenation of HMF to DHMF at 130 °C under 2.8 MPa using Ru-based catalyst supported on materials with high isoelectric points and the selectivity was hinged on the acidity of the aqueous solution. Furthermore, Chen and co-workers¹³⁹ in 2013 reported Ru clusters supported on mesoporous ZrSi nanospheres as an excellent catalyst for the hydrogenation of HMF with good selectivity at room temperature. However, the reaction was carried out under high pressure (5 MPa). In 2019, Tan *et al.*¹⁹¹ demonstrated the effectiveness of the bimetallic Ru-Pd/RGO catalyst for the hydrogenation of HMF at room temperature under 1 MPa. Adsorption of the substrate on Ru and the strong interaction between the two metals facilitated the selective hydrogenation of the carbonyl group.

Besides Ru, Pt- and Pd-based catalysts have equally been reported in seminal publications with performance ranging from good to poor for the selective hydrogenation of the carbonyl group in HMF. For instance, Liu et al., reported the hydrogenation of HMF to DHMF and DHMTHF in 71 and 15% yields respectively using Pd/charcoal in water for 48 h under 50 bar of H₂,¹⁹² while Silva and co-workers carried out hydrogenation of HMF to DHMF using Pd supported on cup-shaped stacked carbon nanotubes (CSCNT) combining with microscale activated carbon (AC) with 76% conversion and 87% selectivity towards DHMF in water for 2 h under 3.4 MPa of H₂.¹⁹³ Both authors agreed that the presence of water in the reaction medium enhanced the catalyst selectivity for the carbonyl group.

1.11 Ring oping of furan derivatives

Typically, selective hydrogenation and hydrogenolysis are considered to be the two methods of choice for the conversion of platform chemicals like HMF and FF into valuable compounds for different industrial applications. One of the products obtained as a result of selective hydrogenation and hydrogenolysis of platform chemicals are 1,5-pentanediol (1,5-PDO) and 1,2-pentanediol (1,2-PDO), which are used as a monomer in the plastic industry. Selective hydrogenation and hydrogenolysis of platform chemicals derived from biomass using a heterogeneous catalyst have been extensively studied for the aforementioned reasons.¹⁹⁴⁻¹⁹⁷ Comparatively, hydrogenolysis requires harsher reaction conditions than selective hydrogenation, however, the transformation of platform chemicals into important industrial feedstocks are feasible with a careful selection of appropriate catalysts and reaction conditions. The adsorption configuration of the furan ring on the catalyst surface has been found crucial for the ring-opening reaction and to improve the efficiency of hydrogenolysis reaction, most researchers nowadays focus on tuning the support, precursor metal, and experimental conditions that could significantly impact the catalyst's performance.¹⁹⁵

1.11.1 Hydrogenolysis of furfural to pentanediol.

FF is one of the platform chemicals whose transformation leads to a wide range of important derivatives. The direct conversion of FF to 1,5-PDO and 1,2-PDO using catalysts under mild reaction conditions has become necessary in view of the importance

of these polyols in the chemical industry.¹⁹⁸ 1,2-PDO is an important intermediate in the synthesis of polyesters, a critical intermediate for the production of anti-microbicide agents, and an intermediate in the production of fungicides, as well as an ingredient in printing ink, disinfectants, and cosmetics.¹⁹⁴⁻¹⁹⁶ (1,5-PDO) is used as a monomer in the manufacture of polyester, polyurethane, and pharmaceutical intermediates. Additionally, this substance can be used as an eco-friendly solvent for the manufacture of chemicals and antifreeze.¹⁹⁷

Adkins and Connor were the first to convert 2-FFA to 1,2-PDO and 1,5-PDO in equal amounts using CuCr_2O_4 as a catalyst under high hydrogen pressure (100–150 atmospheres).¹⁹⁹ In addition to these two products, amyl alcohol, methyltetrahydrofuran and tetrahydrofurfuryl alcohol were equally observed. As a result of the wide application ranges of these diols and increasing demand for efficient catalytic processes by manufacturers, many researchers have designed and synthesised a wide variety of metal catalysts with a view to improving the activity and selectivity for these diols.²⁰⁰

By selective hydrogenation and hydrogenolysis, 1,2-PDO and 1,5-PDO can be accessed from FF. The process involves the hydrogenation of FF to 2-FFA or THFA, and then the C-O bond breaks selectively.^{194, 201} C2-O1 bond or C5-O1 bond cleaves to produce 1,5-PDO or 1,2-PDO, respectively as shown in Scheme 1.11.^{27, 202}

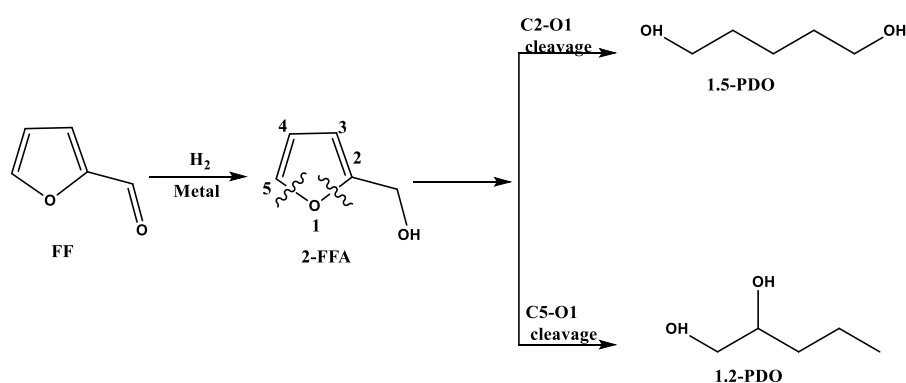
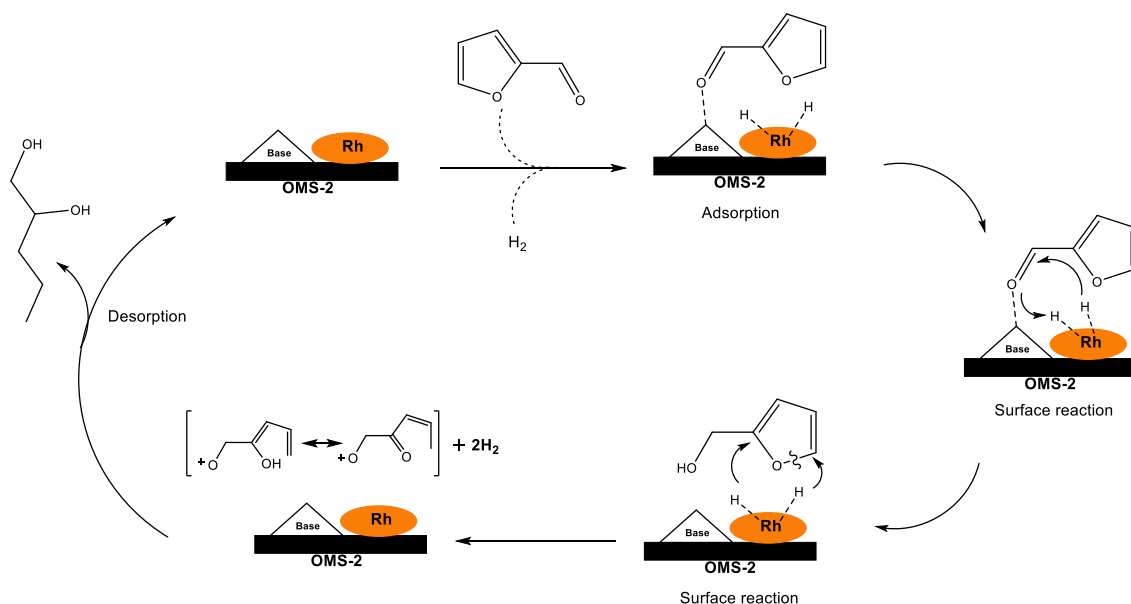


Figure 1.11: Hydrogenation and hydrogenolysis of FF to 1,2-PDO and 1,5-PDO.

1.11.1.1 The direct conversion of furfural to 1,2-pentanediol

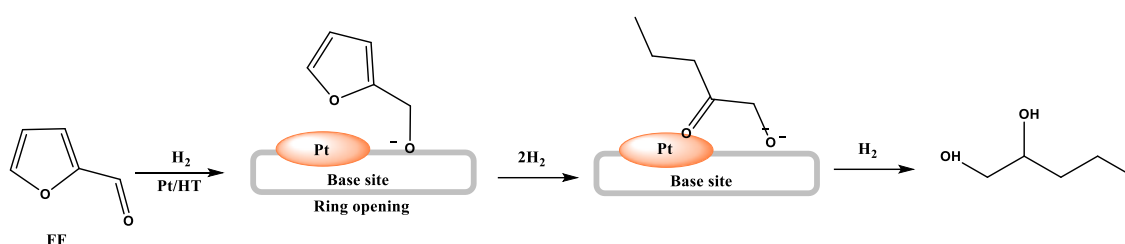
The transformation of FF to 1,2-PDO has been executed using catalysts including but not limited to Pt^{27, 203-205}, Pd²⁰⁶, Ru¹⁹⁴, and Rh.²⁰⁷ Recently, Tan and colleagues conducted

a comprehensive review of the liquid-phase catalytic conversion of FF and their derivatives to diol products.²⁰⁰ They suggested that besides engineering catalysts to become efficient, the acidity/basicity of the support plays a crucial role in selective FF ring opening reaction. For instance, Pt/HT, Pt/CeO₂, Rh/OMS-2, Pd/(MMT-K 10) present efficient selectivity for furan ring opening products, and this results have been hinged on the nature of the supports.^{196, 195, 203, 205} Specifically, Mizugaki *et al.*, reported a 73% yield for the direct transformation of FF to 1,2-PDO using Pt/HT catalyst in isopropanol at 3 MPa of hydrogen for 24 h at 150 °C.²⁰¹ Equally, Date and co-workers¹⁹⁵ suggested the acid functionality of montmorillonite clay support (MMT-K 10) played an important role in the direct conversion of FF to 1,2-PDO with 66% yield. The reaction was carried out using isopropanol as a solvent at 220 °C under 3.5 MPa of H₂ for 5 h. Furthermore, the acidity/basicity of the support influences the mechanism of ring opening of furan leading to either 1,2- or 1,5-pentanediol. Pisal and Yadav proposed a plausible reaction pathway for the conversion of FF to 1,2-PDO over Rh/OMS-2 catalyst as shown in Scheme 1.12, with emphasis on the synergy between Rh and OMS-2 support. H₂ adsorbed dissociatively over Rh while FF was weakly adsorbed via oxygen atom on the basic site. The synergy between the basic sites on the support and the evenly dispersed Rh nanoparticles leads to 1,2-PDO formation (87% yield) in the hydrogenolysis step.¹⁹⁴



Scheme 1.12: Proposed mechanism for hydrogenation of FF to 1,2-PDO over Rh/OMS-2. Adapted from Pisal and Yadav.¹⁹⁴

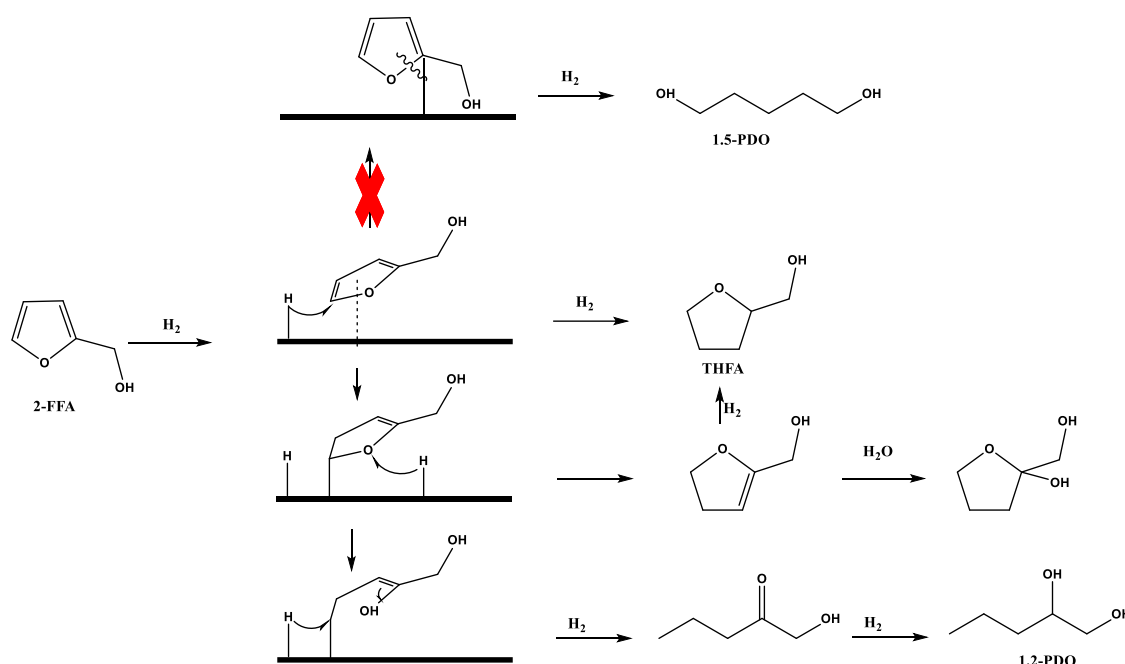
Miguzaki et al., also proposed a reaction pathway as described in Scheme 1.13 for the transformation of FF to 1,2-PDO over Pt/HT catalyst. The cycle started with the selective hydrogenation of the formyl group over the Pt metal surface and the hydrogenation of FF to 2-FFA occurred, after which the 2-FFA adsorbs in vertical adsorption mode on the basic site near the Pt metal. This led to the C5-O1 bond in the furan ring breaking to form the intermediate 1-hydroxy-2-pentanone and lastly, the C=O bond in 1-hydroxy-2-pentanone is hydrogenated to produce 1,2-PDO on the metal site.²⁰³



Scheme 1.13: Proposed mechanism for hydrogenation of FF to 1,2-PDO over Pt/HT. Adapted from Miguzaki et al.²⁰³

1.11.1.2 Indirect conversion of 2-furfuryl alcohol to 1,2- pentanediol and 1,5- pentanediol

Besides FF, 1,2-PDO and 1,5-PDO have been produced by using 2-FFA or THFA as a starting material²⁰⁸⁻²¹⁰ by selective cleavage of the C-O bond in furan ring for 2-FFA or THFA using heterogeneous catalysts.^{196, 211, 212} However, it has been found that the acid support site promoted the formation of dimers, oligomers and polymers of 2-FFA (Lewis and Bronsted acids have been reported to cause self-polymerisation of 2-FFA), which reduces the activity of the catalyst.²⁰⁸ Zhang and co-workers observed that MnO_x support in the Ru/MnO_x catalyst did not only show enhanced selectivity for 1,2-PDO, It equally suppressed the polymerization of 2-FFA during the aqueous phase hydrogenolysis/hydrogenation of 2-FFA to 1,2-PDO. The proposed mechanism for the conversion of 2-FFA to 1,2-PDO is as shown in Scheme 1.14 below and they suggested that the conversion of MnO_x to basic Mn(OH)₂ in the aqueous solution prevents 2-FFA from self-polarising.¹⁹⁴



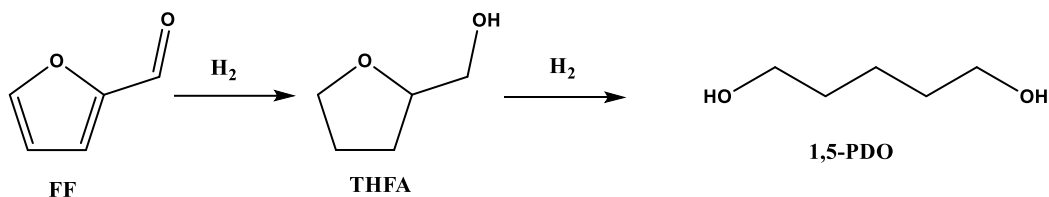
Scheme 1.14: Proposed mechanism for the transformation of 2-FFA to 1,2-PDO over Ru/MnO_x . Adapted from Zhang *et al.*¹⁹⁴

Tong and co-workers revealed the importance of crystal planes of CeO_2 support in the hydrogenolysis of 2-FFA to 1,2-PDO using Pt/CeO_2 -nanocube catalyst. It was found that the terminally exposed CeO_2 -C (100) facet, which can form surface oxygen vacancy, tunes the electronic state of surface Pt which enhanced the selectivity of 1,2-PDO relative to other crystal planes. The metal support interaction between this basic support and Pt on the surface of the Pt/CeO_2 -nanocube controlled by the surface oxygen vacancies of CeO_2 plays a crucial role in the transformation of 2-FFA to 1,2-PDO with a high selectivity (77%) at 165 °C and under 2 MPa of H_2 for 24 h.²¹³

Selective hydrogenolysis of 2-FFA to 1,2-PDO was achieved by Liu *et al.*, using 10 wt% Cu nanoparticles supported on Al_2O_3 . The catalyst was prepared by the precipitation-gel method and the interaction between the dispersed Cu particles and the acidic Al_2O_3 support is critical in the selective transformation of 2-FFA to 1,2-PDO and 1,5-PDO. The Cu/Al_2O_3 catalyst achieved 85.8% conversion with 48.1 and 22.2% selectivity towards 1,2-PDO and 1,5-PDO respectively in ethanol at 140°C, and 8 MPa of H_2 for 8 h.²¹⁴

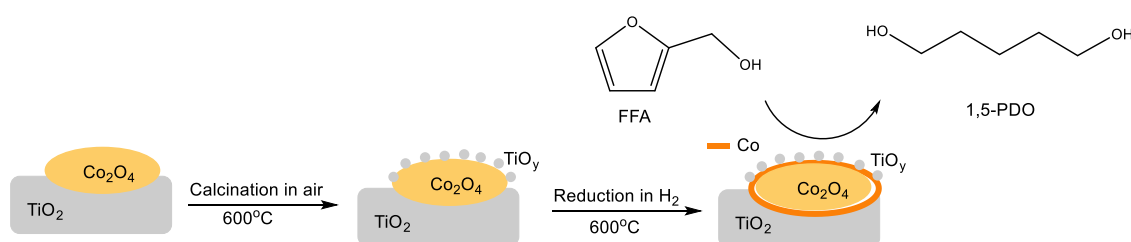
Shimazu and co-workers investigated the ring opening of 2-FFA using Ni supported on Y_2O_3 . It was found that the $Ni-Y_2O_3$ catalyst exhibited high catalyst activity in the

hydrogenolysis of 2-FFA with high selectivity towards 1,5-PDO. In particular, the Ni-Y₂O₃ with 2.5 Ni/Y mole ratio under relatively mild reaction conditions (2.0 MPa H₂, 423 K for 24 h in isopropanol) achieved full conversion of 2-FFA with 41.9% yield of 1,5-PDO. They suggested the reaction pathway proceeded through hydrogenation of the C=C bond in 2-FFA to form THFA which was converted to 1,5-PDO by selective C1-O2 bond hydrogenolysis (Scheme 1.15).²¹⁵



Scheme 1.15: Proposed reaction pathway for the transformation of 2-FFA to 1,5-PDO over Ni-Y₂O₃ by Shimazu et al.²¹⁵

Lee et al., equally observed that high-temperature calcination and reduction of Co particles supported on TiO₂ enhances the metal-support interaction and this effect improved the catalyst selectivity for C-O bond cleavage in furan ring for 2-FFA thereby converting it to 1,5-PDO with 30.3% selectivity at 140°C under 2.34 MPa of H₂ (Scheme 1.16).²⁰⁹

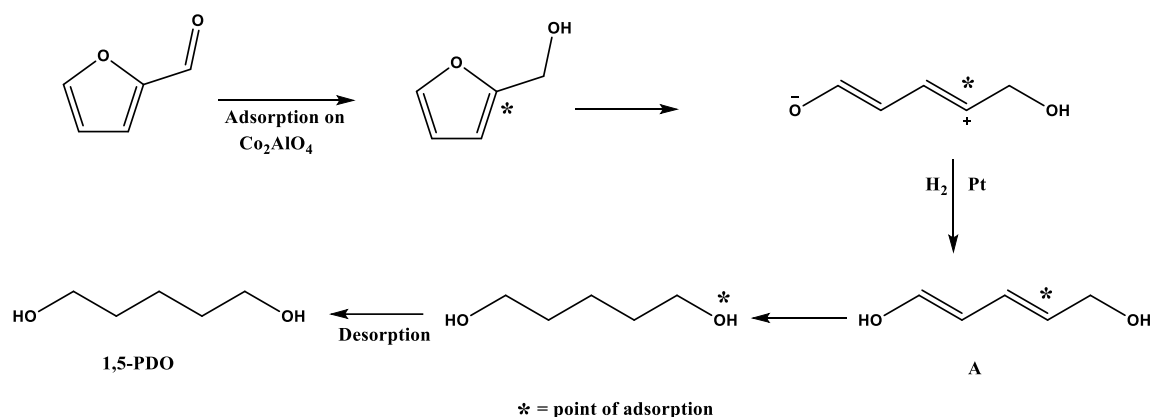


Scheme 1.16: Effect of high-temperature calcination and reduction on Co/TiO₂ for the transformation of 2-FFA to 1,5-PDO. Adapted from Lee et al.²⁰⁹

Furthermore, Sulmonetti and co-workers reported the transformation of 2-FFA to 1,5-PDO on a mixed metal oxide 0.25Cu-2.75Co-Al. This well dispersed mixed metal oxides containing both metal oxides and metallic species exhibited 98.8% activity and 41.6% selectivity towards 1,5-PDO in ethanol at 160°C under 4 MPa of H₂.²¹⁰

1.11.3 Direct conversion of furfural to 1,5- pentanediol

Alternatively, 1,5-PDO could be produced by the one-pot reaction from FF in contrast to the indirect method of preparation described in the last section. 1,5-PDO, just like 1,2-PDO can be produced directly from FF using both noble and non-noble metals on a wide variety of supports. Noble metals such as Pt¹⁹⁸, Pd²⁰⁶, Ir, Rh-Ir²¹⁶ and non-noble metals such as Cu²¹⁷, Co²¹⁸, Ni, Ni-Pd¹¹⁶ have been used, albeit, some non-noble metals (Ni and Co) have been reported with relatively lower selectivity towards 1,5-PDO.^{219, 220} Yeh and co-workers reported an effective and selective transformation of FF to 1,5-PDO over MOF-derived supported Pt on Al₂O₃ in H₂O at 45°C for 8 h with NaBH₄ as reductant. Their strategy involves the use of mild reaction conditions and the catalyst achieved >99% FF conversion and 75.2% selectivity for 1,5-PDO.²²¹ Xu et al., investigated Pt/Co₂AlO₃ bimetallic for the direct conversion of FF to 1,5-PDO. The catalyst exhibits 100% conversion of FF and 27% selectivity to 1,5-PDO at 140°C under 1.5 MPa H₂ for 24 h. In this mechanism, FF was adsorbed through the C=C bond on Co₂AlO₄ and this facilitated the hydrogenation of C=O to form 2-FFA by the Pt. Cleavage of the C-O bond by CoO_x (Co³⁺ ions, especially) leads to intermediate A, which was later reduced by Pt to 1,5-PDO as depicted in Scheme 1.17 below.¹⁹⁸



Scheme 1.17: A proposed catalytic mechanism for the direct conversion of FF to 1,5-PDO over Pt/Co₂AlO₄ catalyst.¹⁹⁸

Kurniawan and co-workers investigated the direct conversion of FF over a Ni-Co-Al trimetallic catalyst in ethanol at 160°C at an initial H₂ pressure of 3 MPa. The catalyst achieved 100% conversion with 47.5% selectivity 1,5-PDO.²²²

The direct conversion of FF to 1,5-PDO over heterogeneous catalysts looks promising, however, this process is plagued with various issues that need to be addressed. Selectivity of 1,5-PDO needs to be improved to reduce the cost of separation via techniques that are energy intensive and time consuming. Research efforts on the use of non-noble metals and relatively mild reaction conditions should be intensified to stem the reliance of this process on noble metals that are highly expensive in order to bring down the production cost via this reaction route. Table 1.6 presented some of the direct conversion of FF to 1,5-PDO/ 1,2-PDO over heterogeneous catalysts and some optimum reaction conditions.

Table 1.6 The direct conversion of FF to 1,5-PDO/ 1,2-PDO over heterogeneous catalyst.

Entry	Catalyst	Reaction conditions					Conv. (%)	Main product/ Selectivity	Yield (%)	Ref.
		Furfural/ catalyst (g/g)	Solvent	Temp. (°C)	H ₂ pres. (MPa)	Time (h)				
75	3%Pd/MMT-K	2.5 g/ 0.25 g	2-PrOH	220 3c	500 psig	5	99	1.2-PDO/66	-	223
76	Pd–Ir–ReO _x /SiO ₂ 2 steps reaction	1g/0.1g	H ₂ O	40 then 100	6 then 8	8 then72		1,5- PDO	71.4%	206
77	Pt(IV)oxide	-	Acetic acid	-	0.14-0.41	-	-	1.2- PDO	100	224
78	Pt/Co ₂ AlO ₄	0.4g/0.2 g	10ml ethanol	140	1.5	24	-	1,5- PDO	35	198

79	1.9 Pt/HT	1 mmol/ metal: 1 mol %	L k	150	3	8	>99	1.2- PDO	73	201
80	Pt/MgO	1 mmol/ metal: 1 mol %	2-PrOH	150	3	8	>99	1.2- PDO	68	201
81	Pt/CeO ₂	1 mmol/ metal: 1 mol %	2-PrOH	150	3	8	>99	1.2- PDO	41	201
82	Pt/CeO ₂	1 mmol/ 0.1 g	2-PrOH	165	3	4	>99	1.2- PDO	54	205
83	Pt/MgO	1 mmol/ 0.1 g	2-PrOH	165	3	4	>99	1.2- PDO	35	205
84	Ni-Y ₂ O ₃			150	2	24	-	1,5- PDO	41.9	215
85	Pt/ MgO	HMF 0.2 mmol/10 mg	H ₂ O	135	3	24	-	1,2,6-HTO	14	42

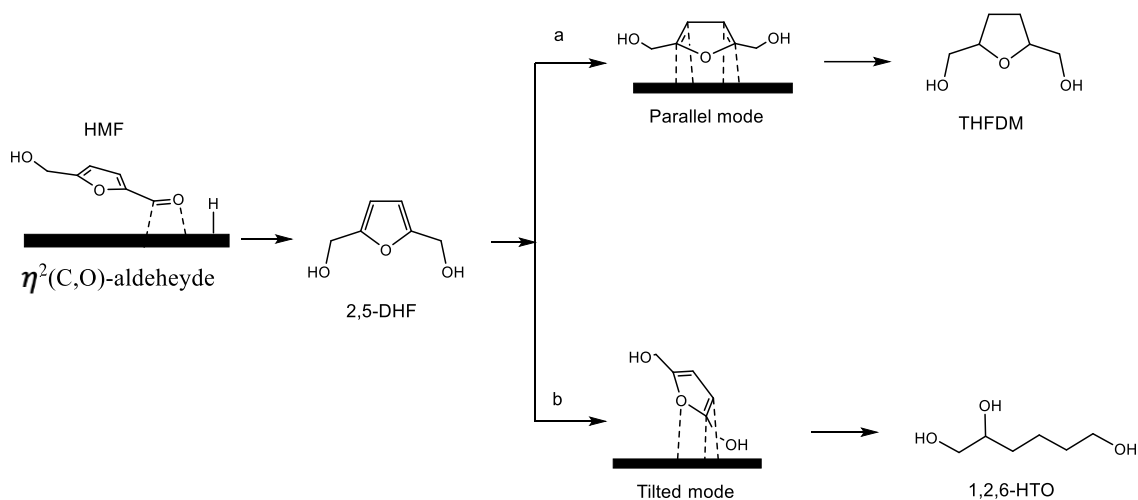
86	Pt/ CeO ₂	HMF 0.2 mmol/10 mg	H ₂ O	135	3	24	-	1,2,6-HTO	27	42
87	Pt/HT	HMF 0.2 mmol/10 mg	H ₂ O	135	3	24	-	1,2,6-HTO	32	42
88	Pt/Al ₂ O ₃	furfural 1 g/catalyst 0.05 g	2-PrOH	240	5 bar N ₂	2	44	1,2-PDO	15	27

1.11.4 Hydrolysis of hydroxymethylfurfural

HMF can be further catalytically transformed into many derivatives of ring-opening products, such as 1,6-hexanediol,²²⁵ 1,2,6-Hexanetriol²²⁶, adipic acid,^{227, 228} 1-hydroxyhexane-2,5-dione,²²⁸ levulinic acid,²²⁹ 1-hydroxy hexane dione,²³⁰ and methyl levulnate.²³¹ All these derivatives can be obtained by hydrogenation/hydrolytic ring opening reactions using various heterogeneous or homogeneous catalysts. The development of hydrogenation or hydrogenolysis of HMF has attracted a lot of interest over the past few years due to its potential applications in a variety of industrial applications.²³² One of the target objectives of this research is to test the effect of a few supports on the ring opening of HMF to 1,6-HDO.

1.11.4.1 Hydroxymethylfurfural hydrogenation to produce 1,2,6-hexanetriol

1,2,6-hexanetriol (1,2,6-HTO) is a versatile platform chemical, used in a variety of chemical applications, including resins, plastics, pharmaceuticals, and cosmetics.²³³⁻²³⁵ 1,2,6-HTO is a humectant, a solvent, a viscosity control agent, and a precursor to hexanediol derivatives.^{234, 235} Typically, it is formed through the dimerization of oil-based acrolein, followed by hydrolysis and hydrogenation.²³⁶ Therefore, one possible way to resolve this problem would be to use the direct conversion of bio-based renewable feedstocks into 1,2,6-HTO which is more sustainable.²²⁶ The mechanism of opening the ring of HMF to 1,2,6-HTO has been proposed and it starts with the hydrogenation of the aldehyde group to produce 2,5-DHF. This is followed by the adsorption of 2,5-DHF on the catalyst surface, which could be in two different modes: parallel (a) and tilted (b). The parallel mode leads to full hydrogenation to produce THFDM, while in tilted mode, the C-O bond is broken, resulting in the production of 1,2,6-HT (Scheme 1.18).^{148, 226, 237}



Scheme 1.18: Proposed mechanism of HMF hydrogenation to 1,2,6-HTO. Adapted from Yao *et. al.*²²⁶

Kataoka and co-workers investigated the effect of acid-base properties of different supports over Pt-supported catalysts in the one-pot conversion of HMF to 1,2,6-HTO. They observed that basic supports such as Pt/HT, Pt/MgO, and Pt/CeO₂, and the adsorption mode of the substrate on the catalyst surface are important for the direct conversion of HMF to 1,2,6-HTO. Pt/HT achieved 32% yield of 1,2,6-HTO, while Co promoted Pt/CeO₂ achieved a maximum yield of 42% 1,2,6-HTO in H₂O at 135°C under 3 MPa of H₂. The activity and selectivity of these catalysts were rationalized to be due to the acid-basic properties of the supports and the adsorption mode of the substrate on the catalyst surface.⁴²

In addition, Yao *et al.*, highlighted the important role of the synergetic effect between Ni and Co nanoparticles in the transformation of HMF to 1,2,6-HTO over Ni-Co-Al mixed oxide catalyst in methanol at 120°C under 4 MPa of H₂ for 4 h. 1,2,6-HTO was obtained in 64.5% yield over Ni-Co-Al catalyst and the reaction pathway was suggested to start with the hydrogenation of the aldehyde group in HMF to form 2,5-DHF. Subsequent hydrogenolysis of 2,5-DHF on the catalyst yields 1,2,6-HTO.²²⁶

Buntara and co-workers published a seminal work on the conversion of biomass-derived THF-dimethanol to 1,2,6-HTO over Rh-ReO_x/SiO₂ catalyst in H₂O at 80°C under 8 MPa of H₂ for 20 h. This catalyst achieved 11% conversion of THF-dimethanol with 29% selectivity for 1,2,6-HTO.²³⁸ 1.7 highlights a few examples of HMF hydrogenation to produce 1,2,6-HTO with the optimise reaction conditions

Table 1.7 HMF hydrogenation to produce 1,2,6-Hexanetriol

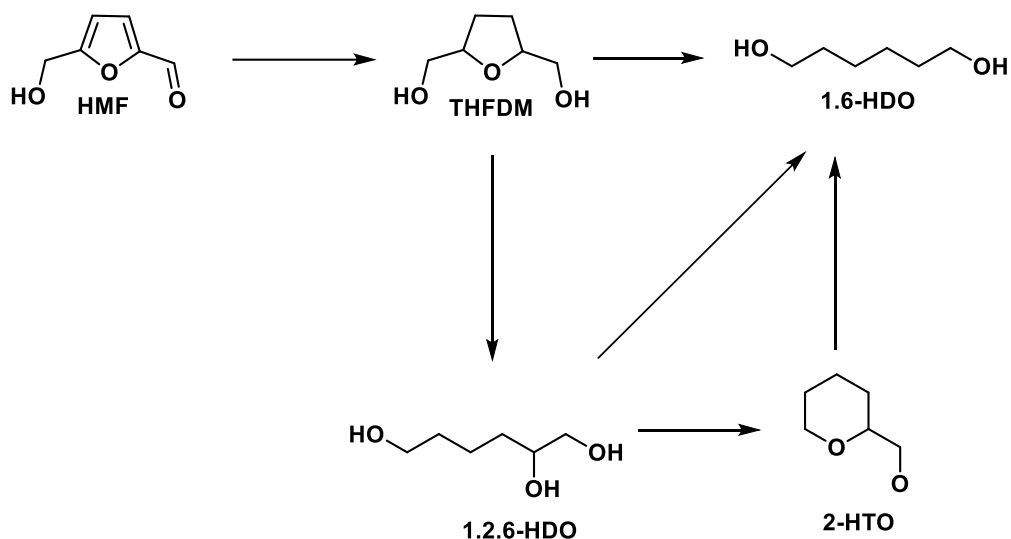
Entry	Catalyst	Reaction conditions					Main product/ Selectivity	Yield (%)	Ref
		Furfural/catalyst (g/g)	Solvent	Temp. (°C)	H ₂ pres. (MPa)	Time (h)			
89	0.5Ni _{2.5} CoAl	1 g/0.2 g	MeOH	120	4	4	1,2,6-HTO	64.5	226
90	Pt ₅ Co ₅ /CeO ₂	0.2 ml/10mg	H ₂ O	135	3	24	1,2,6-HTO/DHTHF	42/41	42

1.11.4.2 Hydroxymethylfurfural hydrogenation to produce 1,6-hexandiol

1,6-hexanediol (1,6-HDO) is another essential monomer used in the formation of polyesters, polyurethane resins, adhesives, and plasticizers.²³⁹ As a result of the growing demand for polyurethane, 1,6-hexanediol (1,6-HDO) market has experienced rapid growth.²⁴⁰ Currently, 1,6-HDO is produced industrially by hydrogenation of adipic acid (AA) or dimethyl adipate using a homogeneous Cu-based catalyst under 25 to 30 MPa of H₂ pressure at 300°C.²⁴¹⁻²⁴³ However, there are several disadvantages to this process, including low 1,6-HDO yield due to the numerous reaction steps required. Additionally, the homogeneous catalyst is difficult to separate from the product mixture. Furthermore, there are significant greenhouse gas emissions resulting from the use of nonrenewable petroleum resources.²⁴⁴ Therefore, using cellulose-derived molecules for the production of 1,6-HDO is highly desirable and has been studied significantly by academic and industrial researchers.

Marcel Faber in 1981 prepared 1,6-HDO from biomass in three steps.²⁴⁵ The First process is depolymerization of biomass using an acid catalyst which leads to the production of HMF. The HMF is subsequently hydrogenated using Raney-Nickel catalyst to 5-tetrahydrofuran diol (THFD), and lastly, hydrogenation of THFD with copper chromite catalyst to give 1,6-HDO. Nonetheless, the formation of humin results in a decrease in HMF yield.^{246, 247}

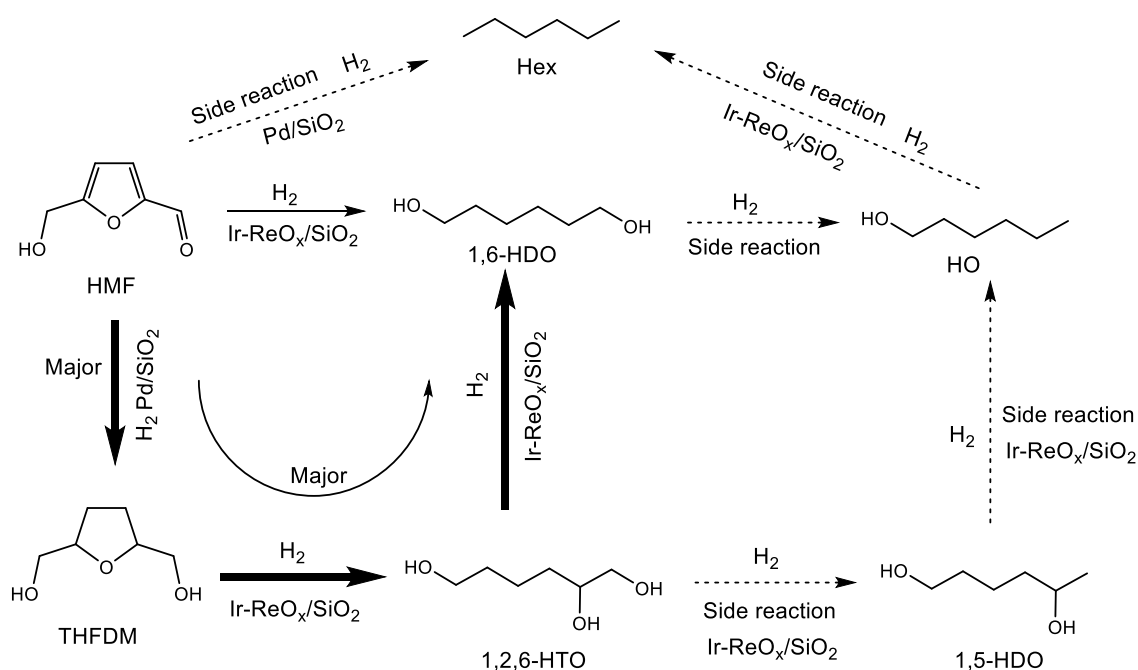
1,6-HDO can be synthesized from HMF directly or via intermediates such as THFD and 1,2,6-HDO via two different routes as depicted in Scheme 1.19. It is equally worth noting that 1,6-HDO can be obtained from 1,2,6-HDO via two different routes.²⁴⁸



Scheme 1.19: Preparation of 1,6-HDO via different reaction pathways. Adapted from Buntara et. al.²⁴⁸

The direct conversion of HMF to 1,6-HDO through one step hydrogenation /or hydrogenolysis is a difficult reaction that often results in low yield and the 1,6-HDO selectivity is sensitive to the nature of support, metals, and reaction conditions. The direct conversion of HMF to 1,6-HDO is fully reviewed in Chapter 5.

Xiao et al reported the transformation of HMF to 1,6-HDO in 58% yield over a double-layered catalyst, Pd/SiO₂ and Ir-ReO_x/SiO₂ in a fixed bed reactor in a mixed solvent (H₂O/THF) at 100°C under 7 MPa H₂. This reaction proceeded via two intermediates, THFDM and 1,2,6-HTO. THFDM is formed by hydrogenation of HMF by Pd/SiO₂ and 1,2,6-HTO is obtained by hydrogenolysis of THFDM using Ir-ReO_x/SiO₂. Hydrogenolysis of 1,2,6-HTO with Ir-ReO_x/SiO₂ leads to the desired 1,6-HDO (Scheme 1.20). The yield of 1,6-HDO improves by gradual replacement of THF solvent with water as a solvent for the reaction with a resultant decrease in the yield of THFDM. The presence of water in increasing amounts led to a decrease in the yield of 1,6-HDO due to the formation of hexanol during hydrogenolysis.²⁴⁹



Scheme 1.20: Reaction pathways of HMF conversion to 1,6-HDO. Adapted from Xiao et al.²⁴⁹

The indirect conversion of HMF derivatives to 1,6-HDO has been described by many researchers. He and Co-workers used THFDM as a start material to produce 1,6-HDO in 70% yield over a Pt-WO_x/TiO₂ catalyst. The reaction proceeded via ring opening of THFDM to form 1,2,6-HTO and this intermediate subsequently underwent hydrogenolysis to give 1,6-HDO with high selectivity. According to their findings, hydrogen spilt over from Pt sites to WO_x/TiO₂, leading to the reduction of the W=O function to form Brønsted acid sites, and the synergistic effect between Pt and the acid sites in the catalyst influenced the selectivity of 1,6-HDO.²⁴⁴ Recently, an assessment of various noble metals supported on WO_x/TiO₂, including Pt, Rh, Pd, and Ru, was conducted in order to study their effectiveness in promoting the formation of 1,6-HDO. The results of the research showed that noble metals had a notable impact on the production of 1,6-HDO, with the highest yield being achieved while using Pt-WO_x/TiO₂ and Rh-WO_x/TiO₂ catalysts. These catalysts have an especially high rate of hydrogenolysis of THFDM leading to 1,6-HDO in high yield. In particular, Pt and Rh are able to reduce W⁶⁺ more effectively than active W⁵⁺, but, these catalysts were deactivated due to the leaching of W.²⁵⁰

Buntara *et al*²³⁵ reported the hydrodeoxygenation of 1,2,6-HTO to 1,6-HDO using Rh-ReO_x/SiO₂ catalyst at 180°C under 8 MPa of H₂ for 20 h in water, leading to full conversion of 1,2,6-HTO with 73% selectivity to 1,6-HDO. Furthermore, the ring opening of tetrahydropyran-2-methanol (2-THPM) leads to 1,6-HDO with 96% selectivity at 26% conversion by Rh-ReO_x/SiO₂ catalyst at 120°C, 80 bar of H₂ for 20 h, ReO_x-promoted Rh/C catalyst has been shown to have good selectivity for C-O cleavage for a broad range of cyclic ethers and polyols.^{207, 251}

1.11.4.3 Hydroxymethylfurfural hydrogenation to produce 1-hydroxy-2,5-hexanedione

1-hydroxy-2,5-hexanedione (HHD) is another hydrogenation/hydrogenolysis derivative of HMF. Nowadays, diketone derivatives are produced from platform chemicals such as HMF²³² and many researchers have investigated the production of HHD using acidic supports which has been found to favour ring-opening reactions.²⁵² In 1991, Descotes and co-workers were the first to report the hydrogenation of HMF into HHD over a Pt/C catalyst in aqueous oxalic acid.²⁵³ Consequently, hydrogenation of HMF to HHD has been achieved using Pd, Pt, and Au metals on different supports. For instance, hydrogenation and hydrolysis of HMF yielded HHD with 28% selectivity over Pd/C catalyst in propanol. HHD resulting from acid-catalysed ring opening of HMF followed by hydrogenation.²⁵⁴ de Vries *et al*²⁴⁸ achieved the full conversion of HMF over bimetallic catalysts Rh-Re/SiO₂ for the production of HHD with 81% selectivity and 6% selectivity for 1,6-HDO as a side product. Ohyama *et al.*, in 2012 reported the hydrogenation of HMF using gold supported on Al₂O₃ without hydrogenolysis of the furan ring, which resulted in excellent transformation to 2,5-bis(hydroxymethyl)furan (BHF) in 96% yield.²⁵⁵ The same research group in 2014 reported the efficient catalytic performance of gold nanoparticles supported on acidic metal oxides (TiO₂, ZrO₂, Ta₂O₅, TiO₂-SiO₂ (TS), and sulfated zirconia (SZ)) for the conversion of HMF to cyclopentanone derivatives via ring rearrangement. HMF was hydrogenated to HHD and several furan products, including 3-hydroxymethyl cyclopentanone (HCPN) and 4-hydroxy-4-hydroxymethyl-2-cyclopentenone (HCPEN), over an Au/Nb₂O₅ catalyst in the presence of 8.5 mM H₃PO₄ with a yield of HHD 60%.²⁵² The ring opening of HMF has been achieved with full conversion to produce HHD with 77% yield via a combination of Pd/C and Amberlyst-15 (an acid catalyst) in a single

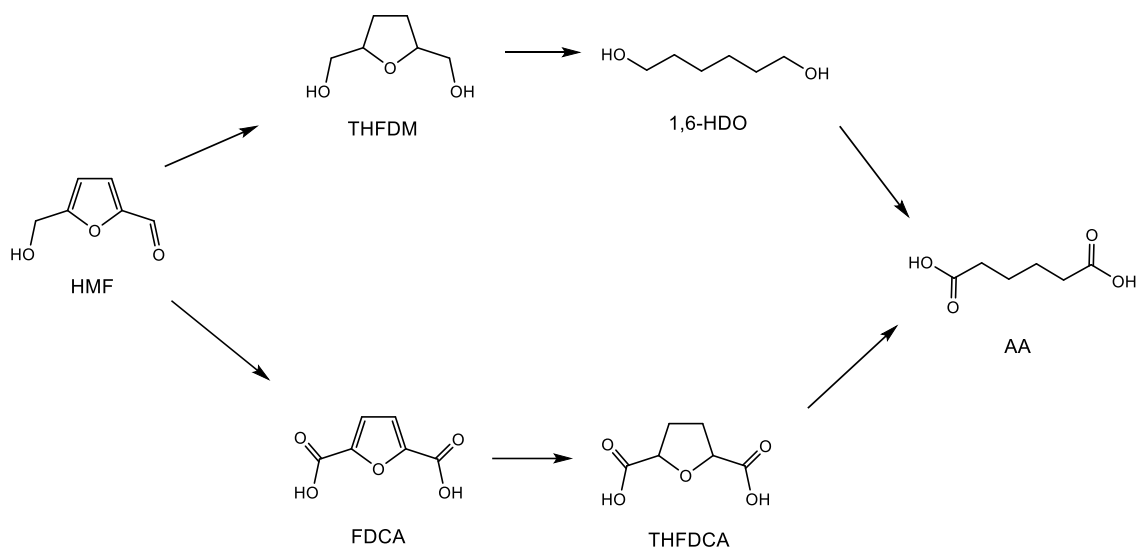
reactor at 80 °C under 50 bar of H₂.¹⁹² Moreover, HMF has been hydrogenated to HHD (yield, >77%) over 7.5 wt% of Pd/C under 3 MPa of H₂ and 1 MPa of CO₂ (the ratio was 3 in the CO₂/H₂ system) in the presence of water as solvent. Water and carbon dioxide were important in generating carbonic acid that facilitated the ring opening of BMF formed from the hydrogenation HMF.²³² Yang *et al.*, reported the production of HHD with 85% selectivity by the hydrogenation of HMF using a Pd/Nb₂O₅ catalyst in water. They confirmed that the acid site is important for HHD production by testing Pd/C in the presence of an acidic or basic state.²⁵⁶

Furthermore, Xu and co-workers²⁵⁷ reported the catalytic hydrogenation of HMF to HHD with a 36.8% yield by MOF-derived bimetallic nickel–copper catalyst at 140°C, under 2.0 MPa H₂ in water/ethanol for 5 h. The hydrogenation of HMF, in the presence of Lewis acid oxides combined with Ni-Cu/C produced HHD in good yield and the combination of solvents is necessary for the ring-opening product. The production of HHD requires an acid site for the opening of the furan ring, however, when excessive acidity and higher temperatures are present, humins will be generated leading to cross-polymerization between the reactants and intermediates.²⁵⁸ Also, polymers derived from humin and other products that are excessively dehydrated may cause a low carbon balance.²⁵⁸⁻²⁶⁰

1.11.4.4 Hydroxymethylfurfural hydrogenation to produce adipic acid

adipic acid (AA) is another compound which can be generated directly from the hydrogenation of HMF. AA is predominantly used in the formation of Nylon-6,6 and polyurethanes.²⁶¹ Currently, AA is prepared by the oxidation of a mixture of cyclohexanol and cyclohexanone in the presence of a large excess from nitric acid with Cu(II) and ammonium metavanadate catalyst.²⁶² In 1983, Wilson's group²⁶³ prepared AA from biomass by hydrolysed biomass in a dilute acid medium to produce HMF which is subsequently hydrogenated via Raney Nickel (RaNi) catalyst under hydrogen gas at 100-200°C to form THFDM. Hydrogenolysis of THFDM Under H₂ pressure (1,000 psi) at 200 to about 350°C gave 1,6-HDO which was bio-oxidised in the presence of a microorganism such as *Gluconobacter oxydans* subspecies, to produce AA.

The formation of AA from HMF is provided by two pathways. The first way is HMF hydrogenation to open the furan ring to form 1,6-HDO which is oxidation to production AA. The second way is the oxidation of HMF to 2,5-furan dicarboxylic acid (FDCA), then hydrogenolysis and ring opening of FDCA to AA (Scheme 1.21).²⁶⁴



Scheme 1.21: Reaction pathways of AA from HMF. Adapted from Gilkey et. al.²⁶⁴

Boussie and co-workers synthesised AA in a two-step reaction involving hydrogenation using Pd on a silica catalyst. The reaction starts with the hydrogenation of 2,5-furandicarboxylic acid FDCA to THFDM in 88% yield at 140 °C for 3 h in acetic acid under high pressure of H₂ (750 psi). In a subsequent step, THFDM is hydrogenated in acetic acid under hydrogen at 160 °C for 3 h to form AA in 99% yield via 5% Pd on silica catalyst in the presence of 0.3 M of HI.²⁶⁵

1.12 Why platinum metal was selected

The design of catalysts to improve C-OH bond cleavage using noble metals with metal oxide support has become a prominent strategy for preparing an efficient catalyst due to the high capacity of hydrogen dissociation with noble metals. Also, the creation of oxygen vacancies catalyzes the dehydration of hydroxyl groups in noble metal catalysts.^{56, 266, 267} However, catalysts based on Pt as the active site has high hydrogenation activity for

carbonyl group and ring opening of the furan ring under moderate reaction conditions compared to other metal supported catalysts such as Pd, Cu, Ni.^{68, 91-95, 117, 268, 269} Platinum is a precious metal with high cost implication, its strong interaction with varying support and ability to facilitate hydrogen spillover over metal oxide support has a significant effect on the catalyst's activity.^{156, 180} Moreover it was found that 2-FFA selectivity increased under low hydrogen pressure, and consequently, non-noble metals like Cu which was found to be more selective for methyl furan, albeit, with a higher Cu loading (and got deactivated over time) has become a good alternative.^{161, 269-274} On the other hand, Pd-based catalysts are more selective towards C=C hydrogenation in the furan ring to form THFA, and poor selectivity for the hydrogenation of carbonyl group especially under low temperature and pressure.^{115, 275} Relatively, Ni-based catalysts are found to be less active than Pd for hydrogenation of FF, but, are more selective for the hydrogenation of FF to 2-FFA. However, at high temperatures, decarboxylation product to produce furan results over Ni-based catalysts.^{129, 269}

1.13 Aim and objective of this thesis

The objectives of this thesis are the selective hydrogenation of furfural to furfural alcohol and the ring opening of the furan ring in the HMF compound via the tuning of catalytic sites. This could be achieved by investigating the role of the supports and the heat treatment on the catalytic activity for selective hydrogenation.

The catalysts were characterised to determine their physical and chemical properties using such techniques as XPS, TEM, CO chemistry, inductively coupled plasma emission spectroscopy (ICP), and TPR.

Chapter 3 focuses on the development of a catalytic for the production of furfural alcohol with high selectivity via investigating the effect of heat treatment protocols on the catalysts. The effect of different supports. The catalyst underwent different heat treatment protocols for the production of furfural alcohol. Moreover, the utilisation of different loads of the metal to produce furfural alcohol. Consequently, the characterization of each catalyst is also explained.

Chapter 4 focuses on investigating the effect of a bimetallic catalyst and investigate their synergistic effect for the FF hydrogenation into 2-FFA. The activity of the Pt monometallic

catalytic will be evaluated against the PtRu bimetallic catalyst supported on TiO₂. The characterizations of bimetallic catalysts are also considered.

The objectives of **Chapter 5** are to investigate the ring opening of HMF using different supports. Also, study the effect of combining two metals for on the ring opening reaction. This chapter also highlights the optimum reaction conditions for the ring opening of HMF over a PtRu catalyst supported by HAP. The characterization of PtRu supported by HAP is elucidated. A reaction pathway is suggested.

Chapter 6 presents a summary of the results of the catalytic study on the hydrogenation of FF and the ring opening of HMF into 2-FFA and 1,6-HDO, respectively. Moreover, the characteristics of the catalysts

1.14 Reference

1. M. A. Rubio Rodríguez, J. D. Ruyck, P. R. Díaz, V. K. Verma and S. Bram, *Appl. Energy*, 2011, **88**, 630-635.
2. B. Wozniak, S. Tin and J. G. de Vries, *Chem Sci*, 2019, **10**, 6024-6034.
3. S. Sadula, O. Oesterling, A. Nardone, B. Dinkelacker and B. Saha, *Green Chem.*, 2017, **19**, 3888-3898.
4. R. A. Sheldon, *ACS Sustain. Chem. Eng.*, 2017, **6**, 32-48.
5. M. Balat, *Energy Sources, Part B: Economics, Planning, and Policy*, 2007, **2**, 167-181.
6. D. M. Alonso, J. Q. Bond and J. A. Dumesic, *Green Chem.*, 2010, **12**, 1493-1513.
7. G. Ertl, H. Knözinger and F. Schüth, *andbook of Heterogeneous Catalysis*, Wiley-VCH Verlag GmbH, 2008.
8. P. Ibarra-Gonzalez and B.-G. Rong, *Chin. J. Chem. Eng.*, 2019, **27**, 1523-1535.
9. S. Behera, R. Arora, N. Nandhagopal and S. Kumar, *Renew. Sust. Energ. Rev.*, 2014, **36**, 91-106.
10. J. N. Chheda, G. W. Huber and J. A. Dumesic, *Angew. Chem. Int. Ed. Engl.*, 2007, **46**, 7164-7183.
11. S. Chen, R. Wojcieszak, F. Dumeignil, E. Marceau and S. Royer, *Chem Rev*, 2018, **118**, 11023-11117.
12. R. Sindhu, P. Binod and A. Pandey, *Bioresour Technol*, 2016, **199**, 76-82.
13. J. Zakzeski, P. C. A. Bruijninx, A. L. Jongerius and B. M. Weckhuysen, *Chem. Rev.*, 2010, **110** 3552–3599.
14. W. Schutyser, T. Renders, S. Van den Bosch, S. F. Koelewijn, G. T. Beckham and B. F. Sels, *Chem Soc Rev*, 2018, **47**, 852-908.
15. Y. Geng and H. Li, *ChemSusChem*, 2022, **15**, e202102495.
16. S. Panthapulakkal, L. Raghunanan, M. Sain, B. Kc and J. Tjong, in *Green Composites*, 2017, DOI: 10.1016/b978-0-08-100783-9.00003-4, pp. 39-72.

17. M. T. A. Li Shuai, Ydna M. Questell-Santiago, Florent Héroguel, Yanding Li, Hoon Kim, Richard Meilan, Clint Chapple, John Ralph,^{2,3,4} Jeremy S. Luterbacher, *Science China Chemistry* 2016, **354**, 329–333
18. A. Yousuf, D. Pirozzi and F. Sannino, in *Lignocellulosic Biomass to Liquid Biofuels*, 2020, pp. 1-15.
19. X. Zhang, K. Wilson and A. F. Lee, *Chem Rev*, 2016, **116**, 12328-12368.
20. W. Fang and A. Riisager, *Green Chem.*, 2021, **23**, 670-688.
21. K. Gupta, R. K. Rai and S. K. Singh, *ChemCatChem*, 2018, **10**, 2326-2349.
22. Q. Fu, H. Jiang, Y. Wang, H. Wang and X. Zhao, *Mater. Chem. Front.*, 2023, 628-642.
23. X. Li, P. Jia and T. Wang, *ACS Catal.*, 2016, **6**, 7621-7640.
24. W. Zhao, F. Wang, K. Zhao, X. Liu, X. Zhu, L. Yan, Y. Yin, Q. Xu and D. Yin, *Carbon Resour. Convers.*, 2023, **6**, 116-131.
25. A. Bohre, S. Dutta, B. Saha and M. M. Abu-Omar, *ACS Sustain. Chem. Eng.*, 2015, **3**, 1263-1277.
26. A. E. Eseyin and P. H. Steele, *Int. J. Adv. Chem.*, 2015, **3**, 42-47.
27. S. Bhogeswararao and D. Srinivas, *J. Catal.*, 2015, **327**, 65-77.
28. J. G. de Vries, *Curr. Opin. Green Sustain. Chem.*, 2023, **39**, 100715.
29. J. P. Lange, E. van der Heide, J. van Buijtenen and R. Price, *ChemSusChem*, 2012, **5**, 150-166.
30. S. Nishimura and K. Ebitani, in *Green Chemical Processing and Synthesis*, 2017, ch. Chapter 3.
31. E. Cousin, K. Namhaed, Y. Peres, P. Cognet, M. Delmas, H. Hermansyah, M. Gozan, P. A. Alaba and M. K. Aroua, *Sci Total Environ*, 2022, **847**, 157599.
32. F. Menegazzo, E. Ghedini and M. Signoretto, *Molecules*, 2018, **23**, 2201.
33. Y. Nie, Q. Hou, W. Li, C. Bai, X. Bai and M. Ju, *Molecules*, 2019, **24**, 594.
34. B. I. G. Ofrasio, M. D. G. de Luna, Y.-C. Chen, R. R. M. Abarca, C.-D. Dong and K.-L. Chang, *Bioresour. Technol. Rep.*, 2020, **11**, 100515.

35. G. Xu, Z. Tu, X. Hu, M. Li, X. Zhang and Y. Wu, *Fuel*, 2023, **339**, 127334.
36. J. Nowicki and N. Stanek, *Biomass and Bioenergy*, 2021, **154**, 106252.
37. Z. Xu, G. Zhang and K. Wang, *Catal. Commun.*, 2023, **175**, 106608.
38. W. Wang, H. Zhou, Q. Guan, L. Shen, L. He, R. Miao, X. Xu and M. Wang, *Fuel*, 2023, **333**, 126389.
39. C. B. T. L. Lee and T. Y. Wu, *Renew. Sust. Energ. Rev.*, 2021, **137**, 110172.
40. G. Marcotullio and W. de Jong, *Carbohydr. Res.*, 2011, **346**, 1291-1293.
41. M. R. Nimlos, X. Qian, M. Davis, M. E. Himmel and D. K. Johnson, *The Journal of Physical Chemistry A*, 2006, **110**, 11824-11838.
42. H. Kataoka, D. Kosuge, K. Ogura, J. Ohyama and A. Satsuma, *Catal. Today*, 2020, **352**, 60-65.
43. Z. F. Hu Li , Richard L. Smith Jr. , Song Yang, *Prog. Energ. Combust*, 2016, **55**, 98–194.
44. M. J. A. Jr., W. S. L. Mok and G. N. Richards, *Carbohydr. Res.*, 1990. , **199** 91-109.
45. B. F. M. Kuster, *Starch - Stärke*, 1990, **42**, 314-321.
46. M. J. Antal, Jr., W. S. L. Mok and G. N. Richards, *Carbohydr. Res.*, 1990, **199**, 91-109.
47. H. E. v. Dam, A. P. G. Kieboom and H. v. Bekkum, *starch - Stärke*, 1986 **38**, 95-101.
48. M. J. Gilkey and B. Xu, *ACS Catal.*, 2016, **6**, 1420-1436.
49. A. M. Ruppert, K. Weinberg and R. Palkovits, *Angew. Chem. Int. Ed. Engl.*, 2012, **51**, 2564-2601.
50. M. Sankar, N. Dimitratos, P. J. Miedziak, P. P. Wells, C. J. Kiely and G. J. Hutchings, *Chem Soc Rev*, 2012, **41**, 8099-8139.
51. H. He, A. Dasgupta, R. M. Rioux, R. J. Meyer and M. J. Janik, *J. Phys. Chem. C*, 2018, **123**, 8370-8378.
52. Y. Nakagawa, M. Tamura and K. Tomishige, *ACS Catal.*, 2013, **3**, 2655-2668.

53. Q. Hou, X. Qi, M. Zhen, H. Qian, Y. Nie, C. Bai, S. Zhang, X. Bai and M. Ju, *Green Chem.*, 2021, **23**, 119-231.
54. G. Millán, G. Sixta and Herbert, *Catalysts*, 2020, **10**, 1101.
55. U. K. Singh and M. A. Vannice, *Appl. Catal. A: Gen.*, 2001, **213** 1–24.
56. Z. Huang, J. Wang, J. Lei, W. Zhao, H. Chen, Y. Yang, Q. Xu and X. Liu, *Front Chem*, 2022, **10**, 925603.
57. H. S. Fogler, *Elements of chemical reaction engineering*, Prentice-Hall., 1992.
58. K. Cavell, S. Golunski and D. Miller, *Handbook of Green Chemistry - Green Catalysis*, 2010.
59. F. Delbecq and P. Sautet, *J. Catal.*, 2002, **211**, 398-406.
60. S. Campisi, D. Motta, I. Barlocco, R. Stones, T. W. Chamberlain, A. Chutia, N. Dimitratos and A. Villa, *ChemCatChem*, 2022, **14**,
61. J. E. Bailie, G. J. Hutchings and S. O’Leary, ed. R. W. C. in: K.H.J. Buschow, M.C. Flemings, B. Ilschner, E.J. Kramer, S. Mahajan, P. Veyssièrè *Encyclopedia of Materials: Science and Technology*, Elsevier Oxford, 2001, pp. 8986-8990.
62. S. Sitthisa and D. E. Resasco, *Catal. Lett.*, 2011, **141**, 784-791.
63. S. Campisi, C. E. Chan-Thaw, L. E. Chinchilla, A. Chutia, G. A. Botton, K. M. H. Mohammed, N. Dimitratos, P. P. Wells and A. Villa, *ACS Catal.*, 2020, **10**, 5483-5492.
64. Z. Yu, X. Lu, X. Wang, J. Xiong, X. Li, R. Zhang and N. Ji, *ChemSusChem*, 2020, **13**, 5185-5198.
65. Y. Nakagawa, K. Takada, M. Tamura and K. Tomishige, *ACS Catal.*, 2014, **4**, 2718-2726.
66. J. Long, W. Zhao, H. Li and S. Yang, in *Biomass, Biofuels, Biochemicals*, eds. S. Saravanamurugan, A. Pandey, H. Li and A. Riisager, Elsevier, Guizhou University, Guiyang, China, 2020, ch. 11, pp. 299-322.
67. Y. Wang, D. Zhao, D. Rodríguez-Padrón and C. Len, *Catalysts*, 2019, **9**, 796.
68. A. Mandalika, L. Qin, T. K. Sato and T. Runge, *Green Chem.*, 2014, **16**, 2480-2489.

69. J. Zhang, D. Mao, H. Zhang and D. Wu, *Appl. Catal. A: Gen.*, 2023, **660**, 119206.
70. K. Yan, G. Wu, T. Lafleur and C. Jarvis, *Renew. Sust. Energ. Rev.*, 2014, **38**, 663-676.
71. M. Kabbour and R. Luque, in *Biomass, Biofuels, Biochemicals*, eds. S. Saravanamurugan, A. Pandey, H. Li and A. Riisager, Elsevier, , Universidad de Cordoba, Cordoba, Spain, 2020, ch. 10, pp. 283-297.
72. D. Liu, D. Zemlyanov, T. Wu, R. J. Lobo-Lapidus, J. A. Dumesic, J. T. Miller and C. L. Marshall, *J. Catal.*, 2013, **299**, 336-345.
73. M. Ghashghaee, S. Shirvani and V. Farzaneh, *Russ. J. Appl. Chem.*, 2017, **90**, 304-309.
74. Y. Wang, Y. Shen, Y. Zhao, J. Lv, S. Wang and X. Ma, *ACS Catal.*, 2015, **5**, 6200-6208.
75. S. Shirvani, M. Ghashghaee, V. Farzaneh and S. Sadjadi, *Biomass Convers. Biorefin.*, 2017, **8**, 79-86.
76. J. Li, J. L. Liu, H. J. Zhou and Y. Fu, *ChemSusChem*, 2016, **9**, 1339-1347.
77. P. Puthiaraj, K. Kim and W.-S. Ahn, *Catal. Today*, 2019, **324**, 49-58.
78. W. Huang, H. Li, B. Zhu, Y. Feng, S. Wang and S. Zhang, *Ultrason Sonochem*, 2007, **14**, 67-74.
79. Z. An and J. Li, *Green Chem.*, 2022, **24**, 1780-1808.
80. P. Yan, H. Wang, Y. Liao and C. Wang, *Renew. Sust. Energ. Rev.*, 2023, **178**, 113219.
81. H. K. G. Ertl, F. Schüth, and J. Weitkamp., *Handbook Of Heterogeneous Catalysis*. , Wiley-VCH., 2009.
82. P. S. Moyo, L. C. Matsinha and B. C. E. Makhubela, *J. Organomet. Chem.*, 2020, **922**, 121362.
83. H. Cai, C. Li, A. Wang and T. Zhang, *Catal. Today*, 2014, **234**, 59-65.
84. C. Xu, E. Paone, D. Rodriguez-Padron, R. Luque and F. Mauriello, *Chem Soc Rev*, 2020, **49**, 4273-4306.
85. B. Campo, M. Volpe, S. Ivanova and R. Touroude, *J. Catal.*, 2006, **242**, 162-171.

86. H. Lee, C. Nguyen-Huy, E. Jeong Jang, J. Lee, E. Yang, M. S. Lee, J. H. Kwak and K. An, *Catal. Today*, 2021, **365**, 291-300.
87. D. M. Alonso, S. G. Wettstein and J. A. Dumesic, *Chem Soc Rev*, 2012, **41**, 8075-8098.
88. C. Liu, W. Luo, J. Liu, L. Sun, Y. Yang, G. Liu, F. Wang, W. Zhong, C. Guild and S. L. Suib, *Catal. Lett.*, 2018, **148**, 555-563.
89. M. G. Prakash, R. Mahalakshmy, K. R. Krishnamurthy and B. Viswanathan, *Catal. Sci. Technol.*, 2015, **5**, 3313-3321.
90. S. Bhogeswararao and D. Srinivas, *J. Catal.*, 2012, **285**, 31-40.
91. M. J. Taylor, L. J. Durndell, M. A. Isaacs, C. M. A. Parlett, K. Wilson, A. F. Lee and G. Kyriakou, *Appl. Catal. B: Environ.*, 2016, **180**, 580-585.
92. Y. Long, S. Song, J. Li, L. Wu, Q. Wang, Y. Liu, R. Jin and H. Zhang, *ACS Catal.*, 2018, **8**, 8506-8512.
93. M. Agote-Arán, S. Alijani, C. Coffano, A. Villa and D. Ferri, *Catal. Lett.*, 2021, **152**, 980-990.
94. C. Wang, Z. Guo, Y. Yang, J. Chang and A. Borgna, *Ind. Eng. Chem. Res.*, 2014, **53**, 11284-11291.
95. X. Chen, L. Zhang, B. Zhang, X. Guo and X. Mu, *Sci Rep*, 2016, **6**, 28558.
96. G. Gao, J. Remón, Z. Jiang, L. Yao and C. Hu, *Appl. Catal. B: Environ.*, 2022, **309**, 121260.
97. D. Yan, J. Li, M. Zahid, J. Li and Y. Zhu, *Appl. Surf. Sci.*, 2023, **609**, 155308.
98. M. Hronec and K. Fulajtarová, *Catal. Commun.*, 2012, **24**, 100-104.
99. A. Fuente-Hernández, R. Lee, N. Béland, I. Zamboni and J.-M. Lavoie, *Energies*, 2017, **10**, 286.
100. N. S. Biradar, A. A. Hengne, S. N. Birajdar, R. Swami and C. V. Rode, *Org. Process Res. Dev.*, 2014, **18**, 1434-1442.
101. Y. Shi, H. Wang, Z. Wang, C. Liu, M. Shen, T. Wu and L. Wu, *J. Energy Chem.*, 2022, **66**, 566-575.

102. W. Tolek, K. Khruachao, B. Pongthawornsakun, O. Mekasuwandumrong, F. J. C. S. Aires, P. Weerachawanasak and J. Panpranot, *Catal. Commun.*, 2021, **149**, 106246.
103. J. Li, M. Zahid, W. Sun, X. Tian and Y. Zhu, *Appl. Surf. Sci.*, 2020, **528**, 146983.
104. W. Yu, Y. Tang, L. Mo, P. Chen, H. Lou and X. Zheng, *Bioresour Technol*, 2011, **102**, 8241-8246.
105. V. V. Ordonsky, J. C. Schouten, J. van der Schaaf and T. A. Nijhuis, *Appl. Catal. A: Gen.*, 2013, **451**, 6-13.
106. P. Reyes, D. Salinas, C. Campos and M. Oportus, *Quim Nova* 2010, **33**, 33-77.
107. M. Tamura, K. Tokonami, Y. Nakagawa and K. Tomishige, *Chem Commun (Camb)*, 2013, **49**, 7034-7036.
108. M. M. Villaverde, T. F. Garetto and A. J. Marchi, *Catal. Commun.*, 2015, **58**, 6-10.
109. W. Gong, C. Chen, H. Zhang, Y. Zhang, Y. Zhang, G. Wang and H. Zhao, *Mol. Catal.*, 2017, **429**, 51-59.
110. W. Gong, C. Chen, H. Zhang, G. Wang and H. Zhao, *Catal. Sci. Technol.*, 2018, **8**, 5506-5514.
111. M. G. Dohade and P. L. Dhepe, *Green Chem.*, 2017, **19**, 1144-1154.
112. J. Wu, C. Liu, Y. Zhu, X. Song, C. Wen, X. Zhang, C. Wang and L. Ma, *J. Energy Chem.*, 2021, **60**, 16-24.
113. X. Gao, S. Tian, Y. Jin, X. Wan, C. Zhou, R. Chen, Y. Dai and Y. Yang, *ACS Sustain. Chem. Eng.*, 2020, **8**, 12722-12730.
114. S. Saknaphawuth, P. Weerachawanasak, L. Chuenchom, P. Praserttham and J. Panpranot, *Catalysts*, 2022, **12**, 393.
115. L. Liu, H. Lou and M. Chen, *Appl. Catal. A: Gen.*, 2018, **550**, 1-10.
116. B. Chen, F. Li, Z. Huang and G. Yuan, *Appl. Catal. A: Gen.*, 2015, **500**, 23-29.
117. A. B. Merlo, V. Vetere, J. F. Ruggera and M. L. Casella, *Catal. Commun.*, 2009, **10**, 1665-1669.

118. H. Li, H. Luo, L. Zhuang, W. Dai and M. Qiao, *J. Mol. Catal. A: Chem.*, 2003, **203**, 267-275.
119. C. Xu, L. Zheng, J. Liu and Z. Huang, *Chin. J. Chem.*, 2011, **29**, 691-697.
120. Rodiansono, S. Khairi, T. Hara, N. Ichikuni and S. Shimazu, *Catal. Sci. Technol.*, 2012, **2**.
121. R. Tu, K. Liang, Y. Sun, Y. Wu, W. Lv, C. Q. Jia, E. Jiang, Y. Wu, X. Fan, B. Zhang, Q. Lu, B. Zhang and X. Xu, *Chem. Eng. J.*, 2023, **452**, 139526.
122. P. W. Jacek Kijeński, *Appl. Catal. A: Gen.*, 2000 **193**, L1-L4.
123. J. O. Martin Bankmann, Thomas Tacke,, *US Pat.*, 1997, **5591873**.
124. S. Sitthisa, T. Sooknoi, Y. Ma, P. B. Balbuena and D. E. Resasco, *J. Catal.*, 2011, **277**, 1-13.
125. F. Dong, Y. Zhu, H. Zheng, Y. Zhu, X. Li and Y. Li, *J. Mol. Catal. A: Chem.*, 2015, **398**, 140-148.
126. D. Vargas-Hernández, J. M. Rubio-Caballero, J. Santamaría-González, R. Moreno-Tost, J. M. Mérida-Robles, M. A. Pérez-Cruz, A. Jiménez-López, R. Hernández-Huesca and P. Maireles-Torres, *J. Mol. Catal. A: Chem.*, 2014, **383-384**, 106-113.
127. B. M. Nagaraja, V. S. Kumar, V. Shasikala, A. H. Padmasri, B. Sreedhar, B. D. Raju and K. S. R. Rao, *Catal. Commun.*, 2003, **4**, 287-293.
128. J. Wu, Y. Shen, C. Liu, H. Wang, C. Geng and Z. Zhang, *Catal. Commun.*, 2005, **6**, 633-637.
129. S. Sitthisa, W. An and D. E. Resasco, *J. Catal.*, 2011, **284**, 90-101.
130. C. P. Jiménez-Gómez, J. A. Cecilia, I. Márquez-Rodríguez, R. Moreno-Tost, J. Santamaría-González, J. Mérida-Robles and P. Maireles-Torres, *Catal. Today*, 2017, **279**, 327-338.
131. C. P. Jiménez-Gómez, J. A. Cecilia, D. Durán-Martín, R. Moreno-Tost, J. Santamaría-González, J. Mérida-Robles, R. Mariscal and P. Maireles-Torres, *J. Catal.*, 2016, **336**, 107-115.

132. C. P. Jiménez-Gómez, J. A. Cecilia, F. I. Franco-Duro, M. Pozo, R. Moreno-Tost and P. Maireles-Torres, *Mol. Catal.*, 2018, **455**, 121-131.
133. B. M. Reddy, G. K. Reddy, K. N. Rao, A. Khan and I. Ganesh, *J. Mol. Catal. A: Chem.*, 2007, **265**, 276-282.
134. X. Ying Hao, W. Zhou, J.-W. Wang, Y.-Q. Zhang and S. Liu, *Chem. Lett.*, 2005, **34**, 1000-1001.
135. H. Zhang, Y. Lei, A. J. Kropf, G. Zhang, J. W. Elam, J. T. Miller, F. Sollberger, F. Ribeiro, M. C. Akatay, E. A. Stach, J. A. Dumesic and C. L. Marshall, *J. Catal.*, 2014, **317**, 284-292.
136. H. R. Prakruthi, B. M. Chandrashekhara, B. S. J. Prakash and Y. S. Bhat, *J. Ind. Eng. Chem.*, 2018, **62**, 96-105.
137. M. A. Jackson, M. G. White, R. T. Haasch, S. C. Peterson and J. A. Blackburn, *Mol. Catal.*, 2018, **445**, 124-132.
138. C. P. Jiménez-Gómez, J. A. Cecilia, R. Moreno-Tost and P. Maireles-Torres, *ChemCatChem*, 2017, **9**, 2881-2889.
139. J. Chen, F. Lu, J. Zhang, W. Yu, F. Wang, J. Gao and J. Xu, *ChemCatChem*, 2013, **5**, 2822-2826.
140. M. Chatterjee, T. Ishizaka and H. Kawanami, *Green Chem.*, 2014, **16**, 4734-4739.
141. A. J. Kumalaputri, G. Bottari, P. M. Erne, H. J. Heeres and K. Barta, *ChemSusChem*, 2014, **7**, 2266-2275.
142. X. Kong, R. Zheng, Y. Zhu, G. Ding, Y. Zhu and Y.-W. Li, *Green Chem.*, 2015, **17**, 2504-2514.
143. Y. Zhu, X. Kong, H. Zheng, G. Ding, Y. Zhu and Y.-W. Li, *Catal. Sci. Technol.*, 2015, **5**, 4208-4217.
144. S. Lima, D. Chadwick and K. Hellgardt, *RSC Advances*, 2017, **7**, 31401-31407.
145. L. Yu, L. He, J. Chen, J. Zheng, L. Ye, H. Lin and Y. Yuan, *ChemCatChem*, 2015, **7**, 1701-1707.
146. D. Hu, H. Hu, H. Zhou, G. Li, C. Chen, J. Zhang, Y. Yang, Y. Hu, Y. Zhang and L. Wang, *Catal. Sci. Technol.*, 2018, **8**, 6091-6099.

147. Y. Feng, G. Yan, T. Wang, W. Jia, X. Zeng, J. Sperry, Y. Sun, X. Tang, T. Lei and L. Lin, *Green Chem.*, 2019, **21**, 4319-4323.
148. S. Fulignati, C. Antonetti, D. Licursi, M. Pieraccioni, E. Wilbers, H. J. Heeres and A. M. Raspolli Galletti, *Appl. Catal. A: Gen.*, 2019, **578**, 122-133.
149. T. Wang, J. Zhang, W. Xie, Y. Tang, D. Guo and Y. Ni, *Catalysts*, 2017, **7**, 92.
150. D. K. Mishra, H. J. Lee, C. C. Truong, J. Kim, Y.-W. Suh, J. Baek and Y. J. Kim, *Mol. Catal.*, 2020, **484**, 110722.
151. M. Mani, G. G. Kadam, L. J. Konwar and A. B. Panda, *Biomass Convers. Biorefin.*, 2022, 1-18.
152. T. M. Townsend, C. Kirby, A. Ruff and A. R. O'Connor, *J. Organomet. Chem.*, 2017, **843**, 7-13.
153. A. S. Gowda, S. Parkin and F. T. Ladipo, *Appl. Organomet. Chem.*, 2012, **26**, 86-93.
154. T. G. P. H. Mark J. Burk, Jeffrey R. Lee, Christopher Kalberg, *Tetrahedron Lett*, 1994 **35**, 4963-4966.
155. N. K. Oklu and B. C. E. Makhubela, *New J. Chem.*, 2020, **44**, 9382-9390.
156. K. An, N. Musselwhite, G. Kennedy, V. V. Pushkarev, L. R. Baker and G. A. Somorjai, *J Colloid Interface Sci*, 2013, **392**, 122-128.
157. R. Šivec, M. Huš, B. Likozar and M. Grilc, *Chem. Eng. J.*, 2022, **436**, 135070.
158. A. Halilu, T. H. Ali, A. Y. Atta, P. Sudarsanam, S. K. Bhargava and S. B. Abd Hamid, *Energy & Fuels*, 2016, **30**, 2216-2226.
159. M. Ghashghaee, S. Shirvani, V. Farzaneh and S. Sadjadi, *Braz. J. Chem. Eng.*, 2018, **35**, 669-678.
160. K. L. MacIntosh and S. K. Beaumont, *Top. Catal.*, 2020, **63**, 1446-1462.
161. B. M. Nagaraja, A. H. Padmasri, B. D. Raju and K. S. R. Rao, *J. Mol. Catal. A: Chem.*, 2007, **265**, 90-97.
162. B. M. Nagaraja, A. H. Padmasri, B. D. Raju and K. S. Rama Rao, *Int. J. Hydrog. Energy*, 2011, **36**, 3417-3425.

163. H. Cui, X. Wu, Y. Chen, J. Zhang and R. I. Boughton, *Mater. Res. Bull.*, 2015, **61**, 511-518.
164. A. J. Estrup, MSc, University of Maine 2015.
165. H. Liu, Q. Hu, G. Fan, L. Yang and F. Li, *Catal. Sci. Technol.*, 2015, **5**, 3960-3969.
166. M. Ghashghaee, S. Sadjadi, S. Shirvani and V. Farzaneh, *Catal. Lett.*, 2017, **147**, 318-327.
167. S. Sadjadi, V. Farzaneh, S. Shirvani and M. Ghashghaee, *Korean J. Chem. Eng.*, 2017, **34**, 692-700.
168. F. F. Tao, *Chem Soc Rev*, 2012, **41**, 7977-7979.
169. S. Srivastava, G. C. Jadeja and J. Parikh, *J. Mol. Catal. A: Chem.*, 2017, **426**, 244-256.
170. W. Zhao, X. Zhu, Z. Zeng, J. Lei, Z. Huang, Q. Xu, X. Liu and Y. Yang, *Mol. Catal.*, 2022, **524**, 112304.
171. J. Wu, X. Zhang, Q. Chen, L. Chen, Q. Liu, C. Wang and L. Ma, *Energy & Fuels*, 2019, **34**, 2178-2184.
172. M. Lesiak, M. Binczarski, S. Karski, W. Maniukiewicz, J. Rogowski, E. Szubiakiewicz, J. Berlowska, P. Dziugan and I. Witońska, *J. Mol. Catal. A: Chem.*, 2014, **395**, 337-348.
173. R. Ferrando, J. Jellinek, and R.L. Johnston, , *Chem. Rev.*, 2008, . **108**, 845-910.
174. S. Alayoglu, A. U. Nilekar, M. Mavrikakis and B. Eichhorn, *Nat Mater*, 2008, **7**, 333-338.
175. Q. Yang, D. Gao, C. Li, S. Wang, X. Hu, G. Zheng and G. Chen, *Appl. Catal. B: Environ.*, 2023, **328**, 122458.
176. Y. Wang, H. Wang, X. Kong and Y. Zhu, *ChemSusChem*, 2022, **15**, e202200421.
177. S. J. Tauster, S. C. Fung and R. L. Garten, *J. Am. Chem. Soc.* , 1978, **100**, 170-175
178. S. J. Tauster, *Acc. Chem. Res.*, 1987, **20**, 389-394.

179. G. L. Haller and D. E. Resasco, in *In: Advances in catalysis.* , Academic Press, 1989, vol. 36, pp. 173-235.
180. L. R. Baker, G. Kennedy, M. Van Spronsen, A. Hervier, X. Cai, S. Chen, L. W. Wang and G. A. Somorjai, *J Am Chem Soc*, 2012, **134**, 14208-14216.
181. L. R. Baker, A. Hervier, H. Seo, G. Kennedy, K. Komvopoulos and G. A. Somorjai, *J. Phys. Chem. C*, 2011, **115**, 16006-16011.
182. A. B. Boffa, A. T. Bell and G. A. Somorjai, *J. Catal*, 1993, **139**, 602.
183. Y. Mueangern, X. Yang, Y. Tang, F. F. Tao and L. R. Baker, *J. Phys. Chem. C*, 2017, **121**, 13765-13776.
184. K. M. Neyman and S. M. Kozlov, *NPG Asia Materials*, 2022, **14**, 59.
185. L. Wang, J. Zhang, Y. Zhu, S. Xu, C. Wang, C. Bian, X. Meng and F.-S. Xiao, *ACS Catal.*, 2017, **7**, 7461-7465.
186. Y. Li, H. Cheng, W. Lin, C. Zhang, Q. Wu, F. Zhao and M. Arai, *Catal. Sci. Technol.*, 2018, **8**, 3580-3589.
187. J. Wang, C.-Q. Lv, J.-H. Liu, R.-R. Ren and G.-C. Wang, *Int. J. Hydrog. Energy*, 2021, **46**, 1592-1604.
188. Y. Yoon, R. Rousseau, R. S. Weber, D. Mei and J. A. Lercher, *J Am Chem Soc*, 2014, **136**, 10287-10298.
189. L. He, F. J. Yu, X. B. Lou, Y. Cao, H. Y. He and K. N. Fan, *Chem Commun (Camb)*, 2010, **46**, 1553-1555.
190. R. Alamillo, M. Tucker, M. Chia, Y. Pagán-Torres and J. Dumesic, *Green Chem.*, 2012, **14**.
191. J. Tan, J. Cui, Y. Zhu, X. Cui, Y. Shi, W. Yan and Y. Zhao, *ACS Sustain. Chem. Eng.*, 2019, **7**, 10670-10678.
192. F. liu, M. Audemar, K. D. O. Vigier, J.-M. Clacens, F. D. Campo and F. Jérôme, *Green Chem.*, 2014, **16**, 4110-4114.
193. W. R. Silva, E. Y. Matsubara, J. M. Rosolen, P. M. Donate and R. Gunnella, *Mol. Catal.*, 2021, **504**, 111496.
194. B. Zhang, Y. Zhu, G. Ding, H. Zheng and Y. Li, *Green Chem.*, 2012, **14**, 3402.

195. N. S. Date, R. C. Chikate, H.-S. Roh and C. V. Rode, *Catal. Today*, 2018, **309**, 195-201.
196. D. S. Pisal and G. D. Yadav, *ACS Omega* 2019, **4**, 1201–1214.
197. J. Guan, J. Li, Y. Yu, X. Mu and A. Chen, *J. Phys. Chem. C*, 2016, **120**, 19124-19134.
198. W. Xu, H. Wang, X. Liu, J. Ren, Y. Wang and G. Lu, *Chem Commun (Camb)*, 2011, **47**, 3924-3926.
199. R. C. Homer Adkins, *J. Am. Chem. Soc.* , 1931, **53** 1091–1095.
200. J.-j. Tan, Y.-h. Su, K. Gao, J.-l. Cui, Y.-z. Wang and Y.-x. Zhao, *J. Fuel Chem. Technol.*, 2021, **49**, 780-790.
201. T. Mizugaki, T. Yamakawa, Y. Nagatsu, Z. Maeno, T. Mitsudome, K. Jitsukawa and K. Kaneda, *ACS Sustain. Chem. Eng.*, 2014, **2**, 2243-2247.
202. R. Karinen, K. Vilonen and M. Niemela, *ChemSusChem*, 2011, **4**, 1002-1016.
203. T. Mizugaki, T. Yamakawa, Y. Nagatsu, Z. Maeno, T. Mitsudome, K. Jitsukawa and K. Kaneda, *ACS Sustain. Chem. Eng.*, 2014, **2** .2243-2247.
204. W. E. Kaufmann and R. Adams, *J Am Chem Soc* , 1923, **45** 3029-3044.
205. T. Tong, Q. Xia, X. Liu and Y. Wang, *Catal. Commun.*, 2017, **101**, 129-133.
206. S. Liu, Y. Amada, M. Tamura, Y. Nakagawa and K. Tomishige, *Green Chem.*, 2014, **16**, 617-626.
207. M. Chia, Y. J. Pagan-Torres, D. Hibbitts, Q. Tan, H. N. Pham, A. K. Datye, M. Neurock, R. J. Davis and J. A. Dumesic, *J. Am. Chem. Soc.* , 2011, **133**, 12675–12689.
208. D. Götz, M. Lucas and P. Claus, *React Chem Eng* , 2016, **1**, 161-164.
209. J. Lee, S. P. Burt, C. A. Carrero, A. C. Alba-Rubio, I. Ro, B. J. O'Neill, H. J. Kim, D. H. K. Jackson, T. F. Kuech, I. Hermans, J. A. Dumesic and G. W. Huber, *J. Catal.*, 2015, **330**, 19-27.
210. T. P. Sulmonetti, B. Hu, S. Lee, P. K. Agrawal and C. W. Jones, *ACS Sustain. Chem. Eng.*, 2017, **5**, 8959-8969.

211. R. Ma, X.-P. Wu, T. Tong, Z.-J. Shao, Y. Wang, X. Liu, Q. Xia and X.-Q. Gong, *ACS Catal.*, 2016, **7**, 333-337.
212. Y. Nakagawa and K. Tomishige, *Catal. Today*, 2012, **195**, 136-143.
213. T. Tong, X. Liu, Y. Guo, M. Norouzi Banis, Y. Hu and Y. Wang, *J. Catal.*, 2018, **365**, 420-428.
214. H. Liu, Z. Huang, H. Kang, C. Xia and J. Chen, *Chinese J. Catal.*, 2016, **37**, 700-710.
215. H. W. Wijaya, T. Kojima, T. Hara, N. Ichikuni and S. Shimazu, *ChemCatChem*, 2017, **9**, 2869-2874.
216. S. Liu, Y. Amada, M. Tamura, Y. Nakagawa and K. Tomishige, *Catal. Sci. Technol.*, 2014, **4**, 2535-2549.
217. F. Gao, H. Liu, X. Hu, J. Chen, Z. Huang and C. Xia, *Chinese J. Catal.*, 2018, **39**, 1711-1723.
218. A. Barranca, I. Gandarias, P. L. Arias and I. Agirrezabal-Telleria, *Catal. Lett.*, 2022, **153**, 2018-2025.
219. Y. Shao, J. Wang, K. Sun, G. Gao, C. Li, L. Zhang, S. Zhang, L. Xu, G. Hu and X. Hu, *Renew. Energ.*, 2021, **170**, 1114-1128.
220. Y. Shao, J. Wang, H. Du, K. Sun, Z. Zhang, L. Zhang, Q. Li, S. Zhang, Q. Liu and X. Hu, *ACS Sustain. Chem. Eng.*, 2020, **8**, 5217-5228.
221. J.-Y. Yeh, B. M. Matsagar, S. S. Chen, H.-L. Sung, D. C. W. Tsang, Y.-P. Li and K. C.-W. Wu., *J. Catal.*, 2020, **390**, 46-56.
222. R. G. Kurniawan, N. Karanwal, J. Park, D. Verma, S. K. Kwak, S. K. Kim and J. Kim, *Appl. Catal. B: Environ.*, 2023, **320**, 121971.
223. N. S. Date, R. C. Chikate, H.-S. Roh and C. V. Rode, *Catal. Today*, 2018, **309**, 195-201.
224. J. F. F. Hilton A. Smith, *Contribution No. 60 from the Department of Chemistry, University of Tennessee*, 1949, **71**, 415-419.
225. J. Tuteja, H. Choudhary, S. Nishimura and K. Ebitani, *ChemSusChem*, 2014, **7**, 96-100.

226. S. Yao, X. Wang, Y. Jiang, F. Wu, X. Chen and X. Mu, *ACS Sustain. Chem. Eng.*, 2013, **2**, 173-180.
227. M. Faber, *U.S. Patent No 4,400,468*,, 1983, 388.
228. S. V. d. Vyver and Y. Roma'n-Leshkov, *Catal. Sci. Technol.*, 2013, **3**, 1465-1479.
229. D. W. Rackemann and W. O. S. Doherty, *Biofuels, Bioproducts and Biorefining*, 2011, **5**, 198-214.
230. J. Ohyama, Y. Ohira and A. Satsuma, *Catal. Sci. Technol.*, 2017, **7**, 2947-2953.
231. L. Zhou, H. Zou, J. Nan, L. Wu, X. Yang, Y. Su, T. Lu and J. Xu, *Catal. Commun.*, 2014, **50**, 13-16.
232. F. Liu, M. Audemar, K. De Oliveira Vigier, J. M. Clacens, F. De Campo and F. Jerome, *ChemSusChem*, 2014, **7**, 2089-2093.
233. K. Endo and T. Sawada, *Colloid Polym Sci*, 2001, **279** 1058-1063.
234. M. H. Y. Miura, M. Yuge, K. Numano, K. Iwakiri, *Contact Dermat*, 1999 **41** 118-119.
235. T. Buntara, S. Noel, P. H. Phua, I. Melián-Cabrera, J. G. de Vries and H. J. Heeres, *Top. Catal.*, 2012, **55**, 612-619.
236. R. W. Tess, R. D. Harline and T. F. Mika., *Ind. Eng. Chem.*, 1957, **49** 374– 378.
237. D. P. Duarte, R. Martínez and L. J. Hoyos, *Ind. Eng. Chem. Res.*, 2015, **55**, 54-63.
238. T. Buntara, I. Melián-Cabrera, Q. Tan, J. L. G. Fierro, M. Neurock, J. G. de Vries and H. J. Heeres, *Catal. Today*, 2013, **210**, 106-116.
239. F. C. A. Figueiredo, E. Jordão and W. A. Carvalho, *Appl. Catal. A: Gen.*, 2008, **351**, 259-266.
240. N. Enjamuri and S. Darbha, *Catal. Rev.*, 2020, **62**, 566-606.
241. Y. Kojima, S. Kotani, M. Sano, T. Suzuki and T. Miyake, *J. Jpn. Pet. Inst.*, 2013 **56**, 133-141.
242. H. Kim, S. Lee, J. Lee and W. Won, *Bioresour Technol*, 2021, **331**, 125009.

243. S. P. Burt, K. J. Barnett, D. J. McClelland, P. Wolf, J. A. Dumesic, G. W. Huber and I. Hermans, *Green Chem.*, 2017, **19**, 1390-1398.
244. J. He, S. P. Burt, M. Ball, D. Zhao, I. Hermans, J. A. Dumesic and G. W. Huber, *ACS Catal.*, 2018, **8**, 1427-1439.
245. Marcel Faber, *US Patent*, 1983, **4**, 468.
246. P. Daorattanachai, S. Namuangruk, N. Viriya-empikul, N. Laosiripojana and K. Faungnawakij, *J. Ind. Eng. Chem.*, 2012, **18**, 1893-1901.
247. S. Yin, Y. Pan and Z. Tan, *Int. J. Green Energy*, 2011, **8**, 234-247.
248. T. Buntara, S. Noel, P. H. Phua, I. Melian-Cabrera, J. G. de Vries and H. J. Heeres, *Angew. Chem. Int. Ed. Engl.*, 2011, **50**, 7083-7087.
249. B. Xiao, M. Zheng, X. Li, J. Pang, R. Sun, H. Wang, X. Pang, A. Wang, X. Wang and T. Zhang, *Green Chem.*, 2016, **18**, 2175-2184.
250. J. He, S. P. Burt, M. R. Ball, I. Hermans, J. A. Dumesic and G. W. Huber, *Appl. Catal. B: Environ.*, 2019, **258**.
251. K. Chen, S. Koso, T. Kubota, Y. Nakagawa and K. Tomishige, *ChemCatChem* 2010, , **2**, 547-555.
252. J. Ohyama, R. Kanao, A. Esaki and A. Satsuma, *Chem Commun (Camb)*, 2014, **50**, 5633-5636.
253. V. Schiavo, Descotes, G., Mentech, J., *Bull. Soc. Chim. Fr.*, 1991, **128**, 704-711.
254. H. van Bekkum, L. Maat, G. C. A. Luijkx, N. P. M. Huck and F. van Rantwijk, *Heterocycles*, 2009, **77**, 1037.
255. J. Ohyama, A. Esaki, Y. Yamamoto, S. Arai and A. Satsuma, *RSC Adv.*, 2013, **3**, 1033-1036.
256. Y. Duan, M. Zheng, D. Li, D. Deng, L.-F. Maa and Y. Yang, *Green Chem.*, 2017, **19**, 5103-5113.
257. S. Zhang, H. Ma, Y. Sun, Y. Luo, X. Liu, M. Zhang, J. Gao and J. Xu, *Green Chem.*, 2019, **21**, 1702-1709.
258. J. Ohyama, R. Kanao, Y. Ohira and A. Satsuma, *Green Chem.*, 2016, **18**, 676-680.

259. B. Girisuta, L. P. B. M. Janssen and H. J. Heeres, *Green Chem.*, 2006, **8**, 701.
260. D. Ren, Z. Song, L. Li, Y. Liu, F. Jin and Z. Huo, *Green Chem.*, 2016, **18**, 3075-3081.
261. L. Suhadolnik, D. Bajec, D. Žigon, M. Čeh and B. Likozar, *Chem. Eng. Technol.*, 2019, **43**, 375-379.
262. B. G. Hermann, K. Blok and M. K. Patel, *Environ. Sci. Technol.*, 2007, **41** 7915–7921.
263. J. Wiley, Kepplinger, P. E. M. & Wilson, F. A. , *US4400468A* 1983, 4–7.
264. M. J. Gilkey, A. V. Mironenko, D. G. Vlachos and B. Xu, *ACS Catal.*, 2017, **7**, 6619-6634.
265. Thomas R. Boussie, Eric L. Dias, Zachary M. Fresco, Vincent J. Murphy, James Shoemaker, Raymond Archer and Hong Jiang, *U.S. Pat. US 2010/031 7823 A1*, 2010.
266. W. Guan, X. Chen, H. Hu, C.-W. Tsang, J. Zhang, C. S. K. Lin and C. Liang, *Fuel Process. Technol.*, 2020, **203**, 106392.
267. K. J. Stephens, A. M. Allgeier, A. L. Bell, T. R. Carlson, Y. Cheng, J. T. Douglas, L. A. Howe, C. A. Menning, S. A. Neuenswander, S. K. Sengupta, P. S. Thapa and J. C. Ritter, *ACS Catal.*, 2020, **10**, 12996-13007.
268. S. T. Thompson and H. H. Lamb, *ACS Catal.*, 2016, **6**, 7438-7447.
269. C. Zhang, Q. Lai and J. H. Holles, *Catal. Commun.*, 2017, **89**, 77-80.
270. C. P. Jimenez-Gomez, J. A. Cecilia, R. Moreno-Tost and P. Maireles-Torres, *ChemSusChem*, 2017, **10**, 1448-1459.
271. A. Barranca, I. Agirrezabal-Tellería, M. Rellán-Piñeiro, M. A. Ortuño and I. Gandarias, *React. Chem. Eng.*, 2023, **8**, 687-698.
272. R. T. K. B. Rajeev S. Rao, M. Albert Vannice *Catal. Lett.*, 1999, **60**, 51–57.
273. S. Srivastava, G. C. Jadeja and J. Parikh, *RSC Advances*, 2016, **6**, 1649-1658.
274. C. Sun, P. Zeng, M. He, X. He and X. Xie, *Catal. Commun.*, 2016, **86**, 5-8.
275. R. Albilali, M. Douthwaite, Q. He and S. H. Taylor, *Catal. Sci. Technol.*, 2018, **8**, 252-267.

Chapter 2: Experimental

2.1 Introduction

This chapter gives an overview of the material used in catalysts preparation, testing and different characterisation techniques employed in this study. This covers details of how the catalysts were prepared and characterised, including reaction specificities and post-reaction protocols.

2.2 Materials

All chemicals used in this work were purchased from commercial sources and used without further purification. Table 2.1 provides details about the substances used and their sources.

Table 2.1: Chemical materials used in this study, along with approximate purity.

No.	Chemical	Chemical detail
1	Co(NO ₃) ₂	Sigma Aldrich, 99 %.
2	NH ₄ ReO ₄	Sigma Aldrich, 99 %.
3	RuCl ₃ .xH ₂ O,	Fisher Scientific, 99.9 %.
4	PdCl ₂	Fisher Scientific, 99.9 %.
5	H ₂ PtCl ₆	Sigma Aldrich, , ≥37.50% Pt basis.
6	HAuCl ₄ .xH ₂ O	Strem Chemicals
7	Titania P25 (TiO ₂)	Degussa.
8	Silicon dioxide (SiO ₂)	Sigma Aldrich, powder 5-15 nm, 99.5%.
9	MgO	BDH, 99.9%.
10	Hydrotalcite (HT)	Sigma Aldrich.
11	HAP	Acros organics.
12	C (Carbon)	DARCO G-60, ACROS.
13	Sulphated zirconia (SZ)	Luxfer MEL Technologies.

14	Tungstated zirconia (WZ)	Luxfer MEL Technologies.
15	Polyvinyl alcohol (PVA)	Sigma Aldrich.
16	Sodium borohydride (NaBH ₄)	Sigma Aldrich, 99.9%.
17	Furfural	Sigma Aldrich, 99%.
18	Furfuryl alcohol	Sigma Aldrich, 98%.
19	n-Octanol	Sigma Aldrich, + 98%.
20	Hydroxymethyl furfural	Sigma Aldrich, 99%.
21	Propylbenzen	Sigma Aldrich, + 99%.
22	Isopropanol	Fisher Scientific, 99.5%.
23	Methanol	Fisher Scientific, 99.5%.
24	Cerium(IV) oxide (CeO ₂)	Sigma Aldrich, 99%.
25	HAuCl ₄ .3H ₂ O	Strem Chemicals.
26	H ₂	BOC gases, 99.99%.
27	5% H ₂ /Ar	BOC gases.
28	HCl	Sigma Aldrich, 37%.

2.3 Hydrogenation of furfural and hydroxymethyl furfural.

2.3.1 Preparation of monometallic and bimetallic catalysts for hydrogenation of furfural

2.3.1.1 Catalyst preparation

Two different methods have been employed for the preparation of the catalysts used for the hydrogenation of furfural (FF). The wet impregnation and sol immobilisation methods were used for the preparation of monometallic and bimetallic catalysts. Bimetallic catalysts are composed of two metals with a molar ratio of 1:1.

2.3.1.1.1 Wet-impregnation method

Wet-impregnation method is an easy and effective technique and one of the most prevalent methods used for the preparation of supported catalysts.¹ Aqueous solutions of Pt, Pd, Ru, Co, Au and Re from the following precursors aqueous precursor: H₂PtCl₆ · 6H₂O (18.57 mg ml⁻¹), RuCl₃·xH₂O (14.70 mg ml⁻¹), PdCl₂ (11.70 mg ml⁻¹), HAuCl₄·3H₂O (12.25 mg ml⁻¹) Co(NO₃)₂, (8.20 mg ml⁻¹) and NH₄ReO₄, (34.22 mg ml⁻¹) respectively, were prepared. It is worth noting that 0.58 M HCl was added to PdCl₂ to facilitate its dissolution. After the preparation of the precursor solutions, Agilent 4200 MP-AES instrument was used to define the exact amount of each metal in the precursor solutions. Metal precursor solutions are quantified as the weight percentage of the metals (wt. %) in the solution. In a typical preparation of 5 wt. %Pt/TiO₂ (2 g) by wet-impregnation method, the calculation of the volume of the metal precursor solution needed is as shown below:

$$\text{Metal amount} = \frac{5}{100} \times 2\text{g} = 0.1 \text{ g of Pt}$$

Equation 2.1

$$\text{Precursors amount (ml)} = \text{Metal amount (0.1 g)} \times \frac{1}{\text{Content of the Pt in the precursor} \frac{\text{mg}}{\text{ml}} \times \frac{1}{1000}}$$

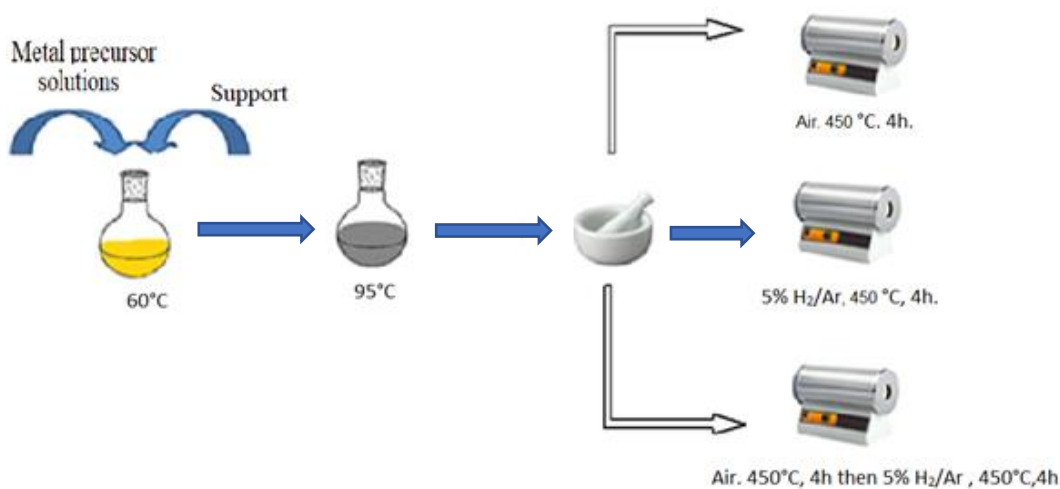
Equation 2.2

$$\text{The support amount TiO}_2 \text{ (g)} = \text{Metal amount (0.1 g)} - \text{weight of the catalyst (2g)}$$

Equation 2.3

A 50 ml round bottom flask (RBF) equipped with a stirrer bar was charged with a required quantity of the precursor as shown in Table 2.1 and distilled water was added to the solution to achieve a total volume of 16 ml of the solution in the RBF. After heating the RBF at 60 °C for 10 minutes, the support was added (1.98 g of TiO₂ (P-25)) over 10 minutes period. The mixture was left for 15 minutes with continuous stirring and the temperature was increased from 60°C to 95°C over a period of 16 hours to facilitate the gradual evaporation of the solvent in air. Finally, the resultant mixture was collected from RBF and ground into a fine powder using a pestle and mortar. This fine powder is referred to as “dried only” sample. Subsequently, 1g of fine powder obtained is calcined in the furnace at 450 °C with a ramp rate of 10 °C/min for 4 h under flow air and the product obtained from this process is referred to as “calcined only” sample. “Reduced only”

sample were made by reducing 1g of dried only sample in the furnace under a flow of 5% H₂/Ar (Argon) at 450 °C with a ramp rate 10 °C/min for 4 h.² Lastly, “calcined + reduced” were made by calcining 1g of dried only sample in the furnace at 450 °C with a ramp rate 10 °C/min for 4 h under flow air and subsequently, the same sample is reduced under a flow of 5% H₂/Ar at 450 °C with a ramp rate 10 °C/min for 4 h. The synthetic protocol for wet-impregnation method is as depicted in Figure 2.1 below.



Scheme 2.1: Illustrations of the preparing supported Pt/TiO₂ catalysts using wet impregnation method. (Ar : Argon)

Table 2.2 required quantity of aqueous precursor.

Precourser	Amount of aqueous precursors (mg ml ⁻¹)
H ₂ PtCl ₆	18.57
RuCl ₃ .xH ₂ O	14.70
PdCl ₂	11.70
HAuCl ₄ .3H ₂ O	12.25
Co(NO ₃) ₂	8.20
NH ₄ ReO ₄ ,	34.22

The equations below were used for the preparation of 5wt. % PtRu/TiO₂ bimetallic catalyst with the two metals in equimolar ratio using a wet-impregnation method.

$$\text{Total metal amount} = \frac{5}{100} \times 2\text{g} = 0.1 \text{ g of RuPt} \quad \text{Equation 2.4}$$

$$\text{Total metal mol} = \text{Metal amount (0.1 g)} \times \frac{1}{\text{Molecular wight of Pt} + \text{Molecular wight of Ru}} \quad \text{Equation 2.5}$$

$$\text{Precursors metal1 (ml)} = \text{Total metals mol} \times \text{Mwt. of metal 1} \times \frac{1}{\text{Content of metal 1 in the precursor} \frac{\text{mg}}{\text{ml}} \times \frac{1}{1000}} \quad \text{Equation 2.6}$$

$$\text{Precursors metal 2 (ml)} = \text{Total metals mol} \times \text{Mwt. metal 2} \times \frac{1}{\text{Content of metal 2 in the precursor} \frac{\text{mg}}{\text{ml}} \times \frac{1}{1000}} \quad \text{Equation 2.7}$$

$$\text{The support amount (TiO}_2\text{) (g)} = \text{Metal amount (0.04 g)} - \text{weight of the catalyst (2g)} \quad \text{Equation 2.8}$$

Precursor solutions of Pt and Ru were prepared as described above. The metal precursor solutions were mixed, stirrer bar and distilled water was added to make the total volume in the RBF to 16 mL solution. The mixture in RBF with a stirrer was placed in an oil bath and continuously stirred for 10 minutes at 60 °C. Subsequently, TiO₂ was added slowly over a 10-minute period. The mixture was stirred further at 60°C for 15 minutes after which the temperature was increased to 95°C and left to run for 16 h until full evaporation of the water occurred. The resulting residue was then ground into fine powder. The fine powder obtained was subjected to different heating protocols as described earlier to generate dried only, calcined only, reduced only and calcined + reduced catalysts. This fine powder is referred to as “dried only” sample. Subsequently, 1g of fine powder obtained is calcined in the furnace at 450 °C with a ramp rate of 10 °C/min for 4 h under flow air and the product obtained from this process is referred to as “calcined only” sample. “Reduced only” sample were made by reducing 1g of dried only sample in the furnace under a flow of 5% H₂/Ar (Argon) at 450 °C with a ramp rate 10 °C/min for 4 h.²

Lastly, “calcined + reduced” were made by calcining 1g of dried only sample in the furnace at 450 °C with a ramp rate 10 °C/min for 4 h under flow air and subsequently, the same sample is reduced under a flow of 5% H₂/Ar at 450 °C with a ramp rate 10 °C/min for 4 h. A similar procedure has also been followed to prepare the catalysts using different supports (Nb₂O₅, CeO₂, SiO₂, C, MgO and HT). All the supports were used without further treatment except for Hydrotalcite (HT), which was calcined at 550 °C for 5 h before catalyst preparation.

2.3.1.1.2 *Sol-immobilisation method*

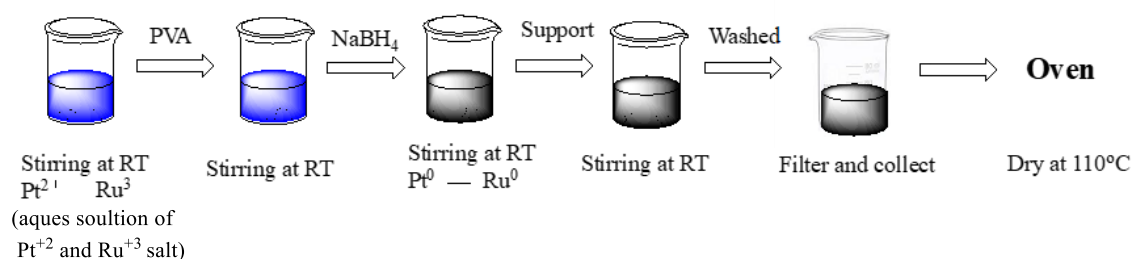
The sol-immobilisation technique is another method commonly used for preparing highly dispersed supported metals. The FF hydrogenation was tested using catalyst prepared by sol-immobilization method. During this process, metal nanoparticles are generated in solution, and subsequently, these nanoparticles are immobilized leading to highly dispersed supported metal nanoparticles. With this technique, a stabilising agent is required to stabilise and control the size of the metal particles by encapsulating them in the stabilising agent, typically a polymer, that covers the metal in a large amount of solution after which the metal ions are then reduced to metal nanoparticles by a reducing agent. Metal nanoparticles are subsequently immobilised onto a support by acidification of the resultant solution at the end of the preparation of metal nanoparticles, which causes the PH of the resultant solution to be lower than the isoelectric of the support.

The metal nanoparticles are attracted to the support due to the electrochemical double layer. Sol-immobilization method is versatile and can be applied to any type of support.

For preparing 5 wt. %Pt/TiO₂ catalyst (2 g), The required amount from H₆PtCl₆ precursor (prepared as described above) was placed in a beaker with 800ml of distilled water with stirring using a magnetic bar at room temperature. The quantity of polyvinyl alcohol PVA/Metal added was 0.65 weight ratio or 1.2 (for bimetallic) taken from freshly prepared 1wt% PVA solution (0.1g in 10 ml solution) and the mixture stirred for 2-3 minutes. 0.1 M NaBH₄ (NaBH₄/Metal= 5 molar ratio) was subsequently added to the mixture as a reducing agent. It is recommended that NaBH₄ solution be used within 5 minutes of preparation, as otherwise NaBH₄ slowly decomposes, lowering its reducing power. The solution was stirred for 30 minutes, followed by adding the desired amount of support (1.98g) to immobilise the colloid. The solution was then acidified using

concentrated sulphuric acid (H₂SO₄) 5-10 drops with vigorous stirring, to lower the pH of the solution. The mixture was left for 1 hour, and the catalyst was filtered to remove excess of PVA, washed with 2 litres of distilled water and dried in an oven at 110 °C for 16 hours without any other further treatment.

This preparation technique produced supported metal nanoparticles that are finely dispersed and exhibit significantly narrower size distributions than those produced using wet impregnation method.



Scheme 2.2: Diagram of the preparing supported Pt/TiO₂ catalysts using Sol-immobilisation method.

2.3.2 Preparation of monometallic and bimetallic catalysts for hydrogenation of hydroxymethyl furfural

Hydrogenation of HMF was carried out using monometallic or bimetallic catalysts. All the catalysts were prepared using wet-impregnation method. The process of preparing the catalysts were identical to that described above using wet-impregnation method. For HMF hydrogenation, reduced-only catalysts were prepared and used for this process. HAP support was used without any further treatment, while sulphated zirconia hydroxide sample (SZ, XZO1720, Luxfer MEL Technologies) and tungstated zirconia hydroxide sample (WZ, XZO1251, Luxfer MEL Technologies) were calcined before being used to prepare the catalyst to form the oxide samples. SZ support was calcined at 620 °C /2hr, with a slow ramp from RT (1C/min) and WZ was also treated at 700 °C /2 h, with a slow ramp from RT (1 °C /min).

2.4 Catalytic testing

2.4.1 Colaver reactor

Hydrogenation of FF was performed in a 50 mL moderate pressure batch glass reactor (Colaver reactor) under 0.3 MPa of hydrogen gas. A 50 mL Colaver glass reactor as shown in Figure 2.1 was employed to conduct the catalyst evaluation. To test the catalyst, the reactor was loaded with 4.45 mmol of FF, the catalyst (molar ratio moles FF/moles metal = 207) and 15 ml of isopropanol. The glass reactor was sealed, purged with nitrogen three times, and then purged with hydrogen three times before it was pressurised with hydrogen to 3 bars of pressure. The experiment was performed under hydrogen flow at 30°C, and the reaction mixture was continuously stirred at 800 rpm with a magnetic stirrer. At the end of the reaction, the reactor was cooled in an ice bath for 10 minutes, and the catalyst was separated from the reaction mixture using 0.45 µm PTFE syringe filter. The gas chromatography (GC) sample was prepared by mixing 10 mL of the reaction mixture with 0.1 mL n-octanol (standard solution) then, 1 mL, was taken for GC analysis.



Figure 2.1: a Colaver reactor® for the catalyst testing.

2.4.2 Autoclave reactor

Hydrogenation of hydroxymethyl furfural (HMF) was studied using an autoclave reactor under 2 MPa of H₂. This study was conducted to investigate the hydrogenolysis of HMF using a 50 mL stainless-steel autoclave reactor "4590 Micro Bench Top Reactor" from

Parr Instruments Company. The autoclave reactor is as depicted in Figure 2.2 and a schematic representation of this high-pressure device is as shown in Figure 2.3 below.



Figure 2.2: 50ml stainless-steel autoclave reactor by Parr Instruments.

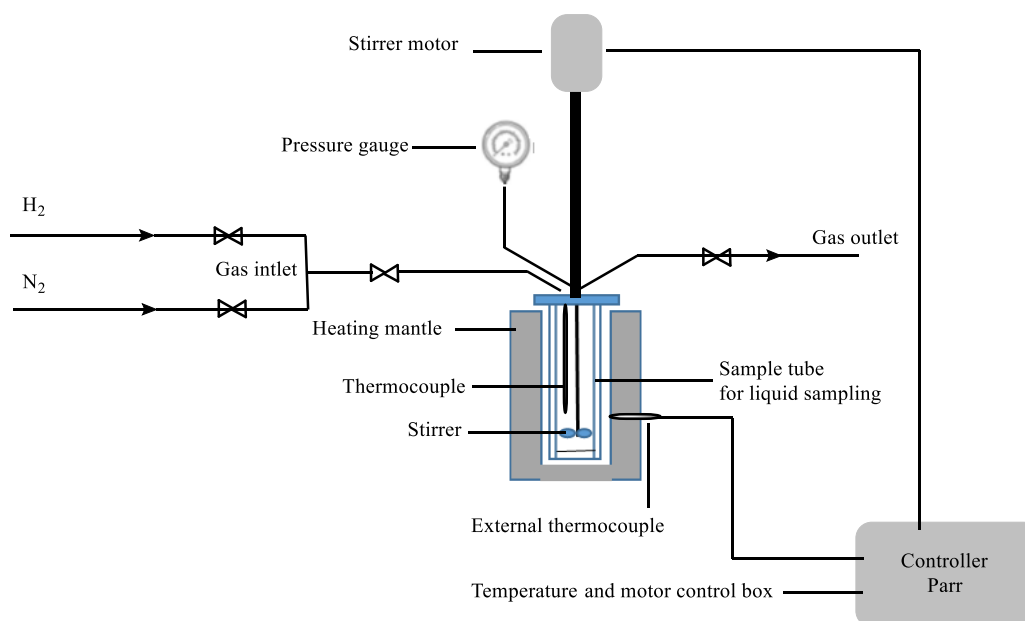


Figure 2.3: Schematic representation of the high-pressure autoclave reactor.³

This reactor is equipped with a mechanical stirrer capable of reaching 2000 rpm, as well as a Type J thermocouple, for the reactor temperature measurement. The reactor is

designed such that it has a heating device housing the stainless-steel reaction compartment and a digital control box, "4848 reactor controller", to monitor and control the pressure, stirring rate, and temperature.

For typical hydrogenation of HMF reaction with 5 wt. % Pt/HAP catalyst, the catalyst (0.04 g), HMF (0.2 g) and 20 ml methanol were added to the liner. The reactor was equipped with a mechanical stirrer and sealed. The molar ratio of the metal to the substrate is maintained at 1:155 in all the reactions. The autoclave was purged three times with nitrogen gas (0.5 MPa) and three times with hydrogen gas (0.5 MPa), after which the reactor was pressurised with 20-bar of hydrogen pressure or as necessary. The mechanical stirrer was turned on (approximately 100 rpm) to ensure effective local mixing while the reaction mixture was heated to achieve the set temperature of 120 °C, after which the remote stirring rate was increased to 1000 rpm. The hydrogenolysis reaction was considered to have officially started once the temperature plateaued at 120 °C, which was also designated as the reaction start time. At the end of the reaction, the reactor was cooled in an ice bath to 5 °C, the reaction mixture was filtered using 0.45 µm PTFE syringe filters to separate the catalyst from the liquid phase and the liquid phase analysed by GC. The aliquot was prepared as described in the previous section and the catalyst was recovered, washed and characterised.

2.5 Stability of the catalyst

After a typical catalytic cycle and due to the effect of solvent, temperature and pressure employed during a reaction, some supported catalysts become deactivated because of leaching and/or poisoning.⁴ Catalyst stability is one of the most important factors when considering industrial applicability.

2.5.1 Reusability of the catalyst

The purpose of these experiments is to evaluate the performance of the catalyst after repeated use in order to assess its reusability. Under the same standard reaction conditions, multiple testing was carried out and the catalyst was retrieved after each reaction by centrifugation. The recovered catalyst from the reaction mixture was washed two times with isopropanol for FF hydrogenation or methanol for HMF hydrogenation, once with acetone and dried overnight at room temperature. Subsequently, the catalysts were further dried at 110 °C in static air for 10 minutes, before being used for the next

reaction to make sure the acetone was completely removed. The dry catalysts were re-tested again under the same standard reaction conditions to compare their reusability by comparing the activity over each cycle to the previous one. To maintain the same weight of the catalyst for each cycle, two reactions were carried out at the same time under the same condition, and the catalyst was collected for the next reaction.

2.5.2 Determination of the quantity of metal(s) in a catalyst

The quantity of metal(s) in the precursors and the catalysts before and after reactions were determined using Microwave Plasma Atomic Emission Spectroscopy and Inductively coupled plasma-mass spectrometry.

2.5.2.1 Microwave plasma atomic emission spectroscopy)

The Microwave Plasma Atomic Emission Spectroscopy (MP-AES) is a spectroscopic instrument that has been extensively used in the analysis of liquid samples to determine their quantitative elemental composition. MP-AES is a valuable resource for investigating heterogeneous catalysts after digestion of the catalyst using Aqua Regia (HCl: HNO₃, 3:1). It can provide insights into the quantity of metals in the precursors and that loaded onto the catalyst, the extent of metal leaching, and the presence of catalytic poisons. The concept behind this is that when a specific amount of energy is applied to an element, one of its valence electrons moves to a higher energy state. This excited electron returns to its original state by emitting light and the resulting spectral lines reveal the distinctive electronic transitions of the element.⁵ Figure 2.4. illustrated the diagram for the emission photons process.⁶

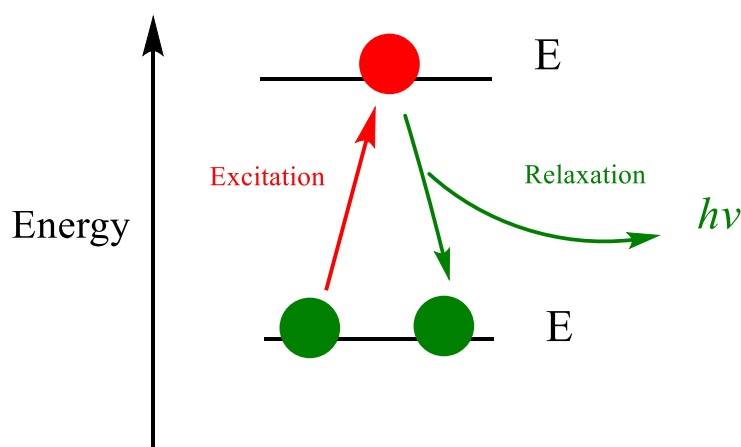


Figure 2.4: illustrates a diagram for the emitting photons process. ⁵

MP-AES makes use of the aforementioned principle for highly accurate elemental analysis of liquid samples. Nitrogen is first passed through a water trap and gas filter before reaching the torch, where it is heated to around 5000 °C by microwave radiation. This causes the nitrogen to break down and become ionized, forming a nitrogen plasma. When elements are exposed to this plasma, they are atomised and subsequently become excited and emit photons of specific energies and wavelengths that are unique to each element. The emitted light is collected and focused by mirrors in the torch chamber onto a monochromatic detector.⁵

Experimental

The elemental analysis of precursors, Pt and Ru catalysts were determined using the Agilent 4100 MP-AES. The composition was determined by analysing two emission lines and to do this, a known amount of the precursor (5 ppm, H₂O) was introduced into a nitrogen plasma stream through a single-pass spray chamber at a pressure of 120 kPa without any air injection. The instrument was calibrated using standard solutions of 2.5 ppm, 5 ppm, and 10 ppm of the element. The analysis was repeated three times for each sample, and the average of the results was calculated.

2.5.2.2 Inductively coupled plasma-mass spectrometry

Inductively Coupled Plasma Mass Spectrometry (ICP-MS) is a method that is highly sensitive and is used for the determination of the composition of materials.^{6, 7} Analyses were carried out using the Agilent Technologies 7900 ICP-MS system in conjunction with the Agilent Integrated Autosampler. It has the capability to identify trace elements at very low detection limits in parts per trillion (ppt).^{7, 8} The purpose of this technique is to determine the catalyst load for the fresh catalyst and for the recovered catalyst after each catalytic run to assess the metal leaching and reusability/stability of the catalyst. ICP-MS is a highly sensitive technique with the highest quantitation accuracy. It is an excellent atomizer and element ionizer for sample molecules or atoms, and it separates and analyses the resulting ions with the coupled mass spectrometer.⁶ The instrument works by inductive heating and this energizes the plasma source (Argon gas) with an electromagnetic coil. The energized plasma contains sufficient concentration of ions, and this plasma is sustained in a torch, consisting of three consecutive tubes and usually made

of quartz. Liquid sample sample is introduced through the central tube by a nebulizer and a solid sample can be introduced using laser ablation. The sample gets into the central channel, evaporates, molecules dissociate, and the constituent atoms ionise at the operating temperature of the plasma. The resulting ions are then sent through ion optics and separated based on their mass-to-charge ratio using a mass spectrometer that operates at room temperature in a high vacuum environment. The ions are detected and counted, allowing for the determination of the elemental composition of the sample.^{7,9} Figure 2.5 illustrated diagrammatic representation of ICP coupled to a MS detector⁶

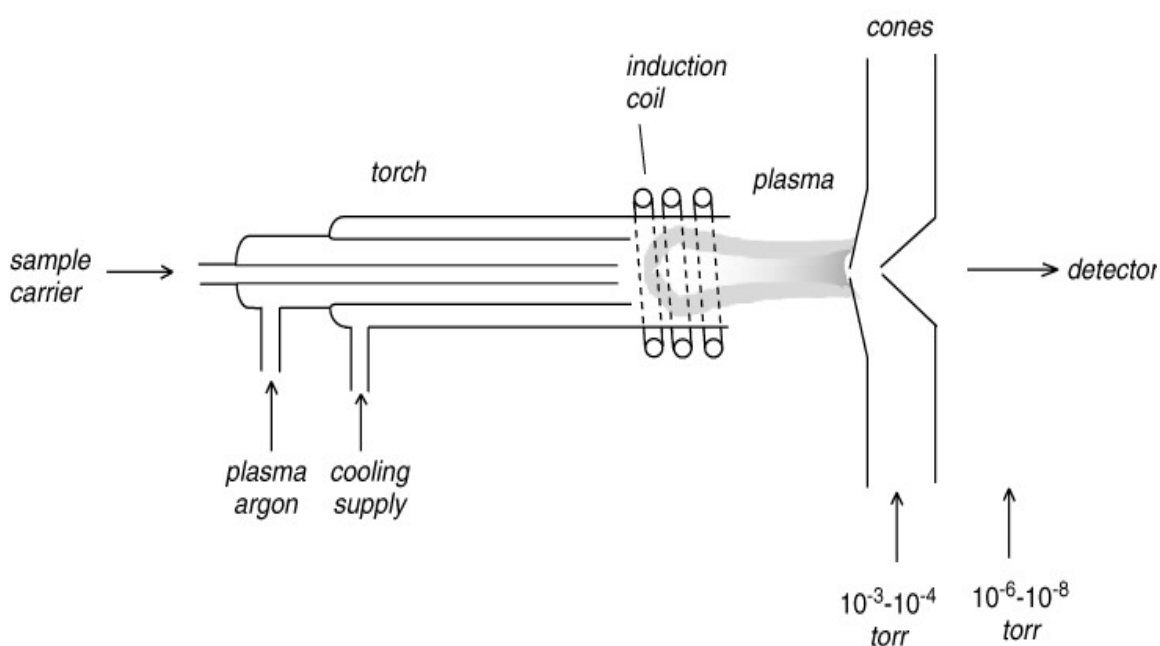


Figure 2.5: Diagrammatic representation of ICP coupled to a MS detector.⁶

Experimental

In this study, the ICP-MS method was employed to assess the elemental composition of the catalyst before and after the reaction, aiming to investigate the potential occurrence of active sites leaching during the chemical process. Elemental analysis was conducted using an Agilent 7900 ICP-MS, with samples pre-digested in Aqua Regia using a microwave reactor. The analysis was overseen by Dr. Simon Waller at Cardiff University.

2.6 Analysis techniques employed for the analysis reactions products

In this study, separation and analysis of the reaction products from the hydrogenation processes were achieved by Gas Chromatography (GC) and Gas Chromatography-Mass Spectrometry (GC-Mass).

2.6.1 Gas chromatography

Gas Chromatography (GC) is an analytical technique used for the separation and analysis of the chemical components of a sample mixture. The components are usually organic molecules that are volatile or gases.⁹ This technique was employed in the separation and analysis of catalytic hydrogenation reaction samples containing a mixture of the reaction products.

Gas Chromatography (GC) uses a carrier gas (argon, helium or nitrogen), which serves as the mobile phase (Figure 2.6). The carrier gas transports the sample through the GC system. The sample is introduced into GC inlet by a syringe via a septum. The GC column, which is a long narrow tube housing the stationary phase is connected to the inlet. This column is held in the column oven, which is heated during the analysis to ensure elution of analytes in the sample. The outlet of the column is inserted into the Flame Ionisation Detector (FID), which responds with a signal as the individual analytes elute from the column.¹⁰

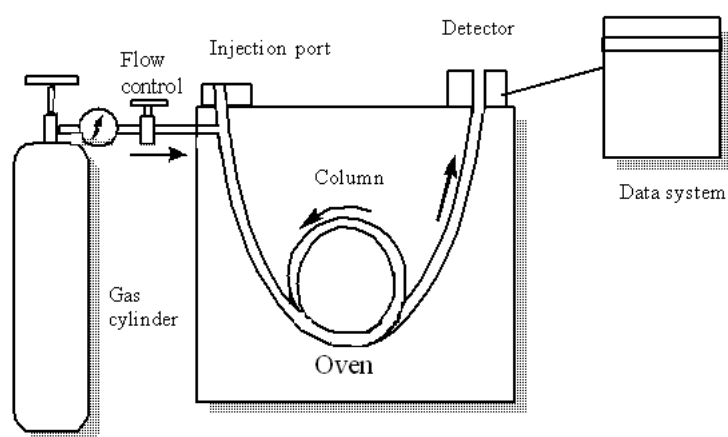


Figure 2.6: diagram illustrated the Gas Chromatography contains.

The components are separated based on the length and polarity of the column. The separation occurs due to the interaction of sample components with the column.¹⁰ The detection of sample using FID is based on sample combustion in hydrogen and air to produce cations that could be analysed. The signal is produced by the flow of electrons from the anode to the cathode, resulting in a signal corresponding to the quantity of carbon-based compounds ignited in the flame. The intensity of the flame could vary, leading to varying product areas. Consequently, a constant area ratio of the products was ensured using an external standard.¹¹

Experimental

The analyses of the reaction mixtures for FF hydrogenation reactions were carried out using Bruker scion 456-GC fitted with a RESTEK Rtx@-1 (60m, 0.32mmID) equipped with FID. The inlet temperature was set at 280°C and the column temperature is set to start at 70 °C, after which it is ramp at 10 °C / min for 2 mins. (Then the sample hold for 2 min) Then at 280 °C, the sample hold for 5 min. The total time taken was 28 mins. Table 2.2 illustrated the GC oven temperature program for the analysis of FF hydrogenation reaction products mixture.

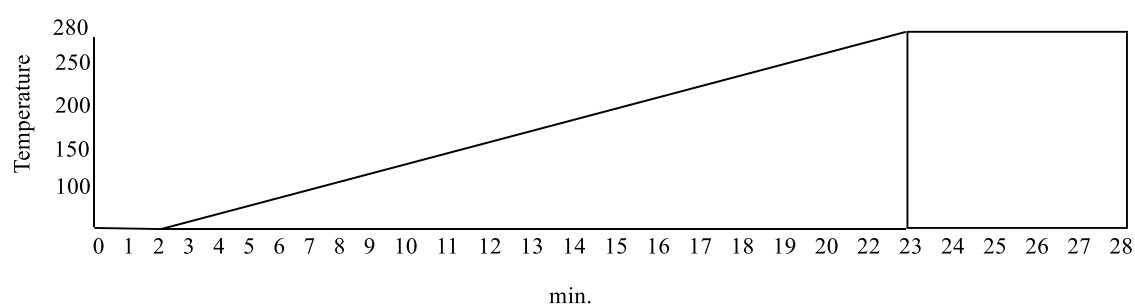


Figure 2.7: GC method for analysis of FF hydrogenation products.

Table 2.2 GC method analysis of FF hydrogenation products

Rate (°C /min)	Temp.	Time (min.)	Total
inlet	70	2	2
10	280	5	28
		Total time	28

For HMF hydrogenation sample analysis The GC parameters employed are as highlighted below. The inlet temperature was set at 280 °C and the column temperature is set to start at 50 °C, after which it is ramped at 15 °C / min for 8 mins, and then at 280 °C, the sample hold for 33 min. The total time taken was 33 mins. The GC oven temperature program for the analysis of HMF hydrogenation reaction products mixture is shown in Table 2.3.

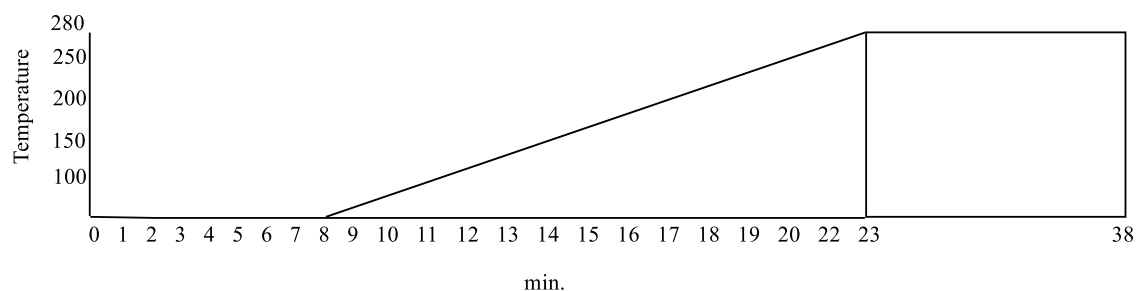


Figure 2.8: GC method for analysis of HMF hydrogenation products

Table 2.2 GC oven temperature program for the analysis of HMF hydrogenation reaction products mixture.

Rate (°C /min)	Temp.	Time (min.)	Total
inlet	50	8	8
15	280	10	33.33
		Total time	33.33

4.6.1.1 Calculations of response factors for each compound

Gas Chromatography (GC) was used to monitor the conversion of the substrates and the products selectivity (Furfuryl alcohol and 1,6-hexanediol) for the catalytic hydrogenation of FF and HMF respectively. The calibration process used to calculate the response factor for the substrates (FF and HMF) and for the expected products that may form during the hydrogenation process involved preparing known sample solutions with different concentrations of each analyte in the substrate and the product mixture that are of interest. The concentration of the prepared mixtures depended on the conversion concentration of the substrates (0%, 20%, 40%, 60%, 80% and 100%) and products. These solutions were diluted using isopropanol or methanol as solvents (using the same volume used in the

prepared of the reaction mixture) for FF and HMF respectively, with a constant mass of the external standard.

For GC analysis, each expected product that was used in the preparation of the calibration mixture and the substrate was injected alone after dilution with solvent to determine the retention time for each. The external standard used in this study were either n-octanol and propyl benzene, for FF and HMF hydrogenation respectively. For hydrogenation of Ff, samples were prepared mixing 10 ml of the products mixture reaction mixture with 0.1 ml n-octanol as external standard. The mixtures were filtered using a 0.45 μm PTFE syringe filter. Sample of reactions involving hydrogenation of HMF were prepared by adding 10 mL of each of the reaction product with 0.2 mL of the external standard (propyl benzene). After thorough mixing of all the samples prepared, 1ml aliquot of each sample was placed in a separate GC vial and subsequently injected into a GC. For accurate measurements, each sample was injected twice and an average area was used for this calculation.

The resulting GC peaks for each product were normalised to the area of the external standard and calibration plots were used to calculate the different response factors (RF). The response factor is determined by plotting the normalised area of the components to the area of the standard, then plotted against their known concentrations of the prepared solution normalised to the area of the standard.

An example of a typical calibration curve for FF and HMF are shown in Figure 2.9 and the slope of the calibration line of best fit is the response factor (RF) and can be employed to determine the quantity of an analyte in a solution. Equations 2.9 to 2.13 are employed for the determination of conversion, selectivity and yield.

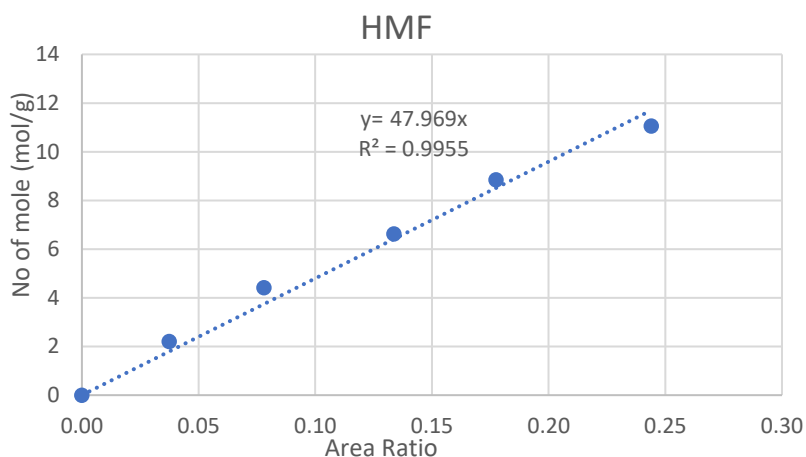
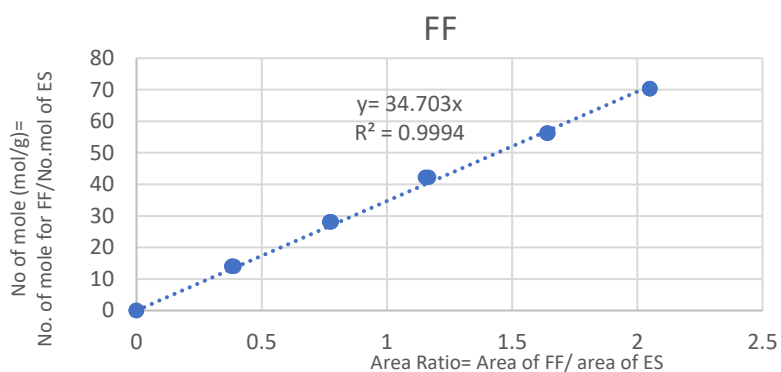


Figure 2.9: Calibration curve of a)- FF and b)- HMF at different concentrations

$$\text{Conversion (\%)} = \frac{\text{Starting moles Substrate} - \text{Remaining moles substrate}}{\text{Starting moles Substrate}} \times 100$$

Equation 2.9

$$\text{Conversion (\%)} = \frac{(\text{actual wight of substrate} \div \text{Mwt of substrate}) - \left(\left(\frac{\text{Area product}}{\text{Area Standard}} \right) \times \text{RF} \times \text{Moles standard} \right)}{(\text{actual wight of substrate} \div \text{Mwt of substrate})} \times 100$$

Equation 2.10

The selectivity of the product was computed by employing Equation 2.11

$$\text{Selectivity} = \frac{\text{Moles of Product}}{\text{Total moles of Products}} \times 100$$

Equation 2.11

$$\text{Selectivity} = \frac{\left(\frac{\text{Area product}}{\text{Area Standard}} \right) \times RF \times \text{Moles standard}}{\left(\frac{\text{Area product A}}{\text{Area Standard B}} \right) \times FR \times \text{Moles standard} + \left(\frac{\text{Area product B}}{\text{Area Standard B}} \right) \times RF \times \text{Moles standard}} \times 100$$

Equation 2.12

The product yield was calculated utilizing Formula Equation 2.11

$$\text{Yield (\%)} = \frac{\text{Selectivity} \times \text{Conversion}}{100}$$

Equation 2.13

2.6.2 Gas Chromatography-mass spectrometry

Gas Chromatography-Mass Spectroscopy (GC-MS) is a method employed to determine the chemical composition of a sample by first separating its components through gas chromatography, and then analysing its components using mass spectroscopy. The purpose of these experiments is to separate and determine the products' mass/charge ratio to identify the unknown products with their fragmentation patterns and with the aid of a library of reference. This is accomplished by directing an electron beam through the separated molecules, producing positive or negative ions/radicals. The positive ions/radicals, produced by the loss of electrons, are more commonly used than the negative ions/radicals resulting from the addition of electrons. Finally, the ions are separated according to their mass to charge ratio using either a Time-of-Flight Analyzer or a Quadrapole Analyzer.

The working principle of a Time-of-Flight (TOF) Detector is based on calculating the time taken by ions to travel from the source to the detector. On the other hand, a Quadrapole Analyzer is composed of four rods that are utilised to quantify ions. The quantification of ions can be done through either an Electron Multiplier or a Faraday Cup. The Faraday Cup is capable of detecting charged molecules with either a negative or positive charge. When these charges get to the ground electrode, they are neutralized. Molecules with higher energy levels strike the cup, generating a shower of secondary electrons that are detected due to the shape of the Faraday Cup, and then the signal is amplified. The Electron Multiplier amplifies the signal by utilising secondary electrons. The ions cause the first dynode to emit secondary electrons, which then move at a faster pace through the electric field and hit the second dynode. This leads to a significant increase in the signal, magnifying it 106 times.¹²

Experimental

Analysis was performed using a Waters GC-TOF equipped with a BPX-5 column. The ionisation method utilised in this study was electron ionisation. Prepared samples were sent for quantitative analysis at the Mass Spectrometry Laboratory of Cardiff University.

2.7 Catalysts characterisation techniques

Through this section, the fundamental concepts of certain characterisation methods utilized in this research are outlined. Thus, catalysts are characterised to provide information on the composition, morphology, and gain valuable insights on catalyst performance, optimisation, and establish a correlation between the physical properties and the activity of the catalyst.

2.7.1 X-ray photoelectron spectroscopy

X-Ray Photoelectron Spectroscopy (XPS) is one of the commonly used techniques based on the photoelectric effect for the characterisation of heterogeneous catalysts. It is a highly sensitive technique for surface analysis, and it provides valuable information about the local bonding environment of an atomic species, i.e., chemical composition, bonding energies and oxidation state(s).¹³⁻¹⁵ The local binding environment is affected by the formal oxidation state, the identity of its nearest-neighbour atoms, and its bonding hybridization to the nearest-neighbour or next-nearest-neighbour atoms. The sample surface is irradiated with X-rays which leads to the absorption of photons of appropriate energy leading to the ejection of a core electron or valence electron with kinetic energy E_k (Equation 2.14).^{15, 16} Figure 2.10 shows a depiction of ejected of photoelectron after an X-ray irradiation.

$$E_k = h\nu - E_b - \phi \quad \text{Equation 2.14}$$

Where

E_k = kinetic energy of the photoelectron

h = Planck's constant

ν = frequency of the exciting radiation

E_b = binding energy of the photoelectron for the Fermi level of the sample

Φ = work function of the spectrometer

The spectra produced display the intensity of detected photoelectrons (a.u.) versus the binding energy in electron volts (eV).¹⁵

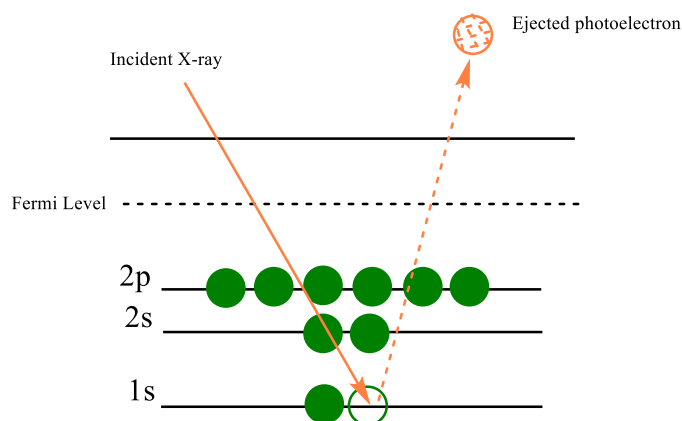


Figure 2.10: A photoelectron is ejected by an X-ray.⁵

The kinetic energy of these photoelectrons is specific to the elements and their chemical state in the material's surface layer, allowing for the identification of elements and determination of their oxidation state.¹⁷ The information depth of this technique varies between 2 and 10 nanometres, depending on the kinetic energy of the photoelectron.¹⁵

Experimental

The purpose of this characterization technique is to determine the oxidation state, percent of the metals on the catalyst (Pt/TiO₂, Ru/TiO₂, PtRu/TiO₂ and PtRu/TiO₂) and the interaction between the metal and the support. Catalysts were investigated using X-ray photoelectron spectroscopy (XPS) on a Thermo Scientific K-Alpha spectrometer. The spectrometer employed monochromatic Al radiation and with a spot size of 400 microns. Dual low energy electron and Ar⁺ neutralisation were employed, and data calibrated to the C(1s) line at 284.8 eV when necessary. All data were analysed using CasaXPS software and using Scofield sensitivity factors corrected with an energy dependence of 0.6 eV, after application of a Shirley background. All catalysts samples were evaluated at the XPS centre at Cardiff University by Dr David Morgan.

2.7.2 *Transmission electron microscopy*

Transmission electron microscopy (TEM) is a technique in which a beam of electrons is transmitted via a sample to form an image. TEM is used to create a highly detailed 2D images of small objects by high-speed electrons. This technique is employed for the determination of particle size, metal distribution and morphology of the supported catalyst.¹⁸ A schematic diagram of a typical electron microscope is shown below in Figure 2.11.⁵ In TEM high magnifications and resolutions are achieved by using a strong electric current to activate the cathode in the electron gun. The heated filament produces a high-energy beam of electrons that are directed via two solenoid coils. The first coil focuses the beam onto a thin stream, and the second focuses it onto a specific area of the sample. The process of TEM involves using the interactions of the electrons with the material to produce a magnified image of its structure. Primary electron beams are highly intense and of high-energy and pass through a condenser to create parallel rays that impinge on sample material. Since the density and thickness of the samples determine the attenuation of the beam, Electrons transmitted from the sample form a two-dimensional projection of its mass, allowing bright field images to be created using electron optics. There are lighter areas of the image that correspond to areas of the sample that were more sensitive to electron transmission (thinner or less dense) and darker areas on the image represent thicker or denser areas in the sample where fewer electrons are transmitted.¹⁸

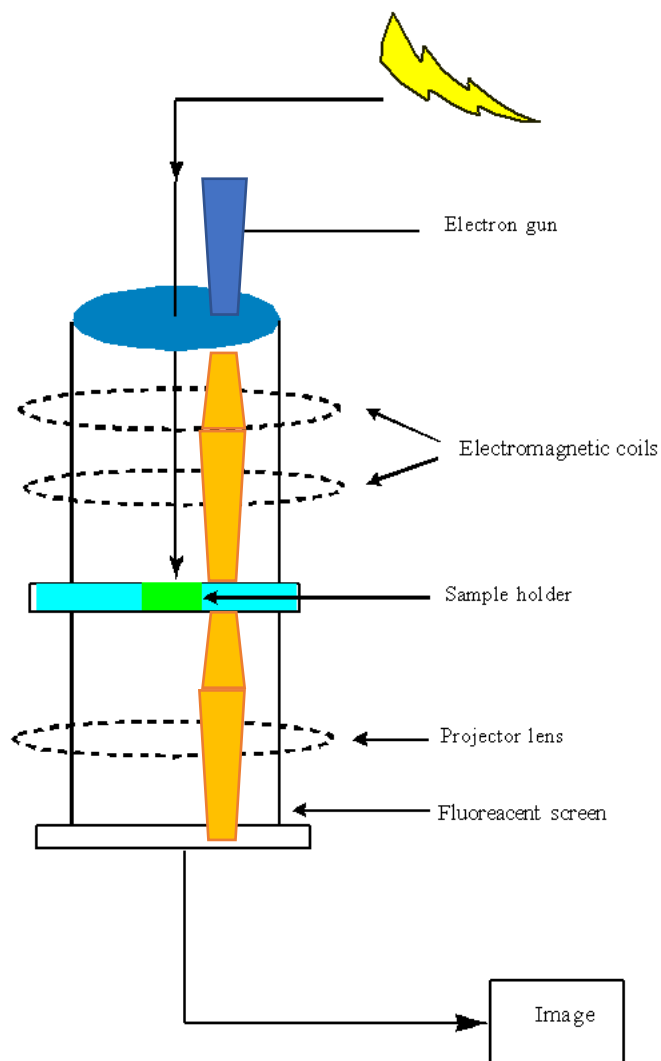


Figure 2.11: A schematic illustration of a conventional electron microscope ⁵

Experimental

TEM was used to determine the size of the metal on the catalyst surface and the distribution of metal particles. To prepare the samples for TEM analysis, they were dry-dispersed on 300 mesh copper grids which had been coated with holey carbon film. The TEM analysis was conducted on a JEOL JEM-2100 instrument operating at 200 kV. All the samples were analysed by Dr Thomas Davies, in Cardiff university.. Image J was used to determine the particle size distribution analysis by analysing the high angle annular dark field of electron micrographs.

2.7.3 *Temperature-programmed reduction*

The Temperature Programmed Reduction (TPR) technique is used to evaluate the ability of a metal oxide (MO) to reduce in a catalyst sample. This process involves heating the sample (gradually) and flowing a mixture of reducing gases over it, usually H₂ mixed with N₂ or Ar. The rate of reduction is measured by changes in the thermal conductivity of the gas consumed because of the reaction between H₂ and O₂, which indicates the concentration of hydrogen consumed by the material. The change in the hydrogen concentration detected by a thermal conductivity detector, (TCD), are displayed in the recorder. Distinct reducible species in the catalyst show up as a peak in the TPR spectrum on the recorder. This experiment permits the determination of the total amount of hydrogen consumed, from which the degree of reduction and thus, the average oxidation state of the catalyst after reduction can be calculated.¹⁹

The catalyst samples are housed in quartz tubes that are surrounded by a compact electric furnace, whose temperature can be linearly increased. Before conducting the TPR experiment, the catalyst sample undergo pretreatment using various gas streams. Afterwards, the gas flow is changed to a mixture of 5% H₂ and 95% N₂, which passes through the thermal conductivity cell, the reactor, and a series of traps designed to eliminate reduction products. The gas then flows through the opposite arm of the thermal conductivity cell, where any reduction process is monitored by measuring the change in hydrogen concentration through changes in thermal conductivity (as hydrogen and nitrogen have vastly different thermal conductivities). The variation in H₂ concentration is documented by a recorder. Given that the gas flow remains constant, the change in H₂ concentration is directly proportional to the rate of catalyst reduction, resulting in distinct reductions.

With this method, it is possible to compare the reducibility profiles of different catalysts, which may be able to explain differences in activity and selectivity that can be attributed to the surface structure.¹⁰

Experimental

TPR was employed to evaluate the reduction behaviour of Pt/TiO₂ under different heat treatment used (reduction-only or calcined followed by reduction) during catalyst sample preparation.

The catalyst (0.5 g) was enclosed in quartz tubes surrounded by a small electric furnace and was pretreated under He gas for 60 minutes at 150 °C. This step cleans the surface of the catalyst by remove any impurity before the actual experiment, TPR, commences. When the sample is ready for TPR analysis, the sample was cooled to room temperature and the gas stream is switched to 10% H₂ in Ar. This gas passes through one arm of the thermal conductivity cell where it is heated with a heating rate of 5 °C/minute to 800 °C. The TPR analysis was performed using a Quantachrome ChemBET instrument.

2.7.4 CO chemisorption

Pulse CO chemisorption analysis was carried out to evaluate the metal active sites and the percentage of metal dispersed. This was achieved by administering a calculated amount of reactant gas onto the sample.¹⁸ The gas that has been introduced undergoes a chemical reaction with the active site until every active site is ‘covered’ with CO. During the initial stages, it is possible that the entire CO is consumed and therefore, no changes in the signal from the detector will be noticed. The measurement of the amount of adsorptive that has not been absorbed by the active metals is monitored using a calibrated thermal conductivity detector (TCD). As the sample reaches saturation, peaks representing the concentration of free CO begin to appear. The number of CO that has undergone chemisorption is calculated by subtracting the amount of reactant gas that did not react with the active sites from the total amount that was initially injected.¹⁸ The typical pulse chemisorption profile is depicted in Figure 2.12. The quantity of CO that was not adsorbed can be calculated based on the area under each peak and by relating this to the total quantity of administered CO, it becomes possible to determine the number of moles of adsorptive gas that has been absorbed per gram of sample, the proportion that wasn't adsorbed, and the mass of the sample.²⁰

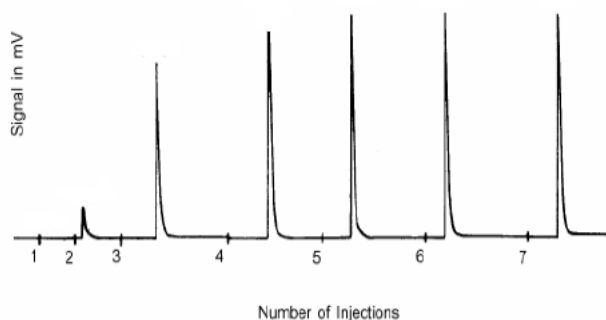


Figure 2.12: Typical output of pulse chemisorption profile. .²⁰

Experimental

CO chemisorption was conducted using a Micromeritics AutoChem II 2920 instrument equipped with a thermal conductivity detector (TCD) signal analyzer (Figure 2.13). The experiments are done in an oxygen-free environment. A sample weight of 0.05 g from (5 wt. % catalysts) or 0.08 g from (0.6 wt.% catalysts). The Pt/TiO₂ samples were inserted into a quartz u-tube between two pieces of quartz wool and pre-treated in a 10% H₂/Ar flow (50 mL·min⁻¹) for 1 h at 300 °C (10 °C·min⁻¹ ramp). Subsequently, the gas flow was changed to Ar (50 mL·min⁻¹) whilst the temperature was fixed at 300 °C to purge the system of residual H₂ for 1 h. The sample was then cooled to 35 °C using air flow and the gas flow was switched to He (50 mL·min⁻¹) to remove the excess H₂ from the system. The TCD baseline was allowed to stabilise and pulses of 1%CO/He were injected until peaks areas remained constant. A total of 10 to 20 pulses of CO were injected into the flow at regular intervals of 3 minutes until the catalyst was saturated with CO.

Particle property information (dispersion, particle size and metal surface area) were calculated following literature procedures. The dispersion (*D*) stoichiometry of CO/Pt was assumed to be 1. Particle size was calculated using the equation $d \text{ (nm)} = 1.12/D$. Platinum surface area was calculated according to the equation $\text{Surface area (m}^2\text{/g}_{\text{Pt}}) = 249.12D$.

The purpose of this experiment is to evaluate the percent of the exposed metal on the catalyst surface, the percentage of the metal active sites and the percentage of metal dispersion on the surface.



Figure 2.13: Micromeritics AutoChem II 2920.

2.8. References

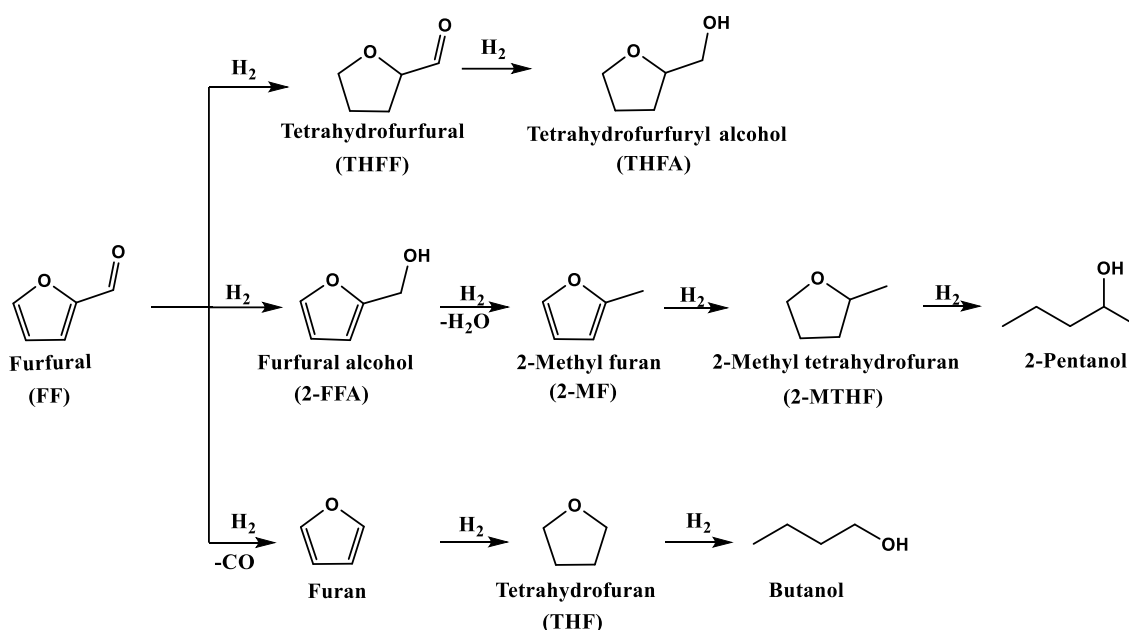
1. B. A. T. Mehrabadi, S. Eskandari, U. Khan, R. D. White and J. R. Regalbuto, 2017, pp. 1-35.
2. M. Macino, A. J. Barnes, S. M. Althahban, R. Qu, E. K. Gibson, D. J. Morgan, S. J. Freakley, N. Dimitratos, C. J. Kiely, X. Gao, A. M. Beale, D. Bethell, Q. He, M. Sankar and G. J. Hutchings, *Nat. Catal.*, 2019, 2, 1132-1132.
3. S. Guadix-Montero, PhD thesis, Cardiff University, 2019.
4. R. Redón, N. G. García-Peña and F. Ramírez-Crescencio, *Recent Pat. Nanotechnol.*, 2014, 8, 31.
5. M. Douthwaite, Cardiff University, 2016.
6. A. A. Ammann, *J Mass Spectrom*, 2007, 42, 419-427.
7. L. Balcaen, E. Bolea-Fernandez, M. Resano and F. Vanhaecke, *Anal Chim Acta*, 2015, 894, 7-19.
8. D. Profrock and A. Prange, *Appl Spectrosc*, 2012, 66, 843-868.
9. S. Guadix-Montero, PhD Thesis, Cardiff University, 2019.
10. O. Aldosari, Cardiff University, 2014.
11. D. Ambrose and B. A. Ambrose, *Gas chromatography*, George Newnes Limited, London, UK, 1961.
12. F. G. Kitson, Barbara S. Larsen and C. N. McEwen, *Gas chromatography and mass spectrometry: a practical guide*, Academic Press, USA, 1996.
13. J. Chastain and R. C. K. Jr, *Handbook of X-ray photoelectron spectroscopy*, Perkin-Elmer Corporation, , 1992.
14. P. Miedziak, PhD thesis, Cardiff University, 2009.
15. J. W. Niemantsverdriet, *Spectroscopy in catalysis: An introduction*, VCH Weinheim, 1995.
16. G. Rothenberg, *Focus on Catalysts*, 2017, 2017.
17. G. Greczynski and L. Hultman, *J. Appl. Phys.*, 2022, 132.

- .18 J. W. Niemantsverdriet, *Appendix: Metal Surfaces and Chemisorption, in Spectroscopy in Catalysis*, Wiley-VCH Verlag GmbH & Co. KGaA, 2007.
- .19 J. M. Thomas and R.M.Lambert, *Characterisation of catalysts*, A Wiley-Interscience, 1980.
- .20 P. A. Webb, *Micromeritics Instrument Corp. Technical Publications*, 2003.

Chapter 3: Chemoselective Hydrogenation of Furfural

3.1 Introduction

The conversion of biomass to renewable energy sources to replace fossil fuels with its unfavourable impact on the environment has been on the increase since the started of twenty-first century.¹⁻³ Economically viable platform chemicals that can be deployed to the production of tetrahydrofurfuryl (THF), tetrahydrofurfuryl alcohol (2-THFA)⁴, 2-methyl furan (2-MF)⁵, furfuryl alcohol (2-FFA) and other derivatives can be obtained by the selective hydrogenation of FF.⁶⁻⁸ The different pathways possible when FF is hydrogenated shown in Scheme 3.1 below.



Scheme 3.1: Schematic representation of the formation of several products during the hydrogenation of Furfural.

Although 2-FFA can be obtained from the hydrogenation of FF, the reaction is limited in selectivity to 2-FFA. This results in various by-products via hydrogenation of the of the C = C bond in the furan ring, (hydrodeoxygenation), ring opening and decarbonylation reactions. The difficulty associated with the hydrogenation of unsaturated aldehyde to alcohol has been reported in the literature.¹⁰ The production of 2-FFA on an industrial scale using FF as a substrate material and the reaction requires an elevated temperature (180°C), a copper chromite catalyst and a pressure of 70 to 100 bars.^{10, 11} However, a by-product of the chromite catalyst is chromate which has been reported to be environmentally harmful due to its toxicity.¹⁰ Consequently, numerous research efforts have been directed to the design and synthesis of catalysts capable of achieving the desired selectivity without toxic by-products for this process.

Pt-based catalysts have been reported to offer greater selectivity when hydrogenating the aldehyde group in FF, researchers have sought to enhance Pt catalysts by incorporating promoters, alloys, and improving Strong Metal-Support Interaction (SMSI) which has been previously reported to improve the catalyst activity.^{12, 13} Platinum nanoparticles (Pt-NPs) supported on TiO₂ or Nb₂O₅ have been found to be efficient in the formation of 2-FFA due to the Interaction between Pt-NPs and the supports.¹⁴

Previous research in FF hydrogenation has confirmed that the catalyst performance is affected by the reaction media while product distribution is governed by several factors including the choice of solvent, the reaction conditions, support, catalytic metal and metal particle size.¹⁵ The rate of hydrogenation can be increased by using alcohols as solvents. For instance, the adsorption of FF on the catalyst surface was found to be enhanced by alcohol solvents because they activate the hydrophilic carbonyl bonds in FF.¹⁶ However, this can result in undesirable side reactions like FF acetalization or esterification when solvents such as isopropanol, ethanol or methanol are used.^{17, 18} Equally, using solvents that are non-polar has the effect of suppressing the formation of such by-products with lower reaction rates of FF hydrogenation.¹⁹ The use of non-polar solvents has been reported to reduce conversion, possibly because hydrogen is less soluble in such solvents.^{16,17} There are additional significant developments in the selectivity profile, with water causing FF to be rearranged and resulting in cyclopentanone.²⁰ A complete conversion with 98% selectivity has been reported by the Fulajtárova group with water as the solvent in the presence of Pd–Cu/MgO catalyst.²¹

Every stage of the catalyst synthesis process offers the opportunity to tune the structural features of the catalyst in order to achieve the desired activity, selectivity or conversion.²² Heat treatment is an accessible way to assert control over the structural properties of heterogeneous catalysts, for example, calcination has been reported to facilitate the decomposition of metal precursors. This is followed by a gas-phase reduction to reduce the metal ions and the generation of the desired metal nanoparticles (NPs).²³

The conversion of FF to 2-FFA via chemoselective hydrogenation of the carbonyl group remain a challenging transformation due to thermodynamic and kinetic barriers.^{24, 25} From a thermodynamics and kinetics perspective, the η^4 adsorption mode make C=C more favourable for hydrogenation.²⁵ Due to these barriers, the C=C bonds are more susceptible to hydrogenation.²⁴⁻²⁸ As a result, it is critical to improve selectivity to a specific group (C=O) to

produce unsaturated alcohol while avoiding hydrogenation of C=C bond.²⁵ Pt-based catalysts and Ru based catalyst are choice candidates for this transformation as they have been reported to be active and more selective towards the aldehyde group rather than the furan ring.^{8, 25, 29} In reference to the relatively broad d-bandwidths of Pt and Ru monometallic catalysts, as well as the differing radial expansion of their d bands, the larger the band, the greater the four-electron repulsive interactions with the C=C bond, and the lower the chance of adsorption.³⁰ For this reason, achieving 100% selectivity of the carbonyl group is challenging with these monometallic catalysts.²⁵ Consequently, numerous attempts have been made to optimise these catalysts.

For selective hydrogenation of FF to 2-FFA, Pt/TiO₂ has been reported due to its strong metal support interaction (SMSI). There are reports that SMSI is beneficial because of the oxygen vacancies on TiO₂ surfaces, as well as the electron-rich metal-support interfacial sites. Nevertheless, it is less well understood how SMSI affects the catalytic hydrogenation of FF into 2-FFA. It was reported that the heat treatment protocol during the catalyst preparation using wet-impregnation method can turning the SMSI in Pt/TiO₂.²³ An SMSI effect, which results in the partial coverage of active Pt sites and a less active catalyst due to heat treatment protocol. For instance, the Pt/TiO₂ reduction-only sample at a high temperature (450 °C) causes coverage of the Pt surface by the TiO₂ overlayer. However, the calcined followed by a high-temperature (450 °C) sample reduced the support coverage of the Pt surface. Thus, for the chemoselective hydrogenation of 3-nitrostyrene to 3-vinylaniline. the calcination followed by reduction sample was found to be more active. Also, it was approved that SMSI tuning of Pt/TiO₂ catalyst is affected by loading and is related to metal particle size. Although catalytic activity of Pt/TiO₂ catalyst with lower Pt loadings (<1 wt.%) was similar to that of the calcined and reduced Pt/TiO₂ catalyst that because the coverage of the Pt surface by TiO₂ for the reduced-only catalyst was minimal.

In this work, Pt- based catalyst on different supports (TiO₂, SiO₂, CeO₂, Nb₂O₅, Carbon, MgO, HT and HAP) catalysts has been subjected to different types of heat treatment procedures namely calcination only, reduction only and calcination followed by reduction to fine-tune the active sites of the catalyst. FF is a candidate of choice because it has two reducible functional group, and it has been used extensively as substrate in chemo-selective hydrogenation reactions. It was found that the catalyst sample (0.6% Pt/TiO₂) that was calcined followed by reduction exhibited a high level of activity. To investigate how SMSI, type of heat treatment

and Pt loading affect catalyst activity, all catalyst samples were characterised with X-ray photoelectric spectroscopy (XPS). Transmission electron microscopy (TEM), and hydrogen gas-temperature programmed reduction (H₂-TPR). It was found that, there is a direct relationship between the creation of exposed Pt sites over TiO₂ support and the Pt/TiO₂ catalysts' activity.

3.2 Objectives and aims

3.2.1 Objectives

The challenges associated with the hydrogenation of FF to 2-FFA have been well reported in the literature, from poor selectivity to harsh reaction conditions. These challenges are due to the preferential hydrogenation of the C=C in FF resulting in a number of unwanted side products rather than the hydrogenation of the carbonyl group. This research work aims to develop solutions to the above challenges by investigating the influence of heat treatment techniques and metal-support interactions (MSI) on the overall efficiency of Pt-based catalysts for the hydrogenation of FF.

3.2.2. Aims

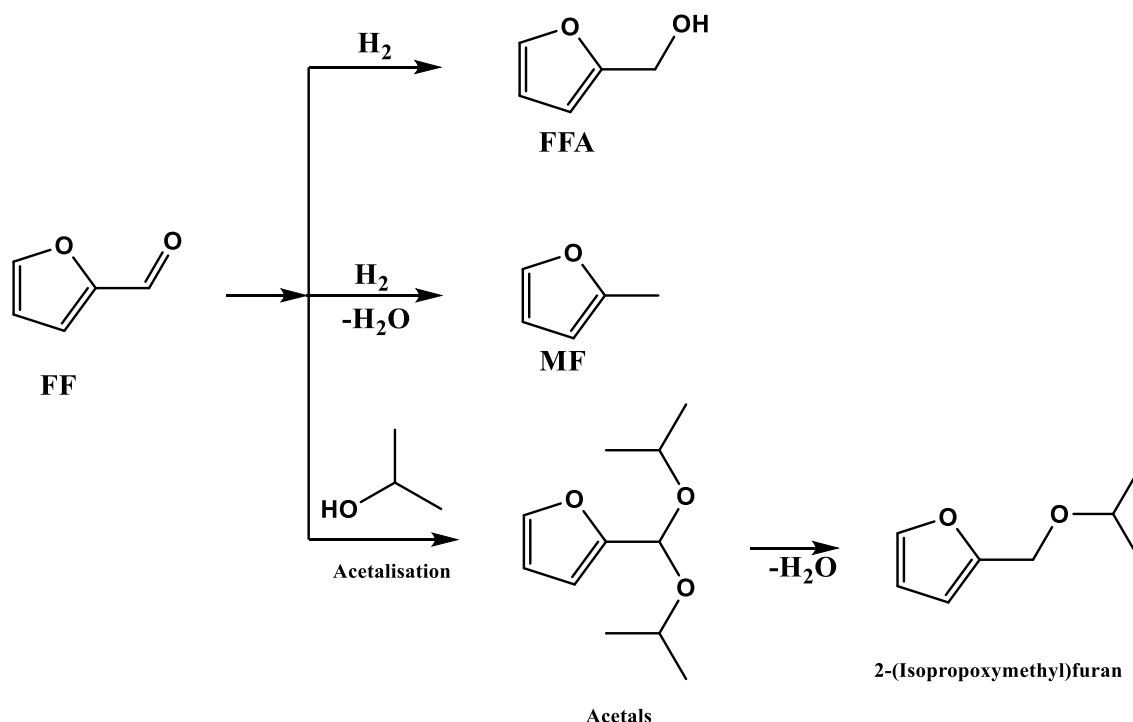
- i) Assess how the support affects the performance of FF hydrogenation
- ii) Assess how the metal particle size affects the catalyst performance.
- iii) Develop a greater understanding of the reaction profile in the effect of the heat treatment procedures on the structural property of Pt/TiO₂ catalyst and further study the effect of them on their catalytic properties during chemoselective hydrogenation of FF.

3.3 Results and discussion

3.3.1 Reducible support Vs non-reducible support

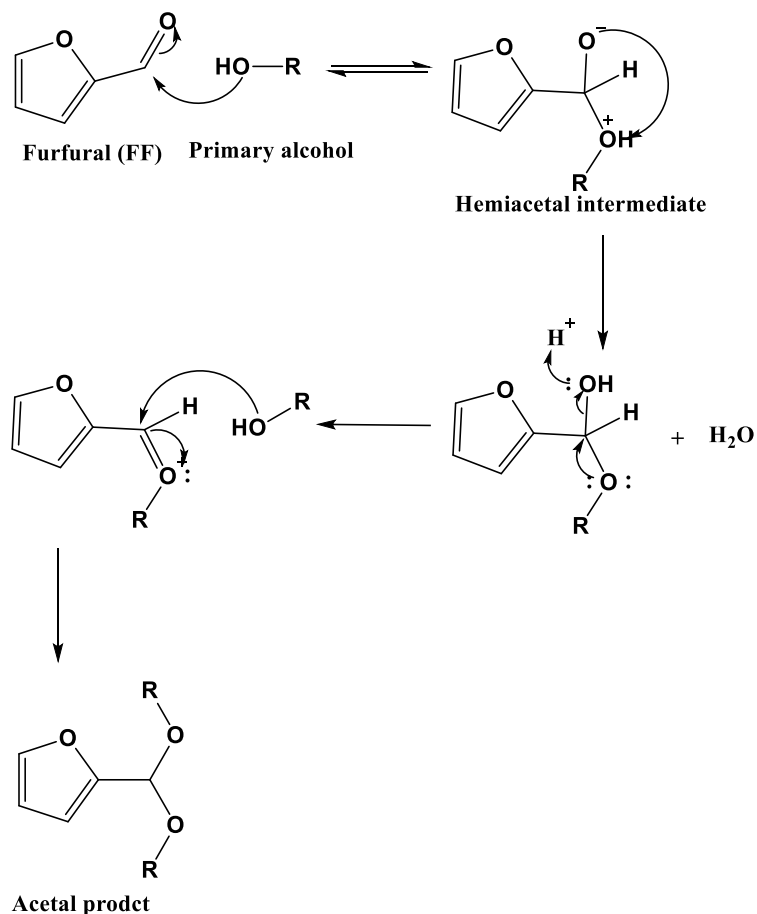
The role of the support material in increasing the activity and selectivity of heterogeneous catalysts has been well documented in chapter 1. In this work, we have utilised various metal oxides (TiO₂, SiO₂, CeO₂, Nb₂O₅, Carbon, MgO, HT and HAP as support in order to improve the selectivity of the catalyst towards the formation of 2-FFA.³¹ Reactions were carried out in the liquid phase under mild conditions at 0.3 MPa of hydrogen pressure at 30 °C using isopropanol as solvent. The selective hydrogenation products were 2-FFA, 2-MF and 2-isopropoxymethyl furan. Other potential products for hydrogenation of FF were not identified

or were only observed in trace quantities for some reactions only. Scheme 3.2 presents the reaction pathways of the products that resulted from the FF hydrogenation using our selected catalysts. As provided in previous studies, 2-isopropoxymethylfuran formed during this reaction due to acetalisation between FF and the solvent (isopropanol).^{19, 32-35} Furthermore, the side solvent product was generated due to acidity left on the catalyst after impregnation.³⁶



Scheme 3.2: Reaction Pathway for FF Hydrogenation

On the roles and effects of solvents, many studies have reported the formation of acetal resulting from the coupling of FF with alcohols (protic polar solvents).^{19, 37, 38} The acetal formation mechanism was proposed by Taylor research³⁹ as illustrated in Scheme 3.2. It was found that the coupling reaction is thermally driven and for this reason, lowering the reaction temperature helps to reduce the acetal products.¹⁹ Taylor research observed that when the reaction temperature decreased from 70 °C to 50 °C, the formation of the solvent product decreased.



Scheme 3.3: The mechanism of the acetal formation in the presence of the primary alcohol with furfural. proposed by Taylor research.³⁹ where R indicates any alkyl group

A blank reaction with all the reactants was performed in the absence of the catalyst(s). This is to confirm the absence of any background activity during the hydrogenation reaction of FF. It was found that, after 3 h reaction, the blank reaction gave 0 % conversion.

All the catalyst samples were prepared using the wet impregnation method as reported in Chapter 2, and MP-AES was used to determine the actual weight loading of the catalysts, and the results are presented in Table 3.1.

Table 3.1: Difference between theoretical loading and actual metal loading (wt. %)

Catalyst	Prepared load (wt.%)	Actual loading (wt.%)
Pt/TiO ₂	4.5	4.2
Pt/Nb ₂ O ₅	4.5	4.3
Pt/CeO ₂	4.5	4.3
Pt/SiO ₂	4.5	4.0
Pt/C	4.5	4.5

Determined by MP-AES

The first liquid-phase hydrogenation of FF was carried out using a 4.2% Pt/TiO₂ calcined-only catalyst. The 4.2% Pt/TiO₂ catalyst was calcined in air at 450 °C for 4 h before being tested. As shown in Figure 3.1, 4.2% Pt/TiO₂ Calc-only catalyst presented 90 % conversion with (42%) selectivity for 2-FFA after 6 h. The 2-FFA conversion was high with Calc-only catalyst, while selectivity improvements are still needed. Also, 4.3% Pt/Nb₂O₅ Calc-only catalyst was tested under the same reaction conditions. Only 11% conversion and 23% selectivity to 2-FFA were achieved with 4.3% Pt/Nb₂O₅ Calc-only. These results suggest that PtO_x particles formed during the calcination process are not selective towards 2-FFA. The catalyst sample with 4.2% Pt/TiO₂ prepared by Red-only using 5% H₂/Ar at 450 °C for 4 h was then tested for the hydrogenation of FF under the same reaction conditions. The catalyst achieved a 25% conversion and 90% selectivity after 6h reaction which is lower than the Calc-only catalyst. Similarly, 4.3% Pt/Nb₂O₅ Red-only catalyst achieved 54% conversion and 77% selectivity towards 2-FFA. The time online for 4.2% Pt/TiO₂ red-only and 4.3% Pt/Nb₂O₅ red-only is shown in Figures 3.2 (a) and 3.3 (a). These results may be attributed to the catalysts' active sites were not available for the desired reaction and were covered by the reducible support particles, TiO₂ and Nb₂O₅ during the high-temperature reduction that they were subjected to. Also, this difference in the conversion and selectivity between Red-only catalysts compared to the Calc-only catalysts confirms how heat treatment protocols affect heterogeneous catalysts for FF hydrogenation to 2-FFA.

It has been reported that the SMSI of Pt/TiO₂ affects its catalytic activity profoundly. SMSI is affected by heat treatment (temperature, environment (oxidizing vs reducing) and metal loading). Subsequently, we have attempted to improve the catalyst activity by tuning a SMSI to increase the conversion and selectivity of the catalysts to the desired product. SMSI has been reported to occur during the high temperature reduction of the sample contain reducible support. This occurs by changes in the electron density of the clusters through polarisation or charge transfer when reducible supports are used. This is possible due to the support decorating the metal.^{40, 41} The next set of catalysts were subjected to calcination using follow air at 450°C for 4 h followed by a reduction using 5% H₂/Ar at 450 °C for 4 h (Calc + Red) before being used to drive the reaction.

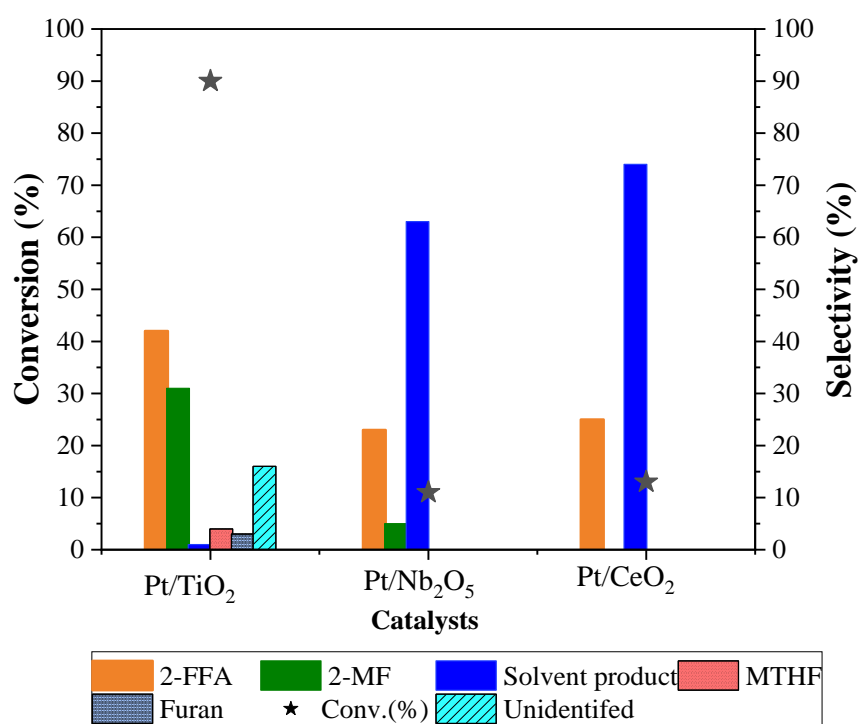


Figure 3.1: The liquid phase hydrogenation of FF over Calcined only catalysts: Pt/TiO₂, Pt/Nb₂O₅ and Pt/CeO₂ under identical reaction conditions. Reaction conditions: FF (4.45 mmol), H₂ (0.3 MPa), *i*-PrOH (15 ml), temp. (30 °C) for 6 h, substrate/metal molar ratio =207.

To investigate the performance of the catalysts subjected to both calcination followed by reduction, 4.2% Pt/TiO₂ and 4.3% Pt/Nb₂O₅ (Calc + Red) were used in the liquid-phase hydrogenation of FF. The conversion observed with 4.2% Pt/TiO₂ and 5% Pt/Nb₂O₅ are 99%

and 98% respectively after 6h (Figures 3.2 (C) and 3.3 (C)). They both showed a better activity compared to the set of catalysts (4.2%Pt/TiO₂ (Red-only) and 5% Pt/Nb₂O₅ (Red-only)) that were subjected to reduction only which achieved 25% and 54% conversion respectively after 6h. Whilst 4.2% Pt/TiO₂ (Calc + Red) had 60% selectivity for 2-FFA, the 4.2% Pt/TiO₂ Calc only catalyst exhibited low selectivity for 2-FFA (42% selectivity).

It can be noted from time online product distribution using a Pt/TiO₂ red-only catalyst and a Pt/TiO₂ calc+red catalyst. that 2-FFA and solvent product (SP) were produced using Pt/TiO₂ catalyst.

For the Pt/TiO₂ calc + red catalyst exhibited the highest selectivity (85%) for 2-FFA after 3h reaction. However, the 2-FFA selectivity gradually decreased due to the formation of the tetrahydrofurfuryl alcohol THFA after 5h of the reaction. Moreover, many byproducts were formed after 6h reaction, such as THFA and 2-MF in 12% and 9%, respectively. The formation of solvent product SP was high at the beginning of the reaction, but it gradually decreased over the reaction time, as it was 45% selectivity after 1h reaction and then reached 1% after 6h reaction.

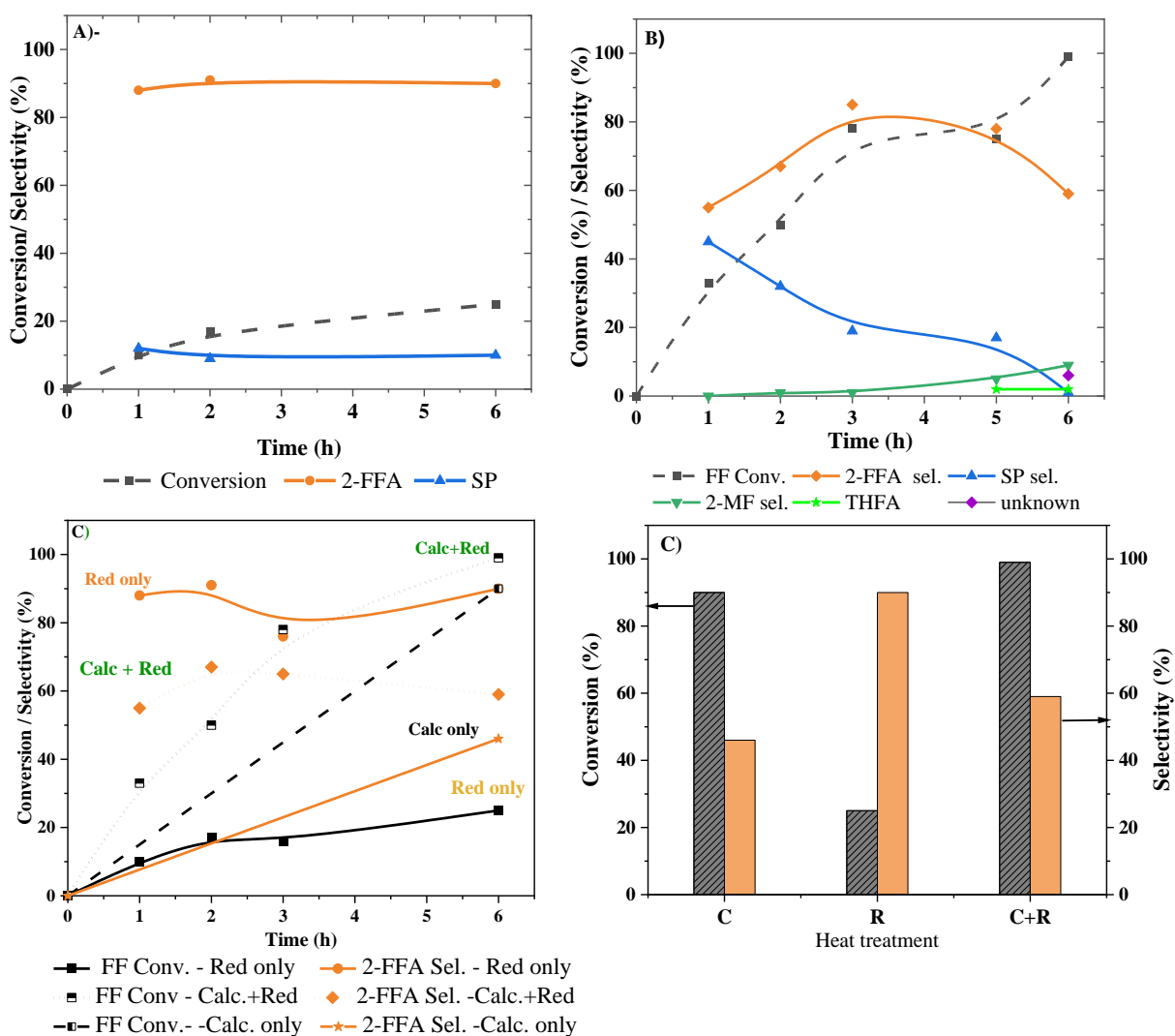


Figure 3.2: Results of the liquid phase hydrogenation of FF using 4.2% Pt/TiO₂, prepared by (A) reduction only and (B) calcination +reduction catalyst and (C) comparison between calcined only Vs reduced only Vs calcined +reduced catalyst. (D) After 6h comparison between calcined only Vs reduced only Vs calcined +reduced catalyst. Reaction conditions: FF (4.45 mmol), H₂ (0.3 MPa), *i*-PrOH (15 ml), temp. (30 °C), substrate/metal molar ratio =207.

The major product using 4.3% Pt/Nb₂O₅ Red only and 4.3% Pt/Nb₂O₅ cal + Red catalyst after 6h of reaction was 2-FFA from the liquid phase hydrogenation of FF. Accordingly, the only products formed over these catalysts were 2-FFA, 2-MF and SP. 4.3% Pt/Nb₂O₅ cal + Red catalyst activity was increased over time, as it increased from 34% conversion, 84% 2-FFA

selectivity after 1h to 98% conversion to 93% 2-FFA selectivity after 6h. however, the solvent product was 16% after 1h reaction and decreased to 5% after 6h reaction.

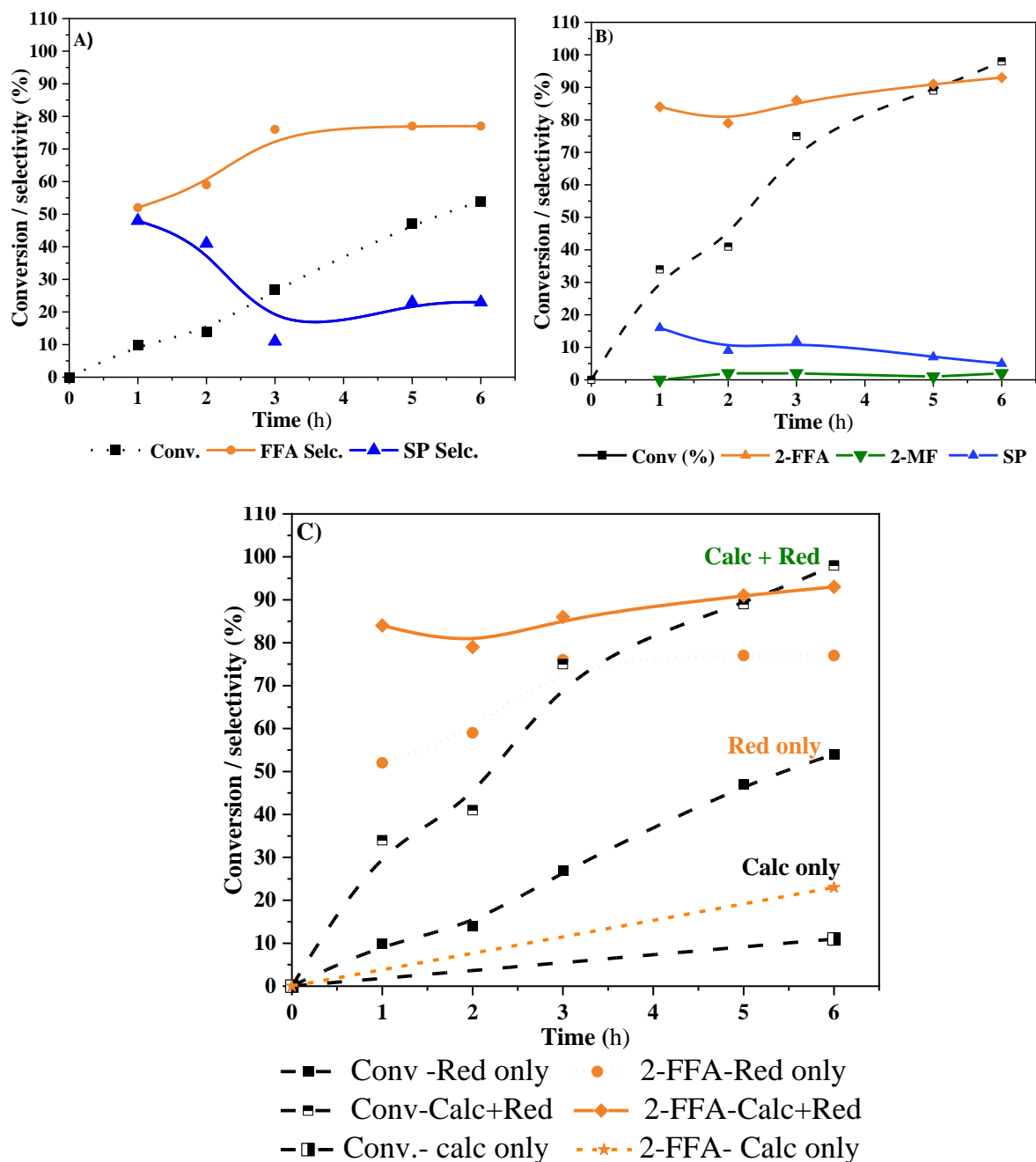


Figure 3.3: Results of the liquid phase hydrogenation of FF by 4.3% Pt/Nb₂O₅ prepared by (A) reduction only, (b) calcination +reduction catalyst and (C) comparison between reduction only Vs calcination +reduction catalyst. Reaction conditions: FF (4.45 mmol), H₂ (0.3 MPa), *i*-PrOH (15 ml), 30 °C, substrate/metal molar ratio =207.

The difference between the activity of 4.3 % Pt/CeO₂ (Red-only) and 4.3% Pt/CeO₂ (Calc + Red) catalysts is subtle, however, 4.3% Pt/CeO₂ (Calc-only) achieved low conversion at 13% (Figure 3.4). This result may be attributed to the competitive side reaction between FF and isopropanol, the solvent used.¹⁹

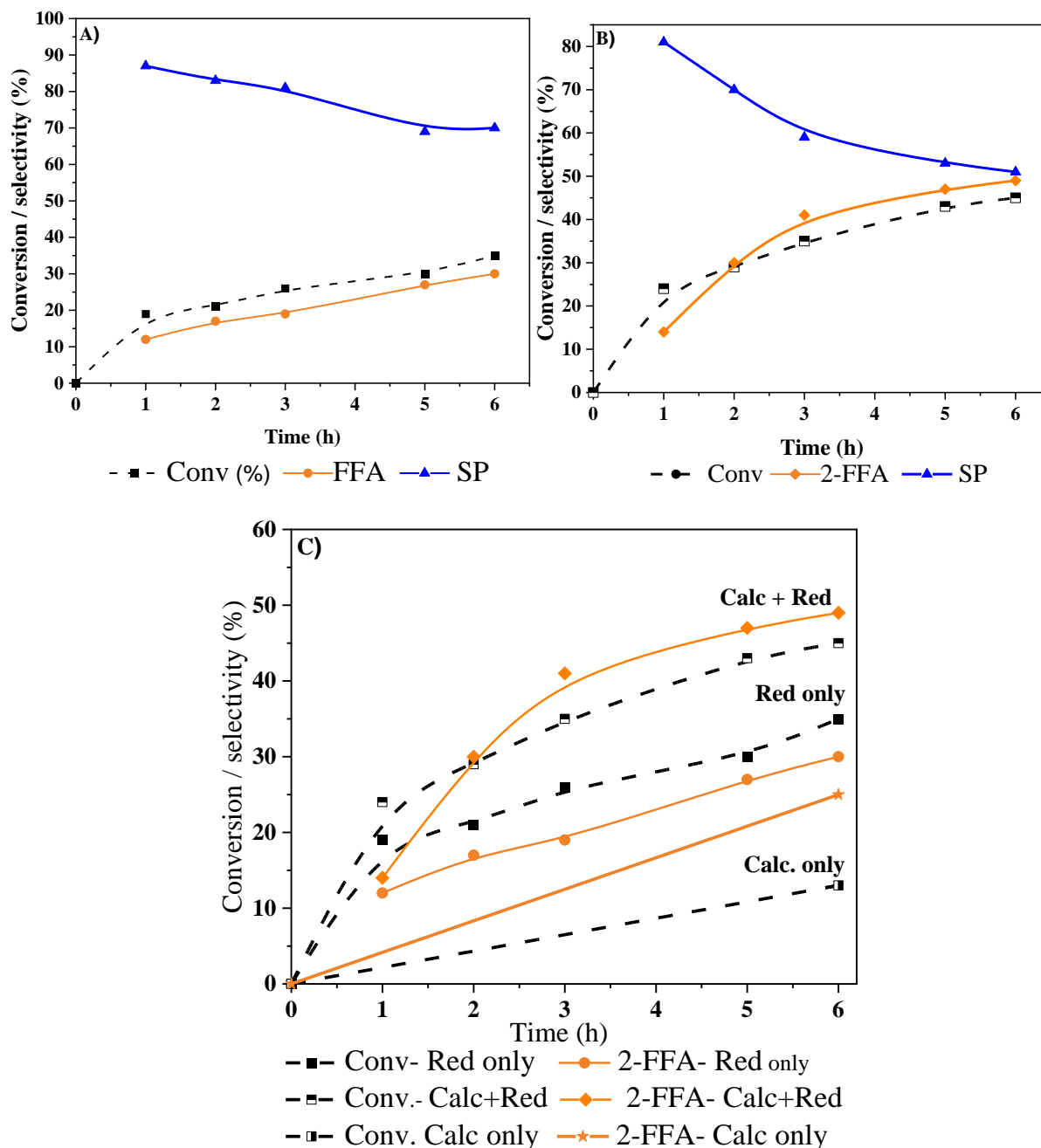


Figure 3.4: Results of the liquid phase hydrogenation of FF by 4.3% Pt/CeO₂ prepared by (A) reduction only, (b) calcination + reduction catalyst and (C) comparison between reduction only Vs calcination + reduction catalyst. Reaction conditions: FF (4.45 mmol), H₂ (0.3 MPa), *i*-PrOH (15 ml), 30 °C, substrate/metal molar ratio =207.

The chemoselective hydrogenation of FF on inert supports such as SiO₂ and carbon (where SMSI are not expected to occur) was carried out. Figures 3.5 and 3.6 show the results obtained for the hydrogenation of FF by 4.5% Pt/C and 4% Pt/SiO₂, respectively. The carbon and SiO₂ supports are inert and no interaction are expected between Pt-NPs and the supports as previously reported.^{40, 41} Consequently, both the Red-only and Calc + Red catalysts exhibited the same activity.

The 4.5% Pt/C Red-only showed 40% conversion with 43% FFA selectivity whilst the catalyst calcined followed by reduced showed 39% conversion with 63% of 2-FFA selectivity after 5h reaction. On the other side, the conversion using 4% Pt/SiO₂ Red-only and Calc + Red catalysts exhibited the same activity (51% and 38% 2-FFA selectivity with 50% and 34% of 2-FFA selectivity respectively after 5h reaction).

This confirms that the performance of these sets of catalysts cannot be improved by calcination followed by reduction. Time online plots for 4% Pt/SiO₂ Red and 4% Pt/SiO₂ calc +red are shown in Figure 3.5 (a) and (b). The major selectivity over these supports was 2-FFA. However, there were many side products observed in trace amounts including THFA, 2-MF, SP and MTHF. On the other side, Figure 3.6 (a) and (b) display the product distribution for 4.5% Pt/C Red catalyst and 4.5% Pt/C Red+ calc catalyst. Both catalysts were more selective to 2-FFA 43% selectivity for 4.5% Pt/C Red only and 63% selectivity for 4.5% Pt/C Red+ calc catalyst after a 5h reaction. Also, a trace amount of 2-MF was observed. The 2-MF selectivity was (6%) for 4.5% Pt/C Red catalyst and 3% selectivity for 4.5% Pt/C calc +red. catalyst after 5h reaction.

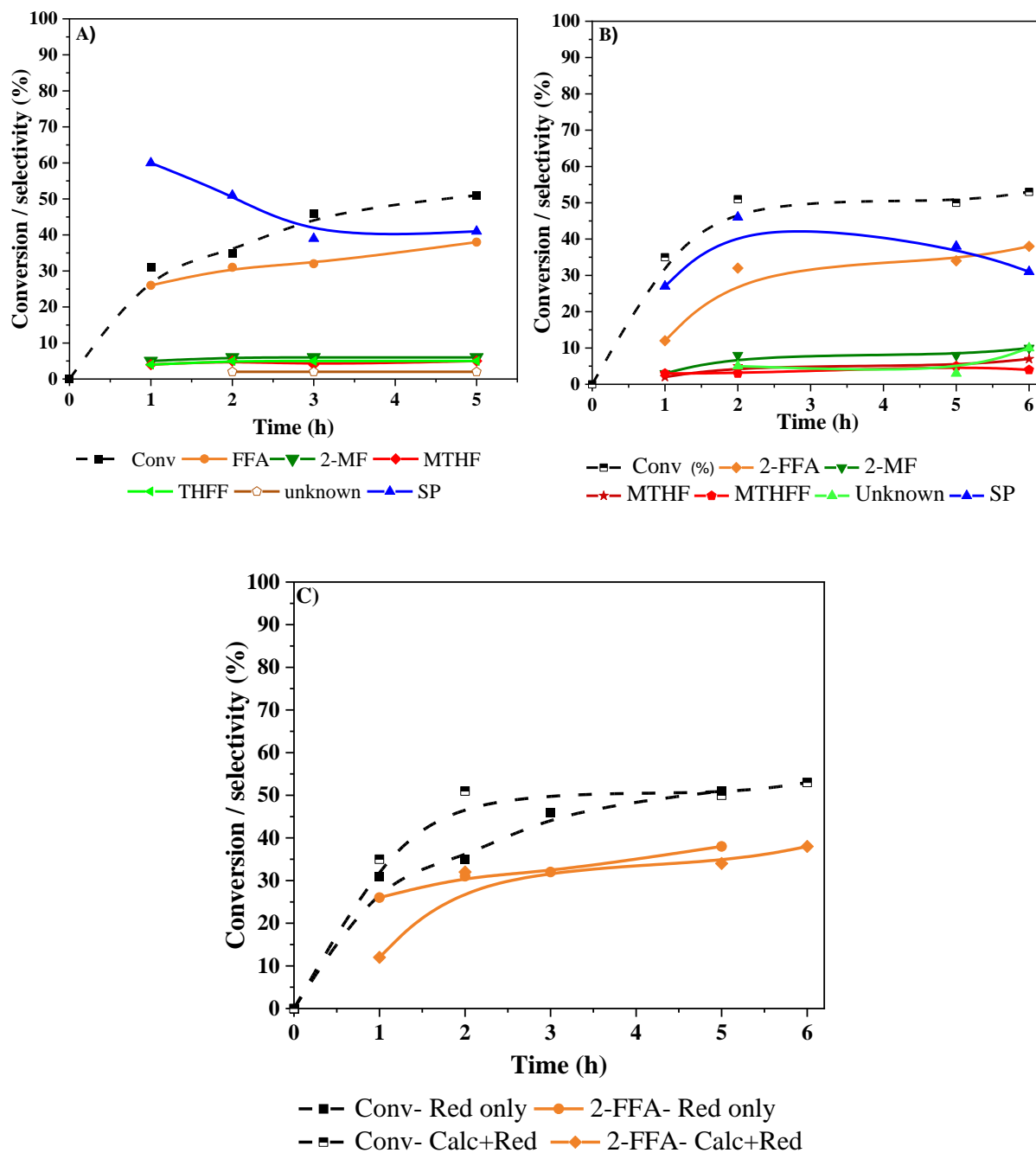


Figure 3.5: Results of the liquid phase hydrogenation of FF by 4% Pt/SiO₂ catalyst (A) reduction only, (b) calcination + reduction catalyst and (C) comparison between reduction only Vs calcination + reduction catalyst. Reaction conditions: FF (4.45 mmol), H₂ (0.3 MPa), i-PrOH (15 ml), temp (30 °C), substrate/metal molar ratio = 207.

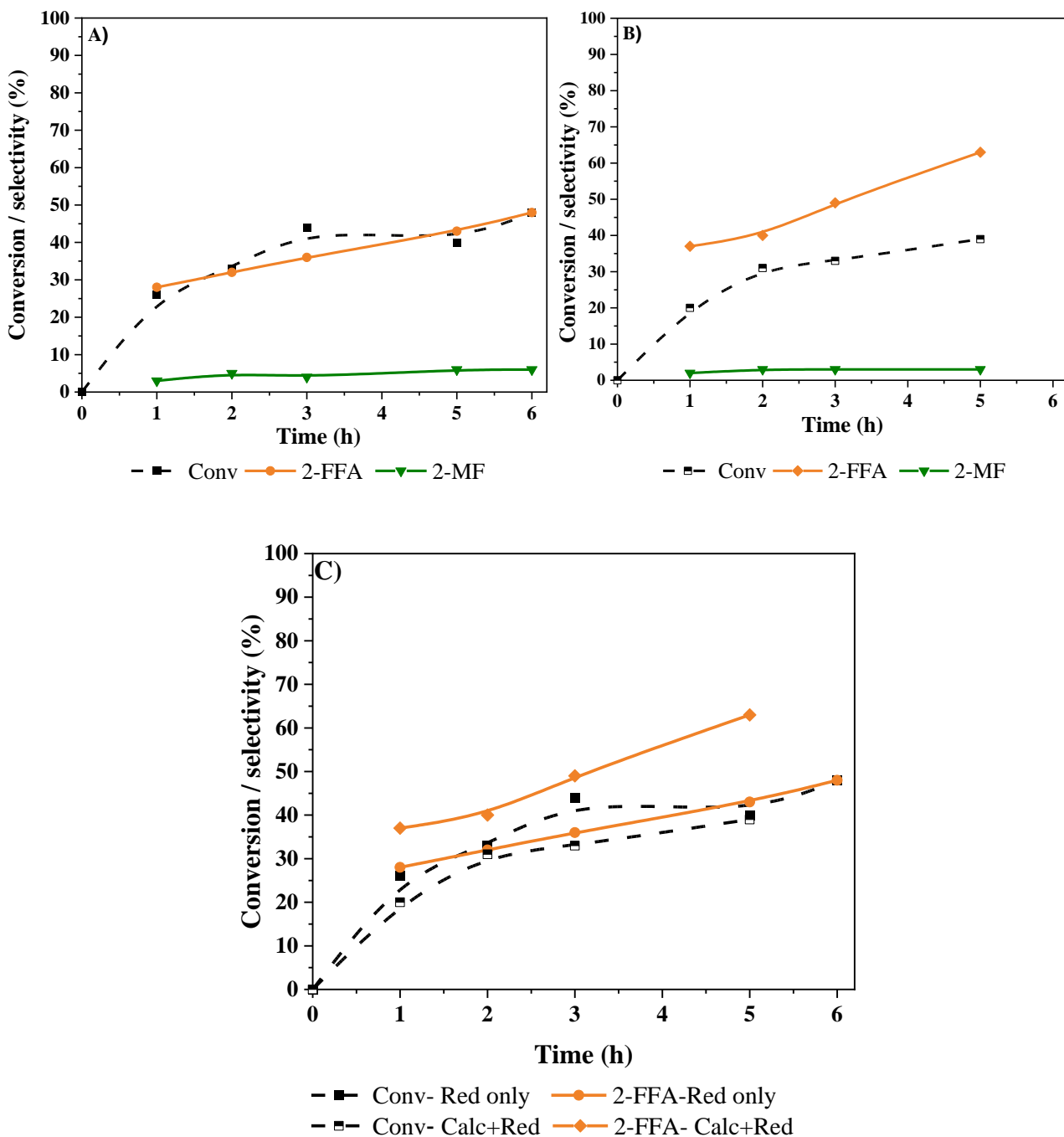


Figure 3.6: Results of the liquid phase hydrogenation of FF by 4.5%Pt/C prepared by (A) reduction only, (b) calcination + reduction catalyst and (C) comparison between reduction only Vs calcination + reduction catalyst. Reaction conditions: FF (4.45 mmol), H_2 (0.3 MPa), *i*-PrOH (15 ml), temp. (30 °C), substrate/metal molar ratio =207.

It is obvious that the heat treatment protocol affects the activities of Pt/TiO₂ and Pt/Nb₂O₅ catalysts. The Calc + Red catalyst is more active than the Red-only or Calc-only catalyst.

The formation of the side product, 2-isopropoxymethylfuran, can be suppressed by using basic catalysts because acetalization is catalysed by acid.¹⁹ To investigate this, Pt-NPs were supported on basic supports (MgO, HT, HAP), and were tested under the same reaction conditions (0.3 MPa of H₂, isopropanol, 30 °C). The results for the hydrogenation of FF by 4.5% Pt/MgO, 4.5% Pt/ HT and 4.5% Pt/HAP Calc + Red catalysts are shown in Figure 3.7.

No side reactions between FF and the solvent (isopropanol) were observed with this set of catalysts. Hence, the main products during these reactions were 2-FFA and trace amounts of 2-MF. However, the conversion over these catalysts varied between 23% - 33% for 4.5% Pt/MgO, 4.5% Pt/ HT, and 4.5% Pt/HAP respectively. These catalysts presented poor activity with high selectivity towards furfuryl alcohol. This finding suggests that the nature of the supports has a pronounced effect on the reaction pathway. These results equally suggest a strong interaction between C=O on furan and basic support which caused a lack of the active site in the catalyst. There are reports in the literature about suppressing the solvent product at low temperatures (50 °C).^{19,42}

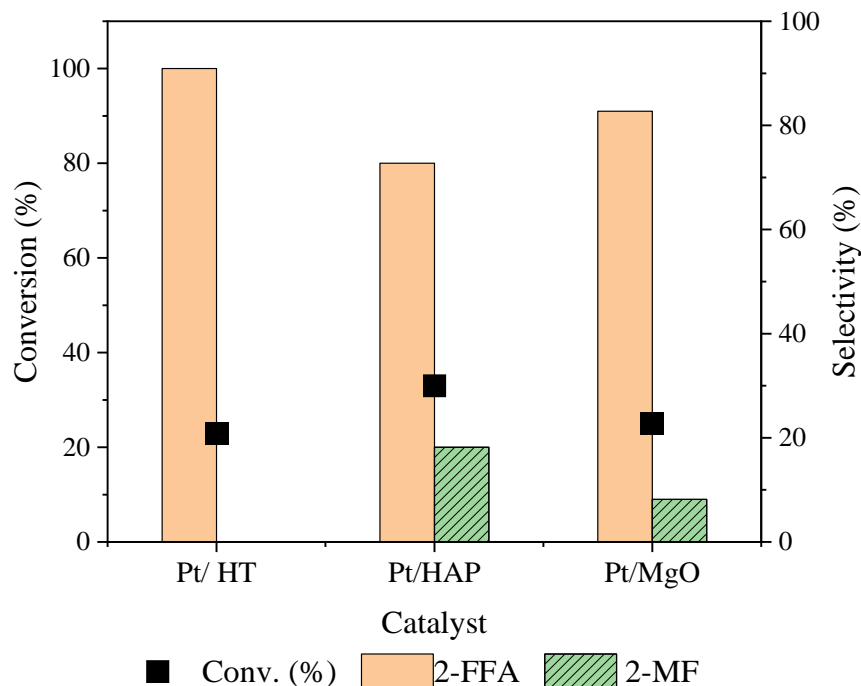


Figure 3.7: Results of liquid phase hydrogenation of FF using basic support, 4.5% Pt/HT, 4.5% Pt/HAP and 4.5% Pt/MgO Calc + Red catalysts respectively under identical reaction conditions. Reaction conditions: FF (4.45 mmol), H₂ (0.3 MPa), *i*-PrOH (15 ml), 30 °C, FF/metal molar ratio 207, 5h.

3.4 Effect of post synthesis heat treatments on the catalysts' performance

Previous research efforts have confirmed the influence of the SMSI on catalyst activity. Moreover, the selectivity of the catalyst has been found to improve if the catalyst is reduced at an elevated temperature.⁴⁰ It has also been established that catalyst conversion is inhibited by increasing the reduction temperature because of the SMSI state.¹³ Considering this, the hydrogenation of FF has been investigated for a range of reduction temperatures. Firstly, 4.2% Pt/TiO₂ catalyst was calcined at 450°C for 4 h, subsequently, the same sample was reduced at different temperatures which are: 400 °C, 450 °C, 500 °C, 550 °C and 600 °C. It was found that the sample calcined followed by reduced at 450 °C achieved the greatest conversion 78% with 87% selectivity (Figure 3.8) and as the reduction temperature increases, the conversion of FF reduces in the following order: 500 (76% with 94% selectivity) > 550 (71% with 97% selectivity) > 600 °C (70% with 98% selectivity). However, selectivity towards 2-FFA increases with an increase in the reduction temperature from 500 to 600. The increase in the

reduction temperature could be enhanced the formation of smaller particles.⁴³ The 4.2% Pt/TiO₂ calc +red 600 °C catalyst increased the selectivity towards 2-FFA. That could be because the high reduction temperature led to an increase in metal dispersion which has been reported in the literature.^{43,44,45}

All these results exhibit that the chemoselective hydrogenation of furfural to furfuryl alcohol, heat treatment impacts the catalytic properties (activity and selectivity) of 4.2%Pt/TiO₂ catalyst.

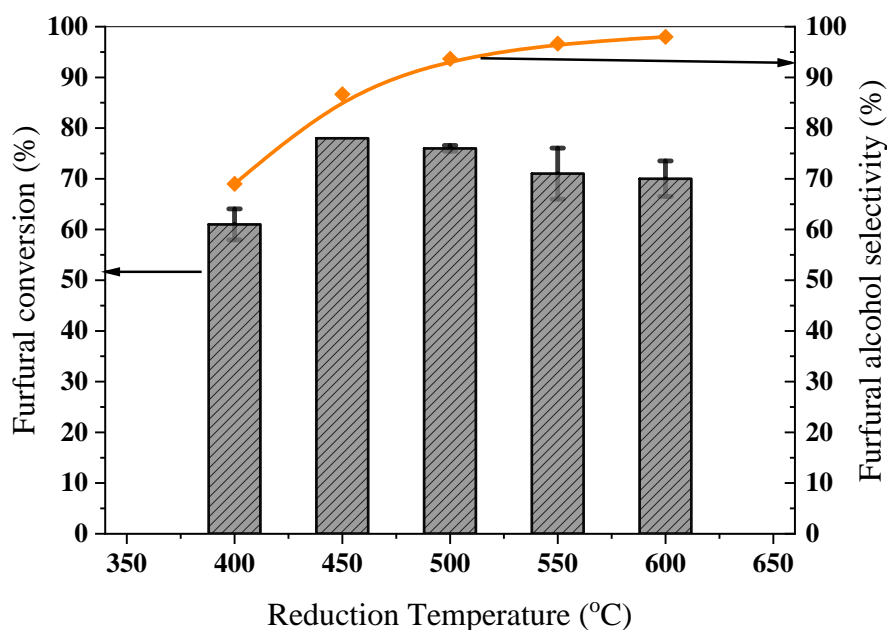


Figure 3.8: Hydrogenation of Furfural by different reduction temperatures (reaction conditions: FF (4.45 mmol), *i*-PrOH (15 mL), temp. (30°C), (0.3 MPa) H₂, substrate/metal molar ratio =207, 3h for 4.2% Pt/TiO₂ calcined at 450 °C then reduced at different temperatures 400, 450, 500, 550 and 600 °C.

To determine the effect of active metal loading on the activity and selectivity of the catalyst, a series of catalysts with various Pt loadings (2.4% Pt/TiO₂, 1.4% Pt/TiO₂, 0.6% Pt/TiO₂) which were all Calc + Red was prepared by wet impregnation. The actual weight loading of the catalysts was determined by MP-AES. The actual loadings of catalysts determined by MP-AES were 2.4% Pt, 1.4% Pt, and 0.6% Pt. This shows that the precursor was completely impregnated on the TiO₂ support during the preparation process. Consequently, the performance of the

different loadings of Pt-NPs was compared under similar reaction conditions for liquid-phase hydrogenation at 30 °C under 3 bars of H₂ pressure for 2 h with FF/metal molar ratio 207 (207 which is moles of FF / moles of metal).

The effect of active metal loading on the activities of the catalysts is shown in Figure 3.9. The performance of the catalysts revealed that the selectivity to 2-FFA and FF conversion followed the trend 4.2% Pt/TiO₂ (50% conversion with 67% selectivity) < 2.4% Pt/TiO₂ (71% conversion with 86% selectivity) < 1.4% Pt/TiO₂ (71% conversion with 89% selectivity) < 0.6% Pt/TiO₂ (81% conversion with 95% selectivity) after 2 h. Comparatively, the 4.2% Pt/TiO₂ exhibited the lowest activity after 2 h of the reaction. However, decreasing the Pt loading from 4.2% to 0.6 % improved the FF conversion from 50% to 81%. Catalyst activity decreased with an increase in the amount of Pt on the catalyst. Side products were formed and detected during this reaction, namely 2-MF and 2- isopropoxymethyl furan (solvent adduct). The solvent adduct was formed by an acetalization reaction between FF and isopropanol. The use of alcohol as a solvents has been reported to influence the size distribution of Pt-NPs in catalysts for this reaction.^{19, 29} With the decrease in the weight loading of Pt from 4.2% to 0.6%, the selectivity of the reaction to 2-FFA increased from 67% to 95% because of the reduction in the selectivity of 2-(isopropoxymethyl) furan from 32% to 4% after 2 h. Furthermore, the 0.6% Pt/TiO₂ catalyst exhibited the highest selectivity to 2-FFA and the lowest selectivity to 2-(isopropoxymethyl)furan. Tetrahydrofurfuryl alcohol (THFA) was found in trace amounts (1-3%) for the 1.4% Pt/TiO₂ catalyst.

Results from the above effect of support study show that the reducible nature of the support is crucial for the catalytic properties this could be because of the presence of the well-reported SMSI in the Pt catalysts supported on reducible oxide.

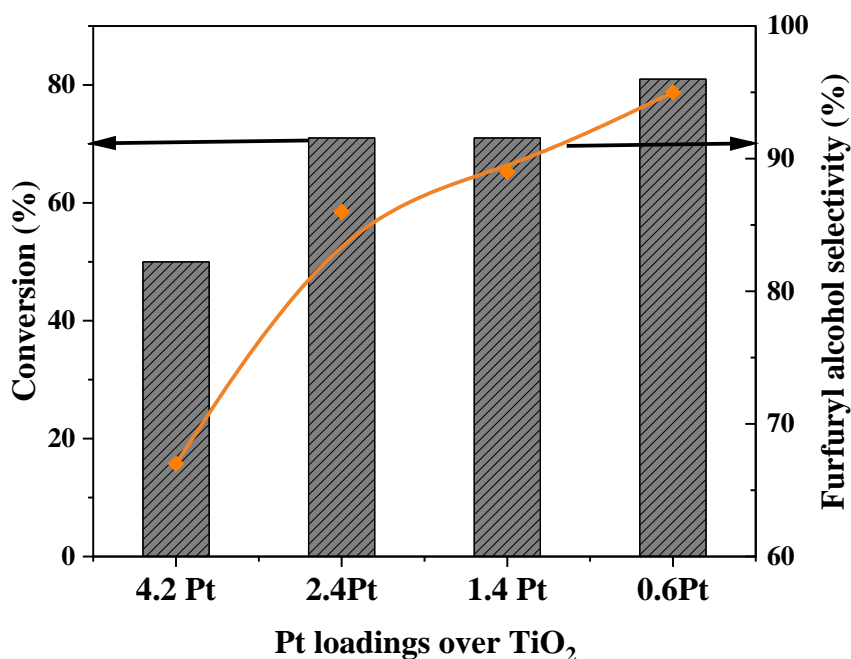


Figure 3.9: liquid-phase hydrogenation of FF by the different loads of Pt under identical reaction conditions. Reaction conditions: FF (4.45 mmol), H₂ (0.3 MPa), *i*-PrOH (15 ml), temp. 30 °C for 2 h with FF/metal molar ratio 207.

Consequently, to identify the catalyst performance over time, time-on-line was studied for 2.4% Pt/TiO₂, 1.4% Pt/TiO₂ and 0.6% Pt/TiO₂ catalysts and the results are shown in Figures 3.10, 3.11 and 3.12 respectively. In the case of the 2.4% Pt/TiO₂ catalyst, the conversion of FF was 52% after 1 h. An increase in the conversion to 100% was observed after 6 h and the selectivity to 2-FFA increased slightly from 87% after 1 h to 94% after 6 h. Equally, the solvent adduct product decreased from 13% (after 1 h) to 4% (after 6 h). These observations indicate that the side reaction between the solvent alcohol and FF is strongly influenced by the duration of the reaction. The products' distribution for hydrogenation of FF by 1.4% Pt/TiO₂ catalyst and 2.4% Pt/TiO₂ reveals that full conversions were achieved in 6 h with 2-FFA as the main product and THFA and 2-MF were produced in low selectivity (1%-4%) using 1.4%Pt/TiO₂ catalyst, while, the 2-FFA was the main product over 0.6%Pt/TiO₂. Moreover, 2-MF compound was formed over 0.6%Pt/TiO₂ in trace selectivity (1%-3%). Meanwhile, the 2-(isopropoxymethyl) furan (solvent product) formation over all different loads of Pt/TiO₂. However, the 2-(isopropoxymethyl) furan selectivity decreased in order 4.2% Pt/TiO₂ (32%)

> 2.4% Pt/TiO₂ (12%) > 1.4% Pt/TiO₂ (6%) 0.6% Pt/TiO₂ (4%) after 2h. This indicates that the selectivity for 2-FFA is strongly influenced by the particle size of the catalysts as well as the interaction between FF and the solvent. As a result, the selectivity to 2-FFA increased and that of the solvent adduct product decreased with a decrease in the Pt-NPs loading on the catalyst. This result is in line with the findings of the Agote-Aran group.²⁹ We also observed that the 0.6% Pt/TiO₂ achieved 97% conversion and highly selective to 2-FFA (95%).

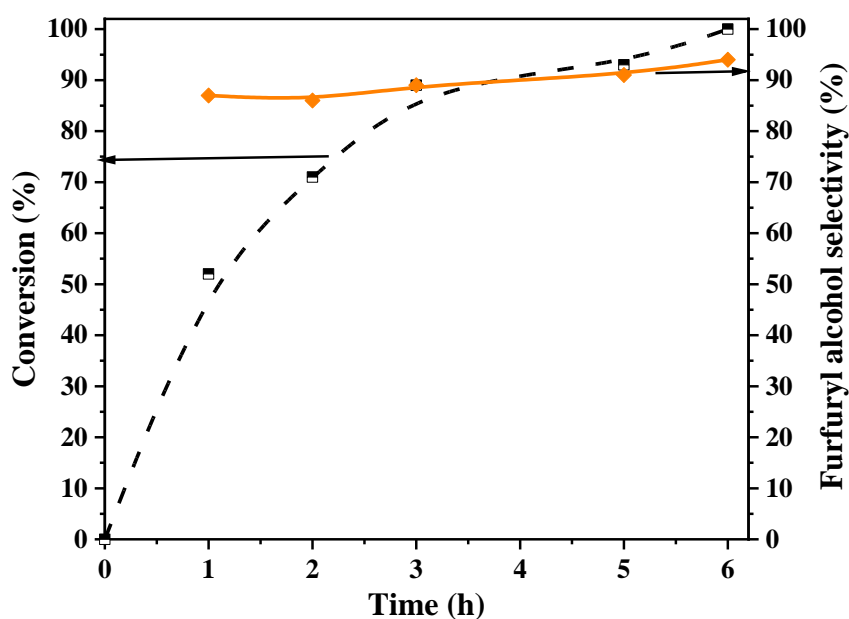


Figure 3.10: Results of the hydrogenation Furfural using 2.4% Pt/TiO₂ calc + red catalyst (reaction conditions: FF (4.45 mmol), *i*-PrOH (15 mL), temp. 30°C, H₂ (0.3 MPa), substrate/metal molar ratio =207, 6 h).

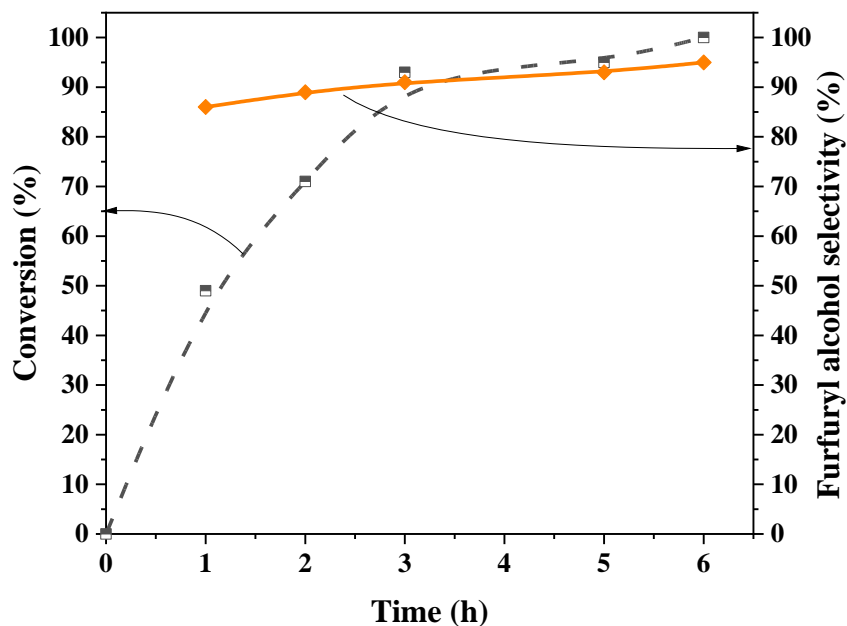


Figure 3.11: Results of the hydrogenation Furfural using 1.4% Pt/TiO₂ calc+red catalyst (reaction conditions: FF (4.45 mmol), *i*-PrOH (15 mL), temp. (30°C), H₂ (0.3 MPa), substrate/metal molar ratio =207, 6 h.

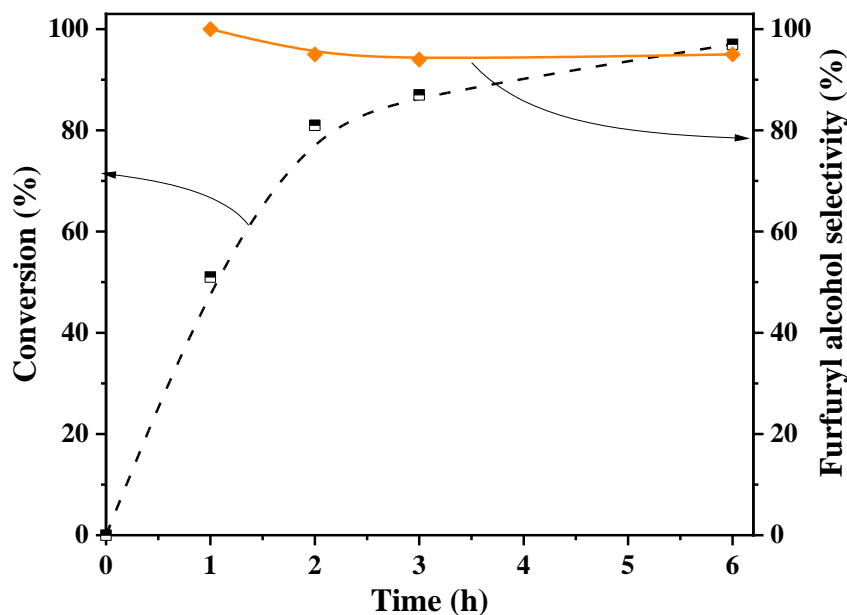


Figure 3.12: Results of the hydrogenation Furfural using 0.6% Pt/TiO₂ calc+red catalyst (reaction conditions: FF (4.45 mmol), *i*-PrOH (15 mL), 30°C, H₂ (0.3 MPa), substrate/metal molar ratio =207, 6 h.

The meaningful comparison of the Pt loadings of the catalytic activities Turnover frequencies (TOF) were detected. The results of TOFs (Figure 3.13) show 0.6 wt.% Pt/TiO₂ calc+red catalyst (83 mol_{FF} mol_{Pt}⁻¹ h⁻¹) has exceptional intrinsic activity. Comparing the TOF value with other Pt loading values 4.2%, 2.4%, 1.4 wt.%, were 52, 73, and 74 mol_{FF} mol_{Pt}⁻¹ h⁻¹, respectively. It is clear that 0.6 wt.% Pt/TiO₂ calc+red material is the most active catalyst compared to other different loads at similar reaction conditions. There were many reports of much higher TOFs in harsh reaction conditions (*i.e.*, higher temperatures, greater H₂ pressure, and higher metal loadings).^{32, 46, 47}

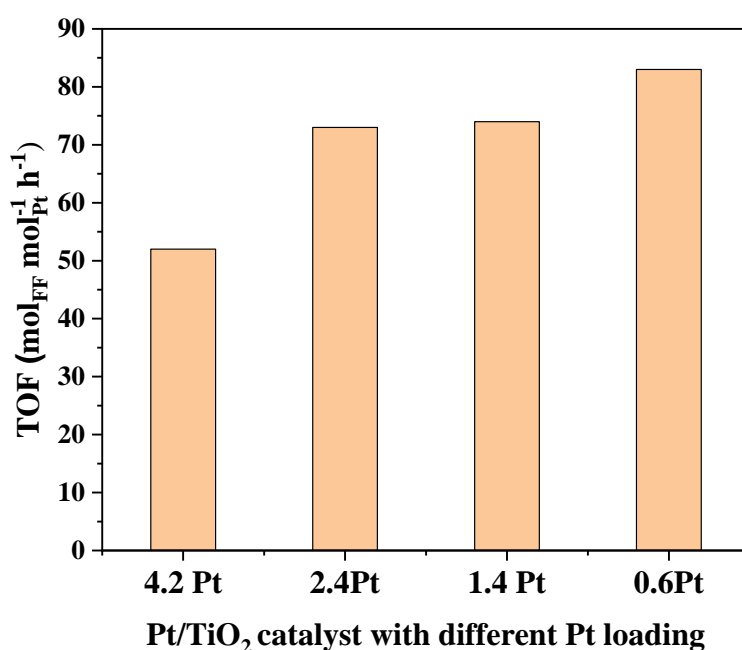


Figure 3.13: Turnover frequencies (TOF) during the selective hydrogenation of FF over Pt/TiO₂ catalysts having different Pt loadings (*i.e.*, 4.2%, 2.4%, 1.4%, 0.6 wt.%) and Effect of heat treatments (calc+red) on the activity. reaction conditions: FF (4.45 mmol), *i*-PrOH (15 mL), temp. 30°C, H₂ (0.3 MPa), substrate/metal molar ratio =207, 2 h.

The influence of the heat treatment on the 0.6% Pt/TiO₂ catalyst activity was investigated. The 0.6 % Pt/TiO₂ calc+red only catalyst (calcined +reduced at 450 °C) was compared with the 0.6% Pt/TiO₂ red catalyst (reduced only at 450 °C). The results for hydrogenation of FF at 30 °C for 6 h under 3 bar of hydrogen gas using 0.6% Pt/TiO₂ red only and 0.6 % Pt/TiO₂ calc+red only catalyst are displayed in Figure 3.14 . The conversion over 0.6% Pt/TiO₂ calc + red catalyst

(97% with 95% selectivity for 2-FFA) was higher than a 0.6% Pt/TiO₂ red only catalyst (70% conversion with 96% selectivity of 2-FFA). These results indicate that heat treatment protocols significantly affect the catalyst activity.

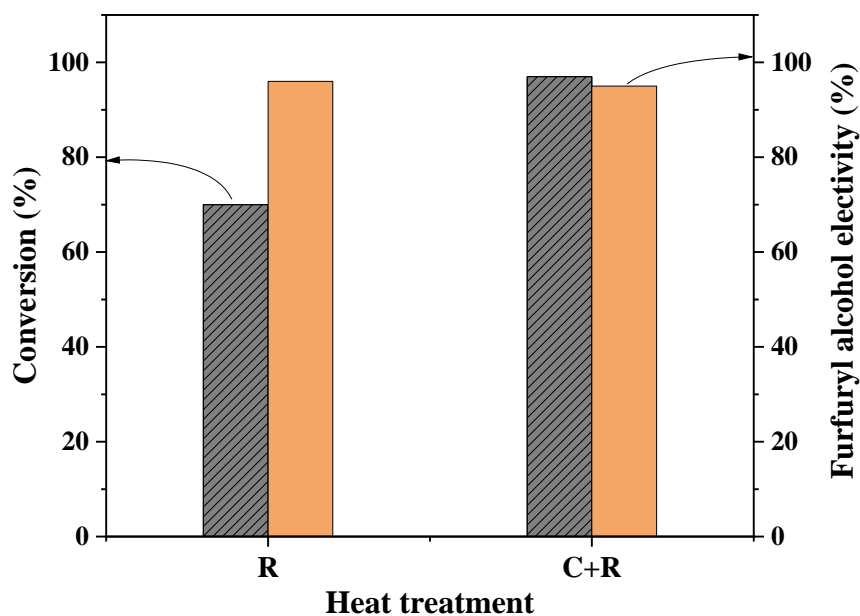


Figure 3.14: Comparison between 0.6% Pt/TiO₂ reduction only (R) vs calcination + reduction (C+R) for the hydrogenation of FF to 2-FFA at 450 °C. Reaction conditions: FF (4.45 mmol), *i*-PrOH (15 mL), temp (30 °C), H₂ (0.3 MPa), substrate/metal molar ratio =207, time (6 h).

3.5 Effect of different preparation techniques on catalytic activity and selectivity

Previous studies have reported how the preparation methods deployed for Pt-based catalysts can significantly influence catalyst performance. A change in the mean particle size is often the cause of this phenomenon.^{14, 48}. To evaluate the effects of different catalyst preparation techniques on particle size, hydrogenation of FF was conducted using 0.6% Pt/TiO₂ catalyst, which was prepared using various methods, including the sol-immobilization method described in Chapter 2. Consequently, the performance of the 0.6% Pt/TiO₂ catalyst prepared by the Sol-immobilisation method was tested for hydrogenation of FF under the same reaction conditions (*i*-PrOH 15 mL, 30 °C, 0.3 MPa. H₂). The time-online plot for this reaction is shown in Figure 3.15.

Comparatively, the 0.6% Pt/TiO₂ catalyst prepared by sol-immobilization method showed lower catalytic activity for hydrogenation of FF with low conversion (28%) and selectivity (47%) than the catalyst prepared by wet impregnation (97% conversion and 95% selectivity) after 6h of the reaction. These results indicate that the performance of 0.6% Pt/TiO₂ catalyst was poor when the catalyst was prepared by sol-immobilisation method which suggests the polyvinyl alcohol (PVA) blocked the interfacial site between the Pt NPs and TiO₂ support.

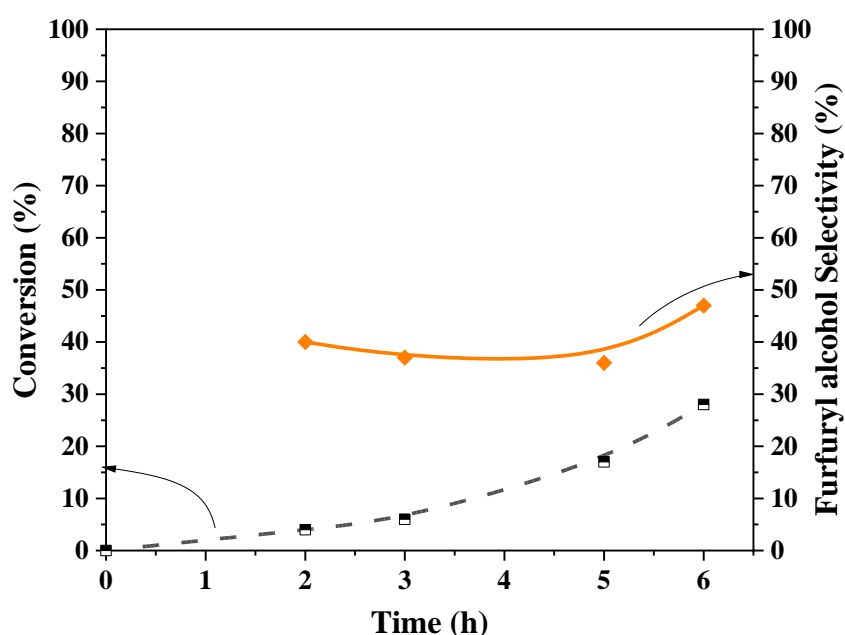


Figure 3.15: Hydrogenation Furfural using 0.6% Pt/TiO₂ prepared by sol-immobilisation method (reaction conditions: FF (4.45 mmol), *i*-PrOH (15 mL), temp. 30°C, H₂ (0.3 MPa), substrate/metal molar ratio =207, 6 h).

3.6 Reusability of catalyst

In terms of industrial applications, a good catalyst must be able to provide a high level of performance over an extended period time with minimal loss of activity and selectivity. In order to evaluate the industrial viability of the optimised catalyst designed in this study, the stability of the 0.6% Pt/TiO₂ catalyst for the hydrogenation of FF to 2-FFA was investigated under the same reaction conditions (3 h, 30°C, 0.3 MPa H₂). Three recycle reactions were carried out to check the reusability potential of the 0.6% Pt/TiO₂ catalyst. Following every

reaction cycle, a centrifuge was used to recover the catalyst and any adsorbed material on the surface of the catalyst was removed by washing using isopropanol and followed by acetone, twice. The catalyst was then allowed to dry at room temperature overnight and subsequently used to drive the next reaction without any pre-treatment. Multiple reactions with the same catalyst were run simultaneously to ensure enough catalyst was present for subsequent tests. Figure 3.16 illustrates the FF conversion as well as 2-FFA selectivity by 0.6% Pt/TiO₂ catalyst after three cycles of reuse.

It was found that 0.6%Pt/TiO₂ catalyst lost activity reducing from 92% for the fresh catalyst to 33% for the spent catalyst after the 3rd recycle as illustrated in Figure 3.16. The 2-FFA selectivity was also decreased from 95% for the fresh catalyst to 51% for the spent catalyst through the 3rd recycle. The 0.6%Pt/TiO₂ catalyst showed a steady decline in the conversion and selectivity from fresh to spent catalyst through 3rd reuse.

There is a gradual decline over three cycles of the conversion and selectivity of the 0.6%Pt/TiO₂ catalyst. There are three probable reasons for this observation: Leaching of the Pt-NPs from the catalyst surface, sintering of the Pt metal, and/or poisoning of the catalyst by irreversible adsorption of the product.⁴⁹ To find the reason for the deactivation of the catalyst, MP-AES was used to investigate the leaching of Pt-NPs. The metal loading of the fresh 0.6% Pt/TiO₂ catalyst prepared was compared with the reused catalyst that underwent three cycles of reaction. We found that both catalysts still retained 100% of their active metal loading of 0.6%. This suggests the absence of leaching of the Pt-NPs and that the Pt-NPs supported on the TiO₂ surface are stable after reuse. The further characterisation will provide a clear explanation of the reason for the catalyst deactivation as explained in the next section.

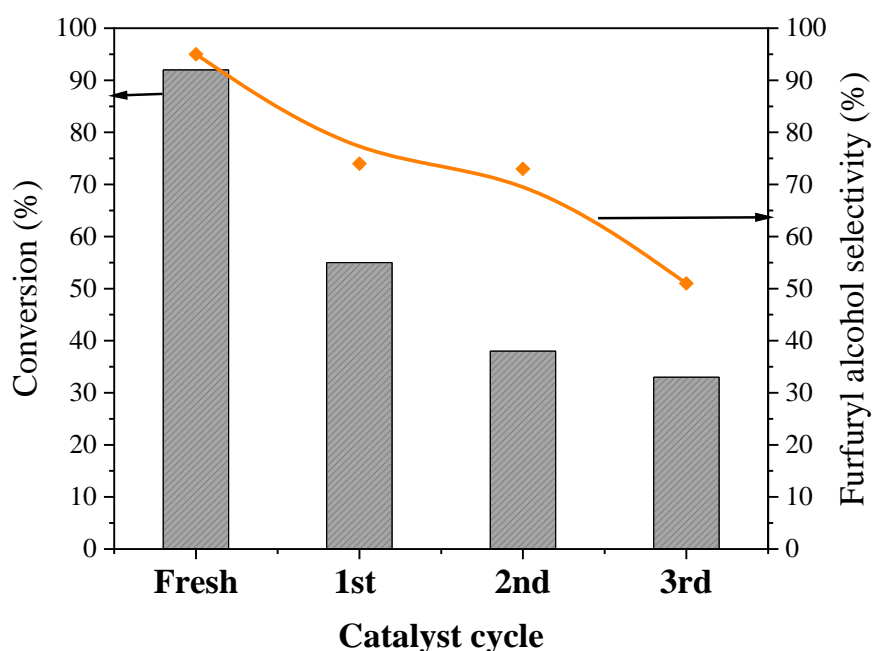


Figure 3.16: 0.6% Pt/TiO₂ Cal+ Red Catalyst reusability test for the the hydrogenation of FF. Reaction conditions: FF (4.45 mmol), *i*-PrOH (15 mL), temp. 30 °C, H₂ (0.3 MPa), substrate/metal molar ratio =207, 3h.

3.7 Catalyst characterisation

To understand the structure-activity relationship of these catalysts, they were characterized with Microwave Plasma Atomic Emission Spectroscopy (MP-AES), X-ray Photoelectron Spectroscopy (XPS), Transmission Electron Microscopy (TEM) and Temperature Programmed Reduction (TPR).

3.7.1 X-ray photoelectron spectroscopy characterisation

The chemical states of the platinum species on Pt/TiO₂ catalysts were evaluated by XPS. This analytical technique was deployed to understand the effect of heat treatment protocols on the oxidation states and to determine the Pt elemental content (atom %) deposited on the different heat treatment protocols. The resulting spectrum for 4.2% Pt/TiO₂ and 0.6% Pt/TiO₂, with different heat treatments, dried only, Calc-only, Red-only and Calc + Red catalysts are illustrated in Figures 3.17 (a-b).

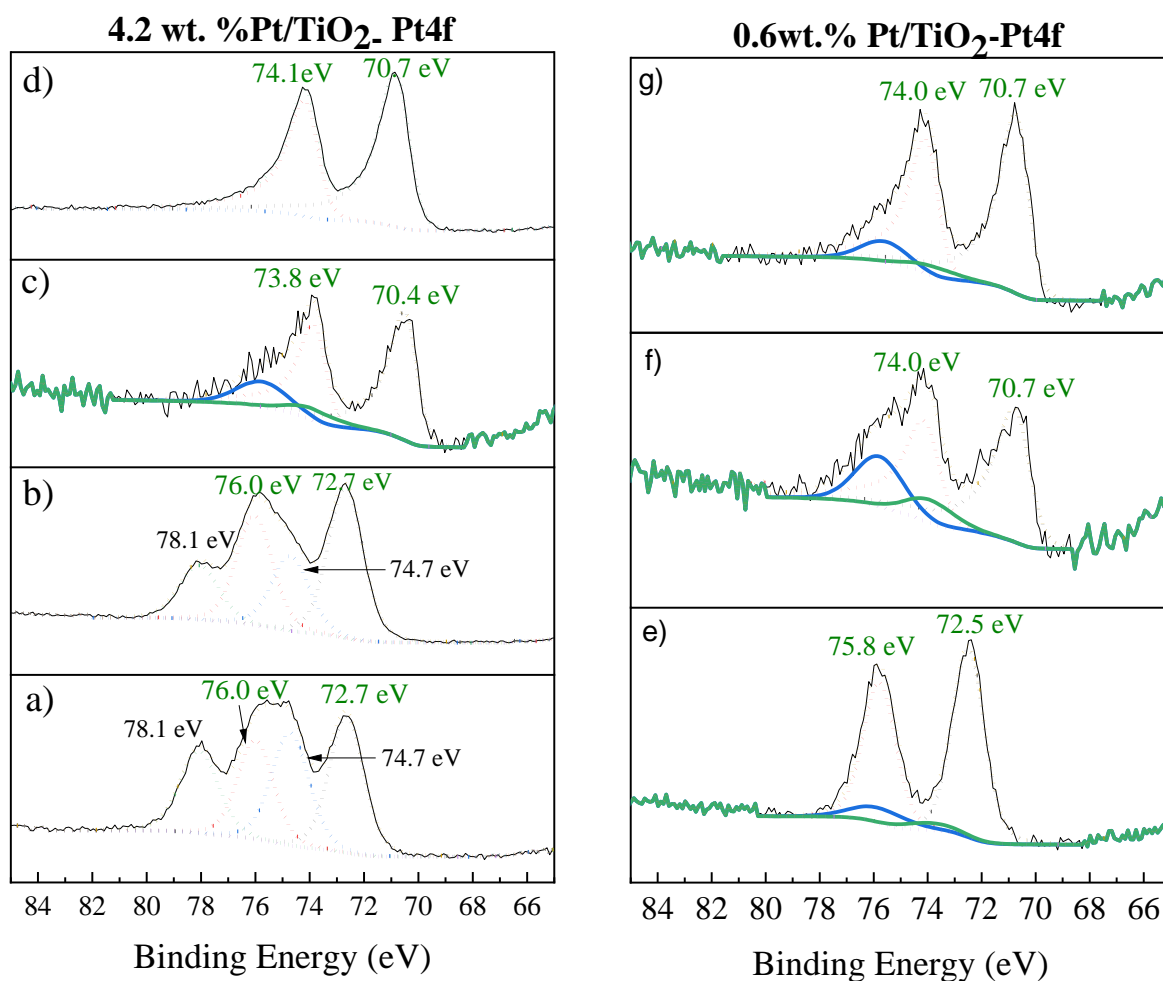


Figure 3.17: XPS profiles of the Pt 4f for different catalysts (a) dried only, (b) calcined-only, (c) reduced-only and (d) calcined+reduced 4.2 %Pt/TiO₂ catalysts and - XPS profiles of the Pt 4f for 0.6% Pt/TiO₂ catalyst with different heat treatment (e) 0.6% Pt/TiO₂ dried only, (f) 0.6% Pt/TiO₂ Red-only, (g) 0.6% Pt/TiO₂ Calc + Red samples.

A doublet signal corresponding to two Pt species Pt 4f_{7/2} and Pt 4f_{5/2} (due to spin-orbit splitting) was observed. Going by the XPS results For 4.2% Pt/TiO₂ dried-only catalyst, the binding energy of Pt 4f_{5/2} appeared at 72.6 eV which is due to the presence of Pt⁺² in Pt(OH)₂. Pt⁺² species have been reported to be present in catalysts prepared at binding energy 72.6 eV. However, the other peak at binding energy 74.7 eV could be assigned to Pt⁺⁴ in PtO₂.

For 4.2% Pt/TiO₂ Calc-only catalyst peaks do not change much for the dried sample as it has a small influence on the ratio of hydroxide to oxide. two peaks were detected. The first peak with a binding energy of 72.6 eV for Pt hydroxide on the catalyst surface²³ This is due to the migration of oxygen species from the support to the Pt species during the calcination process.⁵⁰

The second one, with a binding energy of 74.7 eV for PtO₂ was detected in low intensity for Pt⁺⁴ species. So, in calcined only sample there were not any peaks detected in the range 70-71 eV which is attributed to the metallic Pt form.

However, the strong intense peaks at 70.4 eV for 4f_{7/2} and 70.7 eV for 4f_{7/2} observed for both 4.2% Pt/TiO₂ Red-only catalyst and Calc + Red catalysts respectively confirm that most of the Pt species are present in a metal Pt⁰ form. The intensity of the Pt⁰ signal in the Red-only catalyst is lower than that of the Calc + Red catalyst, this implies that the PtO has been reduced into metallic Pt⁰ during the reduction process at 450 °C for 4 h.

The binding energy for the Red-only sample (70.4 eV) decreased shifts by *ca.* 0.5 eV to 70.4 eV compared to the bending energy for Calc + Red sample (70.7 eV). This decrease is due to charge transfer from the TiO₂ to Pt species and resulted in a rise in electron density on Pt-NPs due to a strong interaction between Pt-NPs and TiO₂ in the reduced sample.^{51, 52, 43, 53} As a result, the Pt was covered by reducible support (TiO₂) and caused the strong metal support interaction phenomena in the reduce only sample. That explains why the catalyst activity for red only sample was lower compared with calc + red sample. The same result was observed with different loading of Pt-NPs. Figure 3.18 displayed XPS analysis for 2.4% Pt/TiO₂ Calc + Red and 1.4% Pt/TiO₂ Calc + Red catalysts. However, the bending energy for both 0.6% Pt/TiO₂ catalysts Red only sample and 0.6% Pt/TiO₂ Calc + Red sample appear at 70.7 eV that due to the SMSI effect decreased with the low load as confirmed by Sankar group²³. Sankar group previous observation that the SMSI was not detected in the reduced-only samples for lower-loading Pt, whereas SMSI was detected in the reduced-only samples for higher Pt, which can be eliminated using calcination followed by reduction. Based on these results, we can conclude that the Pt species are predominantly in metallic Pt (0) form in Calc + Red catalyst. for this reason, the Pt surface is available for the catalytic reduction of FF to FFA.

Accordingly, calcining the catalyst before reduction helps the Pt⁰ species dominate the catalyst surface thereby enhancing the catalyst activity.^{15, 19, 54, 55} This finding may suggest that catalyst activity is improved by the adsorption and activation of FF through the interaction of the carbonyl group to the Pt⁰ species in the catalyst surface.

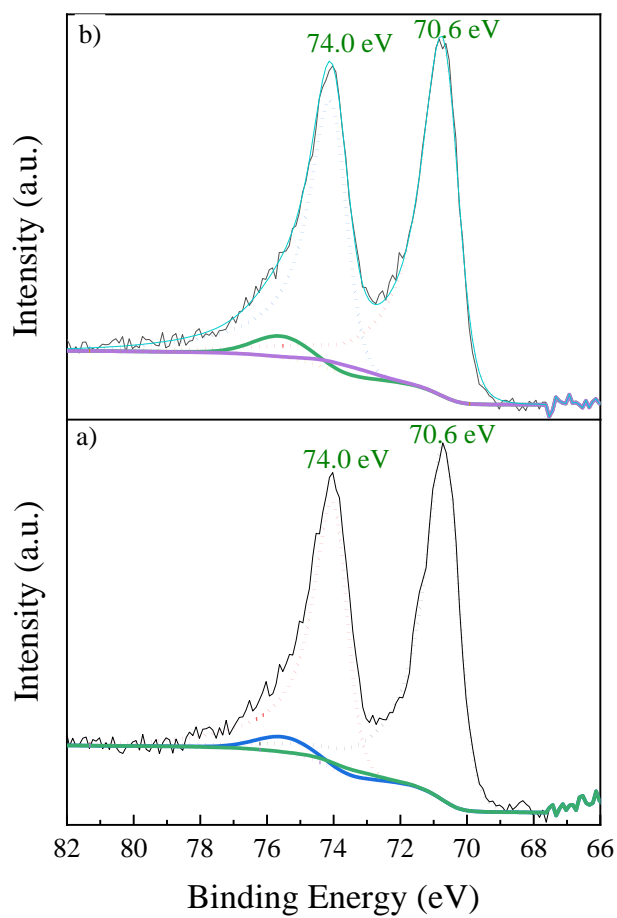


Figure 3.18: XPS profiles of the Pt 4f for different load of catalysts (a) 1.4 %Pt/TiO₂. (b) 2.4%Pt/TiO₂, Calc + Red catalysts.

The oxidation state for the different loading of Pt and the Pt concentration on the catalyst surfaces are summarised in Table 3.2.

Table 3.2: XPS data for 0.6% Pt/TiO₂ and 4.2% Pt/TiO₂ in different heat treatment protocols

<i>Catalyst</i>	<i>Heat Treatment</i>	<i>B.E. / eV (assignment)</i>	<i>Pt species on the surface</i>	<i>Pt % At. Concentration on the surface</i>	<i>Total Pt concentration on the surface</i>
<i>4.2%Pt/TiO₂</i>	<i>Dried only</i>	72.6 (4f(7/2))	Pt ²⁺	0.53	1.74
		74.7	Pt ⁴⁺	0.39	
		76.0	Pt ²⁺	0.47	
		78.1	Pt ⁴⁺	0.35	
	<i>Calcined only</i>	72.7	Pt ²⁺	0.73	1.96
		74.7	Pt ⁴⁺	0.39	
		76.0	Pt ²⁺	0.55	
		78.1	Pt ⁴⁺	0.29	
	<i>Reduced only</i>	70.4	Pt ⁰	0.08	0.14
		73.8	Pt ⁰	0.06	
	<i>Calcined+reduced</i>	70.7	Pt ⁰	0.71	1.24
		74.1	Pt ⁰	0.53	
<i>0.6%Pt/TiO</i>	<i>Dried only</i>	72.5	Pt ²⁺	0.16	0.28
		75.8	Pt ²⁺	0.12	
	<i>Reduced only</i>	70.7	Pt ⁰	0.09	0.15
		74.0	Pt ⁰	0.06	
	<i>Calcined + reduced</i>	70.6	Pt ⁰	0.14	0.24
		74.0	Pt ⁰	0.1	
	<i>Spent catalyst</i>	70.5	Pt ⁰	0.1	0.17

			73.9	Pt ⁰	0.07	
1.4 %Pt/TiO	Calcined reduced	+	70.6	Pt ⁰	0.26	0.46
			74.0	Pt ⁰	0.2	
2.4 %Pt/TiO	Calcined reduced	+	70.6	Pt ⁰	0.4	0.7
			74.0	Pt ⁰	0.3	

According to XPS analysis of the fresh and spent catalysts during the 3rd recycle (Figure 3.19), we found that the oxidation state of Pt-NPs has not significantly changed since Pt remains metallic in both fresh and used catalysts. However, the total Pt concentration in the spent catalyst was 0.17% which is lower than the concentration of the Pt-NPs on the fresh catalyst, which is 0.240 %. That could be due to sintering the catalyst and that could be confirmed using TEM analysis.

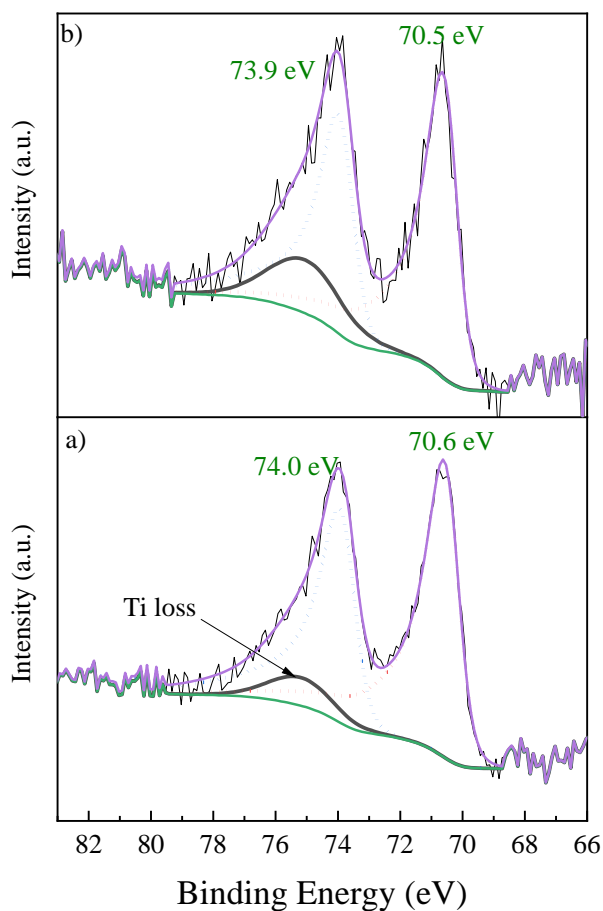


Figure 3.19 XPS results of the (a) 0.6% Pt/TiO₂ calc + red (fresh) (b) 0.6% Pt/TiO₂ calc + red for spent catalyst.

3.7.2 Transmission electron microscopic analysis

To investigate the effect of different heat protocols on the size and distribution of the Pt particles on the catalyst activity, TEM analysis was carried out on the 4.2% Pt/TiO₂ catalyst samples that underwent different post heat treatments. The images obtained are shown in Figures 3.20 and Figure 3.21. The particle size of the dry sample was too small to be measured by TEM. Therefore, the reduction process of the dry sample improves the metal dispersion, this corroborates previous reports in the literature.⁵⁶

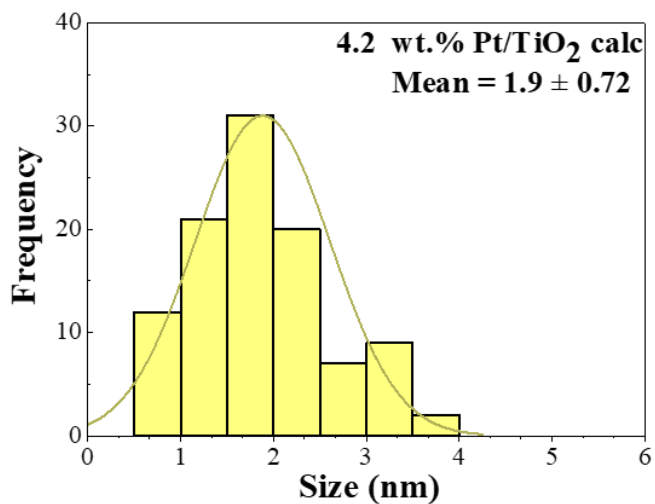
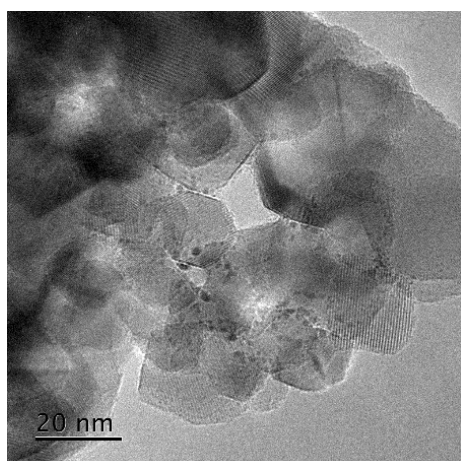
The 4.2% Pt/TiO₂ Calc only catalyst presented the smaller particle size (1.9 nm) that explains the higher catalyst activity. However, the XPS data shows the Pt(II) on the catalyst surface that could reduce under the reaction conditions to Pt⁰.

The TEM images of 4.2% Pt/TiO₂ Calc + Red sample and 4.2% Pt/TiO₂ Red only sample presented the same particle sizes 2.3 nm and 2.4 nm (within the analysis error 0.1 nm). Hence, from XPS data, catalyst activity is related to the presence of Pt⁰ on the catalyst surface and the absence of SMSI.

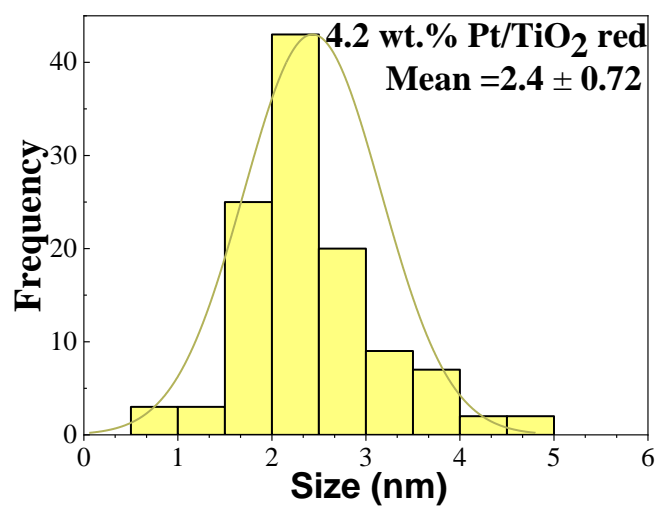
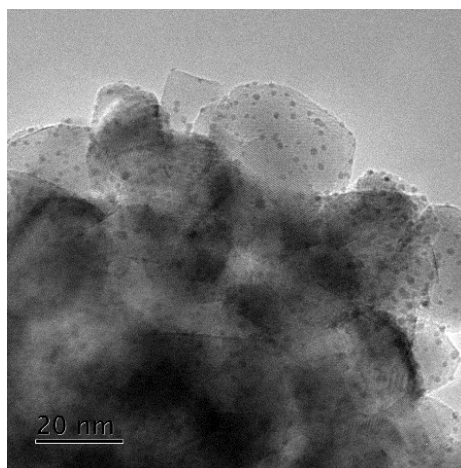
A similar trend was observed for the 0.6% Pt/TiO₂ catalyst samples where the sample subjected to calcination and reduction had a smaller particle size (1.3 nm) with high dispersion. Results from the TEM analysis also confirmed that calcination followed by reduction helps to achieve a uniform dispersion of the active metal NPs on the support.

As shown in Figure 3.20 and Figure 3.21, the average particle size decreases as the Pt loading decreases. The average Pt metal particles size are ± 2.3 nm, ± 1.8 nm, ± 1.5 nm, and ± 1.3 nm for 4.2% Pt/TiO₂, 2.4% Pt/TiO₂, 1.4% Pt/TiO₂, 0.6% Pt/TiO₂, respectively. 0.6% Pt/TiO₂ exhibited the smallest particle size of ± 1.3 nm, with a narrow size distribution on the TiO₂ support. It was found that the smaller Pt-NPs with good dispersion improved the hydrogenation of FF to 2-FFA with high selectivity. This finding is in line with previous research outcomes as reported in the literature.^{23, 54, 57} The heat treatment protocols of calcination followed by reduction of the catalysts assist in achieving the uniform dispersion of the Pt active metal on the TiO₂ support due to the SMSI effect.⁴³ It was approved that the dispersion of the metal was widely, and the activity of the catalyst increased with a high affinity between the metal and the support.⁴³ However, particle size and dispersion are not the only factors affecting the catalyst performance. The SMSI on the catalyst surface affects the catalyst performance as earlier discussed.

A)-4.2% Pt/TiO₂ Calc-only



B)-4.2% Pt/TiO₂ Red-only



C)- 4.2% Pt/TiO₂ Calc + Red

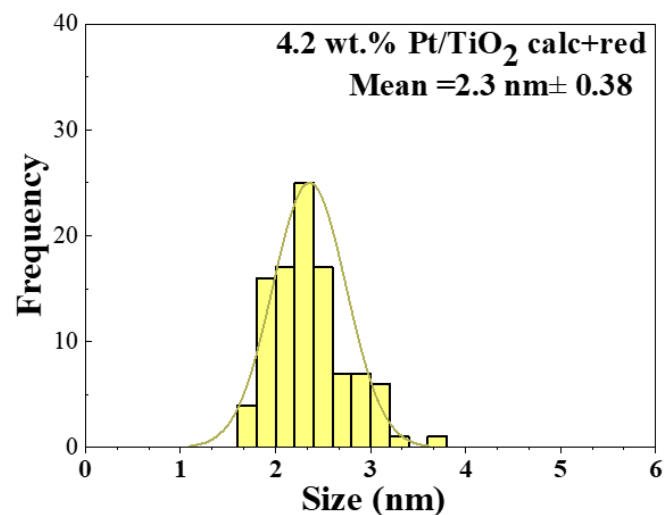
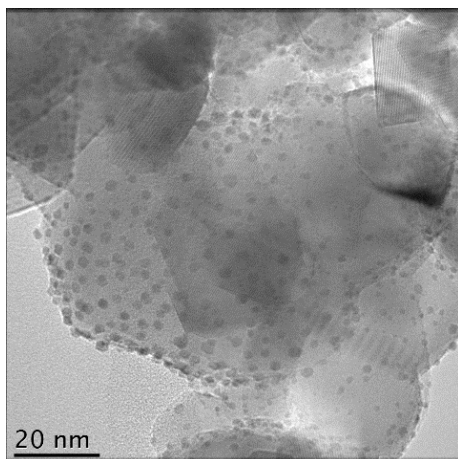
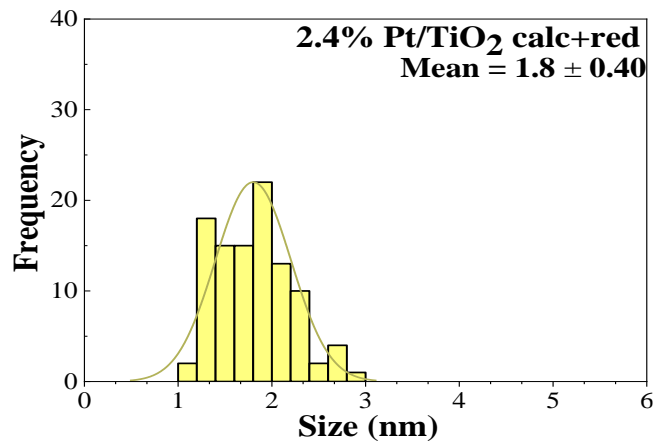
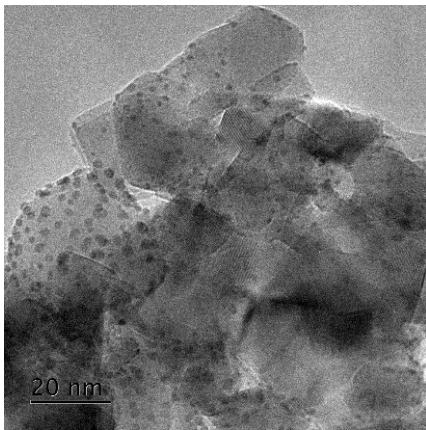
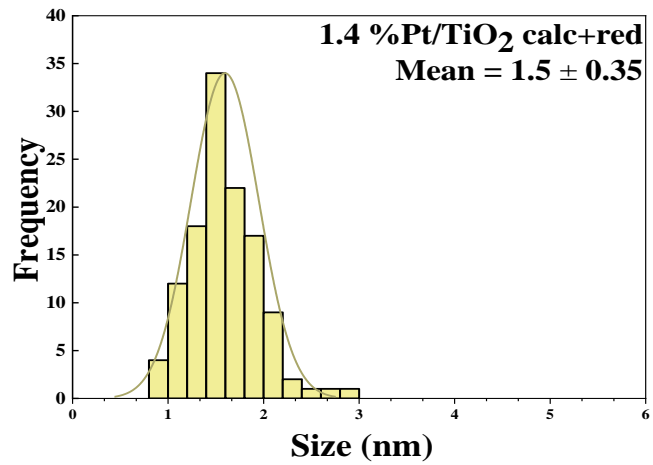
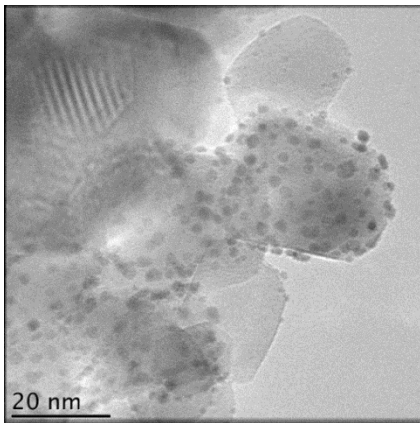


Figure 3.20: TEM image for A)- 4.2% Pt/TiO₂ Calc only, B)- 4.2% Pt/TiO₂ red only and C)- 4.2% Pt/TiO₂ Calc + Red and their corresponding distribution histograms for Pt particles size.

A)- 2.4% Pt/TiO₂ Calc + Red



B)-1.4% Pt/TiO₂ Calc + Red



0.6% Pt/TiO₂ Calc + Red

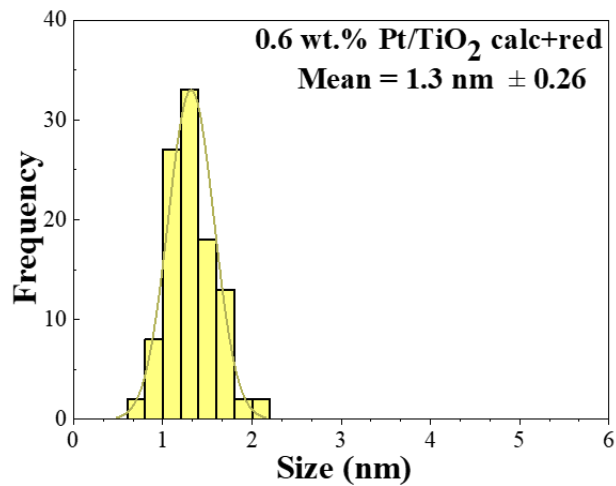
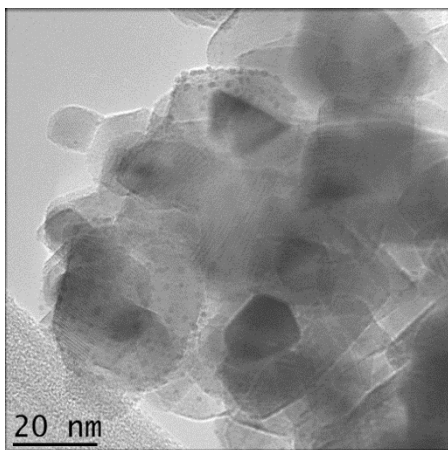


Figure 3.21: TEM image from different scenes of 2.4% Pt/TiO₂ Calc + Red, 1.4% Pt/TiO₂ Calc + Red, 0.6% Pt/TiO₂ Calc + Red and their corresponding distribution histograms for Pt particles size.

Furthermore, the fresh and reused 0.6% Pt/TiO₂ catalysts were characterized after three reaction cycles with TEM, to determine whether Pt-NPs are aggregated. It was found that the size of the Pt-NPs particles increased from 1.3 nm to 1.6 nm (Figure 3.22) after three reuse cycles and this could be attributed to the sintering of the catalyst.

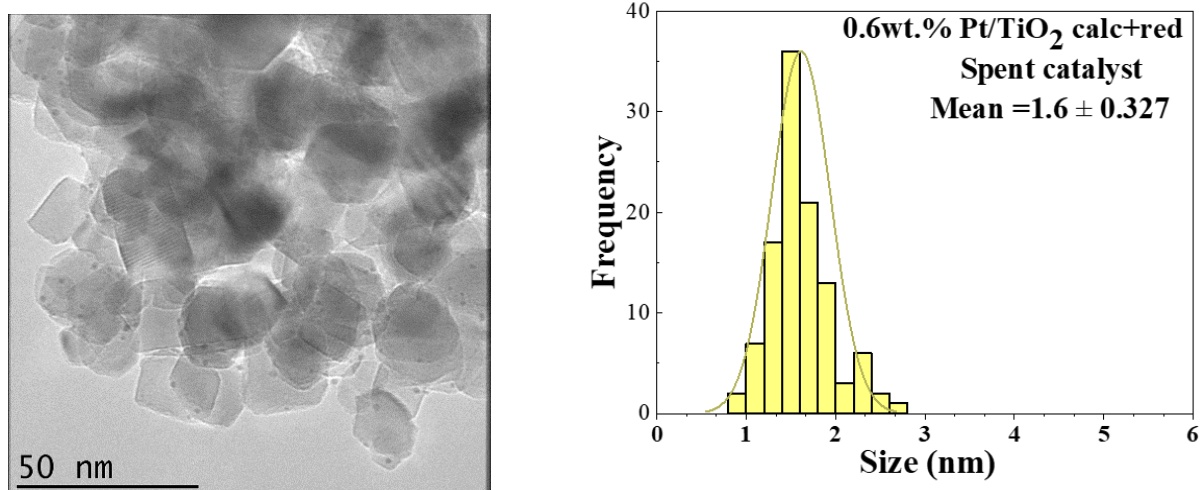


Figure 3.22: TEM images of spent 0.6 wt. % Pt/TiO₂ catalyst and their corresponding distribution histograms for Pt particles size.

It is possible that the catalyst could be deactivated due to the carbonyl group binding too strongly to Pt active site on the catalyst surface. This could prevent the interaction between the Pt-NPs and FF to yield 2-FFA.⁵⁸

3.7.3 CO chemisorption:

CO chemisorption was employed to calculate the particle size of the Pt-NPs and their dispersion on the TiO₂ support. The dispersion of Pt NPs on the support was calculated by assuming one Pt site chemisorbed one CO molecule.⁴⁵ The CO uptake by 0.6% Pt/TiO₂ Calc + Red catalyst shows that the Pt-NPs are well exposed on the support surface and uncovered by the support particles. A core-shell structure of Pt-TiO₂ due to SMSI was not observed. The observed Pt particle size correlates with the results obtained from TEM analysis (1.3 nm) as explained TEM section.

Table 3.3: CO chemisorption data for the supported Pt/TiO₂ catalysts:

Catalyst	CO uptake mmol/g	Dispersion (%)	Surface area (m²/g_{Pt})	Particle size (nm)
0.06 Pt red. only	0.00822	27	66	4.2
0.06 Pt cal+red.	0.0264	86	210	1.3
4.2 Pt red. only	0.00963	4	11	26
4.2 Pt calc. + red.	0.0958	44	110	2.6

The results from CO chemisorption measurements on selected catalysts are shown in Table 3.3. Catalysts reduced at 450 °C display characteristic SMSI behaviour whereby the adsorption of CO is suppressed, resulting in a discrepancy between electron microscopy results and estimates from CO uptake. Interestingly, the 0.6% Pt/TiO₂ catalyst appears to be more resistant to the SMSI state owing to the greater dispersion of this sample. For the Pt/TiO₂ catalysts calcined and reduced at 450 °C, the extent of coverage appears to be lower as CO uptake is higher compared to reduced only samples. This work demonstrates that a high temperature calcination step prior to reduction prevents TiO_x overlayer formation for high loaded Pt catalysts in addition to low loaded catalysts.

3.7.4 Temperature programmed reduction

H₂-TPR was used to study the hydrogen consumption and the reducibility of the Pt-NPs on TiO₂. The H₂-TPR profiles of 4.2% Pt/TiO₂ Red-only catalyst and 4.2% Pt/TiO₂ Calc + Red catalyst are presented in Figure 3.23. The peak at 100 °C is associated with the reduction of Pt oxide (PtO₂ and PtO) to metallic Pt⁰ in Pt/TiO₂ Red-only catalyst. This observation agrees with previously reported data.^{36,59} Based on the TPR profiles of the catalysts, the 4.2% Pt/TiO₂ Calc + Red catalyst took up more hydrogen than the 4.2% Pt/TiO₂ Red-only catalyst. However, the reduction peak of PtO_x was not detected in the 4.2% Pt/TiO₂ Calc + Red.³⁶ Meanwhile, the interaction of TiO₂ support with Pt species appeared as a broad peak at 250 °C to 500 °C in the Calc + Red sample. Moreover, the peak over 500 °C contributed to the surface copping of oxygen in TiO₂ reduction. Pt metal is well known to promote H₂ spill-over on TiO₂ at a

temperature below 473K.^{32,33} As soon as PtO_x was reduced to Pt metal, H_2 molecules dissociated into hydrogen atoms over the Pt metal surface and migrated onto the surface of the support, but this process is reversible. As the temperature was increased further, H atoms migrated from the TiO_2 surface back to the Pt metal surface to replenish the desorbed H_2 molecules in the reverse spill-over process. The negative desorption peak at 331-337 K is attributed to the reverse H_2 spill-over process over the Pt/ $\text{TiO}_2(\text{B})$ nanofiber surface.

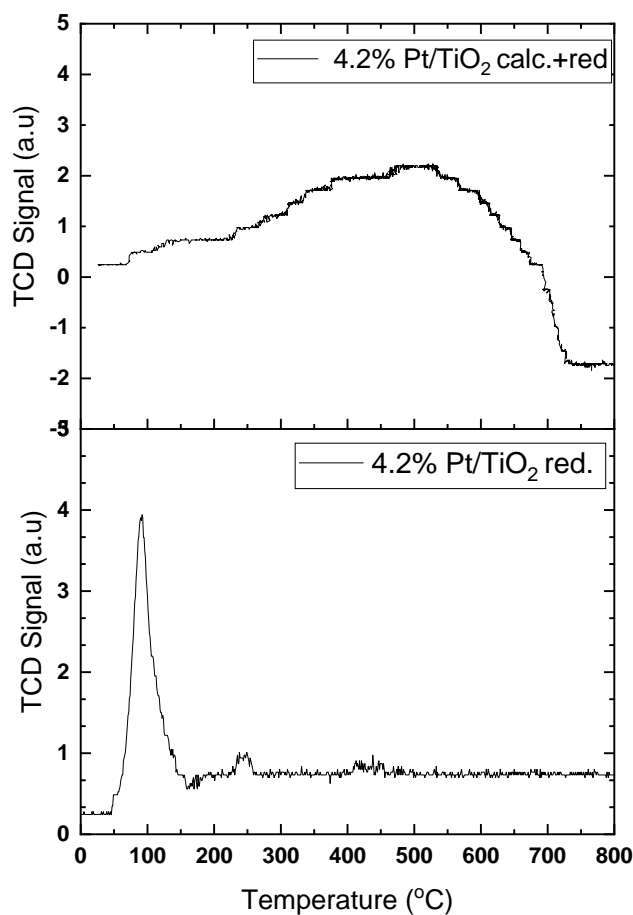


Figure 3.23: Profiles of H_2 -TPR of 4.2% Pt/ TiO_2 with varying post-preparation heat treatments.

The characterization and reaction results indicate that there are different reaction pathways depending on the active metal loading. Accordingly, calcination followed by reduction hindered the migration of TiO_2 over Pt-NPs due to strong metal-support interaction.

It was observed that the Pt⁰ species detected with XPS data reveal that Pt sites are exposed for the catalytic activity. Therefore, it suggests that the Pt⁰ species are more effective than the Pt²⁺ species in the hydrogenation of FF. Optimising the preparation parameters for the 0.6% Pt/TiO₂ catalyst yielded a catalyst with smaller-sized Pt-NPs (1.3 nm) with high percent dispersion.

The XPS and TEM, analyses confirmed that calcination followed by reduction under H₂ flow at 450°C is effective in preventing the migration of the TiO₂ to the Pt-NPs and the Pt-NPs become highly dispersed with nano-sized species smaller than the reduced only Catalyst. The characterisation results confirm that the surface of the catalyst is dominated by Pt⁰ species which enhanced the activity of the catalyst and the selectivity towards the formation of 2-FFA at mild reaction conditions. The only side products observed during the hydrogenation of FF by 0.6% Pt/TiO₂ Calc + Red catalyst were in low quantities, 2-MF and SP. The 0.6% Pt/TiO₂ Calc + Red catalyst reported in this study compares favourably with other reported Pt-based heterogeneous catalysts for the selective hydrogenation of FF as shown in Table 3.3. Compared with those reported in the literature, the improvement of the catalyst performance in this study using post-synthetic heat treatment protocols, strong metal support interaction as well as the control of metal loading were found to considerably improve the activity of the catalyst and selectivity for 2-FFA at room temperature and low H₂ pressure. There are limited research outcomes that indicate the efficiency of Pt⁰ species as responsible for the selective catalytic conversion of the carbonyl group rather than the alkene group in FF. However, in this work, we have successfully controlled the active metal sites and support interaction using different post-synthesis heat treatment protocols for the catalysts. We have been able to achieve excellent conversion of FF (97%) and high selectivity to 2-FFA (95%) by the nano-sized and highly distributed Pt⁰ species on the surface of the support. Previous work¹⁹ indicated that high selectivity to 2-FFA was only possible with catalysts with 4nm particle size, this study has however achieved a higher selectivity (99%) to 2-FFA with smaller nano-sized catalysts (1.6 nm).

Wang group³¹ reported that the Pt/SiO₂-C Calc +Red catalyst presented high activity and selectivity towards 2-FFA due to the physicochemical properties of the catalyst which facilitated interaction between the catalyst and carbonyl group on FF during hydrogenation.

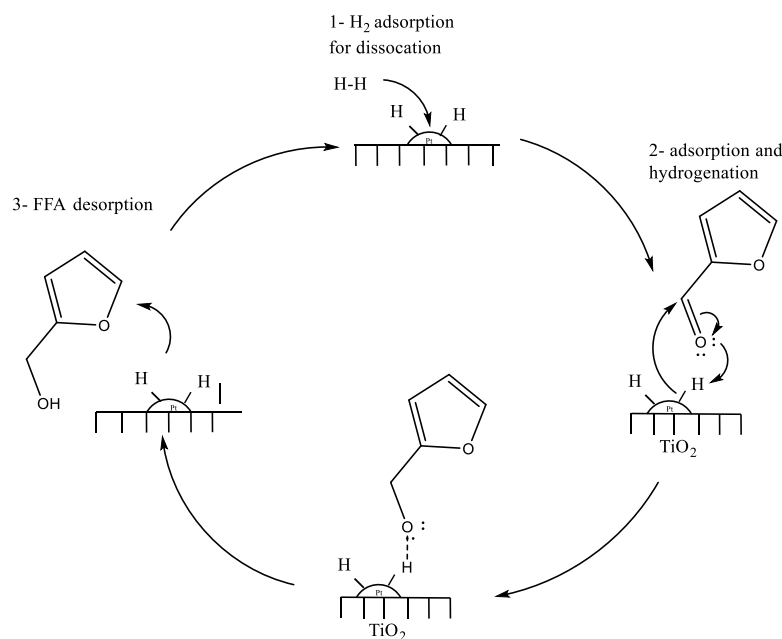
They also reported that optimal metal support interaction exists between Pt-NPs and SiO₂-C, this made the Pt^{+δ} species to be well dispersed and the particle size was (1.8 nm).

Gao et al.⁵⁴ reported that Pt/HT catalyst prepared by the incipient wetness impregnation method followed by calcination and reduction for 1 h each at 400°C showed higher activity (99%) in hydrogenating FF to 2-FFA with 99% selectivity towards 2-FFA. This group hinged the performance of this catalyst to the 2D layered double hydroxides which facilitates the reduction of Pt species effectively and enhances good dispersion of the Pt species. This was reported to be responsible for the selective interaction of the carbonyl group on FF to the catalyst.

Table 3.4: Comparative analysis of previously reported platinum catalysts Vs 0.6% Pt/TiO₂ used in this work.

Catalyst	Preparation method	FF /Catalyst	Temp./Pres./solvent/Time	Conv. (%)	Selec. (%)	Ref
3% Pt/HT	Wetness impregnation method.	FF (0.75 mmols), catalyst (50 mg)	30 °C, /15 bar/ water/ 2 h	99	99	54
3% Pt/SiC–C	Ultrasound promoted impregnation method (calcined 200 °C, 2 h then reduction at 500 °C, 3 h)	FF (0.3 ml), catalyst (20 mg)	25 °C/ 10 bar/ water/ 5h	99	99	31
2.3% Pt/MgO,	Colloidal Pt nanoparticles were prepared adapting the method of Jones et al. ⁶⁰	FF (0.02 mmols), catalyst (20 mg)	50 °C/1.03 bar /methanol/ 7 h	80	99	19
1.4% Pt/CeO ₂	Colloidal Pt nanoparticles were prepared adapting the method of Jones et al. ⁶⁰	FF (0.02 mmols), catalyst (20 mg)	50 °C/ 1.03 bar /methanol/ 7 h	79	97	19
1.9% Pt/ γ -Al ₂ O ₃	Colloidal Pt nanoparticles were prepared adapting the method of Jones et al. ⁶⁰	FF (0.02 mmols), catalyst (20 mg)	50 °C/ 1.03 bar /methanol/ 7 h	77	98	19
0.6% Pt/TiO ₂	Wetness impregnation method (calcined 450 °C, 4 h then reduction at 450 °C, 4 h)	FF (0.3 ml), catalyst (100 mg)	30 °C/ 0.3 MPa /isopropanol/ 6 h	97	95	This study

The reaction mechanism proposed by Gao et al. comprises of four steps as shown in Scheme 3.4.⁵⁴ The first step is the adsorption of the hydrogen from the reaction mixture on the Pt⁰ species of the catalyst. Hydrogen dissociation occurs on the Pt surface when the antibonding orbital of H₂ gains an electron from the d-orbital of Pt species, this makes it easier for the H–H bond dissociate.⁶¹ As more H adsorbs on the catalyst surface, this helps to ensure the optimal adsorption of FF to favour the formation of 2-FFA over ring opening ring or decarbonylation products.⁶² The C=O bond in FF is activated due to the interaction between the C=O (2π*) and Pt (5d)⁶² 61. The adsorbed carbonyl group in FF is then converted to 2-FFA. Finally, the 2-FFA is desorbed from the surface of the catalyst due to the weak adsorption of 2-FFA to the catalyst surface.



Scheme 3.4: Diagram illustrating the catalytic mechanism of selective hydrogenation of FF.

3.8 Conclusions

This work shows how heat treatment protocols can affect the selectivity towards 2-FFA products.

For higher Pt loading catalysts (4.2%Pt/TiO₂) heat treatment plays a crucial role in determining its catalytic activity. 4.2% Pt/TiO₂ calcined + reduced was found

to be much more active than the reduced only sample. Consequently, different Pt loads were tested (2.4% Pt/TiO₂ Calc + Red, 1.4% Pt/TiO₂ Calc + Red, and 0.6% Pt/TiO₂ Calc + Red catalyst) . Among the tested catalysts, 0.6% Pt/TiO₂ Calc + Red catalyst is the most active for the hydrogenation of FF to 2-FFA with high selectivity at 30 °C under 0.3 MPa of hydrogen. A change was made to the catalyst's preparation protocol, which included calcination followed by reduction of the sample before test. Utilising the post heat method helps to prevent the Pt-NPs sites being covered by TiO₂.

The results confirmed that the 0.6% Pt/TiO₂ (Calc + Red) catalyst offers the highest activity level for hydrogenating FF to 2-FFA with 97% conversion of FF with 95% selectivity towards 2-FFA for 6h under mild reaction conditions. It was found that adjusting the synthetic protocols of the catalyst enhanced the catalyst activity. The catalyst presented nanoparticles sized, (1.3 nm), uniform dispersion of Pt⁰ on the catalyst surface. The Pt-NPs on the surface activated the carbonyl compound and subsequently, convert it to alcohol, which ultimately increased the 2-FFA selectivity.

However, the 0.6% Pt/TiO₂ catalyst lost activity gradually after 3 cycles for the reusability test. Characterisation of the spent catalyst using TEM results confirmed the sintering of the catalyst is the main reason for the catalyst deactivation. Furthermore, the MP-AES result showed there was no leaching in the catalyst compared with the fresh catalyst.

3.9 References:

1. C. Li, X. Zhao, A. Wang, G. W. Huber and T. Zhang, *Chem Rev*, 2015, **115**, 11559-11624.
2. L. Wu, T. Moteki, A. A. Gokhale, D. W. Flaherty and F. D. Toste, *Chem*, 2016, **1**, 32-58.
3. Z. Zhang, J. Song and B. Han, *Chem Rev*, 2017, **117**, 6834-6880.
4. J. Wu, X. Zhang, Q. Chen, L. Chen, Q. Liu, C. Wang and L. Ma, *Energy & Fuels*, 2019, **34**, 2178-2184.
5. Q. Yuan, J. Pang, W. Yu and M. Zheng, *Catalysts*, 2020, **10**.
6. J. Kijenski, P. Winiarek, T. Paryjczak, A. Lewicki and A. Mikołajska, *Appl. Catal. A: Gen.*, 2002, **233**, 171–182.
7. S. Srivastava, G. C. Jadeja and J. Parikh, *Chem. Eng. Res. Des.*, 2018, **132**, 313-324.
8. Y. Wang, D. Zhao, D. Rodríguez-Padrón and C. Len, *Catalysts*, 2019, **9**, 796.
9. H. Niu, Y. Cheng, C. Li, S. Li, J. Luo and C. Liang, *Ind. Eng. Chem. Res.*, 2021, **60**, 16939-16950.
10. Q. Yang, D. Gao, C. Li, S. Cao, S. Li, H. Zhao, C. Li, G. Zheng and G. Chen, *Fuel*, 2022, **311**, 122584.
11. F. Hao, J. Zheng, S. He, H. Zhang, P. Liu, H. Luo and W. Xiong, *Catal. Commun.*, 2021, **151**, 106266.
12. T. W. v. Deelen, C. H. Mejía and K. P. d. Jong, *Nat. Catal.*, 2019, **2**, 955-970.
13. C.-J. Pan, M.-C. Tsai, W.-N. Su, J. Rick, N. G. Akalework, A. K. Agegnehu, S.-Y. Cheng and B.-J. Hwang, *J. Taiwan Inst. Chem. Eng.*, 2017, **74**, 154-186.
14. K. An, N. Musselwhite, G. Kennedy, V. V. Pushkarev, L. R. Baker and G. A. Somorjai, *J Colloid Interface Sci*, 2013, **392**, 122-128.
15. Z. Yu, X. Lu, X. Wang, J. Xiong, X. Li, R. Zhang and N. Ji, *ChemSusChem*, 2020, **13**, 5185-5198.
16. X. Gao, S. Tian, Y. Jin, X. Wan, C. Zhou, R. Chen, Y. Dai and Y. Yang, *ACS Sustain. Chem. Eng.*, 2020, **8**, 12722-12730.

17. J. Wang, C.-Q. Lv, J.-H. Liu, R.-R. Ren and G.-C. Wang, *Int. J. Hydrog. Energy*, 2021, **46**, 1592-1604.
18. R. Albilali, M. Douthwaite, Q. He and S. H. Taylor, *Catal. Sci. Technol.*, 2018, **8**, 252-267.
19. M. J. Taylor, L. J. Durndell, M. A. Isaacs, C. M. A. Parlett, K. Wilson, A. F. Lee and G. Kyriakou, *Appl. Catal. B: Environ.*, 2016, **180**, 580-585.
20. S. Zhang, H. Ma, Y. Sun, X. Liu, M. Zhang, Y. Luo, J. Gao and J. Xu, *Chinese J. Catal.*, 2021, **42**, 2216-2224.
21. K. Fulajtárova, T. Soták, M. Hronec, I. Vávra, E. Dobročka and M. Omastová, *Appl. Catal. A: Gen.*, 2015, **502**, 78-85.
22. G. Singh, L. Singh, J. Gahtori, R. K. Gupta, C. Samanta, R. Bal and A. Bordoloi, *Mol. Catal.*, 2021, **500**, 111339.
23. M. Macino, A. J. Barnes, S. M. Althahban, R. Qu, E. K. Gibson, D. J. Morgan, S. J. Freakley, N. Dimitratos, C. J. Kiely, X. Gao, A. M. Beale, D. Bethell, Q. He, M. Sankar and G. J. Hutchings, *Nat. Catal.*, 2019, **2**, 873-881.
24. Y. Yang, D. Rao, Y. Chen, S. Dong, B. Wang, X. Zhang and M. Wei, *ACS Catal.*, 2018, **8**, 11749-11760.
25. X. Wang, X. Liang, P. Geng and Q. Li, *ACS Catal.*, 2020, **10**, 2395-2412.
26. J. Yu, Y. Yang, L. Chen, Z. Li, W. Liu, E. Xu, Y. Zhang, S. Hong, X. Zhang and M. Wei, *Appl. Catal. B: Environ.*, 2020, **277**, 119273.
27. S. Bai, L. Bu, Q. Shao, X. Zhu and X. Huang, *J Am Chem Soc*, 2018, **140**, 8384-8387.
28. Y. Deng, R. Gao, L. Lin, T. Liu, X. D. Wen, S. Wang and D. Ma, *J Am Chem Soc*, 2018, **140**, 14481-14489.
29. M. Agote-Arán, S. Alijani, C. Coffano, A. Villa and D. Ferri, *Catal. Lett.*, 2021, **152**, 980-990.
30. P. Gallezot and D. Richard, *Catal. Rev.*, 1998, **40**, 81-126.
31. G. Wang, R. Yao, H. Xin, Y. Guan, P. Wu and X. Li, *RSC Advances*, 2018, **8**, 37243-37253.

32. X. Chen, L. Zhang, B. Zhang, X. Guo and X. Mu, *Sci Rep*, 2016, **6**, 28558.
33. M. Koehle and R. F. Lobo, *Catal. Sci. Technol.*, 2016, **6**, 3018-3026.
34. P. Panagiotopoulou and D. G. Vlachos, *Appl. Catal. A: Gen.*, 2014, **480**, 17-24.
35. Y. Bonita, V. Jain, F. Geng, T. P. O'Connell, W. N. Wilson, N. Rai and J. C. Hicks, *Catal. Sci. Technol.*, 2019, **9**, 3656-3668.
36. S. Kuhaudomlap, O. Mekasuwandumrong, P. Praserttham, S.-I. Fujita, M. Arai and J. Panpranot, *Catalysts*, 2018, **8**, 87.
37. D. G. K. James M. Bell, P. Sartwell, and Richard G. Zepp, *J. Org. Chem.*, 1965, **30**, 4284-4292.
38. Y. Zheng, X. Wang, X. Fu and K. Wei, *Appl. Organomet. Chem.*, 2007, **21**, 836-840.
39. M. J. Taylor, degree of Doctor of Philosophy, Aston University, 2017.
40. A. Corma, P. Serna, P. Concepcion and J. J. Calvino, *J. Am. Chem. Soc.*, 2008, **130**, 8748-8753.
41. L. R. Baker, G. Kennedy, M. Van Spronsen, A. Hervier, X. Cai, S. Chen, L. W. Wang and G. A. Somorjai, *J Am Chem Soc*, 2012, **134**, 14208-14216.
42. F. Dai, J. Luo, S. Zhou, X. Qin, D. Liu and H. Qi, *J. Bioresour. Bioprod.*, 2021, **6**, 243-253.
43. G. J. Kim, D. W. Kwon and S. C. Hong, *J. Phys. Chem. C*, 2016, **120**, 17996-18004.
44. W. Zhao, D. Zhou, S. Han, Y. Li, J. Liu, Y. Zhou, M. Li, X. Zhang and W. Shen, *J. Phys. Chem. C*, 2021, **125**, 10386-10396.
45. S. Pisduangdaw, O. Mekasuwandumrong, H. Yoshida, S.-I. Fujita, M. Arai and J. Panpranot, *Appl. Catal. A: Gen.*, 2015, **490**, 193-200.
46. C. Liang, H. Li, M. Peng, X. Zhang, Q. Jiang, J. Cui, Y. Ding and Z. C. Zhang, *Appl. Catal. A: Gen.*, 2022, **643**.
47. S. Bhogeswararao and D. Srinivas, *J. Catal.*, 2015, **327**, 65-77.
48. W. Tolek, K. Khruachao, B. Pongthawornsakun, O. Mekasuwandumrong, F. J. C. S. Aires, P. Weerachawanasak and J. Panpranot, *Catal. Commun.*, 2021, **149**, 106246.

49. J. A. Moulijn, A. E. v. Diepen and F. Kapteijn, *Appl. Catal. A: Gen.*, 2001, **212**, 3-16.
50. L. S. Kibis, D. A. Svintsitskiy, A. I. Stadnichenko, E. M. Slavinskaya, A. V. Romanenko, E. A. Fedorova, O. A. Stonkus, V. A. Svetlichnyi, E. D. Fakhrutdinova, M. Vorokhta, B. Šmíd, D. E. Doronkin, V. Marchuk, J.-D. Grunwaldt and A. I. Boronin, *Catal. Sci. Technol.*, 2021, **11**, 250-263.
51. E. J. S. Ringler, M. Boutonnet-Kizling, M. Gothelid *Appl. Surf. Sci.*, 2000 **162–163** 190–197.
52. M. Y. Byun, Y. E. Kim, J. H. Baek, J. Jae and M. S. Lee, *RSC Adv*, 2021, **12**, 860-868.
53. I. Jimenez-Morales, S. Cavaliere, D. Jones and J. Roziere, *Phys Chem Chem Phys*, 2018, **20**, 8765-8772.
54. G. Gao, J. Remón, Z. Jiang, L. Yao and C. Hu, *Appl. Catal. B: Environ.*, 2022, **309**, 121260.
55. Y. Yang, Z. Ren, S. Zhou and M. Wei, *ACS Catal.*, 2021, **11**, 6440-6454.
56. Z. Rui, L. Chen, H. Chen and H. Ji, *Ind. Eng. Chem. Res.*, 2014, **53**, 15879-15888.
57. Y. Zhu, W. Zhao, J. Zhang, Z. An, X. Ma, Z. Zhang, Y. Jiang, L. Zheng, X. Shu, H. Song, X. Xiang and J. He, *ACS Catal.*, 2020, **10**, 8032-8041.
58. M. Besson and P. Gallezot, *Catal. Today*, 2000, **57** 127–141.
59. O. S. Alexeev, S. Y. Chin, M. H. Engelhard, L. Ortiz-Soto and M. D. Amiridis, *J. Phys. Chem.* , 2005, **109**, 23430-23443.
60. M. M. Koebel, L. C. Jones and G. A. Somorjai, *J. Nanopart. Res.*, 2008, **10**, 1063-1069.
61. J. Wu, C. Liu, Y. Zhu, X. Song, C. Wen, X. Zhang, C. Wang and L. Ma, *J. Energy Chem.*, 2021, **60**, 16-24.
62. M. Luneau, J. S. Lim, D. A. Patel, E. C. H. Sykes, C. M. Friend and P. Sautet, *Chem Rev*, 2020, **120**, 12834-12872.

Chapter 4:

Chemoselective Hydrogenation of Furfural over monometallic Pd, Ru, and Au, and bimetallic RuPt, RuPd, AuPt and PtPd catalysts supported on TiO₂

4.1 Introduction

Supported bimetallic catalysts consisting of bifunctional metals are of great interest and have been the subject of substantial research. This catalyst system is achieved by adding a second metal to the primary metal. The added second metal could alter the morphology, microstructure, and electronic structure of the primary metal in the catalyst, leading to a new range of physical and chemical properties.^{1, 2} The alterations in the physical properties of a bimetallic catalyst relative to a monometallic catalyst are caused by the 'synergistic' effects between the two metals in the catalyst.^{2, 3} The 'synergistic' effects have a huge influence on the catalyst activity, selectivity, and stability.⁴ The synergistic effect observed in bimetallic systems could enhance the rate of the reaction by adsorption and activation of reactants, which could improve the activity and selectivity.^{5, 6} Additionally, the activity and selectivity of bimetallic catalysts are also hinged on the change in active metal particle size.⁷⁻⁹

For instance, the synergistic effect between Pd and Au bimetallic catalyst enhanced the catalyst activity and exhibited a significant positive impact on the selective hydrogenation and oxidation of different organic compounds.¹⁰⁻¹³ Although, Hao and coworkers established that the two metals are segregated on the surface of the catalyst, interestingly, the synergistic effect between the two metals led to electron transfer between Au and Pd which enhances activation of the H₂ molecules.^{10, 14, 15, 16} For this reason, many researchers have applied PdAu catalyst in different reactions. Pinto *et al.*⁵ investigated the hydrogenation of cinnamaldehyde using bimetallic PdAu NPs which presented superior catalytic performance (TOF 329 h⁻¹) compared to monometallic Pd NP (TOF 83 h⁻¹). However, monometallic Au NP alone was inactive for this reaction, and these findings suggested that Pd is essential for this catalytic transformation.

Furthermore, it has been observed that the addition of a second metal to Pt-based catalysts could enhance the catalyst's activity, selectivity, and stability.¹⁷ Gallezot and Richard¹⁸ observed that the addition of a second metal to a Pt-based catalyst as a promoter improves the hydrogenation of α , β -unsaturated aldehydes. These bimetallics, PtRu^{19, 20} PdRu²¹, PtAu¹⁵, PtPd²² have been reported to be particularly efficient in the catalytic hydrogenation of carbonyl groups. Equally, bimetallic catalysts such as PtPd exhibit synergetic behaviour, which leads to their application in the hydrogenation of many compounds.²³⁻²⁵ For instance, Chetyrin *et al.*²⁶ found that PtPd/ γ -Al₂O₃ catalyst with low loading of Pt is an efficient catalyst for the oxidation of methane. The catalyst presented superior activity compared to monometallic Pd/ γ -Al₂O₃ catalyst. However, monometallic Pt/ γ -Al₂O₃ did not show any activity for methane oxidation.

Also, PtPd/TiO₂ prepared by co-precipitation method has been reported to exhibit excellent catalyst activity and selectivity in the hydrogenation of FF to FFA under benign conditions.²³ The ultra-small alloy and Pt-rich surface composition of the PtPd catalyst supported on the TiO₂ surface which is a result of the synergistic effect between the two metals are the key factors responsible for its activity and selectivity.

Besides platinum, other noble metals such as gold, ruthenium and palladium have been reported to selectively hydrogenate carbonyls to alcohols.²⁷⁻³² Several metals, including Pt, Ir, Ru, Co, Au, and Ag, have been supported on reducible metal oxides for the hydrogenation of carbonyl group.²⁷⁻³² Although the interaction between the metal and the support is complicated,³³ supported metals have become one of the most investigated classes of heterogeneous catalysts with wide industrial and chemical applications. Due to their nature, the interaction between the support and the metal has been recognised and the importance of this interaction in catalyst activity, selectivity and stability has been reported.³³ In chapter 3, we observed that Pt/TiO₂ catalyst produced 2-FFA with high selectivity compared to CeO₂, Nb₂O₅, SiO₂ and carbon. The high activity of this catalyst could be attributed to the interaction between the Pt and TiO₂ support. As the Ti⁴⁺ is reduced to Ti³⁺, this Ti³⁺ site is electron rich, and this facilitates the adsorption of the carbonyl group in FF, allowing the formation of the C-O bond by electron transfer from the Ti³⁺ cation to the carbonyl group, which causes activation of the C-O bond towards a certain reaction. The C=O bond is activated on metal surfaces by charge transfer, thereby, stabilising the oxy-furfural intermediate on the TiO₂ support^{34, 35} while the C-O bond is hydrogenated on the Pt surface.^{19, 34, 36-38} Furthermore, catalyst preparation protocols are critical in the activity and selectivity of the catalyst,³⁸ and it has become necessary to tune the strong metal-support interaction (SMSI) by heat treatment to increase the metal active sites and make it more active (as previously described in chapter 3).

As described in Chapter 2, Pt/TiO₂ catalysts were prepared using the wet impregnation method, and subsequently subjected to a post-synthesis heat treatment protocols that involves calcining the catalysts first, followed by reduction. The monometallic Pt/TiO₂ with 0.6% wt Pt reported in chapter 3 shows excellent activity for hydrogenation of furfural (FF) to furfural alcohol (2-FFA) at 30°C under 0.3 MPa H₂ gas. The Pt/TiO₂ (0.6%, Cal. + Red) catalyst presented high conversion, 97%, and high selectivity for 2-FFA (95%) after 6 h. Although this catalyst exhibits high activity, gradual loss of activity over three cycles was observed. This poor stability infers that the monometallic Pt/TiO₂ catalyst is not sustainable.

To tune the activity of the monometallic Pt/TiO₂ and improve its stability and sustainability, the 0.6wt% Pt/TiO₂ catalyst was diluted with other metals (Pd, Ru and Au) and the resulting bimetallic catalyst generated were investigated for their catalytic activity and stability. It is important to note that bimetallic catalyst is equally often employed for lowering the amount of platinum and other precious metals in catalytic reactions.³⁹

Consequently, this chapter aims to explore the roles of other metals in the Pt-based bimetallic catalysts (RuPt, RuPd, AuPt and PtPd) supported on TiO₂ in the hydrogenation of FF to 2-FFA. Specifically, their activity and selectivity will be compared to Au, Ru and Pd monometallic catalysts supported on TiO₂. The different bimetallic and monometallic catalysts will be subjected to the same post-synthesis heat treatment protocols described in chapter 2.

The objective of this chapter is to prepare, characterise and compare the catalytic activity and selectivity of monometallic (Ru, Au and Pd) and bimetallic (RuPt, RuPd, AuPt, PtPd) catalysts supported on TiO₂. Furthermore, the stability of the bimetallic catalyst was assessed, and the structure-activity correlation was investigated.

4.2 Results and discussion

4.2.1 Monometallic Vs bimetallic catalysts – catalyst testing:

A series of monometallic catalysts with Ru, Pd and Au, and bimetallic catalysts comprising of PtAu, PtRu, PtPd and PdRu, supported on TiO₂ were prepared using the wet impregnation method and characterised in order to assess their catalytic activity and selectivity in liquid phase hydrogenation of FF. As is well known, noble metals have high hydrogenation activity, albeit, with poor selectivity.⁴⁰ The catalysts were synthesised using the wet impregnation method, followed by calcination at 450 °C for 4 h (using flow air) then reduction at 450°C for 4 h under a flow of 5% H₂/Ar. The molar ratio of the metals in the bimetallic catalyst was made to be 1:1 and the reactions were carried out under identical reaction conditions specified in Chapter 3 (15 ml of the solvent i-PrOH, 30 °C and 0.3 MPa of H₂ for 3 h). It has been reported in some publications that mild reaction conditions present a low chance of forming acetalisation products and prevent the poisoning of the catalyst surface by decarbonylation of the FF.⁴¹⁻⁴³ Metal load of 0.6 wt.% was selected for all further catalysts prepared and we can link their catalyst activity with the increased active site concentration of these catalysts. The product distribution of the liquid phase hydrogenation of FF using monometallic and bimetallic catalysts are as

presented in Figure 4.1 and the hydrogenation products were summarised in Scheme 4.1. The products obtained from the reaction mixtures were analysed using GC and GC-MS. It is possible to hydrogenate various functional groups in FF compounds, such as C=O of the carbonyl groups and C=C in the furan ring.^{17, 29, 44} It is of note that in this study, our target product from the hydrogenation of FF mainly 2-FFA.

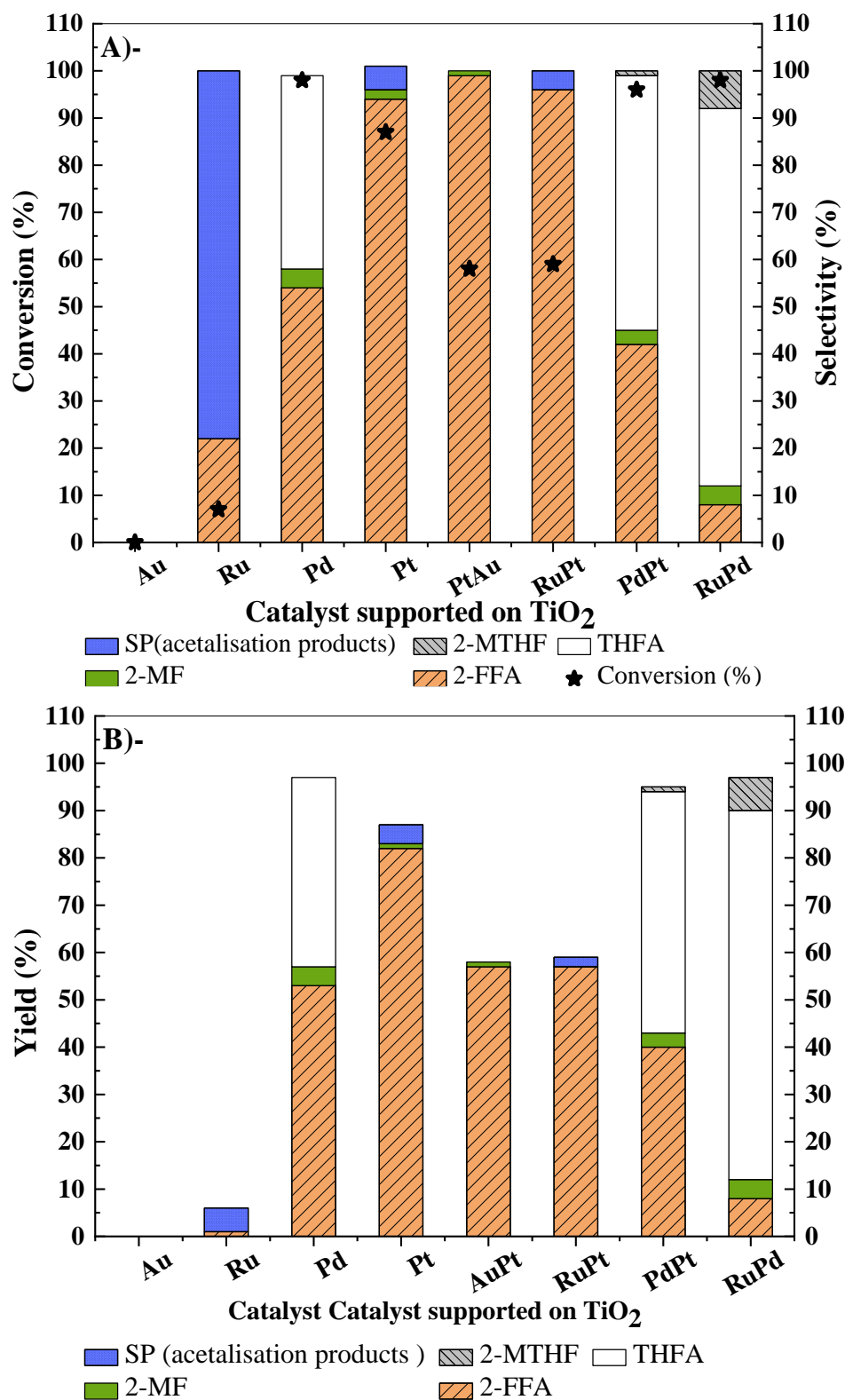
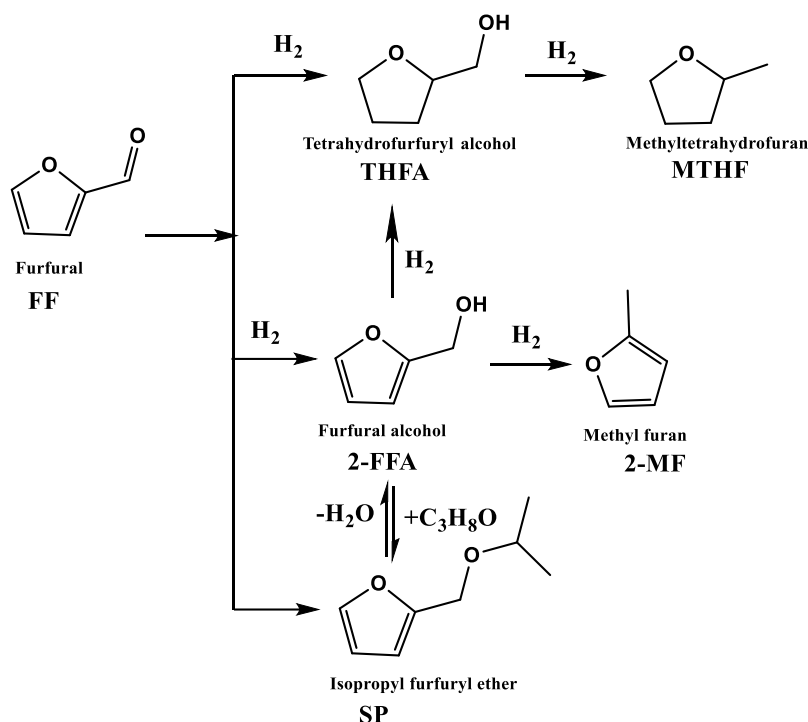


Figure 4.1: Hydrogenation of FF by monometallic and bimetallic catalysts. A)- FFA selectivity. B)- FFA yield. reaction conditions: FF (4.45 mmol), *i*-PrOH (15 mL), temp. 30°C, H₂ (0.3 MPa), substrate/metal molar ratio =207, time (3h).



Scheme 4.1: The observed products for hydrogenation of FF using monometallic and bimetallic catalysts.

Two modes of FF adsorption on the catalyst's surface have been reported in literature and they are as illustrated in Figure 4.2.^{40, 45} FF could be adsorbed in a vertical mode which is favourable to the production of 2-FFA. On the other hand, FF could also be adsorbed in a planar mode via the C=C in the furan ring.^{40, 45} According to theoretical hypotheses about the hydrogenation of the α,β -unsaturated aldehydes put forward by Delbecq and Sautet, the relative adsorption of C=C and C=O groups is reliant on the radial expansion of the metal's d orbitals.⁴⁶

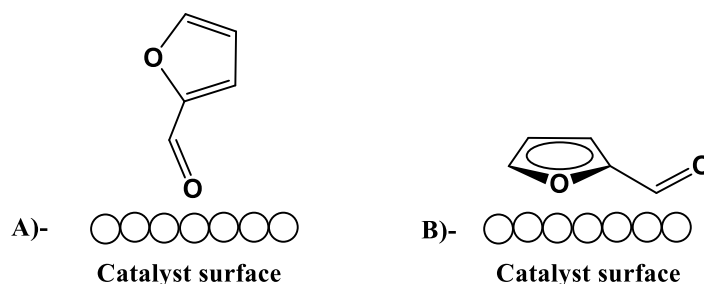


Figure 4.2: The FF Adsorption mode of FF on a metal surface (A) a vertical mode and (B) a planar mode.

For comparing Pd and Pt, the Pd bulk has a slightly higher Fermi level than Pt and more importantly, a d-band width significantly reduced compared to that of Pt, which means that the radial expansion of the Pd d orbitals is smaller than that of the Pt d orbitals. As a consequence, the overlaps of these orbitals with the orbital of the adsorbate molecule are reduced on Pd and the result is a weakening of the interaction between the molecule and the surface, especially the four-electron interaction whose preponderant role has already been underlined. Therefore, the more important the four-electron interaction the more stabilised the corresponding adsorption geometries when Pd replaces Pt. This is the reason, why the ρ_2 modes are more strongly bonded on Pd than on Pt, particularly the π geometries, which decreases the possibility that adsorption would take place through a planar mode. For the Pt/TiO₂ system, the repulsive interaction with the C=C bond would be the greatest so the adsorption of FF through the carbonyl group would be favoured.⁴⁰, Which caused the interaction of each metal with FF in a different way and that caused it to produce different products between each metal. For this reason, different metals were used for the hydrogenation of FF.

The prepared monometallic catalysts present different activities for the catalytic hydrogenation of FF. Pd/TiO₂ (0.6wt%) catalyst presented a complete conversion (98%) of FF, however, the selectivity of 2-FFA is about 54% after 3 h. The selectivity towards 2-FFA is low due to further hydrogenated products like the production of furan hydrogenation products tetrahydro furfuryl alcohol (THFA) with 41% selectivity and hydrolysis product 2-methyl furan (2-MF) 4% selectivity. whereas Pt was very active (87% and 94% selectivity)

Relatively, the Ru/TiO₂ (0.6wt%) catalyst displayed poor activity 7% conversion with 22% selectivity for FFA. Surprising, Ru catalyst is not active for this reaction. Moreover, Au/TiO₂ (0.6wt%) did not show any activity for the hydrogenation of FF.

The conversion of FF over the series of the prepared bimetallic catalyst increased in the following order: AuPt (58%) < RuPt (59%) < PtPd (96%) < RuPd (98%). However, the yield of 2-FFA was found to proceed in the opposite direction as follows: AuPt (57%) , RuPt (57%) > PtPd (40%) > RuPd (8%).

The conversion of FF over PtRu/TiO₂ catalyst was high (59%), with 96% selectivity towards 2-FFA (2-FFA yield = 57%). PdRu/TiO₂ catalyst equally showed high activity for the hydrogenation of FF with a complete conversion of FF (98%) after 3 h. However, the selectivity

of 2-FFA is low (8%) due to the hydrogenation of furan, which led to the formation of THFA (Scheme 4.1 and Figure 4.1).

Interestingly, the main product of FF hydrogenation over PtRu/TiO₂ and PtAu/TiO₂ catalysts is 2-FFA. PtAu/TiO₂ bimetallic catalyst displays high conversion (58%) with and 99% selectivity that is marginally better than PtRu/TiO₂ catalyst (59% conversion with 96% selectivity). While PtPd/TiO₂ exhibit 96% activity and 42% selectivity towards 2-FFA. Additionally, (THFA) was produced in 54% selectivity over PtPd/TiO₂. The PtRu/TiO catalyst selectivity is different from the selectivity displayed by PtPd/TiO₂ and PdRu/TiO₂ catalysts. The main product over PtPd/TiO₂ is THFA. It should be noted that adding Pd to the Pt/TiO₂ catalyst showed slightly lower selectivity because of the hydrogenation of furan ring and carbonyl compound to production THFA as compared to the corresponding Pt/TiO₂ catalyst. These results demonstrate that the addition of the second metal could block the active site, hence, reducing the chemoselectivity of hydrogenation reaction over Pt metal site.

The overall outlook suggests that Pt-based catalysts (both monometallic and bimetallic) are more selective for hydrogenation of the C=O group on FF to produce 2-FFA. However, Pd-based catalysts show medium to low selectivity towards the C=O. Adsorption configurations and site preferences can significantly influence reaction selectivities,^{47, 48} and these results suggest that the Pd species have strong adsorption to the π -electrons and the carbonyl group in the furan ring, resulting in parallel adsorption of FF to the catalyst surface.^{47,49} In contrast, the Pt particles preferentially interact with the carbonyl group in the FF compound. The selectivity of the Pt-based catalysts can be attributed to the strong electronic repulsion between the d-electrons and π -electrons in C=C bond in the furan ring.^{50, 51 47}

4.2.2 Time-on-line studies

The FF conversion over a monometallic Ru/TiO₂ catalyst increases with an increase in the reaction time (1-6 h) as expected (Figure 4.3). 2-FFA was produced by monometallic Ru/TiO₂ catalysts, however, the catalyst presented poor catalyst activity (2-14% conversion). This result is in line with the report by Aldosari *et al.*⁵² They achieved excellent selectivity towards 2-MF (52 %) and 2-FFA (45 %) over RuPd/TiO₂, albeit with 36% conversion of FF at RT under 3 bar of H₂ in octane. This is a reasonable compromise compared to the high conversion of FF

(65%) over Pd/TiO₂ with diverse product distribution 36% selectivity for 2-MF and 29% selectivity for 2-FFA). Addition of Ru to Pd/TiO₂ changed the catalyst selectivity and product distribution.

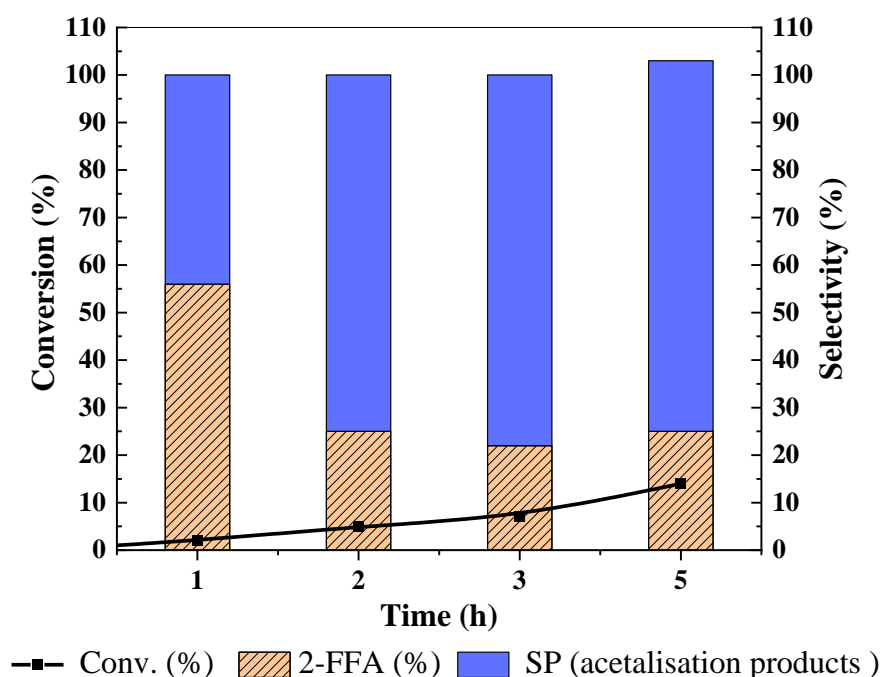


Figure 4.3: Hydrogenation Furfural over 0.6% Ru/TiO₂ calc + red catalyst (reaction conditions: FF (4.45 mmol), *i*-PrOH (15 mL), temp. 30°C, H₂ (0.3 MPa), substrate/metal molar ratio =207, time (6h).

The conversion of FF over 0.6% Ru/TiO₂ is 8%, with 22% selectivity for 2-FF in 3 h at 30°C under 0.3 MPa of H₂. Adding Pt to Ru/TiO₂ catalyst improves the catalyst activity and selective towards 2-FFA significantly. In addition, the acetal product was also reduced to 7% (Figure 4.4). From the results, PtRu/TiO₂ catalyst show higher activity and selectivity than pure monometallic Ru/TiO₂ catalyst. The only products formed over PtRu/TiO₂ in this reaction were 2-FFA and 3-7% acetalisation product. However, after 9h reaction time, further hydrogenation of the product is observed resulting in the formation of THFA and 2-MF. Over time, the conversion of FF over bimetallic PtRu/TiO₂ increases from 29% to 94% from 1 to 9 h.

Relative to the monometallic Pt/TiO₂ (0.6wt%, (cal + red)) catalyst, this bimetallic RuPt/TiO₂ catalyst presents a lower catalytic performance in the liquid phase hydrogenation of FF to 2-FFA. At iso-conversion, the product selectivity for monometallic Pt/TiO₂ and bimetallic

PtRu/TiO₂ is shown in Figure 4.5. At 50% Furfural conversion level, Pt/TiO₂ catalyst produces 2-FFA as the major product with 100% selectivity while PtRu/TiO₂ catalyst produces 93% selectivity for 2-FFA with 7% of other products.

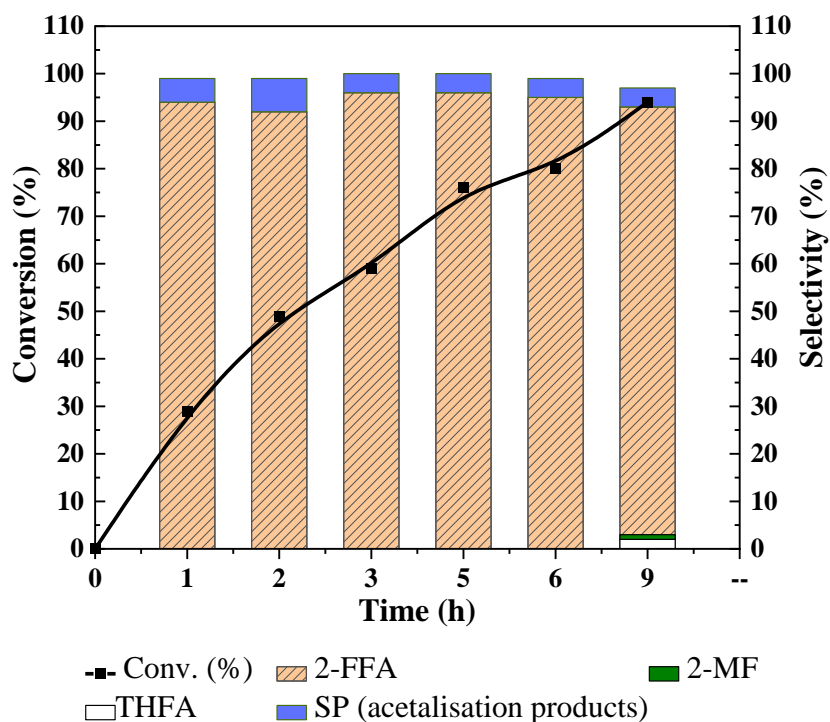


Figure 4.4: Hydrogenation Furfural over 0.6%PtRu/TiO₂ (reaction conditions: reaction conditions: FF (4.45 mmol), *i*-PrOH (15 mL), temp. 30°C, H₂ (0.3 MPa), substrate/metal molar ratio =207, time (9h).

This result could be attributed to the small Ru particle size, which favors formation of 2-MF product.⁵³ The conversion of FF over RuTiO₂ is too low to be included in the iso-conversion comparative analysis.

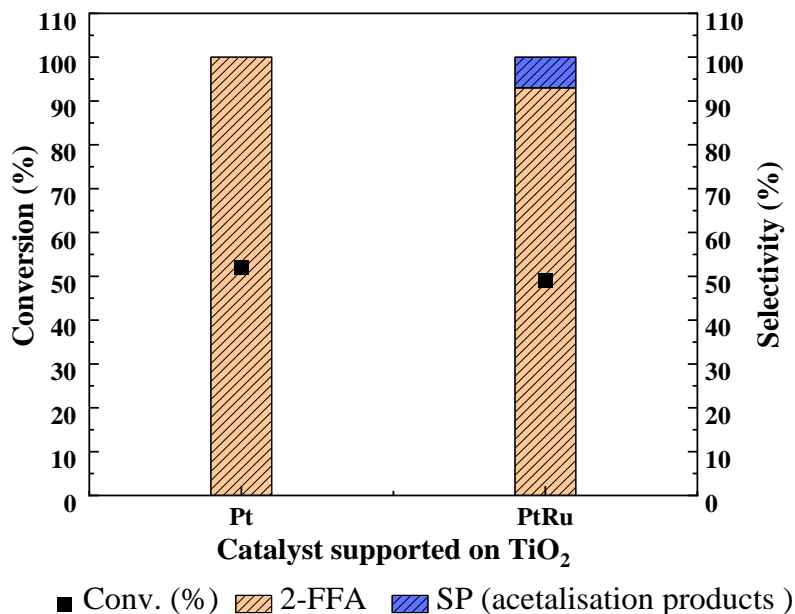


Figure 4.5: Hydrogenation products distribution of FF by 0.6%PtRu/TiO₂ and Pt/TiO₂ at iso-conversion values (filled squares) of 49-52% conversion, (reaction conditions: FF (4.45 mmol), *i*-PrOH (15 mL), temp. 30°C, H₂ (0.3 MPa), substrate/metal molar ratio =207).

Figure 4.6 below shows the time online results for FF hydrogenation using RuPd/TiO₂ catalyst, with 96% conversion achieved in 1 h. In the initial stage, after 1 h, 2-FFA was produced with high selectivity, however, the 2-FFA yield decreased over time, due to further hydrogenation of product resulting in the formation of THFA. Over time, 2-FFA was fully consumed and THFA was further hydrogenated to 2-MTHF as presented in Scheme 4.2.

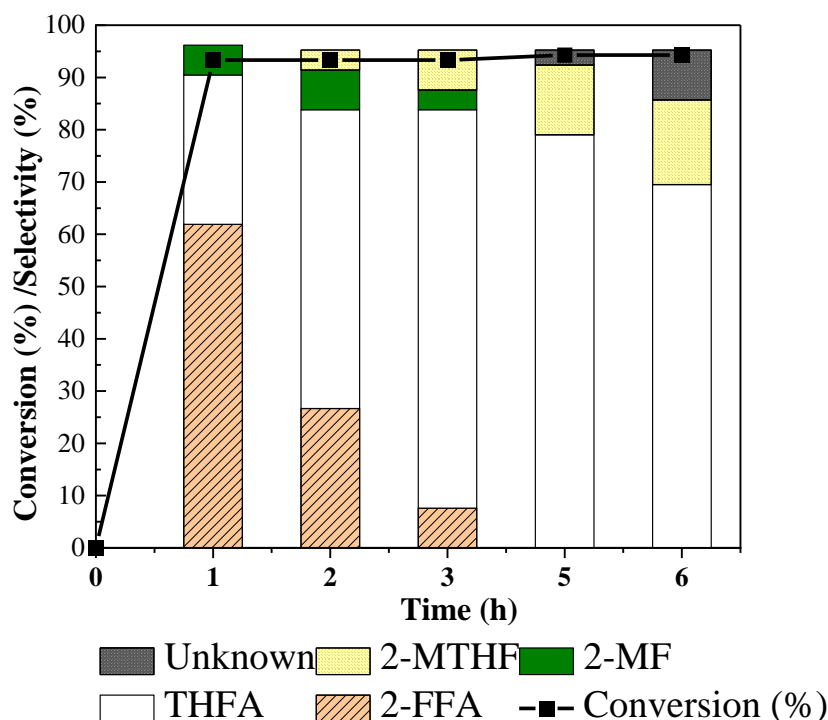


Figure 4.6: Time online plot for hydrogenation Furfural over 0.6% PdRu/TiO₂ catalyst. (Reaction conditions: FF (4.45 mmol), *i*-PrOH (15 mL), temp. 30°C, H₂ (0.3 MPa), substrate/metal molar ratio =207.

4.3 Catalyst stability

Besides activity and selectivity, catalyst stability is another important parameter that determines the lifetime of a catalyst and hence, its recyclability. In FF hydrogenation, catalyst stability is crucial just like catalyst activity and selectivity and the stability of the catalyst makes it suitable for industrial application. It has been reported that catalyst stability could be improved by structural promoters⁵⁴ and bimetallic catalyst with second metal promoter often present high catalyst stability. For instance, Bharath et al.⁵⁵ reported that bimetallic RuPd supported on hexagonal boron nitride (h-BN) presented high stability for hydrogenation of FF to 2-FFA. They found the catalyst to be stable for 5 cycles without losing its activity, and the hydrogenation did not impact any change in the structure of the catalyst. Synthetic protocols have been observed to be vital for catalyst stability. Ru-Pd/BN NCs were successfully produced on the surfaces of BN nanosheets by microwave irradiation for 30 s, resulting in Ru-Pd nanoclusters that self-assemble into spherical-like Ru-Pd bimetallic catalytic sites.⁵⁵ Also, RuCo/C catalyst presented high stability for the hydrogenation of the FF due to strong metal-support interaction.⁵⁶ The PtRu/SiO₂ catalyst showed stability for use in three cycles for

hydrogenation of the carbonyl group.⁵⁷ This bimetallic cluster catalyst was loaded on mesoporous silica by making a slurry and the mesopore-cluster was activated by heating at 195 °C in vacuo for 2 h.

For these reasons, we were hoping that the addition of Ru to Pt/TiO₂ catalyst could improve the catalyst stability. The stability of the catalyst was tested for three cycles at 30°C under 3 bar of hydrogen using isopropanol as solvent. The catalyst was recovered after each cycle and then washed twice using isopropanol and once with acetone to remove any impurities on the catalyst surface. Consequently, the catalyst was left to dry at room temperature before the next run.

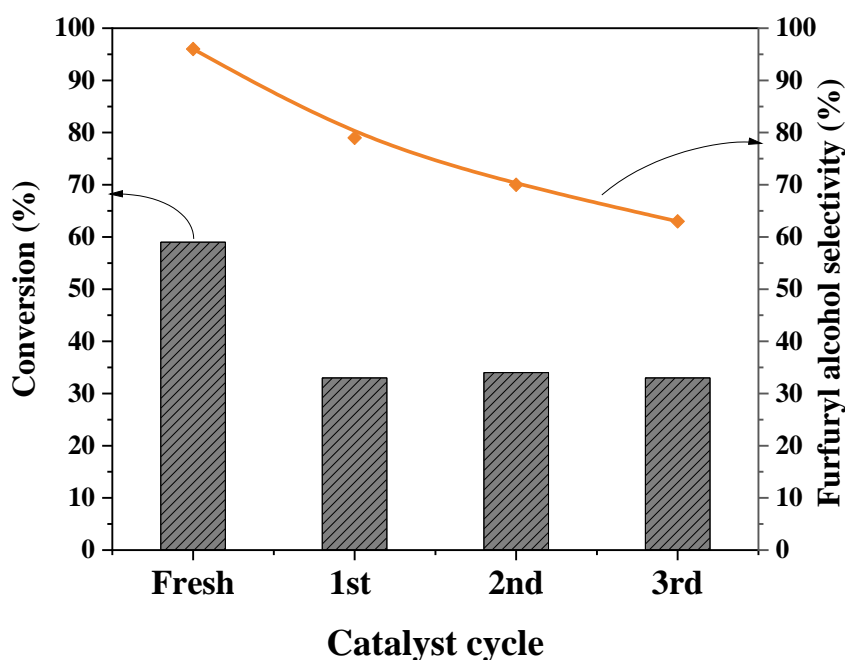


Figure 4.7: 0.6%RuPt/TiO₂ Catalyst reusability for FF hydrogenation. reaction conditions: FF (4.45 mmol), *i*-PrOH (15 mL), temp. 30°C, H₂ (0.3 MPa), substrate/metal molar ratio =207, time (3h).

The stability of PtRu/TiO₂ (cal + red) catalyst reusability and performance was assessed by multiple successive catalytic runs and the result obtained is shown in Figure 4.7 above. The catalyst activity decreased by 25% after the first reuse and remained stable after the second and third consecutive runs. The conversion over Fresh catalyst presented 59% with a 96% selectivity for 2-FFA, while through the 3rd reuse, the spent catalyst displayed a 33%

conversion with a 63% selectivity for 2-FFA. The Bimetallic 0.6% RuPt/TiO₂ catalyst activity deactivated during reuse and 2-FFA selectivity decreased gradually from 96% to 63% from the initial to the third consecutive runs.

The trend observed is in line with the report by Guadix-Montero et al.⁵⁸ where they found a gradual loss of activity of the bimetallic PtRu catalyst during the hydrogenolysis of glycerol. Sintering, leaching, and poisoning are some of the many ways by which metal catalysts get deactivated, and it is important to unravel the mode of deactivation of the PtRu/TiO₂ catalyst

4.4 Catalyst characterisation

To study and possibly unravel the reason(s) for the observed differences in the catalysts performances, XPS and TEM were employed to analyse both the monometallic Ru/TiO₂ catalyst and the bimetallic PtRu/TiO₂ catalyst.

4.4.1 X-ray photoelectron spectroscopy

The catalysts are characterised using XPS technique, which provides valuable information about the local bonding environment of the species on the surface of the catalysts, i.e., chemical composition, bonding energies and oxidation state(s).⁵⁹⁻⁶¹ The XPS analysis proved information about the effect of heat treatment protocols on the oxidation states and surface concentrations of Ru/TiO₂ catalyst and the bimetallic 0.6% PtRu/TiO₂ (calc + red) catalyst. The XPS analysis of Ru/TiO₂ catalyst revealed the nature of the species at the surface of the catalyst and the oxidation state of Ru species on the support (TiO₂) for dried only sample and calcined + reduced sample, as shown in Figure 4.8. For Ru/TiO₂ dried only catalyst, the binding energy of Ru 3d spectrum exhibited a pair of peaks for Ru 3d_{5/2} at 280.7 eV and 3d_{3/2} at 284.8 eV which can be attributed to RuO₂ species.⁶²

The Ru/TiO₂ (calc + red) catalyst signal shifted to lower binding energy compared to the Ru/TiO₂ dried only catalyst. This catalyst presented two different environments for Ru 3d as shown in Figure 4.8. The first signal with a binding energy of 279.2 eV indicates the formation of metallic Ru⁰,⁶³⁻⁶⁵ while the other signal at 279.8 eV is associated with RuO_x. This RuO_x species may be present due to oxidise the atmosphere the oxygen species on the surface of the catalyst during calcination in the furnace.^{30, 62, 65, 66} The adventitious carbon binding energy (C 1s) at 284.8 eV overlapped with Ru 3d for all the present samples.⁶⁷

Figure 4.9 shows the XPS profiles of the bimetallic 0.6%PtRu/TiO₂ (calc + red) catalyst. The XPS results revealed there are no significant changes in the binding energy for Ru 3d and Pt 4f in the bimetallic catalyst compared with the monometallic Ru catalyst. The binding energy of the Ru 3d and Pt 4f in the bimetallic catalyst, presented at 279.4 eV and 70.5 eV, and these values can be attributed to Ru⁰ and Pt⁰ on the catalyst's surface. Comparing these results with the binding energy for Pt⁰ 4f_{7/2} (70.6 eV) for the monometallic 0.6%Pt/TiO₂ (chapter 3)). This suggests that there is no charge transfer between them. That could be because the electronegativity difference between Ru and Pt in the bimetallic catalyst does not occur.

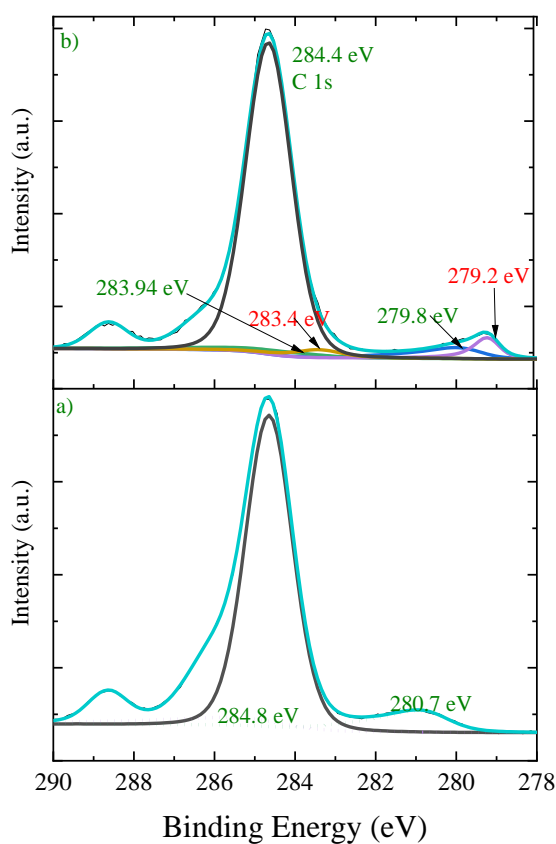


Figure 4.8: XPS profiles of the Ru 3d for 0.6%Ru/TiO₂ with different heat protocols- from (a) dried only catalyst,(b) calcined + reduced catalyst.

The binding energy for Ti 2p is observed at 458.4 eV and does not present any change in the spectrum. This result suggests that the TiO₂ support is stable under the conditions employed

for the preparation of this catalyst.⁶⁵ The metal concentration on the catalyst's surface obtained using XPS analysis is shown in Table 4.1.

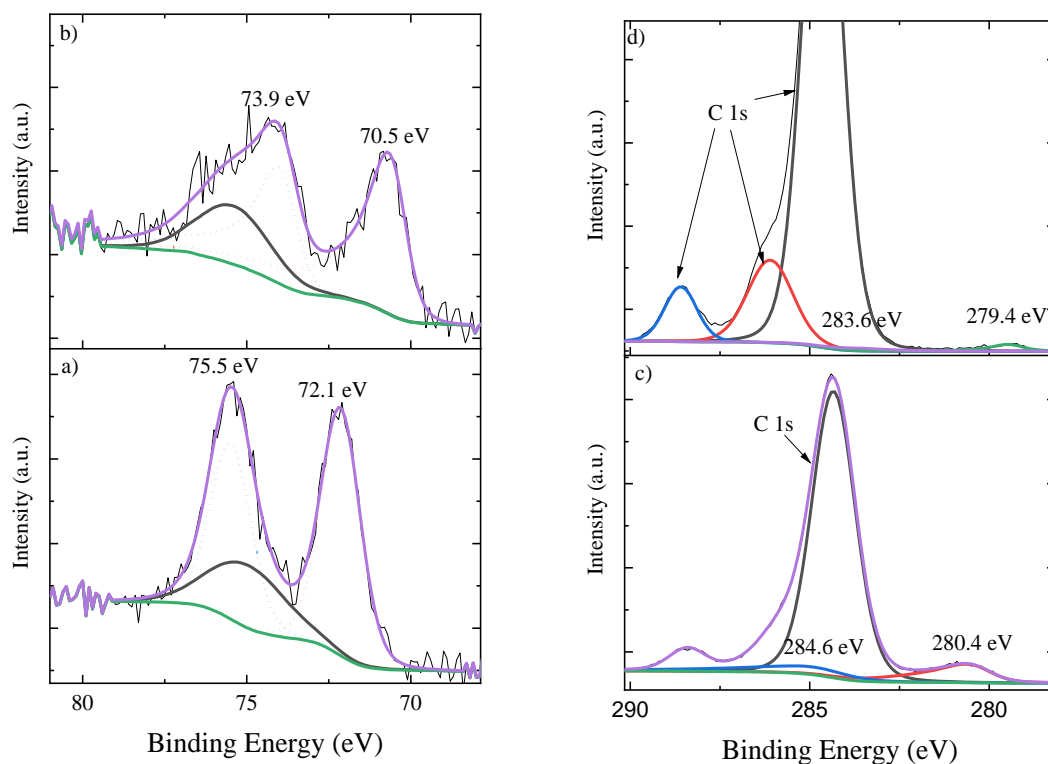


Figure 4.9: XPS profiles of (a) 0.6%PtRu/TiO₂ dried catalyst (Pt4f) and (b) 0.6%PtRu/TiO₂ calc+red catalyst (Pt4f), (c) 0.6%PtRu/TiO₂ dried catalyst (Ru 3d), (d) 0.6%PtRu/TiO₂ calc+red catalyst (Ru 3d).

The obtained results are closely similar to what has been documented in the literature.^{65, 66} The Pt–Ru alloy loaded on TiO₂ support was calcined and reduced and the results obtained from XPS characterisation is in agreement with the results reported by Zhang, *et al.*⁶⁵

Table 4.1: The XPS data for different monometallic and bimetallic.

Catalyst	Ru 3d	Ru 3d Metal	Pt 4f	Pt 4f Metal
0.6%Pt/TiO ₂ Calc + red	-	-		0.28
0.6%Ru/TiO ₂ dry	0.5	-	-	-
0.6%Ru/TiO ₂ Calc+ red	0.17	0.16	-	-
0.6%PtRu/TiO ₂ dry	0.25	-	0.19	-
0.6%PtRu/TiO ₂ Calc+ red	-	0.06		0.09
0.6%PtRu/TiO ₂ Calc+ red used		0.05	-	0.05

XPS technique was used to analyse the spent catalyst and the result obtained was compared with that of the fresh catalyst. It was found that the Pt concentration on the catalyst surface of the spent catalyst was less compared to the fresh catalyst as shown in Table 4.1. The Pt concentration was 0.09% on the fresh catalyst and 0.05% on the used catalyst. In addition, there were no changes in the binding energy of Pt NPs in the XPS analysis of the fresh catalyst and spent catalyst. This indicates that during the reduction reaction, the oxidation state of the Pt is no changed.

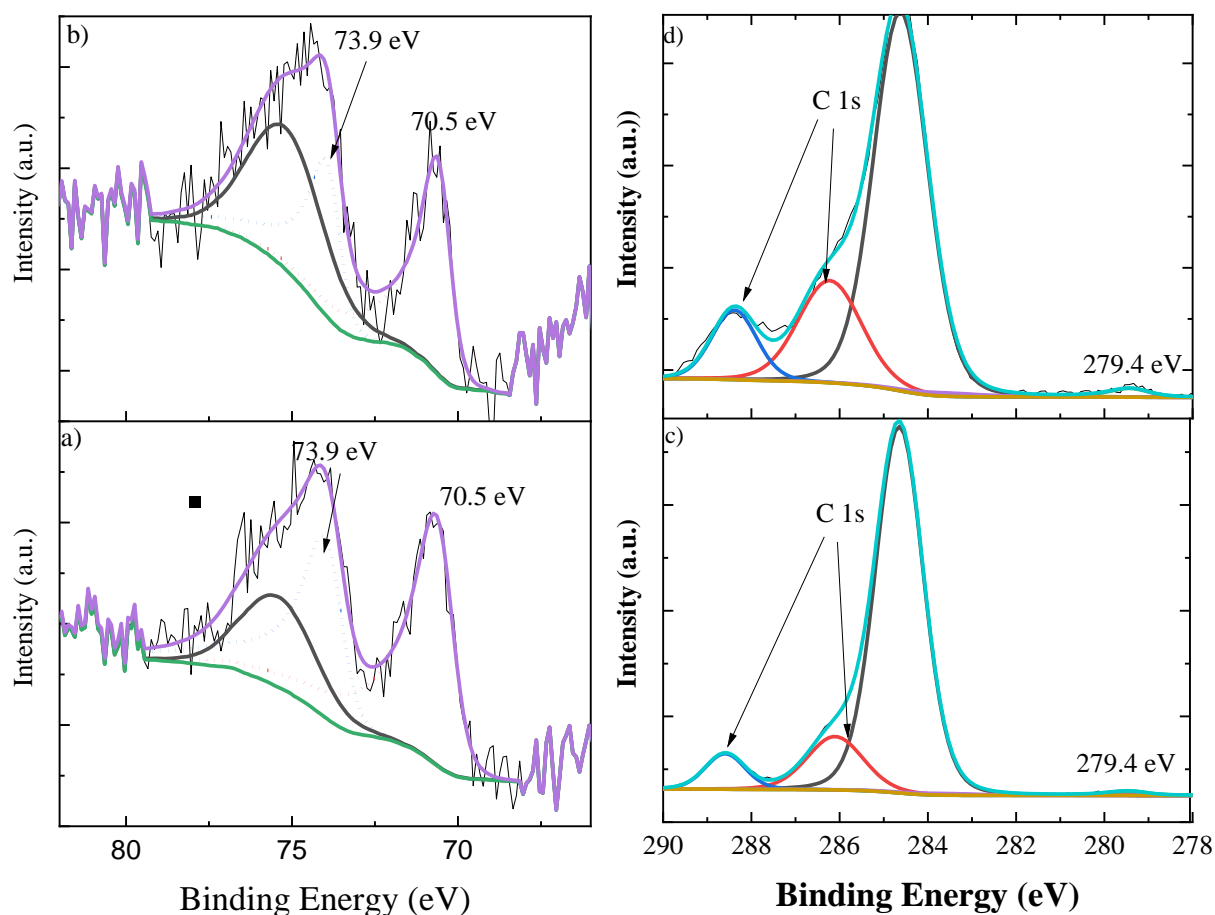


Figure 4.10: XPS profiles of 0.6%PtRu/TiO₂ (a) fresh catalyst and (b) spent catalyst for Pt4f, (c) fresh catalyst and (d) spent catalyst for Ru3d, .

The fresh and spent PtRu/TiO₂ catalyst were analysed using ICP to identify any leaching of the content of the metals in the catalysts. The ICP results indicated that the content of the metal in the fresh catalyst and spent catalyst was stable. Therefore, there was no leaching of metals from the catalyst as the content of the Pt NPs and Ru NPs was 0.2 wt.% and 0.05 wt.% in fresh catalyst and 0.2 wt.% and 0.04 wt.% in spent catalyst, respectively.

4.4.2 Transmission electron microscopy

The particle size distributions for monometallic Ru/TiO₂ catalyst and bimetallic PtRu/TiO₂ catalyst were investigated using TEM. Figure 4.11 shows the representative images and the distributions of associated particle size. The Ru/TiO₂ catalyst has a mean particle size ± 2.1 nm,

while that of the bimetallic RuPt is ± 1.3 nm. The reference Pt/TiO₂ catalyst has been previously characterised (Chapter 3) with a mean particle size of ± 1.3 nm.

Interestingly, the PtRu/TiO₂ catalyst presented the same mean particle size (± 1.3 nm) as the Pt/TiO₂ catalyst, however, there is a significant difference in their catalytic activity and product distribution in the hydrogenation of FF.

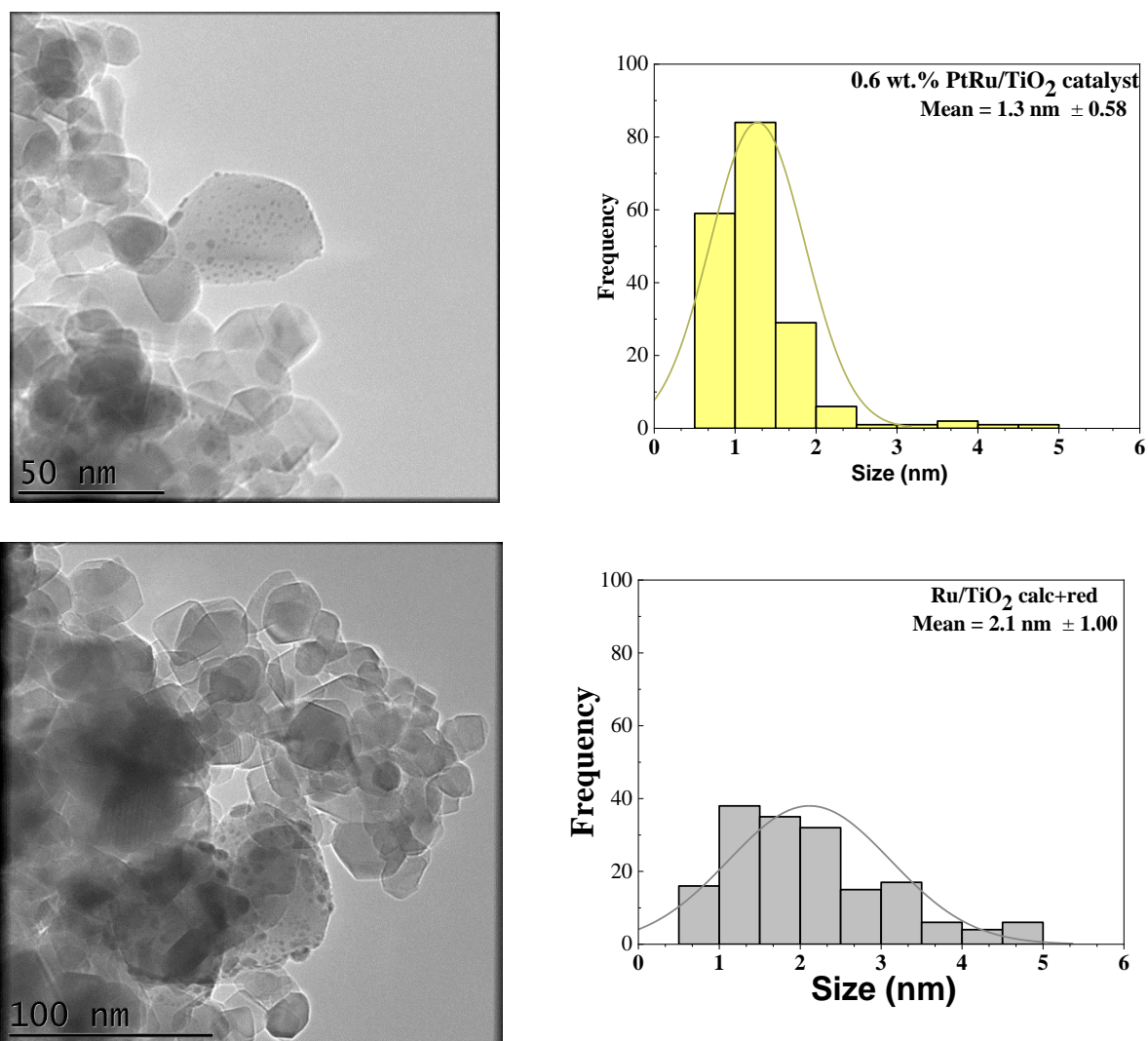


Figure 4.11: TEM micrographs and the size distribution histogram for PtRu/TiO₂ catalyst and Ru/TiO₂ catalyst (200 particles)

The activity of the bimetallic 0.6%PtRu/TiO₂ catalyst was marginally lower than the monometallic 0.6 % Pt/TiO₂ catalyst, albeit, with some side products. While the activity of

monometallic Ru is the least comparatively could be attributed to the size of the particles size are bigger (2.1 nm). TEM results suggest that the particle size in the monometallic 0.6% Pt/TiO₂ catalyst and the bimetallic 0.6 %RuPt/TiO₂ catalyst were similar (1.3 nm). However, the Pt⁰ species on the reducible TiO₂ support are required for high activity and selectivity in the hydrogenation of FF to 2-FFA. Through XPS analysis, the reference Pt catalysts were found majorly in a metallic Pt⁰ state on the catalyst surface, suggesting that Pt⁰ is the active site and responsible for the high activity and selectivity during the hydrogenation of FF.⁶⁸ It has also been observed that Pt species on the monometallic catalyst surface are usually higher than on the bimetallic catalyst surface, via XPS investigation. From the results presented earlier, the concentration of Pt⁰ species on the Pt/TiO₂ surface is 0.28 %, and 0.09% on the bimetallic RuPt/TiO₂. That could be the Ru particles do not hydrogenation of the carbonyl bond. Thus, the difference in the catalytic activity of the bimetallic catalyst compared to that of monometallic Pt could be explained by the fact that the large particle size of Ru particles could hinder the interaction of FF with the active Pt⁰ metallic site on the catalyst surface. as Obaid *et al.*⁵² reported that the large particle sizes of the Ru metal prevent the substrate FF from interacting with the Pd species on the RuPd/TiO₂ catalyst.

The Ru/TiO₂ catalyst presented a mean particle size of 2.1 nm, which could be the reason for the poor catalytic activity and selectivity. The observed phenomenon may be attributed to the concentration of Ru on the catalyst's surface, as XPS results indicated 0.5 Ru 3d on the Ru/TiO₂ reported that the large particle sizes of the Ru metal prevent the substrate (FF) from interacting with the Pd species on the RuPd/TiO₂ catalyst. particle sizes of the Ru metal in Ru/TiO₂ catalyst.

These results revealed that synthetic strategies, metal and particle size, are crucial to achieving extremely high catalytic activity. For instance, Luo *et al.*²¹ reported that Ru/TiO₂ catalyst prepared using modified impregnation methodology without using excess HCl (M_{Im}, 0M HCl) has a better catalyst with high activity for the hydrogenolysis of levulinic acid (LA) to *gamma*-valerolactone (GVL) but with poor selectivity relative to RuPd/TiO₂ catalyst. They suggest that the most active site of the Ru/TiO₂ catalyst was poisoned or blocked by the second metal, Pd. In addition, Obaid *et al.*⁵² reported a Pd/TiO₂ catalyst with higher activity than the bimetallic PdRu/TiO₂ catalyst. These authors proposed that the large particle sizes of the Ru metal prevent the substrate (FF) from interacting with the Pd species on the RuPd/TiO₂ catalyst. More recently, Tolek *et al.*²⁸ reported that Pt/TiO₂ catalyst prepared using the flame spray method presented high activity for the hydrogenation of FF to 2-FFA, and equally found that adding a

second metal, Co, to the catalyst impacted the catalyst negatively. They found Pt/TiO₂ catalyst to be more active than the bimetallic PtCo/TiO₂ due to the Pt dispersion and formation of Pt-TiO_x interface sites, which positively impact the hydrogenation of FF to 2-FFA. As a result of the uniform high dispersion and higher content of metallic Pt⁰, small particle size (1.3 nm) and a high catalyst surface, they approved a more active site on the catalyst⁶⁸. Thus, the substrate interacted better with the active site due to the strong interaction between the Pt⁰ and the TiO₂ support. This phenomenon is also ratified by the Sun and coworkers.⁶⁸ In their report, They found remarkable activity and selectivity of Pt/(Fe, Co)-BTC for the hydrogenation of FF to 2-FFA to the well-dispersed small-sized Pt NPs (approximately 1.7 nm) with a significantly greater content of surface Pt⁰ on the catalyst surface.⁶⁸ Mn- or co-modified MIL-100 (Fe) supports were prepared using a one-pot hydrothermal method. Subsequently, Pt nanoparticles were immobilized on MIL-100 (Fe, Co) through a simple and environmentally friendly ultrasonic impregnation-assisted hydrothermal polyol reduction method. For clarity in experiment descriptions, they refer to the reduction method as Pt/(Fe, Co)-BTC. BTC is 1,3,5-benzenetricarboxylate.

Transmission Electron Microscopy (TEM) was equally used to examine the fresh and spent catalyst to detect if there is any metal particle agglomeration.

The results in Figure 4.12 show that the partial size distribution of the spent PtRu/TiO₂ catalyst was raised by around 35% from 1.3nm for fresh PtRu/TiO₂ catalyst to 2 nm for spent PtRu/TiO₂ catalyst which suggests agglomeration of the bimetallic catalysts, and consequently, the active metallic species on the surface of the catalyst was lost. For this reason, we could suggest that the major deactivation pathway of this catalyst over three cycles in the reusability test is the sintering of the metal NPs.⁶⁹ The sintering issue is irreversible, and there is no way to regenerate the catalyst. For this reason, the replacement of this catalyst is a requirement.⁵⁴

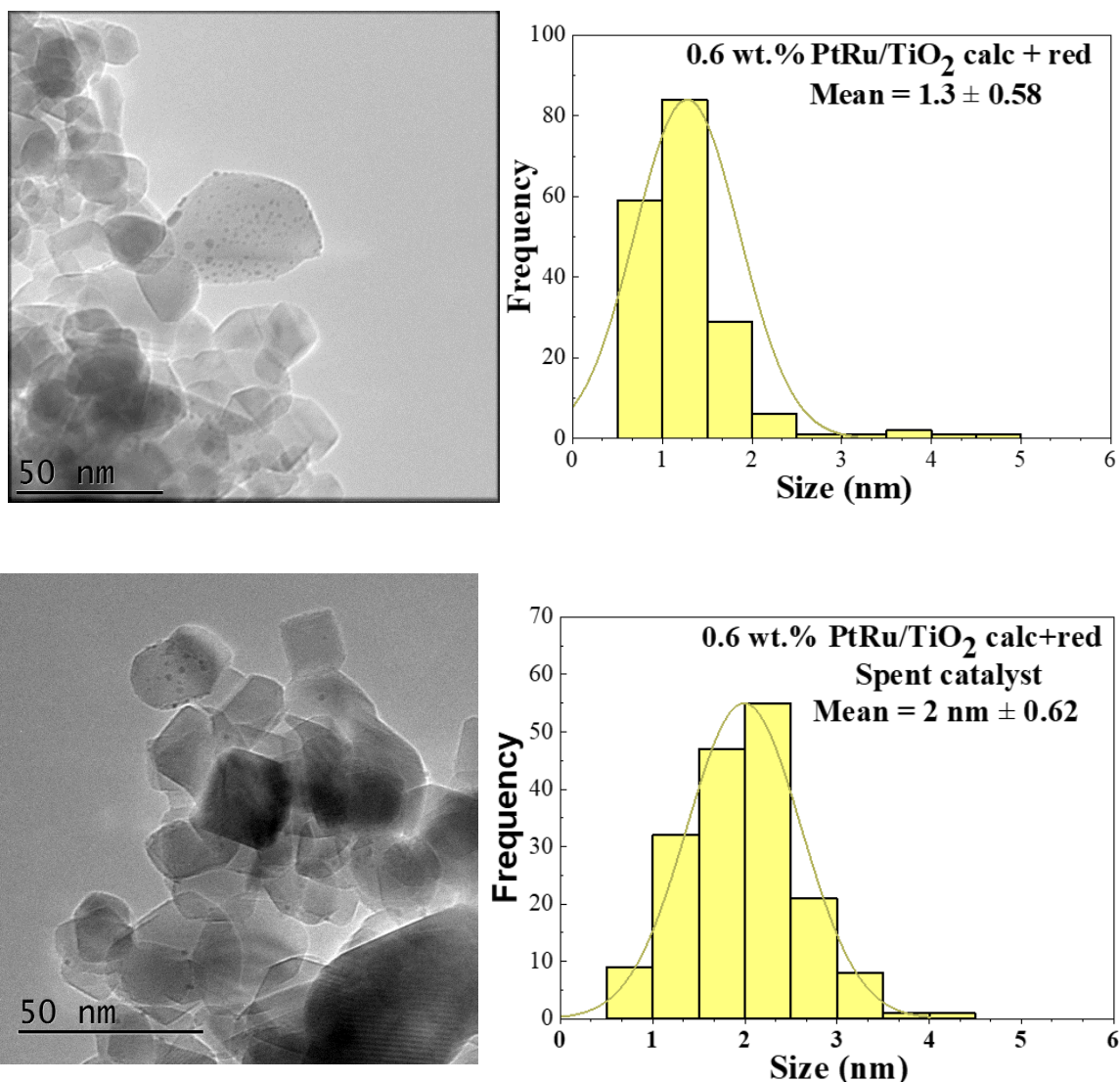


Figure 4.12: TEM micrographs and the size distribution histogram for a) fresh PtRu/TiO₂ catalyst b) PtRu/TiO₂ used catalyst (200 particles)

4.5 Conclusion

In this chapter, the primary objectives were to increase the activity and stability of Pt-based catalysts. Many studies have found that supported bimetallic catalysts have higher catalytic activity and stability than their monometallic counterparts. Hydrogenation of FF to 2-FFA can be affected by exploring alternative metals to platinum. Metals such as Au, Pd and Ru and bimetallics such as PtPd, PtAu, PtRu and RuPd on TiO₂ support have been explored.

All the bimetallic catalysts we worked on show good conversion of FF. Interestingly, both bimetallic PtRu and PtAu on TiO₂ support show good selectivity of 2-FFA, however, PtPd and RuPd display poor selectivity towards 2-FFA due to further hydrogenation of product(s). Both the Au/TiO₂ and Ru/TiO₂ catalysts show poor activity towards FF, however, Pd/TiO₂ display high activity towards FF but with low selectivity for 2-FFA.

TEM and XPS analyses of the bimetallic PtRu catalyst revealed valuable insights. The XPS results confirmed that the oxidation state of the Pt- and Ru-NPs on the catalyst are an essential factor for the selectivity of 2-FFA and the high selectivity on this catalyst could be attributed to the presence of Pt⁰ and Ru⁰ metals. This effectively makes it more selective towards the C=O bond. TEM indicate that small particle sizes are required for high conversion of FF and selectivity towards 2-FFA.

In spite of the high catalytic activity and selectivity of the bimetallic PtRu, the catalyst lost its stability after 3 cycles. The ICP result confirmed there was no leaching of active metals on the surface of the catalyst. Furthermore, the TEM result confirmed that the size of the metal particles increased by 35% compared to the fresh catalyst indicating the catalyst was deactivated over time due to the sintering.

Overall, in this work, we found that the best catalyst for hydrogenation of FF to 2-FFA with high activity and selectivity is 0.6% Pt/TiO₂ calc +red catalyst as reported in Chapter 3. Thus, modification of the 0.6% Pt/TiO₂ calc +red catalyst by adding a second metal did not improve the catalyst activity or stability for the hydrogenation of FF. So, the bimetallic catalysts is not better than the monometallic catalyst for the hydrogenation of FF.

4.6 References

1. Z. Jiang, S. Guo and T. Fang, *ACS Appl. Energy Mater.*, 2019, **2**, 7233-7243.
2. N. G. Dlamini, A. K. Basson and V. S. R. Pullabhotla, *Appl. Nano*, 2023, **4**, 1-24.
3. M. Sankar, N. Dimitratos, P. J. Miedziak, P. P. Wells, C. J. Kiely and G. J. Hutchings, *Chem Soc Rev*, 2012, **41**, 8099-8139.
4. N. Toshima, M. Harada, T. Yonezawa, K. Kushihashi and K. Asakura, *J. Phys. Chem.*, 1991, **95**, 7448-7453.
5. J. J. Pinto, A. Weilhard, L. T. Norman, R. W. Lodge, D. M. Rogers, A. Gual, I. Cano, A. Khlobystov, P. Licence and J. Alves Fernandes, *Catal. Sci. Technol.*, 2023, **13**, 4082.
6. Q. Wang, G. Wang, H. Xin, J. Liu, G. Xiong, P. Wu and X. Li, *Catal. Sci. Technol.*, 2019, **9**, 3226-3237.
7. U. K. Singh and M. A. Vannice, *Appl. Catal. A: Gen.*, (2001) **213** 1–24.
8. A. Silva, O. Santos, M. Mendes, E. Jordão and M. Fraga, *Appl. Catal. A: Gen.*, 2003, **241**, 155–165.
9. J. Fontana, C. Vignado, E. Jordao, F. C. A. Figueiredo and W. A. Carvalho, *Catal. Today*, 2011, **172**, 27-33.
10. C. H. Hao, X. N. Guo, M. Sankar, H. Yang, B. Ma, Y. F. Zhang, X. L. Tong, G. Q. Jin and X. Y. Guo, *ACS Appl Mater Interfaces*, 2018, **10**, 23029-23036.
11. S. Cattaneo, S. J. Freakley, D. J. Morgan, M. Sankar, N. Dimitratos and G. J. Hutchings, *Catal. Sci. Technol.*, 2018, **8**, 1677-1685.
12. M. Bao, Y. Liu, J. Deng, L. Jing, Z. Hou, Z. Wang, L. Wei, X. Yu and H. Dai, *Catalysts*, 2023, **13**.
13. N. Dimitratos, J. A. Lopez-Sanchez, D. Morgan, A. F. Carley, R. Tiruvalam, C. J. Kiely, D. Bethell and G. J. Hutchings, *Phys Chem Chem Phys*, 2009, **11**, 5142-5153.
14. A. Wang, X. Y. Liu, C.-Y. Mou and T. Zhang, *J. Catal.*, 2013, **308**, 258-271.
15. L. Luo, Z. Duan, H. Li, J. Kim, G. Henkelman and R. M. Crooks, *J Am Chem Soc*, 2017, **139**, 5538-5546.

16. R. W. J. Scott, O. M. Wilson, S.-K. Oh, E. A. Kenik and R. M. Crooks, *J. Am. Chem. Soc.*, 2004, , **126** 15583-15591.
17. Á. O'Driscoll, J. J. Leahy and T. Curtin, *Catal. Today*, 2017, **279**, 194-201.
18. P. Gallezot and D. Richard, *Catal. Rev.*, 1998, **40**, 81-126.
19. X. Lan and T. Wang, *ACS Catal.*, 2020, **10**, 2764-2790.
20. J. Teddy, A. Falqui, A. Corrias, D. Carta, P. Lecante, I. Gerber and P. Serp, *J. Catal.*, 2011, **278**, 59-70.
21. W. Luo, M. Sankar, A. M. Beale, Q. He, C. J. Kiely, P. C. Bruijninx and B. M. Weckhuysen, *Nat Commun*, 2015, **6**, 6540.
22. C. Han, L. Du, M. Konarova, D.-C. Qi, D. L. Phillips and J. Xu, *ACS Catal.*, 2020, **10**, 9227-9235.
23. P. de Souza, L. Silvester, A. da Silva, C. Fernandes, T. Rodrigues, S. Paul, P. Camargo and R. Wojcieszak, *Catalysts*, 2019, **9**, 132.
24. V. G. Baldovino-Medrano, G. Pollefeyt, V. Bliznuk, I. V. Driessche, E. M. Gaigneaux, P. Ruiz and R. Wojcieszak, *ChemCatChem*, 2016, **8**, 1157-1166.
25. S. Shafii, W. Lihua, M. R. Nordin and L. K. Yong, *J. Chem. Eng. Process. Technol.*, 2012, **3**.
26. I. A. Chetyrin, A. V. Bukhtiyarov, I. P. Prosvirin, A. K. Khudorozhkov and V. I. Bukhtiyarov, *Top. Catal.*, 2020, **63**, 66-74.
27. W. E. Kaufmann and R. Adams, *J. Am. Chem. Soc.*, 1923, **45**, 3029–3044.
28. W. Tolek, K. Khruachao, B. Pongthawornsakun, O. Mekasuwandumrong, F. J. C. S. Aires, P. Weerachawanasak and J. Panpranot, *Catal. Commun.*, 2021, **149**, 106246.
29. J. J. Musci, A. B. Merlo and M. L. Casella, *Catal. Today*, 2017, **296**, 43-50.
30. W. Tolek, N. Nanthasanti, B. Pongthawornsakun, P. Prasertthdam and J. Panpranot, *Sci Rep*, 2021, **11**, 9786.
31. Q. Wang, S. Santos, C. A. Urbina-Blanco, W. Zhou, Y. Yang, M. Marinova, S. Heyte, T.-R. Joelle, O. Ersen, W. Baaziz, O. V. Safonova, M. Saeys and V. V. Ordonsky, *Appl. Catal. B: Environ.*, 2022, **300**, 120730.

32. B. Li, G.-S. Hu, L.-Y. Jin, X. Hong, J.-Q. Lu and M.-F. Luo, *J. Ind. Eng. Chem.*, 2013, **19**, 250-255.
33. J. L. Snider, V. Streibel, M. A. Hubert, T. S. Choksi, E. Valle, D. C. Upham, J. Schumann, M. S. Duyar, A. Gallo, F. Abild-Pedersen and T. F. Jaramillo, *ACS Catal.*, 2019, **9**, 3399-3412.
34. G. Kennedy, L. R. Baker and G. A. Somorjai, *Angew. Chem. Int. Ed. Engl.*, 2014, **53**, 3405-3408.
35. A. Boffa, C. Lin, A. T. Bell and G. A. Somorjai, *J. Catal.*, 1994, **149**, 149– 158.
36. K. An, N. Musselwhite, G. Kennedy, V. V. Pushkarev, L. R. Baker and G. A. Somorjai, *J Colloid Interface Sci*, 2013, **392**, 122-128.
37. L. R. Baker, G. Kennedy, M. Van Spronsen, A. Hervier, X. Cai, S. Chen, L. W. Wang and G. A. Somorjai, *J Am Chem Soc*, 2012, **134**, 14208-14216.
38. E. Gross and G. A. Somorjai, *Top. Catal.*, 2013, **56**, 1049-1058.
39. M. H. Jang, O. Kizilkaya, A. J. Kropf, R. L. Kurtz, J. W. Elam and Y. Lei, *J Chem Phys*, 2020, **152**, 024710.
40. Y. Zheng, X. Wang, X. Fu and K. Wei, *Appl. Organomet. Chem.*, 2007, **21**, 836-840.
41. J. M. Bell, D. G. Kubler, P. Sartwell and R. G. Zepp, *J. Org. Chem.* , 1965., **30**, 4284–4292.
42. N. Minne and H. Adkins, *J. Am. Chem. Soc.* , 1933, **55**, 299–309.
43. M. J. Taylor, L. J. Durndell, M. A. Isaacs, C. M. A. Parlett, K. Wilson, A. F. Lee and G. Kyriakou, *Appl. Catal. B: Environ.*, 2016, **180**, 580-585.
44. C. Especel, D. Duprez and F. Epron, *C. R. Chim.*, 2014, **17**, 790-800.
45. H. Rojas, G. Borda, D. Rosas, J. J. Martínez and P. Reyes, *Dyna*, 2008, **75**, 115-122.
46. F. Delbecq and P. Sautet, *J. Catal.*, 1995, **152**, 217-236.
47. B. Liu, L. Cheng, L. Curtiss and J. Greeley, *Surf. Sci.*, 2014, **622**, 51-59.
48. S. H. Pang, A. M. Román and J. W. Medlin, *J. Phys. Chem. C*, 2012, **116**, 13654-13660.
49. S. Bhogeswararao and D. Srinivas, *J. Catal.*, 2015, **327**, 65-77.
50. F. Delbecq and P. Sautet, *J. Catal.*, 2002, **211**, 398-406.

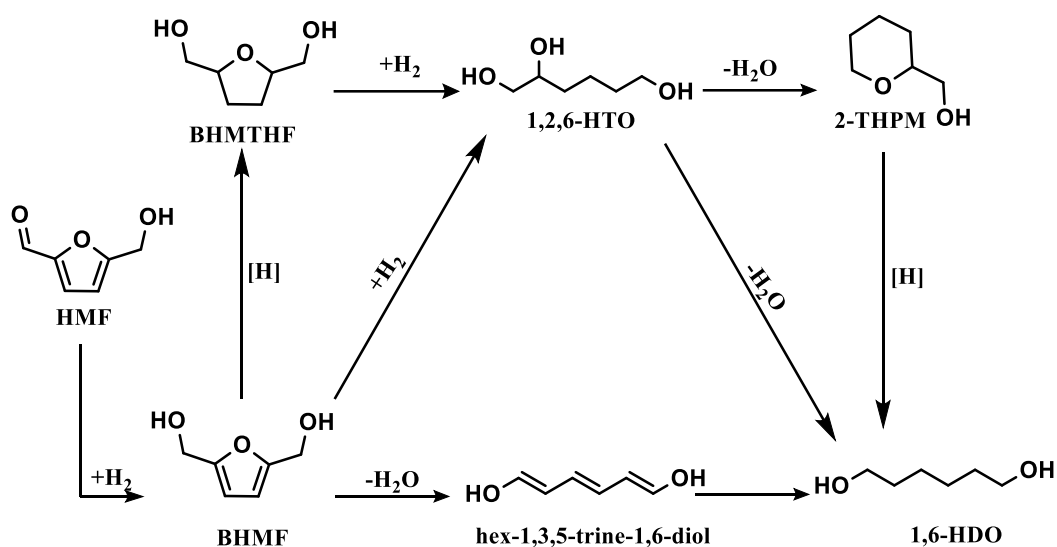
51. A. Richel, P. Maireles-Torres and C. Len, *Curr. Opin. Green Sustain. Chem.*, 2022, **37**.
52. O. F. Aldosari, S. Iqbal, P. J. Miedziak, G. L. Brett, D. R. Jones, X. Liu, J. K. Edwards, D. J. Morgan, D. K. Knight and G. J. Hutchings, *Catal. Sci. Technol.*, 2016, **6**, 234-242.
53. B. Wang, C. Li, B. He, J. Qi and C. Liang, *J. Energy Chem.*, 2017, **26**, 799-807.
54. G. Ertl, H. Knözinger, F. Schüth and J. Weitkamp, *Handbook of Heterogeneous Catalysis*, KGaA, Wiley-VCH Verlag GmbH, 2008.
55. G. Bharath, K. Rambabu, A. Hai, F. Banat, S. Rajendran, D. D. Dionysiou and P. Loke Show, *Fuel*, 2021, **290**.
56. Z. Gao, L. Yang, G. Fan and F. Li, *ChemCatChem*, 2016, **8**, 3769-3779.
57. R. Raja, T. Khimyak, J. M. Thomas, S. Hermans and B. F. G. Johnson, *Angew. Chem. Int. Ed.*, 2001, **40**, 4638-4642.
58. S. Guadix-Montero, PhD thesis, Cardiff University, 2019.
59. J. Chastain and R. C. K. Jr, *Handbook of X-ray photoelectron spectroscopy.*, erkin-Elmer Corporation, , 1992.
60. P. Miedziak, PhD thesis, Cardiff University, 2009.
61. J. W. Niemantsverdriet, *Spectroscopy in catalysis: An introduction*, VCH Weinheim, 1995.
62. D. J. Morgan, *Surf. Interface Anal.*, 2015, **47**, 1072-1079.
63. N. Hamzah, N. M. Nordin, A. H. A. Nadzri, Y. A. Nik, M. B. Kassim and M. A. Yarmo, *Appl. Catal. A: Gen.*, 2012, **419-420**, 133-141.
64. H. Over, A. P. Seitsonen, E. Lundgren, M. Smedh and J. N. Andersen, *Surf. Sci.*, 2002, **504** L196–L200.
65. T. Zhang, S. Wang and F. Chen, *J. Phys. Chem. C*, 2016, **120**, 9732-9739.
66. E. A. Paoli, F. Masini, R. Frydendal, D. Deiana, C. Schlaup, M. Malizia, T. W. Hansen, S. Horch, I. E. L. Stephens and I. Chorkendorff, *Chem Sci*, 2015, **6**, 190-196.
67. H. Wang, P. Ning, Q. Zhang, X. Liu, T. Zhang, J. Fan, J. Wang and K. Long, *Appl. Catal. A: Gen.*, 2018, **561**, 158-167.

68. W. Sun, L. Luo, J. Li, X. Tian, D. Yan and Y. Zhu, *Catal. Lett.*, 2021, DOI: 10.1007/s10562-021-03656-y.
69. M. Bowker, *The Basis and Applications of Heterogeneous Catalysis*, oxford science publications, 1998.

Chapter 5: Hydrogenolysis of 5-hydroxymethyl furfural to 1,6-hexanediol

5.1 Introduction

The direct transformation of hydroxymethylfurfural (HMF) to 1,6-hexanediols (1,6-HDO) by heterogeneous catalysts offers an attractive route toward preparing high-value chemicals from renewable feedstocks. HMF can be produced from cellulose, sugar, or lignocellulosic biomass.¹⁻⁴ HMF is one of the 12 platform molecules recognized by the U.S. Department of Energy (DOE)⁵ and it can serve as feedstock for the production of 1,6-HDO. 1,6-HDO contains dihydroxyls at the molecule terminals, making it an ideal monomer in polymer synthesis⁶ and it is used in the preparation of polyesters, polyester polyols, and polyurethanes.⁶⁻⁸ The unique properties of 1,6-HDO, such as high mechanical strength, low glass transition temperature, high heat resistance and high level of performance with minimal environmental impact make it an intermediate of choice, highly sought after by manufacturers.⁹ 1,6-HDO is currently produced by catalytic reduction of adipic acid using a cobalt catalyst (homogeneous catalyst).¹⁰ ¹¹ This route has many disadvantages, including low 1,6-HDO yield and using non-renewable petroleum feedstocks responsible for global warming.⁹ Therefore, the green synthesis of 1,6-HDO from biomass offers numerous advantages and has attracted significant attention recently.^{9, 12} There are two possible ways of preparing 1,6-HDO from catalytic hydrogenation/hydrogenolysis of HMF. One pathway is the direct furan ring opening followed by hydrogenation of the C=O and the C=C bond,¹³ or by HMF hydrogenation to 2,5-dihydroxy methyl tetrahydrofuran (DHMTHF) followed by hydrogenolysis (ring-opening) of the furan ring.¹⁴ Selective and sequential hydrogenation/hydrogenolysis of HMF is still a challenging reaction because HMF contains hydroxyl, aldehyde, and C=C in the furan ring. If the catalyst employed is not highly selective towards a particular functionality, it could lead to the generation of many other possible by-products and intermediates products such as 2,5-dihydroxymethylfuran (DHMF), 2,5-dihydroxy methyl tetrahydrofuran (DHMTHF), 1,6-hexanediol (1,6-HDO) and 1,2,6-hexanetriol (1,2,6-HTO) during HMF hydrogenation as shown in the Scheme 5.1.^{9, 10, 12, 15, 16} Therefore, highly selective catalysts are crucial and required to obtaining the desired product.



Scheme 5.1: The pathway production of 1,6-HDO from HMF.

There have been several attempts to open the furan ring in HMF and furfural (FF) to produce diol and triol using Pt-based catalysts on basic/acidic supports such as Pt catalysts supported on hydrotalcite, MgO, CeO₂ and Al₂O₃.^{17-19, 9, 20} Basic sites on the support has been reported to facilitate the adsorption of C=O and C-O-C bonds with a resultant increase in the rate of ring opening.²¹

Moreover, the acid sites were suggested to be responsible for the cleavage of the furan ring and loss of the furan oxygen.^{13, 22} The reaction mechanism for diol production using a Pd catalyst supported on zirconium phosphate (ZrP) with acid sites was proposed by Tuteja *et al.*¹³ In this mechanism, HMF was adsorbed by electrostatic interactions onto the catalyst surface with hex-1,3,5-triene-1,6-diol as an intermediate. In addition, a reaction mechanism using Pt nanoparticles supported on hydrotalcite (HT) with basic sites was proposed by Mizugaki and co-workers in 2019.¹⁹ On the basic Pt/HT, a reaction path for the ring opening of FF is put forward which involves hydrogenation of the carbonyl group of FF to generate FFA. The scission of the C5–O1 bond in the furan ring in FFA resulted in 1-hydroxy-2-pentanone as an intermediate, and subsequent reduction of the keto group led to 1,2-PDO.¹⁹

Equally, non-noble metal catalysts such as Ni and Cu have been used to convert biomass to 1,2,6-hexanetriol and 1,2-hexanediol respectively.^{16, 21} However, there is still a challenge associated with the direct conversion of HMF into 1,6-HDO using a one-step process. The first

attempt at the direct transformation of HMF to 1,6-HDO was achieved using a mixture of copper chromate and Pd/C under harsh reaction conditions (270 °C, 150 bar) with hydrogen as the reductant.²³ Under these conditions, the biomass conversion is quantitative, however, 1,6-HDO selectivity was only 4%.²⁴ In 2009, Koso et al. were able to achieve chemoselective transformation of tetrahydrofurfuryl alcohol to 1,5-pentanediol (1,5-PDO) by opening the tetrahydrofuran ring using Rh–ReO_x/SiO₂ catalyst.²⁵ Xiao and coworkers in 2015 used a double-layered Pd/SiO₂ and Ir–ReO_x/SiO₂ in a fixed bed reactor to convert HMF to 1,6-HDO at 373 K, 7 MPa H₂ employing a mixture of H₂O and THF as solvent. This system achieved 58% of 1,6-HDO and investigation revealed Bronsted acid sites were generated on the catalyst in the presence of H₂O.⁶

Furthermore, Tuteja and coworkers achieved 43% yield of 1,6-HDO by catalytic transfer hydrogenation at 140°C using formic acid as hydrogen source, by hydrogenolytic ring opening of HMF using Pd/ZrP catalyst.¹³ They suggest that the acidity of the catalyst surface and furfural alcohol dissociation on Pd sites are crucial for the ring opening reaction.¹³

At present, there are challenges associated with direct conversion of HMF to 1,6-HDO. Long reaction times are required for full HMF conversion and selectivity towards 1,6-HDO is below 50%, which is not economical for industrial application.

Factors such as reaction conditions, synergistic effect between active metal and support, dispersion of the metal on the support, have been found to influence the product selectivity of hydrogenation/hydrolysis of biomass (FF/HMF). In addition, Pt- and Ru-based catalysts have been widely employed for furan ring opening reaction with good efficiency.^{19, 22, 26, 27} For instance, Mizugaki *et al.* reported that the Pt/HT catalyst was efficient for ring opening of FF to 1,5-PDO with a high yield of 73% due to the cooperation of Pt NPs and the basic sites in HT support.¹⁹ The reaction was carried out at 150°C under 3 MPa using isopropanol as solvent. The 1,2-PDO product formed due to the basic surface of hydrotalcite facilitating strong interactions between the hydroxyl group of the intermediate furfuryl alcohol and the support. Subsequently, the interaction between the furan ring and the Pt catalyst led to the cleavage of C5-O bond.

Huber group²² confirmed that the Brønsted acid sites in Pt-WO_x/TiO₂ catalyst are important for the ring opening of tetrahydrofuran-dimethanol (THFDM) leading to the production of 1,6-HDO with up to 70% yield. More recently, Ma *et al.*,²⁷ reported the ring opening of FFA was achieved via a Pt/CeO₂ catalyst using water as solvent. In order to produce the desired ring-

opening products, the catalyst would have to affect both hydrogenation and hydrogenolysis of the furan ring.²⁸

Utne *et al.*²³ identified temperature as an important parameter in controlling selectivity and found temperatures between 100-140°C, to be the optimum for the hydrogenolysis of the furan ring for selectivity towards 1,2,6-hexanetriol.¹⁶

In this research, a variety of factors have been tested for the hydrogenation/hydrogenolysis of HMF to 1,6-HDO including reaction time, temperature, hydrogen pressure, and different monometallic and bimetallic catalysts. Bimetallic catalysts were used to assess the effect of the synergy between metals.²⁹ Moreover, different supports were investigated for the liquid-phase hydrogenation of HMF, including hydrotalcites (HT), magnesium Oxide (MgO), tungstated zirconia (WZ), sulfated zirconia (SZ), cerium dioxide or ceria (CeO₂) and hydroxyapatite (HAP). This is important because support has been reported to influence catalyst selectivity due to cooperative catalysis between metal nanoparticles and the support surface.³⁰

Hydrotalcites (HT), known also as layered double hydroxide (LDHs) is a double layered lamellar clay, used as solid basic catalyst in different applications.^{31,32} The general formula for HT is $[M(II)_{1-x}M'(III)_x(OH)_2](A_{x/n}^{n-}) \cdot mH_2O$. For example, M(II) could be Mg(II), Fe(II), Ni(II), Cu(II), Co(II), Mn(II), Zn(II), or Cd(II) while M'(III) denotes trivalent cations such as Al(III), Fe(III), Ga(II), or Cr(III). The anion, A, represents CO₃²⁻, NO₃³⁻, SO₄²⁻, Cl⁻, and organic anions.^{33,34} The anion and the water molecules are intercalated within the structure.³² The effectiveness of Mg-Al based HTs as a support in the production of biofuel-derived chemicals, with a high yield of 1,2 pentanediol was reported by Mizugaki and coworkers in 2014, and the result was hinged on the interaction between Pt and HT.¹⁹

Magnesium oxide (MgO) is a basic metal oxide which has been employed as a basic support for various chemical transformations.³⁵⁻³⁷ Wang *et al* reported the role of basic sites on the selectivity of the hydrogenation of HMF to dihydroxy methyl furan (DHMF) using Pt/MgO catalyst. The basicity of the MgO support was found to enhance the catalyst selectivity.³⁶

Cerium dioxide or ceria (CeO₂) is classified as a basic oxide and largely considered a weak base.¹⁸ The direct hydrogenation/hydrogenolysis of furfural using Pt/CeO₂ was reported by Tong group¹⁸ with 1,5-HDO as the major product. The authors suggested that the weak base support played a crucial role in promoting the activity and stability of the catalyst by providing oxygen vacancies that could participate in the reaction.¹⁸

Sulfated zirconia (SZ) consists of zirconium oxide (ZrO_2) with sulfate (SO_4^{2-}) ions adsorbed on its surface.³² SZ is a solid acid catalyst that has been used in different catalytic reactions often with high activity and selectivity, making it useful in various chemical processes including biomass conversion.^{32, 38} The active sites in SZ support are the strong acid sites that are created by the adsorption of sulfate ions on the surface of the ZrO_2 support^{38, 39} which act as a proton donor, creating Brønsted acid sites with high acidity that can facilitate a variety of chemical reactions.⁴⁰ The specific nature and distribution of the active sites in SZ support can depend on several factors, including the method of preparation, the type and amount of sulfate used, and the calcination conditions.⁴¹ In general, the density and strength of the active sites can be tuned by adjusting these factors, which could affect the catalyst's performance in specific applications.⁴¹

Tungstated zirconia (WZ) is a composite material consisting of zirconium oxide (ZrO_2) and tungsten oxide (WO_3). It is a solid acid composite also known as a tungsten oxide-zirconia ($\text{WO}_x\text{-ZrO}_2$) and has been employed as a support for the hydrogenation of glycerol to 1,3-propanediol.⁴²⁻⁴⁵ SZ and WZ supports are typically calcined at different temperature ranges before being used as support in order to: remove any water or solvent molecules/precursor that may be adsorbed on the surface of the SZ/WS supports, which can interfere with its activity;⁴¹ to activate SZ/WZ supports by removing any residual sulfate or that may not be strongly adsorbed on the surface;^{39, 46} and to stabilize their crystal structure and enhances their thermal stability.^{41, 41}

Hydroxyapatite (HAP), $\text{HCa}_5\text{O}_{13}\text{P}_3$, possesses acid-base properties and can exchange and stabilize a wide variety of ions. The surface sites are able to behave as a bifunctional catalyst.⁴⁷ ⁴⁹ HAP comprises approximately 70% of bone and teeth mass⁵⁰ and several studies have been initiated to investigate the acidic and basic sites on the hydroxyapatite (HAP) surface. Nevertheless, it is still unclear what role they play in HAP's catalytic properties.⁵⁰ HAP's coexistence of acidic and basic sites in single crystals allows the co-adsorption of molecules with different acid-base properties.⁵⁰⁻⁵² Additionally, the acidic and basic sites on the surface of HAP can be tuned by controlling the bulk Ca/P ratio during the preparation of the catalyst.⁵³ For instance, HAP has the unusual property of being acidic when the Ca/P ratio is 1.50 (low ratio), while it is basic when the Ca/P ratio reaches 1.67 (high ratio).^{50, 51, 54} As a result, HAP catalysts with acidic and basic properties can be produced by controlling Ca/P ratios between 1.50 and 1.67.^{50, 51} A study by Tsuchida group⁵¹ suggests that the ratio of Ca/P of HAP

influences the distribution of acid sites and basic sites on the catalyst surface with Ca^{2+} ions acting as Lewis acid sites, O atoms in PO_4^{3-} and OH groups acting as Lewis base sites, and the PO–H as Brønsted acid sites.^{50, 55-57}

5.2 Objective and aims

Herein, I focus on the direct transformation of HMF to 1,6-HDO by mono or bimetallic heterogeneous catalysts and explore the influence of Pt supported on basic or acidic support for the catalytic hydrogenation of HMF.

Our hypothesis is that a bifunctional support (acid-base properties of the support) would be crucial to enhance the efficiency of biomass-derived substrate selectivity, because of the complexity of biomass-derived substrates. Bifunctional catalysts have two different active sites, acid-base sites would enable them to perform effectively and selectively.⁵⁸⁻⁶⁰

For these reasons, hydroxyapatite (HAP) supported Pt-NP and bimetallic heterogeneous catalysts containing Re, Pd, Ru and Pt on HAP or SZ support were investigated.

My objective in this work is:

to clarify the role of supports in the direct transformation of HMF to 1,6-HDO.

to understand the reaction pathway in the presence of different supported heterogeneous catalysts

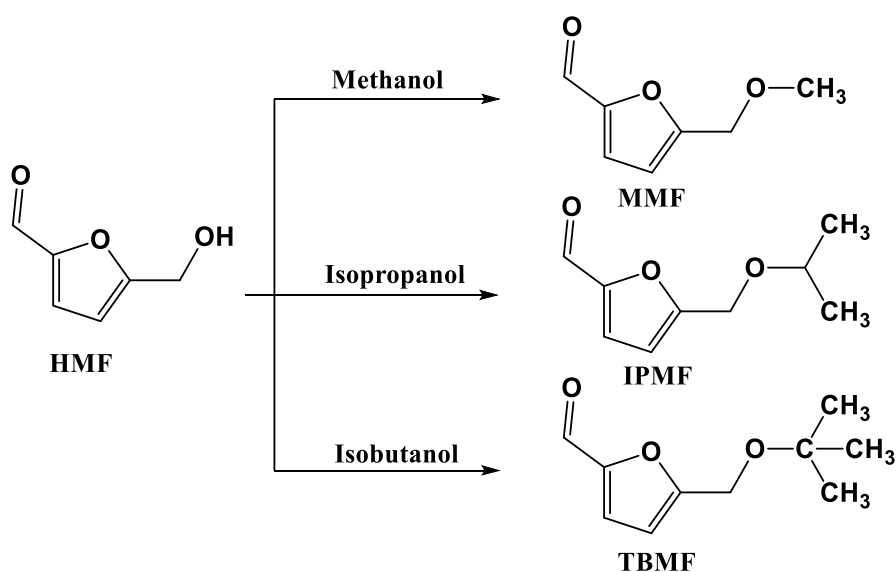
To establish the influence of the reaction conditions (solvent, pressure, and temperature) on the 1,6-HDO selectivity. This chapter also attempts to correlate structured activities relationship.

5.3 Results and discussion

5.3.1 Blank reaction

Blank reaction was carried out with HMF, methanol as solvent under 2 MPa of H_2 for 8 h (In this project, a pressure of 2 MPa was necessary to initiate the opening of the furan ring). The HMF was largely converted (70%) to the solvent product (97%) with trace amount of DHMF (3%) observed. The solvent product results from the reaction of the aldehyde group in HMF with the hydroxy group in methanol (solvent).

The solvent product, alkoxymethylfurfurals (AMFs) which are the resulting products formed due to etherification of HMF with different polar protic solvents^{61, 62} have the OH group on HMF replaced with varying alkoxy groups. Hence, in the presence of methanol, isopropanol and isobutanol, methoxymethylfurfural, (MMF), isopropoxymethylfurfural, (IPMF), and tert-butoxymethylfurfural (TBMF) are produced respectively as shown in Scheme 5.2.⁶³ In our result the solvent products were confirmed by GC-MS analyses were the two AMFs observed. The selectivity of solvent products was 6% for MMF and 14% for IPMF. However, we did not observe any TBMF in our reaction and this could be referred to the steric hindrance.



Scheme 5.2. HMF Etherification with Methanol, Isopropanol and Isobutanol as a solvent.⁶³

5.3.2 Effects of different polar protic solvents on conversion and selectivity

Catalytic transformation of HMF to 1,6-HDO involves hydrogenation and hydrogenolysis of HMF and this is often achieved by direct hydrogenation using H₂ under varying conditions. To ensure the source of the hydrogen in this reaction is the hydrogen gas pressure rather than the polar protic solvent(s) the reaction was carried out in the presence of N₂ (2 MPa), HMF and the catalyst with methanol as solvent. Without H₂, the main product was methoxymethylfurfural (MMF) resulting from etherification of HMF with methanol. We did not observe any hydrogenation products and we can infer that the source of hydrogen in the catalytic hydrogenation of HMF is the H₂.

The choice of solvent has been found to be significant in catalytic transformation, especially on the conversion and selectivity of the reaction.⁶⁴ In order to choose the best protic solvent with positive effect(s) on the prepared catalyst different protic polar solvents such as methanol, isopropanol and isobutanol were screened to test the effect of solvent on the hydrogenation of HMF using 5 wt.% Pt/SZ catalyst with 2 MPa of H₂. Interestingly, methanol presented the highest conversion of HMF (95%), while isobutanol and isopropanol achieved 66% - 67% respectively. The selectivity of 1,6-HDO was also affected by the solvent choice and the result is as shown in Figure 5.1. The selective of 1,6-HDO using methanol, isopropanol or isobutanol were 19%, 0% and 22% respectively. However, with isopropanol, 1,2-HDO with 6% selectivity was also observed and this is in line with the findings of other researchers.^{18, 21, 65} As a result, methanol was selected to be the solvent for the hydrogenation of HMF to 1,6-HDO with our catalyst. Subsequently, methanol was used for all the experiments carried out in this research. Non-polar solvents exhibit poor solubility of H₂, and for this reason, these solvents haven't been tested.⁶⁶

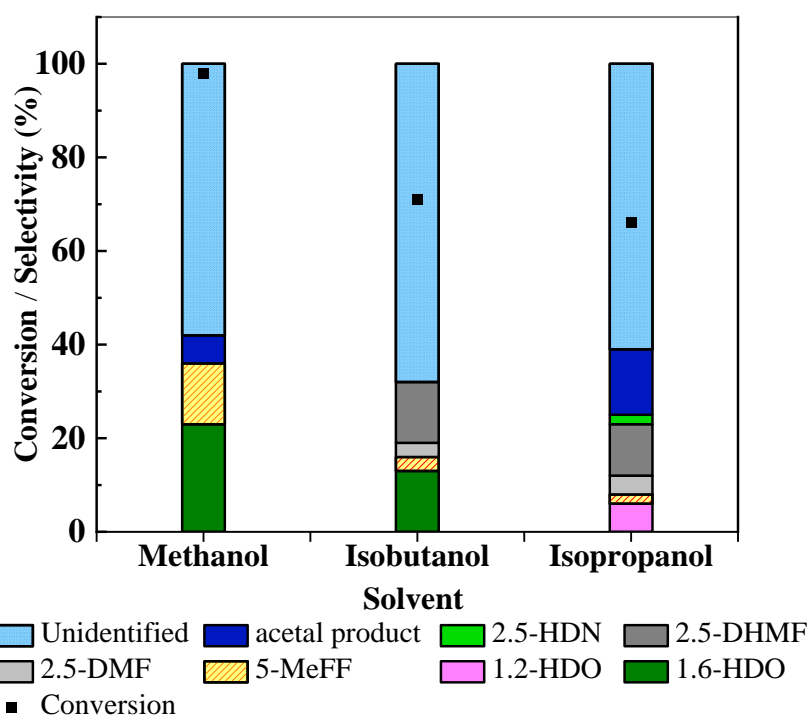
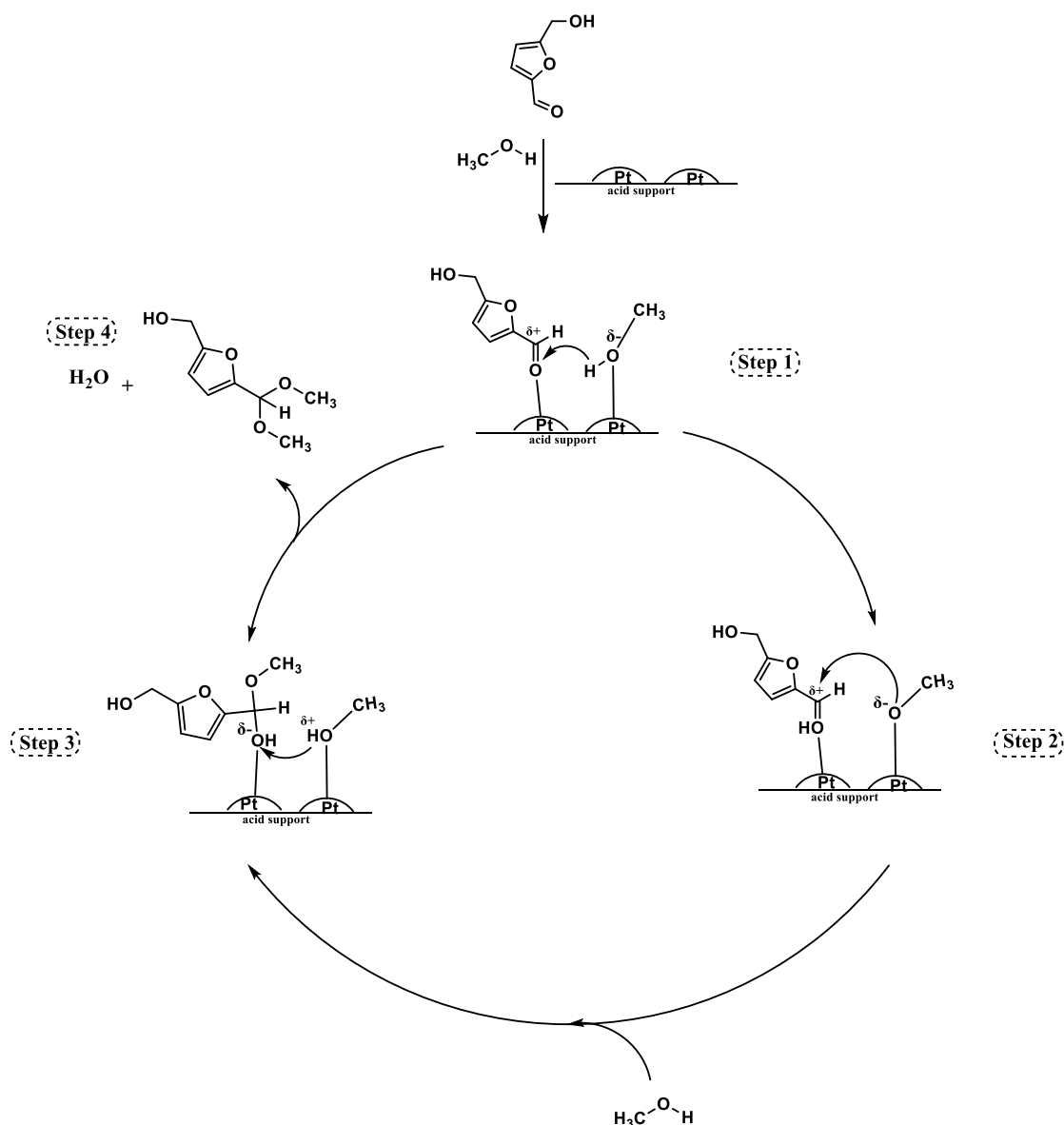


Figure 5.1: Hydrogenation of HMF using different solvents. Reaction conditions: HMF 1.59 mmol, Solvents: methanol, isobutanol or isopropanol 20 mL, using 5 wt.% Pt/SZ catalyst 40 mg under H₂ pressure 2 MPa, 120 °C for 6 h. HDN: 2,5-hexanedione.

The formation of solvent product in the liquid phase hydrogenation of HMF using methanol as a solvent and Pt/SZ catalyst depends on the solubility of HMF and hydrogen in the chosen solvent. The polarity and the solubility aided the formation of H-bonding between HMF and methanol after which, they both diffuse to the catalyst surface.⁶⁷ The mechanism of Pt/SZ-catalysed acetalization for HMF is proposed based on the solvent (methanol) and the substrate (HMF) adsorbing onto the SZ support. It has also been reported that the Pt-NPs on the catalyst surface also aided the formation of acetal. The acetal formed due to the activity of the Pt-NPs on the active sites of the catalyst, and intermediary species such as $\text{Pt}^{\delta+}(\eta^1\text{-O,C-HMF})$ generated methoxide for the production of acetal.⁶⁸ At the beginning of the reaction, polarisation of the C=O bond of HMF by the Pt occurred, thus, the oxygen atom of carbonyl coordinated to the Pt(0) centre, forming $\text{Pt}^{\delta+}(\eta^1\text{-O,C-HMF})$ species that could increase the electrophilicity in the carbonyl's group.⁶⁹ At the same time, the catalyst also interacts with the solvent (methanol) (Step 1, Scheme 5.3)⁶⁸ and promoting the transfer of the hydride to the oxygen atom of the carbonyl group in HMF and generating a Pt-ethoxide intermediate (Step 2, Scheme 5.3).⁶⁸ Followed by the O atom of the methanol nucleophilic attack protonated carbonyl group.⁷⁰ Afterwards, to add methanol to the Pt centre, a second molecule is added (Step 3, Scheme 5.3). This last species releases the acetalisation product and a water molecule (Step 4, Scheme 5.3).⁷¹

In general, the acetalization reaction required an acid catalyst in the reaction mixture to produce a protonate hydroxy group, which then underwent $\text{S}_{\text{N}}2$ substitution and subsequently deprotonation to form the acetal product.



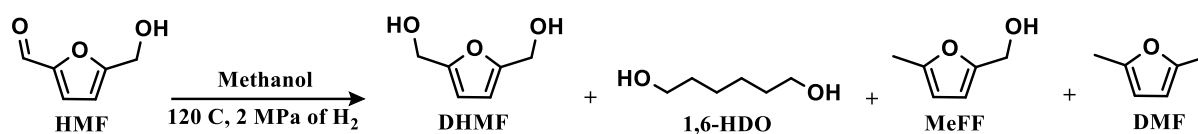
Scheme 5.3: The proposed mechanism of HMF etherification with methanol, as a solvent and Pt/SZ catalyst.

5.3.3 Effect of different support on 1,6-HDO selectivity

5.3.3.1 Monometallic catalysts.

Liquid phase hydrogenation and hydrogenolysis of HMF to 1,6-HDO using Pt-based heterogeneous catalysts was investigated. Pt-based catalyst was chosen because it is more active for the direct conversion of HMF to 1,6-HDO over other metals.^{18,19,27} Pt-based catalysts are very active, and selective to hydrogenation of the carbonyl group due to the *d*-orbitals of Pt exhibiting a large degree of radial expansion.⁷² A metal's *d*-band correlates with its selectivity

towards unsaturated alcohols. The metal surface is more likely to interact with C=C and C=O bonds as electron density and *d*-orbital population increase.⁷² Moreover, the repulsive four-electron interaction between the C=C bond and the metal surface increases.⁷² Also, the nature of the support has been found to influence catalyst selectivity,⁷³ consequently, different supports (HT, MgO, WZ, SZ, CeO₂ and HAP) were used to prepare the catalyst used with 5wt.% Pt loading. The catalysts were prepared by wet impregnation method using an aqueous solution of chloroplatinic acid hexahydrate, H₂PtCl₆.6H₂O (Sigma-Aldrich). This precursor was selected because the presence of residual chlorine in the catalyst has shown a positive impact on the α,β -unsaturated aldehydes hydrogenation.⁷⁴ Afterwards, all the dried samples were reduced using flow 5% H₂/Ar at 450 °C for 4 h. The freshly prepared catalysts were screened under 2 MPa of H₂ at 120 °C with stirring (1000 rpm) and the mole ratio of HMF/catalyst used was 155. Intermediates like DHMF, MeFF, hexanedione (HDN) and DMF were observed to be predominant during the hydrogenation of HMF using GC and GCMS techniques, with subsequent conversion of DHMF mostly into 1,6-HDO. This observation is in agreement with the results of Tuteja *et al.*¹³ All the reaction products are shown in Scheme 5.4. HMF has both C=C and C=O functionalities and as such, selective hydrogenation of HMF towards 1,6-HDO, which is our desired target, is a challenging reaction and one of our aims is to study the mechanism of the 1,6-HDO route.



Scheme 5.4: HMF hydrogenolysis using Pt/support catalysts.

There is a wide variation in product distributions and the catalysts conversions were between 85 – 100% except for Pt/HT with 48% conversion after 5 h (Figure 5.2). From Figure 5.2, the products distributions of HMF hydrogenation using Pt/MgO, Pt/HT, Pt/WZ, Pt/SZ, Pt/CeO₂ and Pt/HAP catalysts confirms the supports have a major effect on selectivity towards 1,6-HDO. Pt/WZ, Pt/SZ, and Pt/HAP demonstrated the ability to convert HMF to 1,6-HDO while the other three catalysts tested (Pt/MgO, Pt/HT, and Pt/CeO₂) displayed no selectivity towards 1,6-HDO but were able to transform HMF to DHMF. The highest selectivity (35%) towards

1,6-HDO was observed with Pt/WZ. HMF conversion increased in order: Pt/HT < Pt/HAP < Pt/HT < Pt/SZ < Pt/WZ < Pt/CeO₂.

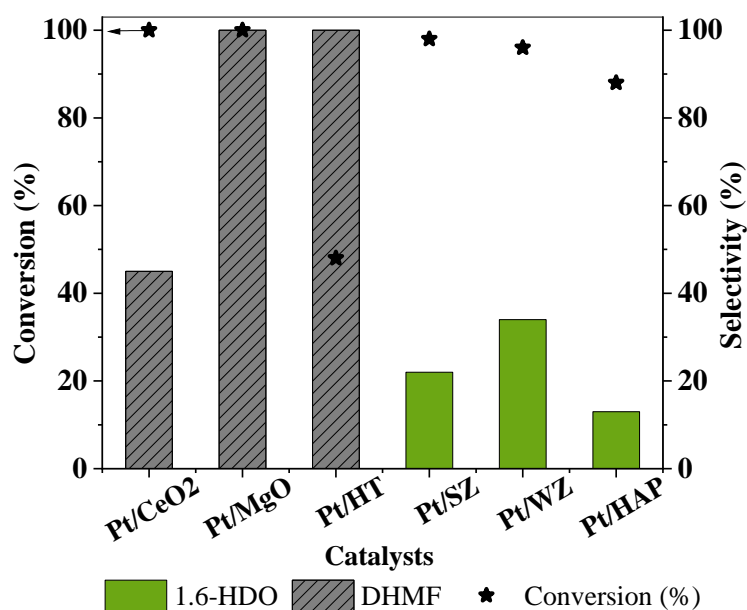


Figure 5.2: HMF conversion and the products selectivity using Pt-based catalysts on different supports. Reaction conditions: HMF 1.59 mmol, Methanol 20 mL, catalyst 40 mg, H₂ pressure 2 /-MPa, 120°C, 5h. The mole ratio of HMF/catalyst (155).

It was found that HMF conversion increases with reaction time as shown in Figure 5.3. Pt/CeO₂ displayed the highest activity for the conversion of HMF with selectivity towards DHMF and other byproducts due to the hydrogenation of the hydroxy group in HMF. It is worth noting that 5% selectivity towards 1,6-HDO was observed by Pt/CeO₂ after 6 h and this could be referred to the weak basic sites on the CeO₂ support as speculated by Tong and coworkers.¹⁸ Time online for liquid hydrogenation of HMF using 5% Pt/CeO₂ is shown in Figure 5.3(A). It is apparent that the direct hydrogenolysis of HMF requires weak basic sites for this reaction to be observed and it has been proposed that the weak basic support stabilized the adsorbed furan ring and facilitated the C-O bond breaking to open the furan ring.¹⁸

Although MgO and HT are basic supports,⁷⁵ Pt/MgO and Pt/HT catalysts did not produce 1,6-HDO even after extended reaction times. Time online for hydrogenation of HMF over 5 wt.%

Pt/MgO catalyst presented 100% selectivity for DHMF as shown in Figure 5.3 (b). The conversion was 100% after 6 h, moreover, the selectivity for DHMF was 100% over Pt/MgO.

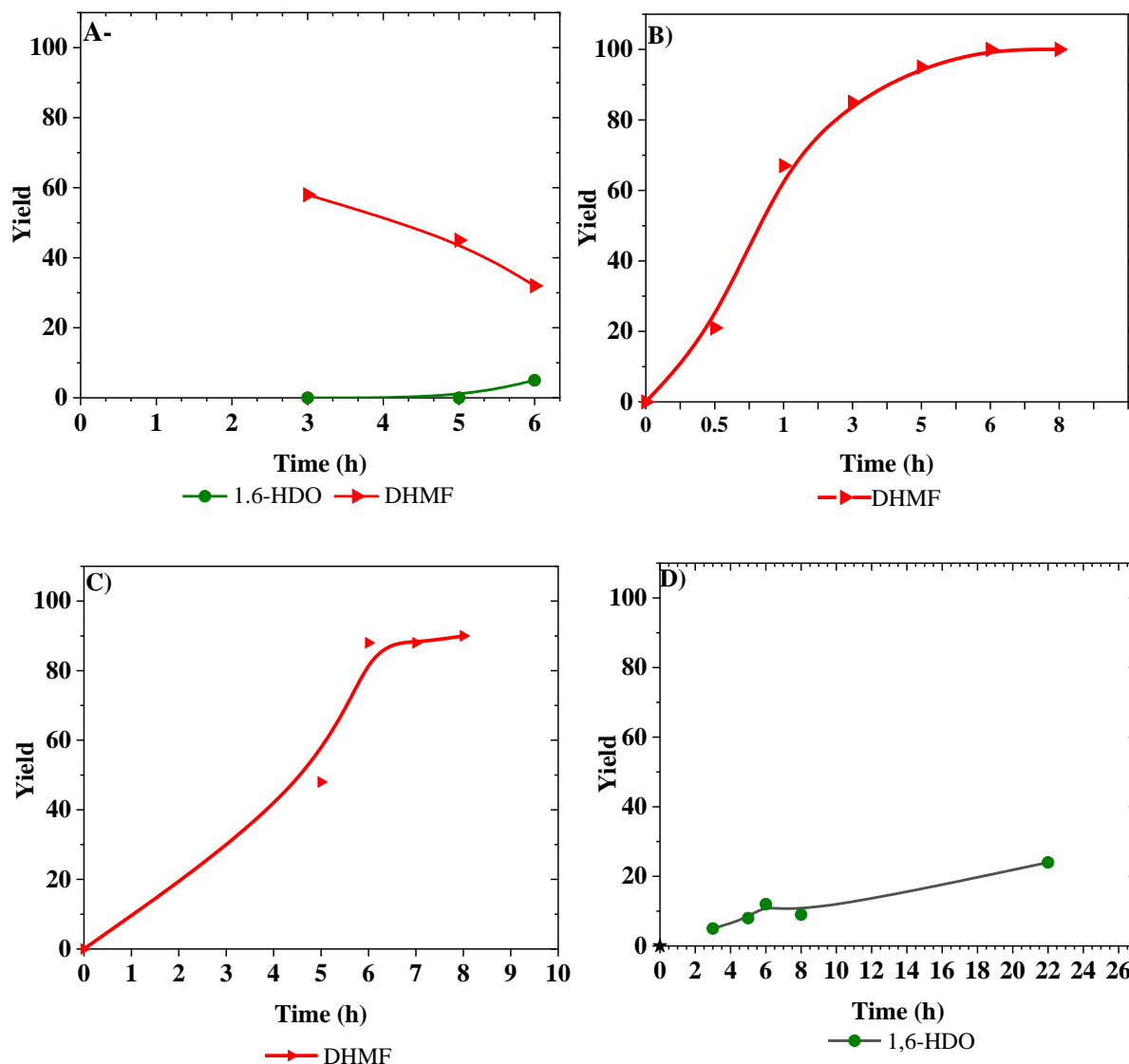


Figure 5.3: Hydrogenation of HMF by (A) 5%Pt/CeO₂, (B) 5%Pt/MgO, (C) 5%Pt/HT And (D) 5%Pt/HAP Reaction conditions: HMF 1.59 mmol, Methanol 20 mL, catalyst 40 mg, H₂ pressure 2 MPa, 120°C. The mole ratio of HMF/catalyst (155).

This result agrees with Wang *et. al.* observation³⁶ and it is worth noting that to achieve repeatability and reproducibility for the activity of Pt/MgO, the catalyst should be reduction in the furnace just before each reaction. This could be due to the effect of air (anything in air could adsorb onto MgO) and moisture on the oxidation state of Pt/MgO. Equally, the solvent

employed (methanol) should be in a dry state to prevent spontaneous ignition of the catalyst during the addition of the catalyst to the reaction matrix.

Pt/HT catalyst presented 100% selectivity for DHMF with 89% conversion after 8 h, as presented in Figure 5.3(C). The high selectivity for DHMF over the basic support is due to the aforementioned adsorption mode of HMF on basic support. This mode (vertical) is more selective for the hydrogenation of the carbonyl group in HMF as displayed in Figure 5.4. Wang *et al.*³⁶ reported the basic sites of metal oxide coordinated with the aldehyde group of HMF. They confirmed the adsorption mode of HMF over the basic support using the infrared spectroscopy (IR) of HMF molecules. As a result of comparing HMF adsorbed on the Pt catalysts with that of HMF. They showed that the C=O stretching and C=C stretching in the IR spectrum are stronger in the basic support Pt/MgO catalyst, indicating that the chemical interactions between the HMF molecules and the active sites on Pt/MgO are less than those on the acidic catalyst. That required less energy during the hydrogenated HMF's desorption. Under the same reaction conditions, they point out that basic support Pt/MgO catalysts exhibit higher activity than acidic support.

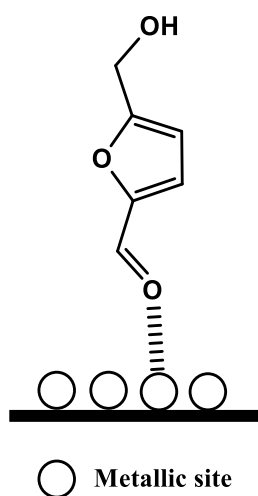
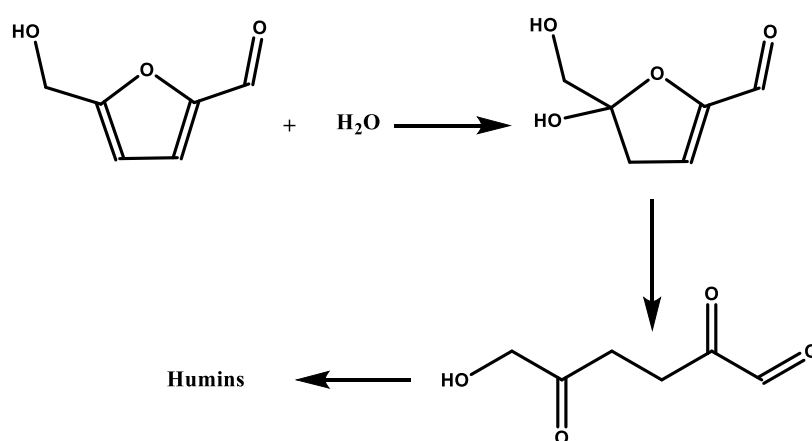


Figure 5.4: Mode of HMF adsorption on the basic active site. reproduced from reference.³⁶

In contrast to the observed trend with basic support, hydrogenolysis of the furan ring in HMF is affected by acidic support such as SZ and WZ.^{76, 77} For instance, Pt/SZ and Pt/WZ were screened for the hydrogenation of HMF and these catalysts presented 98% and 96%, respectively for HMF conversion, and (35%) and (20%) selectivity for 1,6-HDO respectively, after 8 h. The solvent products were equally detected as a byproduct in the presence of acid

support due to the interaction between the solvent (methanol) and the aldehyde group of HMF, so the acid catalyst promotes the acetalization reaction in the solvent (methanol).^{36, 78, 79}

Furthermore, hydrolysis product, 2,5-DMF and poor carbon balance due to polymerisation of HMF were observed over Pt/SZ and Pt/WZ catalysts. The carbon balance were 88 and 84% over Pt/SZ and Pt/WZ respectively, as a result of polymerisation of HMF over acid catalysts²⁷.⁸⁰ The HMF polymerisation reaction generates brown-solid products known as humins. It has been reported that the mechanism for HMF polymerisation is a complex reaction. Horvat and co-workers⁸¹ and later Lund *et al.*,⁸² reported that the formation of 2,5-dioxo-6-hydroxyhexanal by hydration of HMF is a main step in the production of humins, as shown in Scheme 5.5. Aldol condensation is responsible for polymerisation.⁷⁷ 2,5-dioxo-6-hydroxyhexanal contains several α -hydrogen atoms, which contributed to the formation of the polymer networks.⁷⁷



Scheme 5.5: HMF hydration to produce 2,5-dioxo-6-hydroxyhexanal.⁷⁷

HAP surface exhibits acid–base properties⁴⁷ and the Pt/HAP catalyst employed in this work achieved 84 % conversion of HMF and the selectivity towards the desired product, 1,6-HDO, is 12% after 5h reaction. To highlight the importance of Pt in this reaction, a blank reaction of HMF with HAP under 2MPa of H₂ with methanol as solvent was carried out. After 8 h, the conversion was 1% with DHMF and acetal product observed as products.

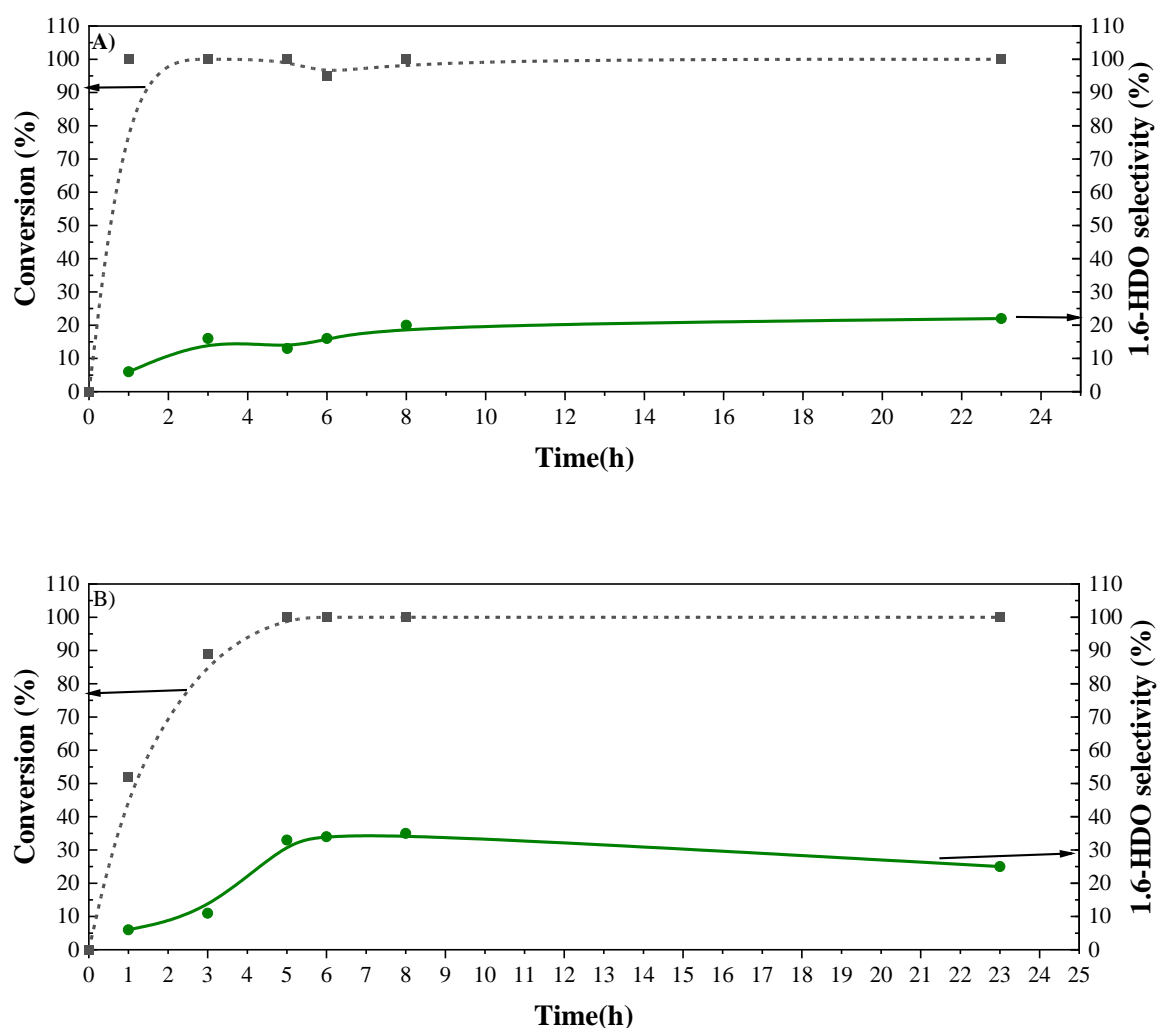


Figure 5.5: Hydrogenation of HMF by A)- 5%Pt/SZ And B)- 5%Pt/WZ . Reaction conditions: HMF 1.59 mmol, Methanol 20 mL, H₂ pressure 2 MPa, 120°C, The mole ratio of HMF/catalyst (155).

The catalysts employed in this work exhibit strong correlations between their acidic or basic properties and 1,6-HDO selectivity. We found that the selectivity of 1,6-HDO increased in this order: Pt/CeO₂ < Pt/HAP < Pt/SZ < Pt/WZ. This suggests that basic site supports are more selective towards adsorption of the carbonyl group in HMF. DHMF is produced over basic sites as a result of hydrogenation of the C=O group on the surface of the catalyst and the basic sites stabilize the hydroxymethyl moiety. Interestingly, acetalisation products were not observed over basic support.^{36, 83}

The HMF adsorption mode to the catalyst surface plays a critical role in the product selectivity as displayed in Figure 5.6. The parallel mode is more selective towards C=C adsorption and by extension hydrogenolysis of the HMF ring. Hence, Pt catalysts with acidic supports interact more with C=C in the furan ring, due to the parallel mode of adsorption which makes HMF more susceptible to both hydrogenation and hydrogenolysis.^{16, 36} The cleavage of C-O bond in the furan ring by acidic support observed in this work is in agreement with previous research findings.^{15, 80, 84, 85}

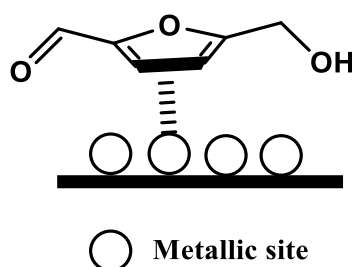


Figure 5.6: Mode of HMF adsorption on the acid active site.³⁶

5.3.3.2 Bimetallic catalyst

The studies of the performance of a range of monometallic catalysts based on Pt with different supports have yielded a great deal of information on hydrogenation/ hydrogenolysis of HMF and selectivity towards 1,6-HDO and how this is dependent upon the adsorption mode of HMF on the catalyst surface. Obviously, the activity of these Pt-based monometallic catalysts are very high,⁷² however, selectivity towards 1,6-HDO remains a challenge. The screening of the monometallic catalysts revealed 5 wt.% Pt/SZ, 5 wt.% Pt/WZ (acid support)^{76,17} and 5 wt.% Pt/HAP (bifunctional support, acid–base properties)^{47,16}, to be selective towards 1,6-HDO.

In order to come up with a catalyst with improved activity and selectivity we have modified the Pt based catalyst by adding a second metal. With this modification, we hope there will be a synergistic interaction between the two metals and the resulting bimetallic catalyst would have improved selectivity towards 1,6-HDO

Therefore, metals such as Ru, Co, Pd and Re have been used as second metal to generate a range of bimetallic catalysts towards improving the selectivity of 1,6-HDO for Pt/SZ and Pt/HAP. HMF conversion for these catalysts was 100% after 8 h (Figures 5.7 and 5.8) and the

selectivity towards 1,6-HDO varies between 3 - 28% for Pt/SZ derived bimetallic catalysts, decreasing in the order PtRu/SZ > PtPd/SZ > PtRe/SZ > PtCo/SZ as shown in the Figure 5.7. Unfortunately, the bimetallic supported on SZ did not present high selectivity for 1,6-HDO.

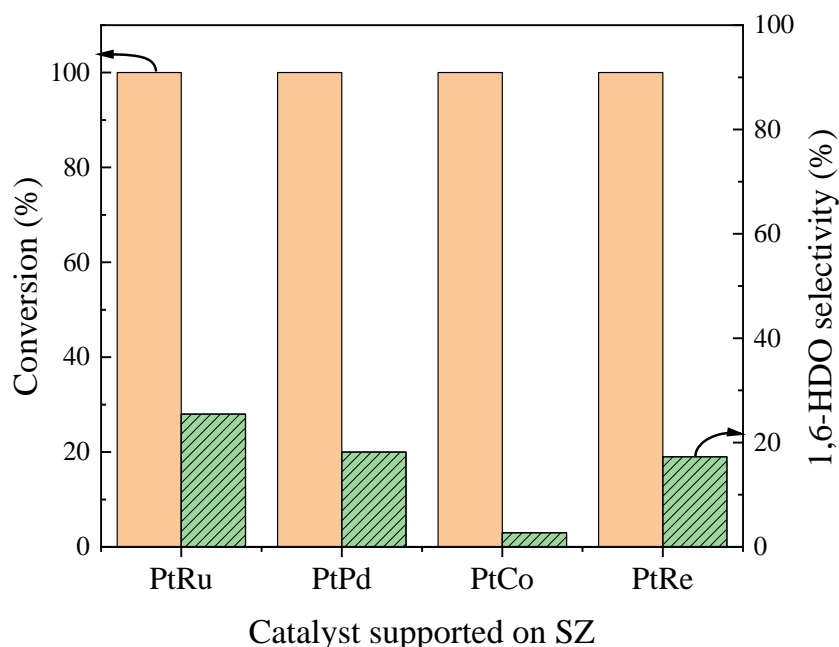


Figure 5.7: Hydrogenation of HMF by bimetallic supported on SZ. Reaction conditions: HMF 1.59 mmol, Isopropanol 20 mL, H₂ pressure 2 MPa, 120 °C, 8h. The mole ratio of HMF/catalyst (155). Acetals was expressed as Solvent Product (SP).

It has been reported that hydroxyapatite (HAP) with acid-base properties is a more efficient support in the catalytic hydrogenation of organic compounds containing oxygen.⁴⁷ Bimetallic catalysts supported on HAP (5 wt.% PtRu/HAP, 5 wt.% PtPd/HAP, 5 wt.% PtCo/HAP, 5 wt.% PtRe/HAP) were screened in the hydrogenation/hydrogenolysis of HMF and the results are as shown in Figure 5.8 (a). The conversions over PtRu/HAP, PtPd/HAP, PtRe/HAP range between 83%-84%, while that of PtCo/HAP is 75%. Varying 1,6-HDO selectivity was observed over these bimetallic catalysts with 1% over PtPd/HAP, 9% over PtCo/HAP, 25% over PtRe/HAP and 57% over PtRu/HAP. 5 wt.% PtRu/HAP bimetallic catalyst yields the best selectivity for the direct opening of the furan ring. However, 1,6-HDO selectivity was poor selectivity over the analogues monometallic catalyst Ru/HAP catalyst and 10% selectivity over Pt/HAP in the iso conversion 73 %, 84% and 84% using Ru/HAP, Pt/HAP and PtRu/HAP catalyst respectively. The results are clearly illustrated in Figure 5.8 (b).

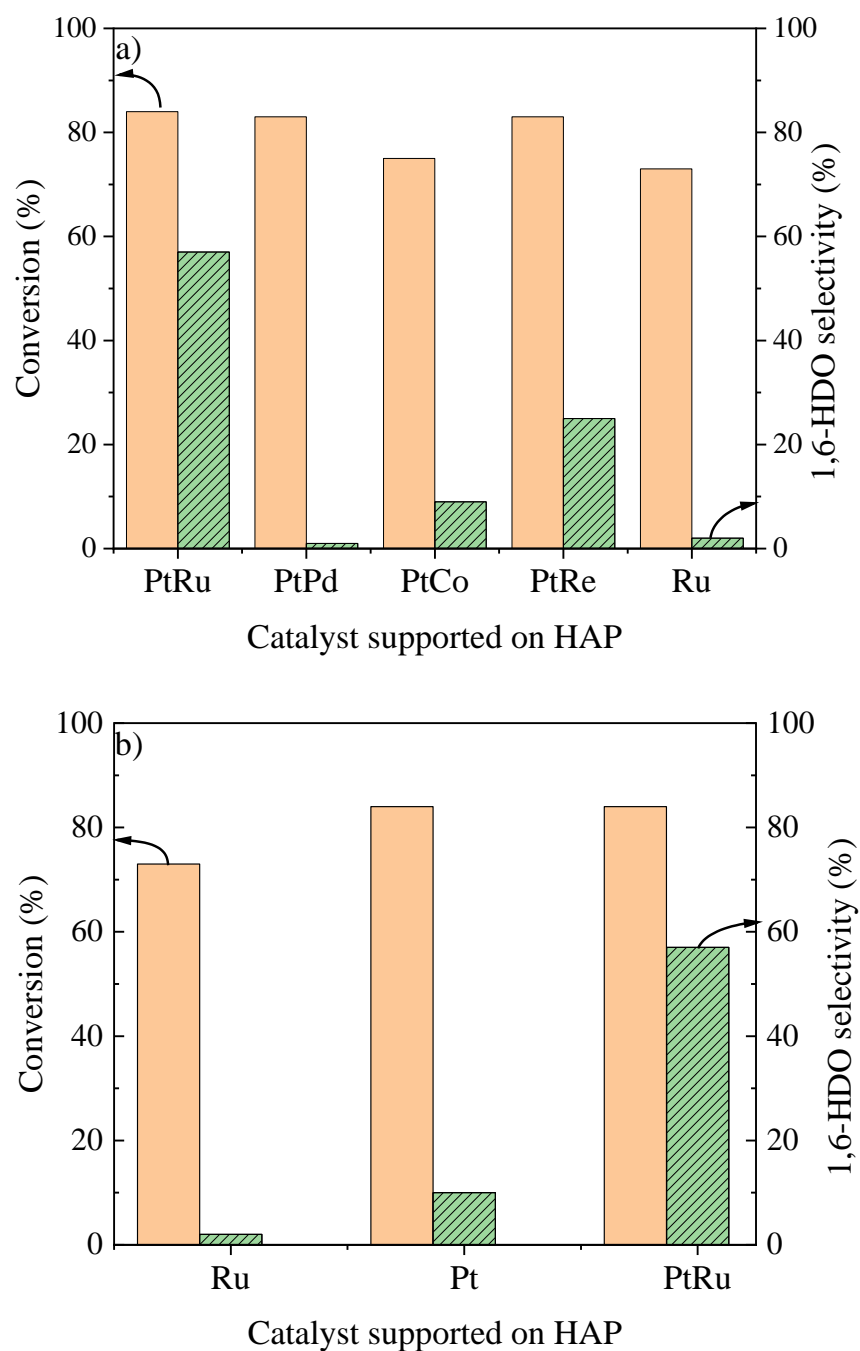


Figure 5.8: Hydrogenation of HMF by (a) bimetallic catalysts supported on HAP. And Ru/HAP catalyst (b) comparison between monometallic Ru/HAP and Pt/HAP and bimetallic PtRu/HAP catalyst. Reaction conditions: HMF 1.59 mmol, Isopropanol 20 mL, H_2 pressure 2 MPa, 120°C, 8h. The mole ratio of HMF/catalyst (155).

Furthermore, the time dependence was studied over 5% PtRu/HAP bimetallic catalyst under 2 MPa of H₂ pressure at 120 °C. It was noted that the conversion of HMF and the selectivity towards 1,6-HDO increases as time increases during the hydrogenation of HMF. The selectivity and conversion to 1,6-HDO was 84% with 57% selectivity after 8h, then did not improve after 8 h, accordingly, 8 h is considered the optimal reaction time (Figure 5.9). Also, it is noted that the acetal product was detected after 1 hour of the reaction, but it decreased over time, which could be the acetal reaction being reversible with the aldehyde group. As the acetal products are hydrogenated, they convert into aldehyde groups, finally disappearing over time.⁸⁶

It was found that the acid supported catalyst, led to a poor mass balance and gave rise to some oligomers. In order, basic support, gave a better mass balance.⁸⁷

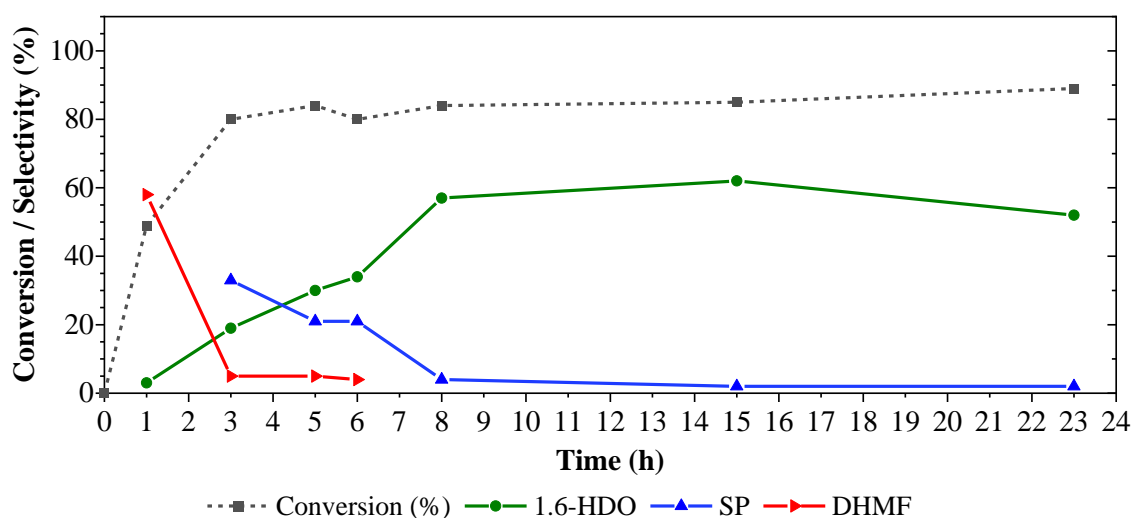


Figure 5.9: Hydrogenation of HMF by 5%PtRu/HAP. Reaction conditions: HMF 1.59 mmol, Methanol 20 mL, H₂ pressure 2 MPa, 120°C, The mole ratio of HMF/catalyst (155).

The next catalyst tested for the hydrogenation of HMF was the PtRe/HAP catalyst. Equally, the conversion of HMF over PtRe/HAP catalyst and selectivity towards 1,6-HDO increase over time, while the selectivity of 2,5-DHMF and solvent product decrease as reaction progresses (Figure 5.10). For instance, after 1 and 5 h reaction times, the solvent product selectivities were 43% and 3% respectively.

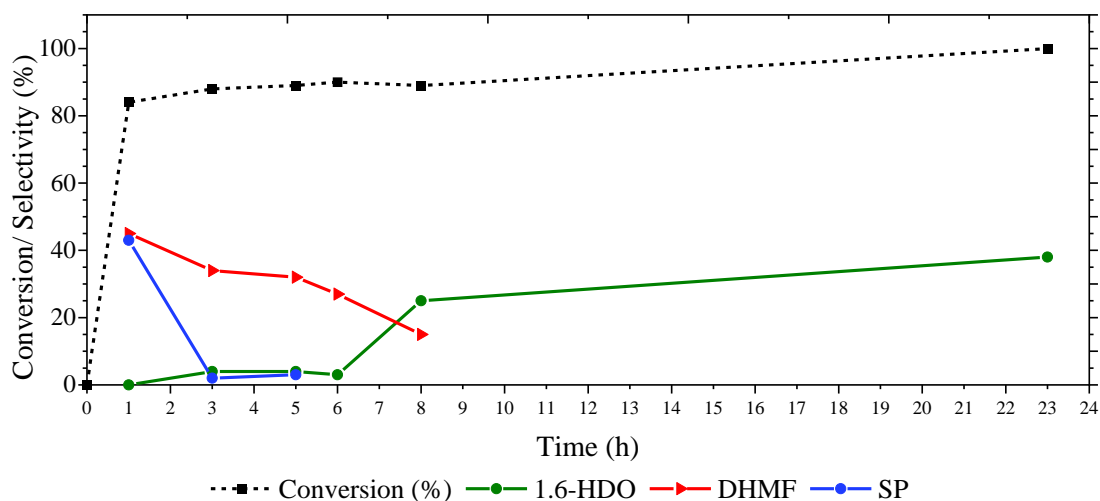


Figure 5.10: Hydrogenation of HMF by 5%PtRe/HAP. Reaction conditions: HMF 1.59 mmol, Methanol 20 mL, H₂ pressure 2 MPa, 120°C, The mole ratio of HMF/catalyst (155).

As a result, we suggest that the acid-base nature of HAP support is an important factor in the direct ring opening of HMF. This finding is in good agreement with previous reports.^{18, 19, 88} The cleavage of the C-O bond in the furan ring is facilitated by the acidic site due to the enhanced stability of adsorbed HMF on the acidic support. Some researchers have also reported that acidic support such as SiO₂ can also facilitate the ring opening of the furan ring in HMF.^{6, 89-91} In addition, it could be possible that the ring opening was a result of the vital cooperation between Pt and Ru and the support, HAP.

1,6-HDO was applied as a substrate under identical reaction conditions (2 MPa, 120 °C and using methanol as a solvent) used in the hydrogenation of HMF to make sure there are no further reactions after product 1,6-HDO formation over time. It was found that no further hydrogenation/ hydrogenolysis products were observed, and the conversion was 0% from the reaction. That means no further reactions after product 1,6-HDO formation over time.

5.4 Influence of different reaction conditions on catalyst's performance

The effects of the reaction conditions for hydrogenation /hydrogenolysis of HMF to 1,6-HDO were investigated. Different H₂ pressures and varying temperatures were investigated to achieve optimum reaction conditions for the conversion of HMF and selectivity towards 1,6-HDO over 5 wt.%PtRu/HAP catalyst.

5.4.1 Influence of hydrogen gas pressure on catalyst's performance

The effect of H₂ pressure on the conversion of HMF and selectivity towards 1,6-HDO was investigated using different H₂ pressures over 5wt.% PtRu/HAP. The reaction was performed under a range of H₂ pressure 0.5, 1, 2 and 3 MPa for 5h at 120 °C and the results are as shown in Figure 5.11. The conversion of HMF was 80% at 0.5 MPa of H₂ and moved up to 83% for 1 MPa and 84% for 2 and 3 MPa. However, the selectivity towards 1,6-HDO increased moderately with an increase in H₂ pressure. This indicates the incomplete hydrogenation of HMF into 1,6-HDO at lower H₂ pressure. The highest selectivity for 1,6-HDO (32%) was achieved using 2 MPa and this could be due to an increase in the concentration of dissolved H₂ in methanol as the hydrogen pressure increases.⁹² However, increasing the pressure of H₂ beyond 2 MPa did not improve the selectivity for 1,6-HDO, and, instead, the selectivity dropped to about 26%. This could be attributed to the formation of oligomers under this condition over the hydrogenated products.^{88,92} It is clear to note that the activity of the catalyst increased with increased H₂ pressure and as a result, 2 MPa was found to be the optimal pressure.

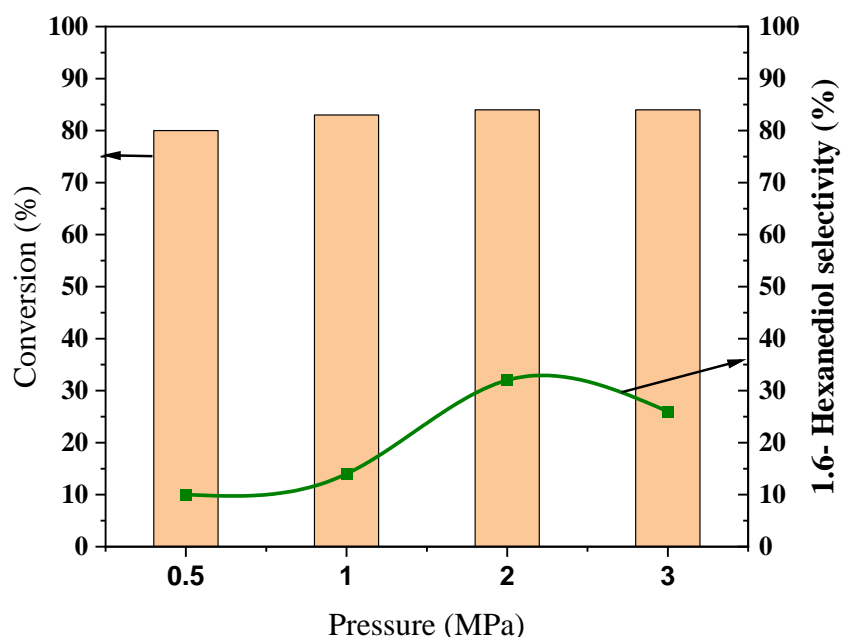


Figure 5.11: Effect of the hydrogen pressure on the Hydrogenation of HMF using 5%RuPt/HAP. Reaction conditions: HMF 1.59 mmol, Methanol 20 mL, H₂ pressure, 120 °C, 5h, The mole ratio of HMF/catalyst (155).

5.4.2 Influence of reaction temperature on catalyst's performance

Reaction temperature has been reported as one of the most important factors for controlling conversion and product selectivity.²³ Effects of different reaction temperatures ranging from 80 -160 °C on the hydrogenation/hydrogenolysis of HMF and selectivity towards to 1,6-HDO was investigated over 5wt.% RuPt/HAP catalyst under 2 MPa of hydrogen for 5 h. As presented in Figure 5.12, the temperature of the reaction strongly affects the catalyst performance and selectivity towards 1,6-HDO. With the starting temperature set at 80 °C, 1,6-HDO was not detected over the duration of the reaction (5 h). A steep increase in 1,6-HDO selectivity (2 % - 51 %) was observed as the temperature of the reaction was increased from 100 °C to 120 °C. However, the selectivity improved slightly on raising the temperature from 120-140 °C. It was found that the selectivity did not improve on raising the temperature from 140 – 160 °C. Furthermore, it was observed that the selectivity for DHMF was high at 80 °C and 100 °C, while, 1,6-HDO selectivity peaked at 140 °C. Accordingly, 140 °C was found to be the optimal temperature.

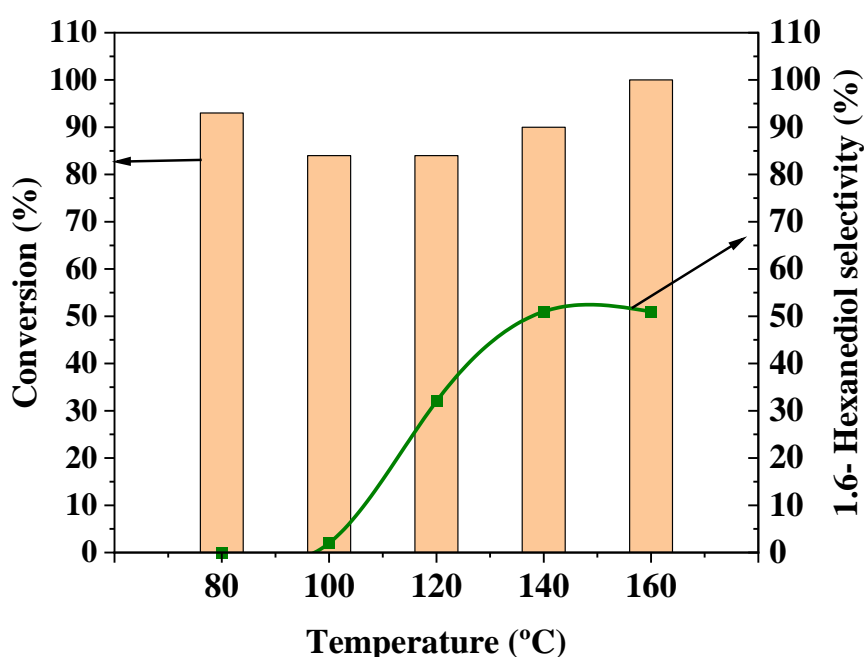


Figure 5.12: Effect of the reaction temperature on the hydrogenation of HMF using 5%RuPt/HAP. Reaction conditions: HMF 1.59 mmol, Methanol 20 mL, 5h, The mole ratio of HMF/catalyst (155).

As a result, the direct transformation of HMF to 1,6-HDO is affected by the reaction conditions. The optimum reaction condition for the ring opening of HMF was 2 MPa of H₂ at 140 °C using methanol as a solvent via a 5% PtRu/HAP catalyst.

5.5 *Recyclability of the catalyst*

The recyclability of PtRu/HAP bimetallic catalyst was assessed over three cycles and the results are as shown in Figure 5.13. The recyclability study of PtRu/HAP for hydrogenation/hydrogenolysis of HMF was carried out under 2 MPa of H₂ at 120 °C for 2 h. After each reaction, the catalyst was collected from the reaction mixture by centrifugation and the recovered catalyst was washed 2 times with methanol and once with acetone to remove any organic compound or adsorbed species from the catalyst surface and the catalyst left to dry for 24 h. The recovered catalyst was reused again under the same reaction conditions and the catalyst's overall weight was kept constant by adding the weight difference from the last run. The catalyst showed nearly stable activity for the conversion of HMF and the selectivity of 1,6-HDO over 3 cycles without losing its activity. Over three cycles, the conversion of HMF and 1,6-HDO selectivity were constant at 84% and 6% respectively. The spent catalyst was characterized to investigate the continued activity of the catalyst over three catalytic runs using ICP-AES, XPS, and TEM. The Inductively coupled plasma atomic emission spectroscopy, ICP-AES, results showed that there was no leaching of the active metal from the catalyst as the metal load remained fairly stable on the spent catalyst after three cycles compared to the fresh catalyst as shown in Table 5.1.

Table 5.1: Results of analysis of fresh and spent catalysts.

Catalyst	Ru/Pt
5 % PtRu/HAP (fresh)	1.5/3.4
5 % PtRu/HAP (spent)	1.5/3.22

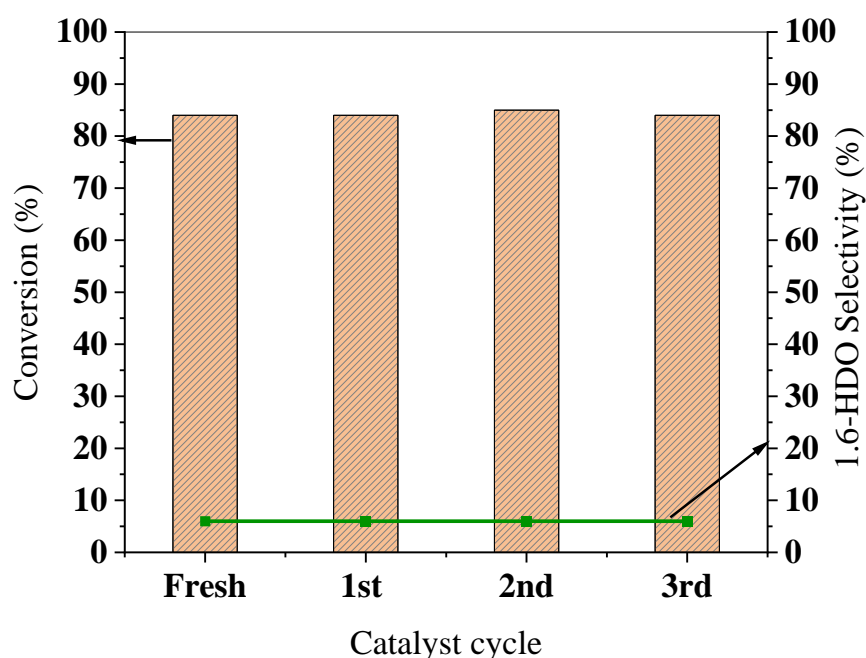


Figure 5.13: Reusability of 5%PtRu/HAP catalyst. Reaction conditions: HMF 1.59 mmol, Methanol 20 mL, H₂ pressure 2 MPa, 120 °C, 2h, The mole ratio of HMF/catalyst (155).

5.6 Catalyst characterisation

5.6.1 X-ray photoelectron spectroscopy analysis

X-ray photoelectron spectroscopy (XPS) was used to study the changes in the chemical state of the catalyst before and after heat treatment of the catalyst (reduction of the sample using flow hydrogen at 450°C for 4 h with ramp rate 10 °C /min). The XPS spectra of Pt(4f) derived from 5wt.% Pt/HAP and 5wt.% PtRu/HAP catalysts are as shown in Figure 5.14 and Figure 5.15 respectively. From the XPS analysis, the binding energy of Pt/HAP red catalyst exhibits a strong peak at 71.5 eV and 74.8 eV for 4f_{7/2} and 4f_{5/2} which can be attributed to metallic Pt⁰ species.⁴⁸ On the XPS spectrum of PtRu/HAP catalyst, the binding energy shifted to lower values at 71.4 and 74.7 eV related to the error of the analysis technique. Moreover, observed for PtRu/HAP were binding energies at 72.8 eV and 76.1 eV attributed to 4f_{7/2} and 4f_{5/2}, and this confirms the presence of Pt²⁺ species as PtO_x or Pt(OH). This species may be present due to adsorbed oxygen species on the surface of the catalyst during preparation of the catalyst.⁹³⁻⁹⁶ On the other hand, Ru⁰ and Ru^{+δ} were observed at 280.1 eV and 280.9 eV, respectively as the Ru species present on the surface of the catalyst.

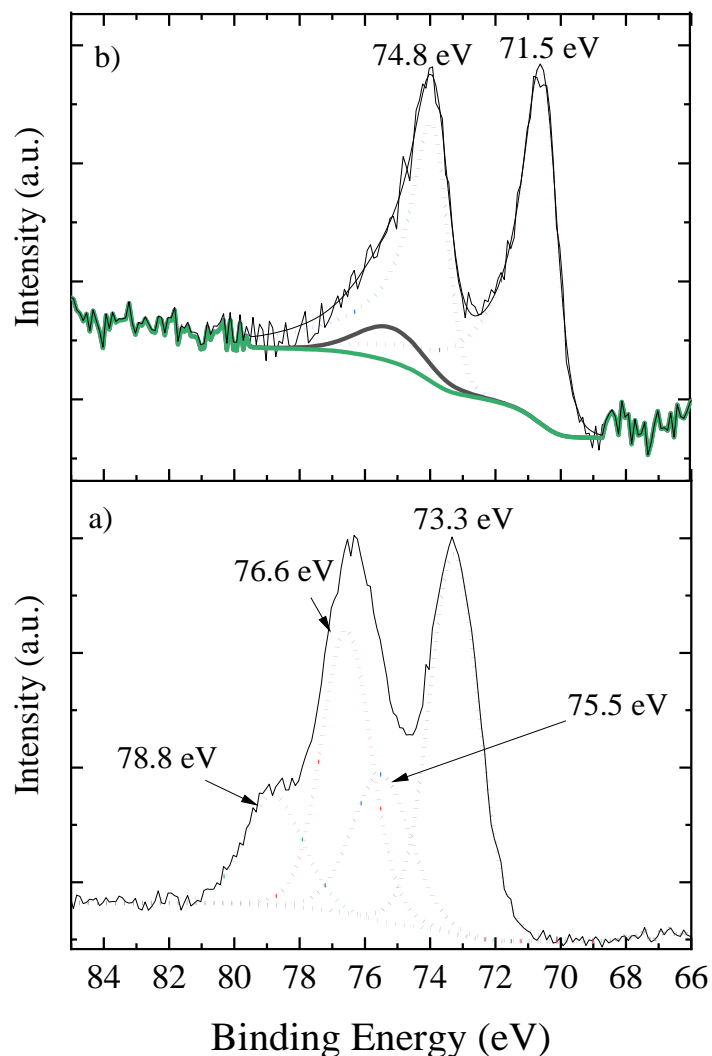


Figure 5.14: (A) XPS spectra at Pt 4f orbitals (a) Pt/HAP dried, (b) Pt/HAP red catalyst

This catalyst could be a random alloy or core-shell, and we need to analyse it using STEM XEDS.

The XPS spectra of Ru/HAP red and Ru/HAP dry catalyst are presented in Figure 5.16 (A) and (B). The profile for Ru/HAP red catalyst presented double peaks with binding energy for Ru 3d_{5/2} and 3d_{3/2} at 280.6 and 284.8 eV respectively attributed to Ru⁰ species. The peaks at 282.4 and 286.6 eV were assigned to Ru⁴⁺ (3d_{3/2}) attributed to the presence of RuO₂ on the catalyst surface. This RuO_x species may be present due to adsorbed oxygen species on the surface of the catalyst during preparing the catalyst.⁹⁴ with a complete overlap between the C 1s peak and

the Ru 3d_{3/2} peak. The profile for the Ru/HAP dry sample shows double peaks with binding energy for Ru 3d_{5/2} and 3d_{3/2} at 282.4 and 286.6 eV respectively attributed to RuCl₃. The Cl⁻ ion residual from the precursor solutions during the preparation of the catalyst.

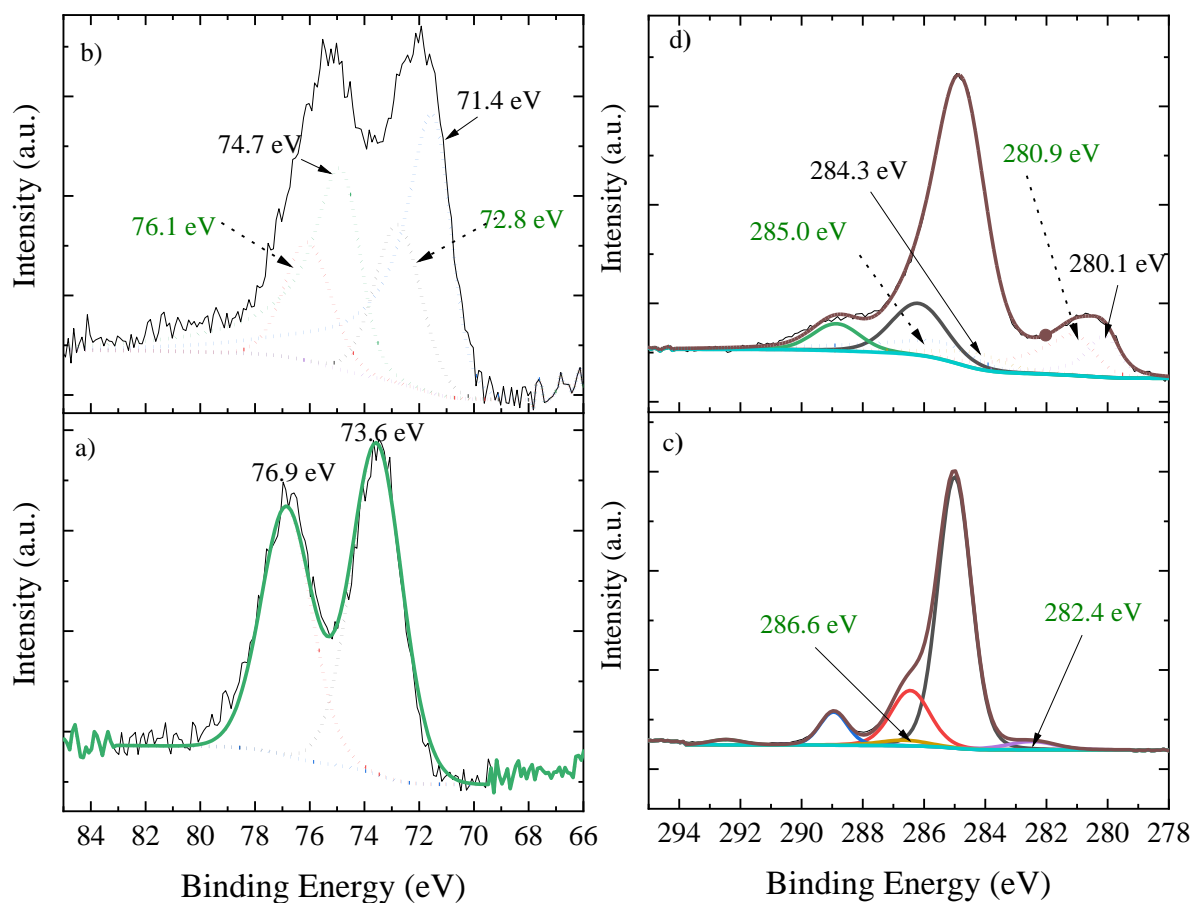


Figure 5.15: XPS analysis for PtRu-HAP catalyst of (a) PtRu/HAP dried (b) PtRu/HAP red catalyst for Pt 3d, (c) PtRu/HAP dried catalyst (d) PtRu/HAP red catalyst for Pt 3d for Ru 3d

The quantitative analysis of the supported bimetallic catalyst obtained from the regions of the XPS spectrum described above is provided in Tables 5.2 and 5.3 and based on previous studies, all levels of the spectrum were aligned with C 1s which has a binding energy of 284.8 eV.

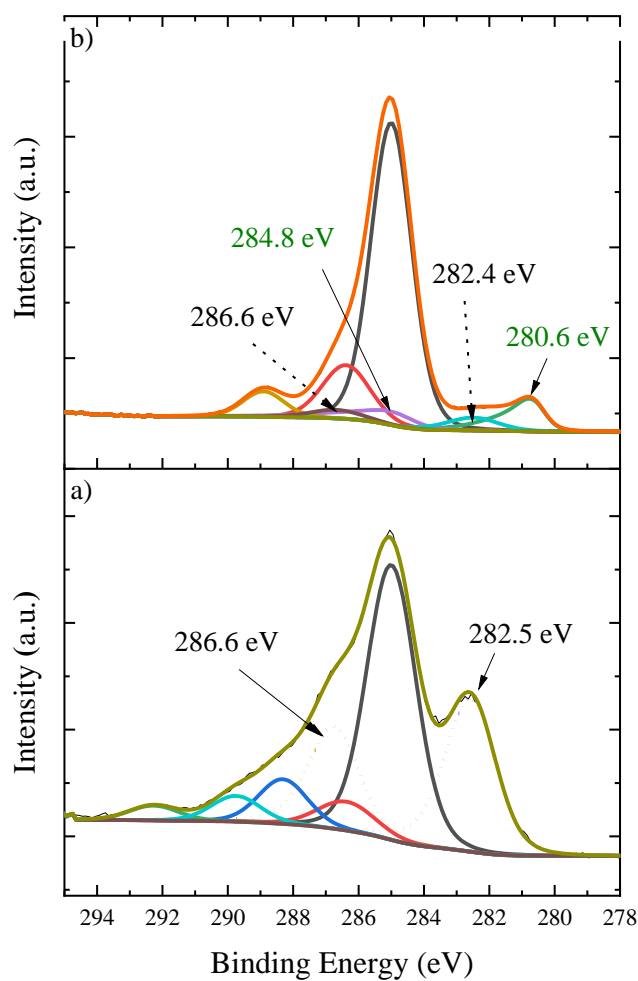


Figure 5.16: XPS analysis for Ru-HAP catalyst of Ru 3d.(a) Ru/HAP dried, (b) Ru/HAP red catalyst.

Table 5.2 the XPS data for quantitative analysis of the supported platinum catalysts.

5%wt. Metal/ HAP Catalyst	Pt	Ru	Ca	P
	% At.Conc.	% At. Conc.	% At. Conc.	% At. Conc.
Pt	0.28	-	8.38	5.21
Ru	-	0.4	11.01	7.61
PtRu	0.4	0.52	17.22	11.45

Table 5.3 the XPS data for the Relative concentration of the oxidation species on the supported catalysts.

5%wt. Metal/ HAP Catalyst	Pt 4f (0) % Conc.	Pt 4f (II) % Conc.	Ru 3d (0) % Conc.	Ru 3d (IV) % Conc.
Pt	0.28	-	-	-
Ru	-	-	0.4	0.19
PtRu	0.4	-	0.52	-

Table 5.4 The XPS data for metal ratio of the oxidation species on the supported platinum catalysts

5%wt. Metal/ HAP Catalyst	Ca/P molar ratio
Pt	1.608
Ru	1.446
PtRu	1.503

The ratio of the acid-base sites in HAP support can be evaluated by finding the Ca/P ratio^{51, 53} and changes in Ca/P ratio can significantly modulate HAP catalyst's activity.⁹⁷ The relationship between the Ca/P ratio of HAP catalysts and the number of acids and basic sites present in the catalyst are determined by Ca²⁺ ions content; in other words, its basic property results from the presence of Ca²⁺ ions, while its acidic property occurs when Ca²⁺ is deficient.⁵¹ In addition, HAP crystals grow along their α -axis, so that the α -faces, which contain phosphate groups related to acidity, are mainly exposed.⁵¹ HAP behaves as an acid catalyst with the presence of basic sites when the Ca/P ratio is 1.50, however, with a Ca/P ratio of 1.67, HAP acts as a basic catalyst (Table 5.4). Based on this phenomenon, the Ca/P ratio in PtRu/HAP catalyst has been found to be 1.503, acting as an acid catalyst with the existence of basic sites. In contrast, the ratio between Ca/P in Pt/HAP catalyst is 1.608. Hence, HAP support in Pt/HAP acts as a basic catalyst with the existence of acid sites. The Ca/P ratio in Ru/HAP is found to be 1.4.

The variety in the surface of the Pt/HAP and PtRu/HAP catalysts could lead to different performances for HMF adsorption and ring opening of furan over the catalytic surface. Therefore, a higher activity of PtRu/HAP than Pt/HAP could be due to the acid surface facilitating the adsorption of HMF molecules. The 2p doublet was symptomatic of Ca 2p in PtRu/HAP catalyst appeared at 347.5 eV, the binding energy of the P element is at 133.4 eV, while that of O 1s is at 531.2 eV. These results agree with the previous study.⁹⁸ Therefore, it is easy to understand a higher activity of PtRu/HAP because the acidic surface facilitates the capture of HMF molecules and open the ring.

Figure 5.17 shows the results of the XPS analyses of the fresh and spent bimetallic catalyst. X-ray photoelectron spectroscopic data of Pt (4f) and Ru (3d) of fresh and spent PtRu/HAP revealed that the catalyst is in a predominantly oxide state, however, there is no difference in the catalytic activity between the fresh and spent sample.⁹⁹ That means the bimetallic catalyst PtRu/HAP catalyst has a crucial effect and the oxidation state has no effect on the catalyst activity.

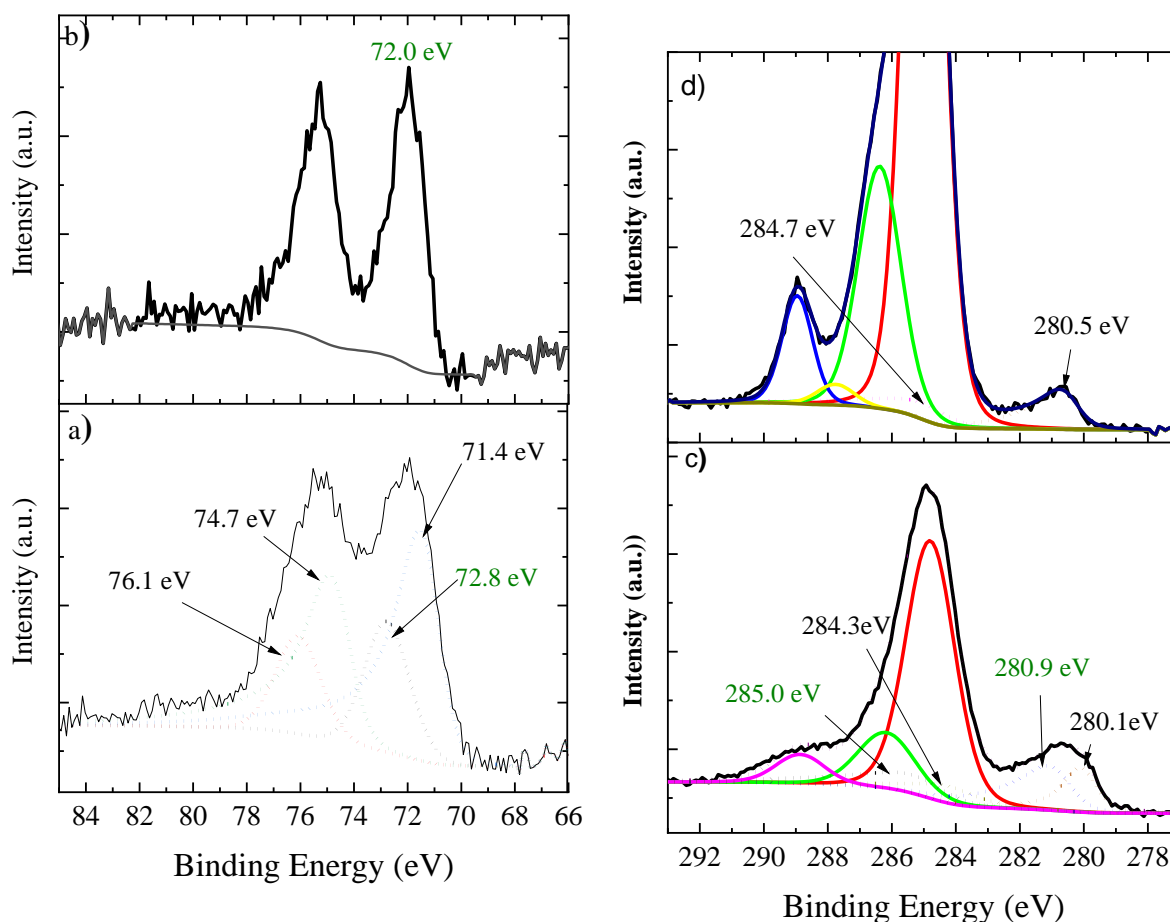


Figure 5.17: XPS analysis for PtRu-HAP reduction and spent catalyst of Ru 3d and Pt 3d (a) PtRu/HAP fresh catalyst, (b) PtRu/HAP spent catalyst for Pt 3d, (c) PtRu/HAP fresh catalyst, d)- PtRu/HAP spent catalyst for Ru 3d.

5.6.2 Inductively coupled plasma atomic emission spectroscopy analysis

Inductively coupled plasma atomic emission spectroscopy (ICP-AES) was performed for elemental analysis. It was determined that the sample was stoichiometric by measuring the Ca and P contents (Ca/P ratio of ~ 1.57) in Pt/HAP and PtRu/HAP bimetallic catalysts. However, the Ca/P ratio for HAP support alone (fresh support) was 1.59. The Pt content in Pt/HAP catalyst was 4.7 wt %. It was also confirmed the Pt and Ru NPs quantity in bimetallic catalysts were 1.5 and 3.4 respectively.

Table 5.5: ICP-AES results for the atomic ratio of Ca/ P for the catalysts

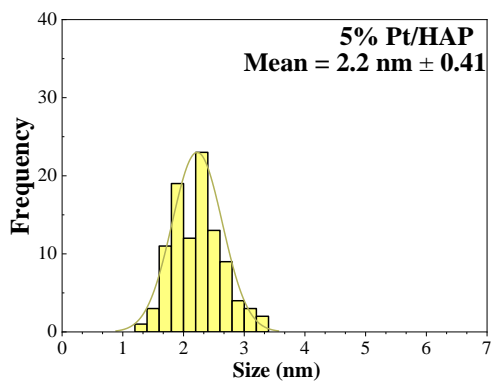
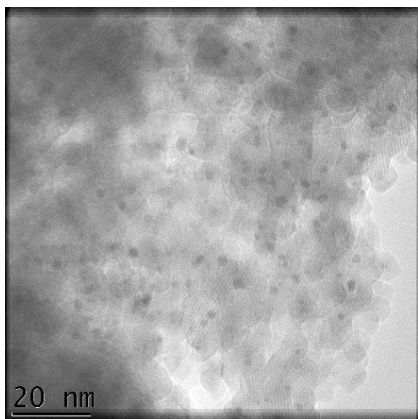
<i>Catalyst</i>	<i>Ca (g/g)</i>	<i>P (g/g)</i>	<i>Ca/P molar ratio</i>	<i>Pt wt% - Ru wt%</i>
<i>HAP</i>	<i>27.358</i>	<i>17.156</i>	<i>1.59</i>	<i>-</i>
<i>Pt/ HAP</i>	<i>26.938</i>	<i>17.091</i>	<i>1.57</i>	<i>4.7</i>
<i>PtRu/ HAP</i>	<i>25.874</i>	<i>16.453</i>	<i>1.57</i>	<i>1.5/3.4</i>

Comparative analysis of the Ca/P ratios obtained from XPS analysis on the surface of PtRu/HAP (Table 5.4) and bulk analysis by ICP-AES for RuPt/HAP catalyst (Table 5.5) revealed that the surface HAP particles have a lower Ca/P ratio (1.54) relative to the bulk (1.57). For this reason, we infer that, calcium ions, which are related to basic properties of HAP support are not readily expressed on the surface.⁵¹

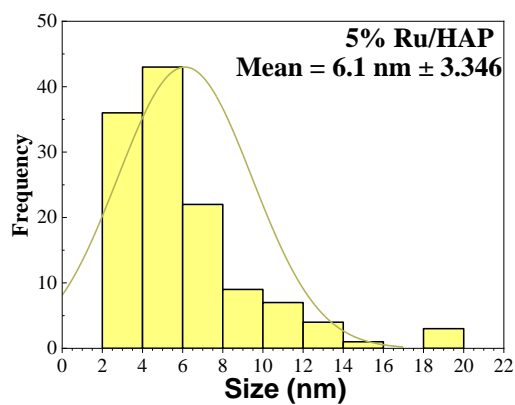
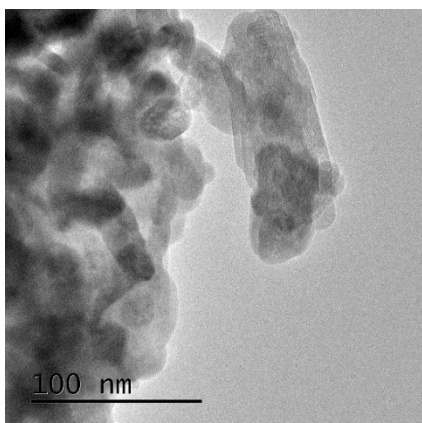
5.6.3 Transmission electron microscopy analysis

Transmission Electron Microscopy (TEM) was used to evaluate the morphology of the Pt-based catalysts. The supported monometallic Pt/HAP and Ru/HAP and bimetallic catalysts PtRu/HAP reduced at 450 °C for 4 h were analysed and the TEM images and particle distribution are as shown in Figure 5.18. According to the results, the Pt/HAP catalyst and PtRu/HAP catalyst are well dispersed uniformly on the surface of HAP supports, however, Ru/HAP showed non-uniform distribution. These results suggested the precursor, H₂PtCl₆, is uniformly dispersed on HAP⁹⁸ and the vague boundary between Pt and HAP was an indication of the strong interaction between them.¹⁰⁰ An interesting finding is that the estimated average size (d_M) of the metal on the catalyst surface depends on the active metal in the following order: d_{Pt} (2.2 nm) < d_{PtRu} (2.5 nm) < d_{Ru} (6.1 nm).

5 % Pt/HAP



5 % Ru/HAP Catalyst



5 % PtRu/HAP Catalyst

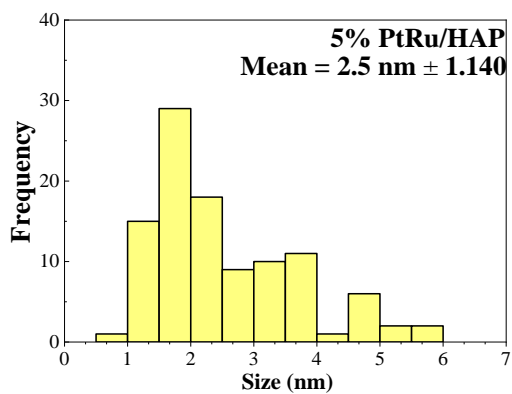
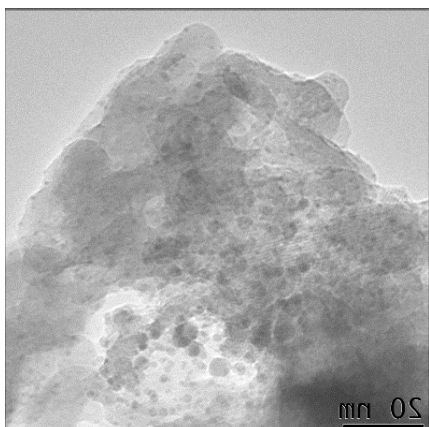


Figure 5.18: TEM images and particle size distribution of reduced 5 % wt. Pt/HAP, Ru/HAP, PtRu/HAP catalysts.

Based on the TEM results presented in Figure 5.19, the spent catalyst does not exhibit any sintering on the metal grain size when compared to the fresh catalyst. The particle sizes of the fresh and the spent catalysts were ± 2.5 nm respectively and this finding suggests that the reduction of the catalyst prevents the sintering of mixed metal oxides (NPs) and enhances the catalyst's stability.²¹ Also, Since Pt, Ru and HAP interact strongly, even after high-temperature treatments, small Pt nanoparticles may remain stable, and resistance to particle sintering may result in high activity and catalyst stability over three cycles.⁴⁸ HAP surface phosphate groups have been reported to anchor platinum nanoparticles by electron-donating interactions¹⁰¹ and the result of this interaction is a highly stable heterogeneous catalyst with high efficiency.

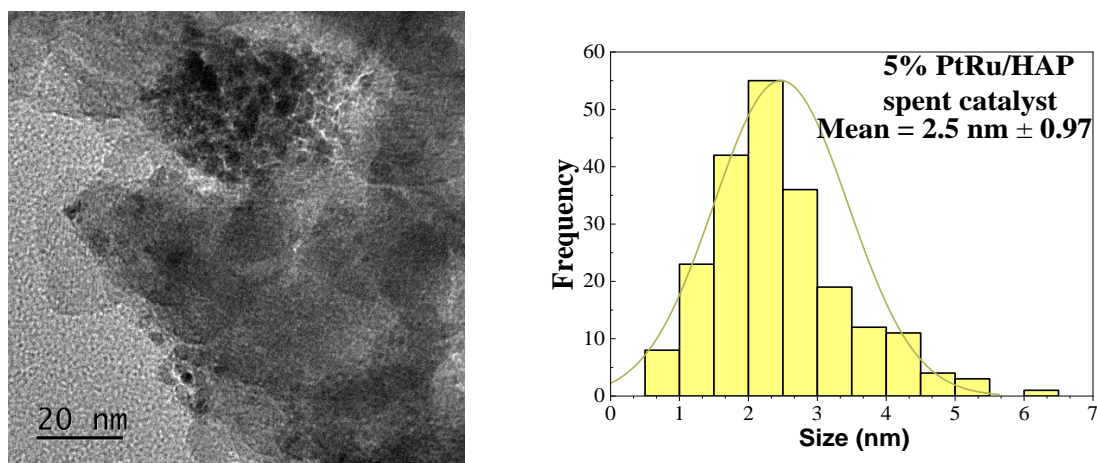
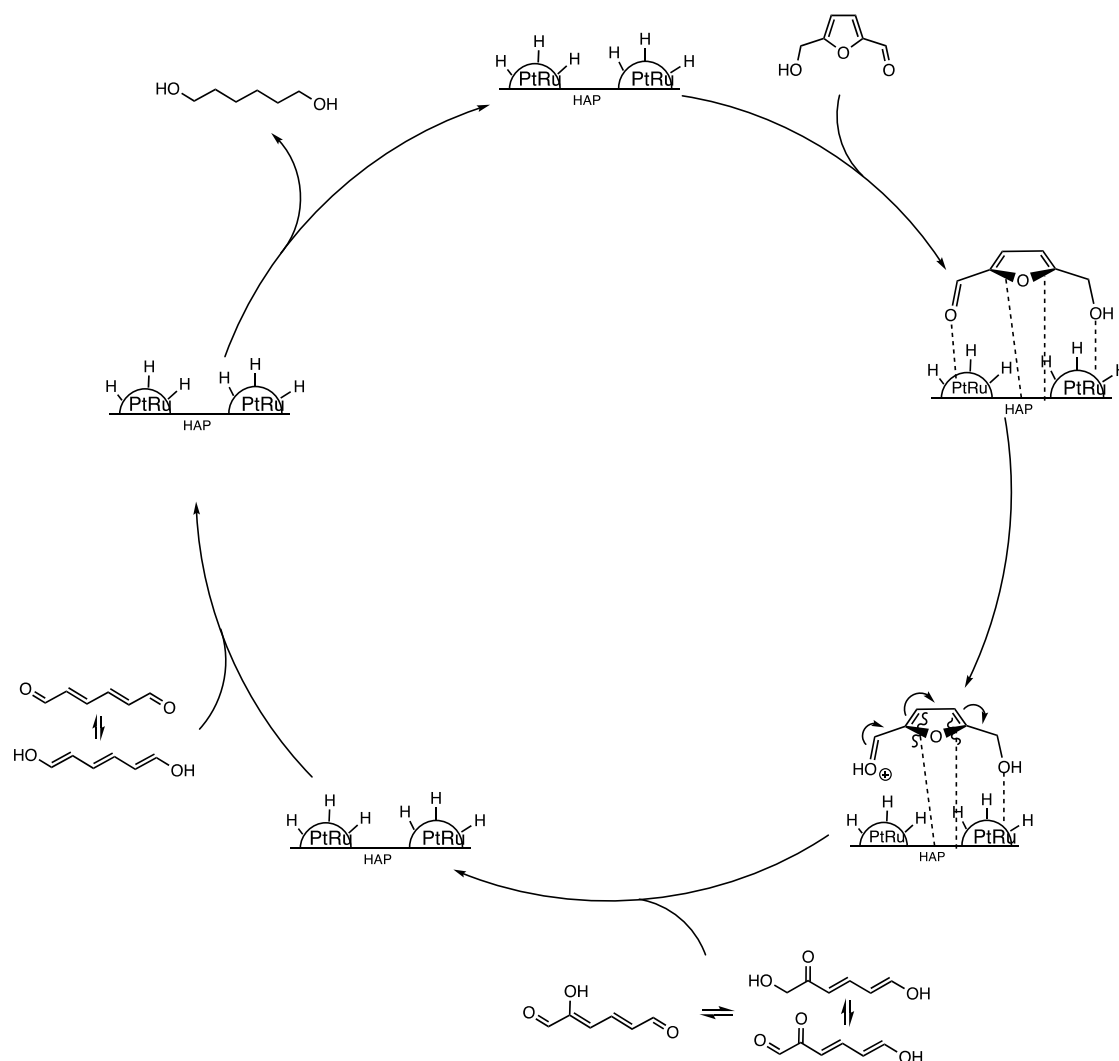


Figure 5.19: TEM image and Particle size distribution of used 5 % wt. PtRu/HAP catalyst based on TEM.

5.7 Proposed reaction mechanism

Based on the evidence gathered from the different characterisation techniques, data analysis and previous literature,^{13, 102, 103} hydrogenation/hydrogenolysis of HMF has been proposed to proceed by five major steps on bimetallic PtRu/HAP. The first step is the electrostatic interaction from both the metal and the acidic site in the support leading to HMF adsorption to the catalyst surface through the three oxygen atoms in HMF.¹³ Subsequently, the furan ring opens with loss of furan oxygen and this is adduced to the acidic site on the support as reported in the literature.¹⁰² This ring opening step led to the formation of hex-1,3,5-triene-1,6-diol,

which was detected by GC-MS. The third step is the keto-enol tautomerism of the intermediate, hex-1,3,5-triene-1,6-diol, to hexa-2,4-dienedial. However, the hex-1,3,5-triene-1,6-diol was assumed to be more stable in a polar solvent. Finally, 1,6- HDO is produced due to hydrogenation of the double bonds on the hex-1,3,5-triene-1,6-diol on the catalyst surface.^{48, 50, 99, 100} All the reaction steps are shown in (Scheme 5.6).



Scheme 5.6 Reaction mechanism proposed for the hydrogenation of HMF using PtRu/HAP catalyst.

Many studies have confirmed that basic or acidic support is efficient for opening of the furan ring. He *et al.*,²² reported that Brønsted acid sites are a requirement for C – O bond cleavage and the Pt sites are essential for hydrogenation. Also, the Pt-WO_x/TiO₂ catalyst's high activity

and selectivity can be adduced to the synergistic effect between Pt and WO_x, enabled by the reducible support. Tuteja and co-workers¹³ reported that 7wt% Pd on zirconium phosphate (ZrP) catalyst exhibited a 43% selectivity for 1,6-HDO via direct hydrogenolysis due to Brönsted/Lewis acid ratio in ZrP support. However, hydrogenation/hydrogenolysis of HMF to 1,6-HDO using Pd supported on zeolites, Al₂O₃, SiO₂–Al₂O₃, Nb₂O₅ and sulfated ZrO₂ showed lower catalytic activity than zirconium phosphate (ZrP) supported catalyst.¹³ In our research, we found a positive correlation in the interaction between acid site in HAP and PtRu NP which plays an essential effect on the ring opening of HMF. Moreover, the synergistic effect, between Pt and Ru led to an improvement in both conversion and selectivity.¹⁰⁴

In this study the XPS results confirmed the Ca/P molar ratio to be 1.5 which showed that the HAP support acts as an acid site while the TEM results revealed the strong interaction between the active metal and HAP which is important for ring opening.⁵⁵ On the other words, the catalyst which contains acid supports and noble metal is effective for the selective catalytic ring cleavage to obtain diols.^{105,51} TEM results showed a small particle size with a uniform dispersion of the active metals, Pt and Ru, over HAP support. The optimum reaction conditions are 5wt% PtRu/HAP for 5 h at 140 °C under 2 MPa of H₂, to achieve high conversion and 51% selectivity towards 1,6-HDO. The PtRu/HAP catalyst was stable over three cycles without significant loss of either activity or selectivity.

5.8 Conclusions

In this work, a monometallic Pt catalyst and a series of bimetallic catalysts on varying supports have been synthesised, characterised and explored as catalysts in hydrogenation/hydrogenolysis of HMF to 1,6-HDO.

Platinum (Pt) catalysts supported on HT, CeO₂, MgO, HAP, SZ and WZ achieved 48 – 100% HMF conversion. Pt/CeO₂, Pt/HT and Pt/MgO are not selective towards 1,6-HDO while Pt/HAP, Pt/SZ and PtWZ presented 10%, 20% and 35% selectivity respectively for 1,6-HDO after 8h. This result confirmed that acidic support is essential for hydrogenolysis.

To better the selectivity towards 1,6-HDO, a series of bimetallic catalysts, PtPd, PtCo, PtRu and PtRe, on acidic supports were investigated in hydrogenation/hydrogenolysis of HMF to 1,6-HDO. Among all the catalysts tested, RuPt supported on HAP produced 1,6-HDO with 57% selectivity after 8 h. The reaction was optimised using different reaction conditions and It

was observed that high 1,6-HDO selectivity was achieved over PtRu/HAP at 140 °C under 2 MPa H₂ for 5 h.

An analysis of the bimetallic PtRu/HAP catalyst by TEM and XPS revealed important insights. The XPS result proved that the oxidation state of the Pt- and Ru-NPs on the catalyst has no effect on 1,6-HDO selectivity. The Ca/P ratio confirms the surface of the HAP support is acidic, which is essential for hydrogenolysis of HMF. TEM showed the catalyst is dispersed uniformly on HAP, with small particle sizes (d_{PtRu} 2.5 nm) which are necessary for high HMF conversion and 1,6-HDO selectivity. The cooperation between the HAP and PtRu NPs, which leads to the strong interaction between PtRu and HAP, and the acid properties of HAP are essential for the ring opening of furan.

The catalyst was found stable after 3 cycles without losing its activity. ICP-AES analysis of the spent catalyst revealed there was no leaching of the active metals from the catalyst surface. Furthermore, the TEM result confirmed that the size of the metal particles was stable relative to fresh catalyst indicating the catalyst was stable over time.

In sum, 5wt% PtRu/HAP was found to be the best catalyst for hydrogenation/ hydrogenolysis of HMF to 1,6-HDO with high activity and selectivity. In addition, insights from this work would be beneficial in catalytic hydrogenation/hydrogenolysis leading to ring opening in a wide variety of substrates.

5.9 References

1. M. Zunita, D. M. Yuan and A. S. Laksono, *Chem. Eng. J. Adv.*, 2022, **11**.
2. L.-K. Ren, L.-F. Zhu, T. Qi, J.-Q. Tang, H.-Q. Yang and C.-W. Hu, *ACS Catal.*, 2017, **7**, **3**, , 2199–2212.
3. Y. Yao, S. Chen and M. Zhang, *Front Chem*, 2022, **10**, 880603.
4. X. Li, R. Xu, J. Yang, S. Nie, D. Liu, Y. Liu and C. Si, *Ind. Crops Prod.*, 2019, **130**, 184-197.
5. R.-J. v. Putten, J. C. v. d. Waal, E. d. Jong, C. B. Rasrendra, H. J. Heeres and J. G. d. Vries, *Chem Rev*, 2013, **113**, 1499-1597.
6. B. Xiao, M. Zheng, X. Li, J. Pang, R. Sun, H. Wang, X. Pang, A. Wang, X. Wang and T. Zhang, *Green Chem.*, 2016, **18**, 2175-2184.
7. G. Lligadas, J. C. Ronda, M. Galia and V. C. diz, *Biomacromolecules*, 2010, **11**, 2825-2835.
8. N. Kolb and M. A. R. Meier, *Eur. Polym. J.*, 2013, **49**, 843-852.
9. N. Enjamuri and S. Darbha, *Catal. Rev.*, 2020, **62**, 566-606.
10. S. H. Krishna, K. Huang, K. J. Barnett, J. He, C. T. Maravelias, J. A. Dumesic and G. W. Huber, *AIChE*, 2018, **64**, 1910-1922.
11. X. Kong, Y. Zhu, Z. Fang, J. A. Kozinski, I. S. Butler, L. Xu, H. Song and X. Wei, *Green Chem.*, 2018, **20**, 3657-3682.
12. Z. Huang, J. Wang, J. Lei, W. Zhao, H. Chen, Y. Yang, Q. Xu and X. Liu, *Front Chem*, 2022, **10**, 925603.
13. J. Tuteja, H. Choudhary, S. Nishimura and K. Ebitani, *ChemSusChem*, 2014, **7**, 96-100.
14. M. Faber, *US Pat.* , 1983, **4,400**, 468.
15. T. Buntara, S. Noel, P. H. Phua, I. Melian-Cabrera, J. G. de Vries and H. J. Heeres, *Angew. Chem. Int. Ed. Engl.*, 2011, **50**, 7083-7087.
16. S. Yao, X. Wang, Y. Jiang, F. Wu, X. Chen and X. Mu, *ACS Sustain. Chem. Eng.*, 2013, **2**, 173-180..

17. H. Kataoka, D. Kosuge, K. Ogura, J. Ohyama and A. Satsuma, *Catal. Today*, 2020, **352**, 60-65.
18. T. Tong, Q. Xia, X. Liu and Y. Wang, *Catal. Commun.*, 2017, **101**, 129-133.
19. T. Mizugaki, T. Yamakawa, Y. Nagatsu, Z. Maeno, T. Mitsudome, K. Jitsukawa and K. Kaneda, *ACS Sustain. Chem. Eng.*, 2014, **2**, 2243-2247.
20. S. Bhogeswararao and D. Srinivas, *J. Catal.*, 2015, **327**, 65-77.
21. Y. Shao, J. Wang, K. Sun, G. Gao, M. Fan, C. Li, C. Ming, L. Zhang, S. Zhang and X. Hu, *ACS Appl. Nano Mater.*, 2022, **5**, 5882-5894.
22. J. He, S. P. Burt, M. Ball, D. Zhao, I. Hermans, J. A. Dumesic and G. W. Huber, *ACS Catal.*, 2018, **8**, 1427-1439.
23. T. Uine, Warrenville, J. D. Garber, Westfield and R. E. Jones, *US3083236*, 1963.
24. T. Buntara, S. Noel, P. H. Phua, I. Melián-Cabrera, J. G. de Vries and H. J. Heeres, *Angew. Chem.*, 2011, **123**, 7221-7225.
25. Y. Nakagawa, M. Tamura and K. Tomishige, *Catal. Surv. Asia*, 2015, **19**, 249-256.
26. Y. Wang, H. Wang, X. Kong and Y. Zhu, *ChemSusChem*, 2022, **15**, e202200421.
27. R. Ma, X.-P. Wu, T. Tong, Z.-J. Shao, Y. Wang, X. Liu, Q. Xia and X.-Q. Gong, *ACS Catal.*, 2016, **7**, 333-337.
28. R. Alamillo, M. Tucker, M. Chia, Y. Pagán-Torres and J. Dumesic, *Green Chem.*, 2012, **14**.
29. S. Gupta, T. S. Khan, B. Saha and M. A. Haider, *Ind. Eng. Chem. Res.*, 2019, **58**, 16153-16163.
30. S. Campisi, D. Motta, I. Barlocco, R. Stones, T. W. Chamberlain, A. Chutia, N. Dimitratos and A. Villa, *ChemCatChem*, 2022, **14**.
31. M. Baki, The University of Texas 2008.
32. L. Wang and F.-S. Xiao, *Green Chem.*, 2015, **17**, 24-39.
33. K. Shekoohi, F. S. Hosseini, A. H. Haghighi and A. Sahrayian, *MethodsX*, 2017, **4**, 86-94.
34. M. Ulibarri, *Chem. Mater.*, 1991, **3**, 626-630.

35. A. Gervasini and A. Auroux, *J. Catal.*, 1991, **131** 190-198.
36. J. Wang, J. Zhao, J. Fu, C. Miao, S. Jia, P. Yan and J. Huang, *Appl. Catal. A: Gen.*, 2022, **643**.
37. M. A. Aramendia, V. Borau, C. Jiménez, A. Marinas, J. M. Marinas, J. R. Ruiz and F. J. Urbano, *J. Mol. Catal. A: Chem.*, 2004, **218**, 81-90.
38. K. Suwannakarn, E. Lotero, J. Goodwinjr and C. Lu, *J. Catal.*, 2008, **255**, 279-286.
39. G. Yadav and J. Nair, *Micropor. Mesopor. Mat.*, 1999, **33**, 1-48.
40. Y. Sun, S. Ma, Y. Du, L. Yuan, S. Wang, J. Yang, F. Deng and F.-S. Xiao, *J. Phys. Chem. B* 2005, **109**, 2567-2572.
41. N. Tangchupong, W. Khaodee, B. Jongsomjit, N. Laosiripojana, P. Praserthdam and S. Assabumrungrat, *Fuel Process. Technol.*, 2010, **91**, 121-126.
42. Y. Fan, S. Cheng, H. Wang, J. Tian, S. Xie, Y. Pei, M. Qiao and B. Zong, *Appl. Catal. B: Environ.*, 2017, **217**, 331-341.
43. T. Kurosaka, H. Maruyama, I. Naribayashi and Y. Sasaki, *Catal. Commun.*, 2008, **9**, 1360-1363.
44. L. Gong, Y. LÜ, Y. Ding, R. Lin, J. Li, W. Dong, T. Wang and W. Chen, *Chinese J. Catal.*, 2009, **30**, 1189-1191.
45. L.-Z. Qin, M.-J. Song and C.-L. Chen, *Green Chem.*, 2010, **12**.
46. R. Kourieh, V. Rakic, S. Bennici and A. Auroux, *Catal. Commun.*, 2013, **30**, 5-13.
47. A. Nakagiri, K. Imamura, K. Yanagisawa and A. Onda, *Nanomaterials (Basel)*, 2021, **11**.
48. S. Lei, S. Qin, B. Li and C. Zhao, *J. Catal.*, 2021, **400**, 244-254.
49. Z. Boukha, B. de Rivas, J. R. Gonzalez-Velasco, J. I. Gutierrez-Ortiz and R. Lopez-Fonseca, *Materials (Basel)*, 2021, **14**.
50. H. Brasil, A. F. B. Bittencourt, K. C. E. S. Yokoo, P. C. D. Mendes, L. G. Verga, K. F. Andriani, R. Landers, J. L. F. Da Silva and G. P. Valença, *J. Catal.*, 2021, **404**, 802-813.

51. T. Tsuchida, J. Kubo, T. Yoshioka, S. Sakuma, T. Takeguchi and W. Ueda, *J. Catal.*, 2008, **259**, 183-189.
52. J. J. Lovón-Quintana, J. K. Rodríguez-Guerrero and P. G. Valença, *Appl. Catal. A: Gen.*, 2017, **542**, 136-145.
53. A. Fihri, C. Len, R. S. Varma and A. Solhy, *Coord. Chem. Rev.*, 2017, **347**, 48-76.
54. S. J. Joris and C. H. Amberg, *J. Phys. Chem.*, 1971 **75** 3167.
55. S. Diallo-Garcia, M. B. Osman, J.-M. Krafft, S. Casale, C. Thomas, J. Kubo and G. Costentin, *J. Phys. Chem. C*, 2014, **118**, 12744-12757.
56. L. Silvester, J.-F. Lamonier, J. Faye, M. Capron, R.-N. Vannier, C. Lamonier, J.-L. Dubois, J.-L. Couturier, C. Calais and F. Dumeignil, *Catal. Sci. Technol.*, 2015, **5**, 2994-3006.
57. M. B. Osman, S. D. Garcia, J.-M. Krafft, C. Methivier, J. Blanchard, T. Yoshioka, J. Kubob and G. Costentin, *Phys Chem Chem Phys*, 2016, **18**, 27837-27847.
58. M. J. Gilkey, P. Panagiotopoulou, A. V. Mironenko, G. R. Jenness, D. G. Vlachos and B. Xu, *ACS Catal.*, 2015, **5**, 3988-3994.
59. I. Klein, C. Marcum, H. Kenttämäa and M. M. Abu-Omar, *Green Chem.*, 2016, **18**, 2399-2405.
60. S. Sawadjoon, A. Lundstedt and J. S. M. Samec, *ACS Catal.*, 2013, **3**, 635-642.
61. A. Iriondo, I. Agirre, N. Viar and J. Requies, *Catalysts*, 2020, **10**, 895.
62. F. Yang, S. Zhang, Z. C. Zhang, J. Mao, S. Li, J. Yin and J. Zhou, *Catal. Sci. Technol.*, 2015, **5**, 4602-4612.
63. L. Hu, L. Lin, Z. Wu, S. Zhou and S. Liu, *Renew. Sust. Energ. Rev.*, 2017, **74**, 230-257.
64. Y. Yang, Y. Wang, S. Li, X. Shen, B. Chen, H. Liu and B. Han, *Green Chem.*, 2020, **22**, 4937-4942.
65. T. Mizugaki, T. Yamakawa, Y. Nagatsu, Z. Maeno, T. Mitsudome, K. Jitsukawa and K. Kaneda, *ACS Sustain. Chem. Eng.*, 2014, **2**, 2243-2247.
66. K. Gupta, R. K. Rai and S. K. Singh, *ChemCatChem*, 2018, **10**, 2326-2349.

67. W. Gong, C. Chen, Y. Zhang, H. Zhou, H. Wang, H. Zhang, Y. Zhang, G. Wang and H. Zhao, *ACS Sustain. Chem. Eng.*, 2017, **5**, 2172-2180.
68. N. Castellanos-Blanco, G. Taborda and M. Cobo, *ChemistrySelect*, 2020, **5**, 3458-3470.
69. A. Talebian-Kiakalaieh, N. A. S. Amin, N. Najaafi and S. Tarighi, *Front Chem*, 2018, **6**, 573.
70. M. J. da Silva and M. G. Teixeira, *Mol. Catal.*, 2018, **461**, 40-47.
71. G. Ferreira, C. Carvalho and S. Nakagaki, *Catalysts*, 2019, **9**.
72. E. Bailón-García, F. Maldonado-Hódar, A. Pérez-Cadenas and F. Carrasco-Marín, *Catalysts*, 2013, **3**, 853-877.
73. R. M. Mironenko, V. P. Talsi, T. I. Gulyaeva, M. V. Trenikhin and O. B. Belskaya, *React. Kinet. Mech. Catal.*, 2018, **126**, 811-827.
74. B. Bachiller-Baeza, A. Guerrero-Ruiz and I. Rodríguez-Ramos, *Appl. Catal. A: Gen.*, 2000, **192**, 289-297.
75. M. H. Haider, N. F. Dummer, D. W. Knight, R. L. Jenkins, M. Howard, J. Moulijn, S. H. Taylor and G. J. Hutchings, *Nat Chem*, 2015, **7**, 1028-1032.
76. C. Mondelli, G. Gozaydin, N. Yan and J. Perez-Ramirez, *Chem Soc Rev*, 2020, **49**, 3764-3782.
77. E. Rossmedgaarden, W. Knowles, T. Kim, M. Wong, W. Zhou, C. Kiely and I. Wachs, *J. Catal.*, 2008, **256**, 108-125.
78. P. Lanzafame, D. M. Temi, S. Perathoner, G. Centi, A. Macario, A. Aloise and G. Giordano, *Catal. Today*, 2011, **175**, 435-441.
79. I. Viil, A. Bredihhin, U. Mäeorg and L. Vares, *RSC Advances*, 2014, **4**, 5689.
80. Y. Nakagawa, M. Tamura and K. Tomishige, *ACS Catal.*, 2013, **3**, 2655-2668.
81. S. K. R. Patil and C. R. F. Lund, *Energy & Fuels*, 2011, **25**, 4745-4755.
82. S. K. R. Patil, J. Heltzel and C. R. F. Lund, *Energy & Fuels*, 2012, **26**, 5281-5293.
83. A. Navajas, G. Arzamendi, F. Romero-Sarria, M. A. Centeno, J. A. Odriozola and L. M. Gandía, *Catal. Commun.*, 2012, **17**, 189-193.

84. M. Chia, Y. J. Pagan-Torres, D. Hibbitts, Q. Tan, H. N. Pham, A. K. Datye, M. Neurock, R. J. Davis and J. A. Dumesic, *J. Am. Chem. Soc.*, 2011, **133**, 12675–12689.
85. J. Ohyama, A. Esaki, Y. Yamamoto, S. Arai and A. Satsuma, *RSC Adv.*, 2013, **3**, 1033-1036.
86. Q. Cao, W. Liang, J. Guan, L. Wang, Q. Qu, X. Zhang, X. Wang and X. Mu, *Appl. Catal. A: Gen.*, 2014, **481**, 49-53.
87. Y. Wang, D. Zhao, D. Rodríguez-Padrón and C. Len, *Catalysts*, 2019, **9**, 796.
88. B. Chen, F. Li, Z. Huang and G. Yuan, *Appl. Catal. A: Gen.*, 2015, **500**, 23-29.
89. M. Chia, B. J. O'Neill, R. Alamillo, P. J. Dietrich, F. H. Ribeiro, J. T. Miller and J. A. Dumesic, *J. Catal.*, 2013, **308**, 226-236.
90. B. Wozniak, Y. Li, S. Tin and J. G. de Vries, *Green Chem.*, 2018, **20**, 4433-4437.
91. S. Liu, Y. Amada, M. Tamura, Y. Nakagawa and K. Tomishige, *Catal. Sci. Technol.*, 2014, **4**, 2535-2549.
92. D. S. Pisal and G. D. Yadav, *ACS Omega* 2019, **4**, 1201–1214.
93. E. A. Paoli, F. Masini, R. Frydendal, D. Deiana, C. Schlaup, M. Malizia, T. W. Hansen, S. Horch, I. E. L. Stephens and I. Chorkendorff, *Chem Sci*, 2015, **6**, 190-196.
94. D. J. Morgan, *Surf. Interface Anal.*, 2015, **47**, 1072-1079.
95. W. Tolek, N. Nanthasanti, B. Pongthawornsakun, P. Prasertthdam and J. Panpranot, *Sci Rep*, 2021, **11**, 9786.
96. T. Zhang, S. Wang and F. Chen, *J. Phys. Chem. C*, 2016, **120**, 9732-9739.
97. D. Miao, A. Goldbach and H. Xu, *ACS Catal.*, 2016, **6**, 775-783.
98. S. Lei, S. Qin, B. Li and C. Zhao, *J. Catal.*, 2021, **400** 244-254.
99. G. Xu, Y. Zhang, Y. Fu and Q. Guo, *ACS Catal.*, 2017, **7**, 1158-1169.
100. Z. Xu, G. Huang, Z. Yan, N. Wang, L. Yue and Q. Liu, *ACS Omega*, 2019, **4**, 21998-22007.
101. G. Xu, J. Guo, Y. Zhang, Y. Fu, J. Chen, L. Ma and Q. Guo, *ChemCatChem*, 2015, **7**, 2485-2492.

102. R. Weingarten, G. A. Tompsett, W. C. Conner and G. W. Huber, *J. Catal.*, 2011, **279**, 174-182.
103. K. Nakajima, T. Fukui, H. Kato, M. Kitano, J. N. Kondo, S. Hayashi and M. Hara, *Chem. Mater.*, 2010, **22**, 3332-3339.
104. H. Vu, F. Goncalves, R. Philippe, E. Lamouroux, M. Corrias, Y. Kihn, D. Plee, P. Kalck and P. Serp, *J. Catal.*, 2006, **240**, 18-22.
105. S. Diallo-Garcia, D. Laurencin, J.-M. Krafft, S. Casale, M. E. Smith, H. Lauron-Pernot and G. Costentin, *J. Phys. Chem. C*, 2011, **115**, 24317-24327.

Chapter 6. Conclusions and Future Work.

6.1 Conclusions

In this work, we have designed and synthesized supported heterogeneous catalysts for the chemoselective hydrogenation of bio-derived, furan-based platform molecules. These catalysts have been tuned in order to make them more active and selective. Different approaches were taken to tune catalysts' active site to improve their activity and selectivity. The first approach taken was tuning metal sites via a post-synthetic heat treatment procedure. The second approach was by employing different supports via testing different reducible/nonreducible and acid/base supports. The third approach taken was tuning the metal support interaction to prevent strong metal support interaction (SMSI) and prevent the support cover the Pt NPs surface via a heat-treatment protocol that involves calcination followed by reduction. The catalysed reactions screened in this study include hydrogenation of FF to FFA and hydrogenation/hydrogenolysis of HMF to 1,6-HDO.

Among the different catalysts tested, Pt-based catalyst over TiO₂ support with post-synthesis heat treatment (Calc + Red) displays the highest selectivity for the hydrogenation of the carbonyl group in FF compound. 0.6 wt % Pt loading displayed the highest activity (100%) and selectivity (95%) towards FFA. The 0.6wt.% Pt/TiO₂ catalyst has been characterised using XPS, TEM and CO-chemisorption. The particle size on the 0.6wt.% Pt/TiO₂ catalyst was found to be ± 1.3 nm with uniform dispersion of Pt⁰ on the catalyst surface. The Pt⁰ species is found to be more selective towards carbonyl group adsorption and by extension, the improved activity and selectivity towards FFA could be attributed to this. However, the activity of the 0.6% Pt/TiO₂ catalyst diminishes gradually over 3 cycles. Characterisation of the spent catalyst using TEM and CO-chemisorption confirmed sintering as the main reason for catalyst deactivation. Furthermore, MP-AES analysis showed there was no leaching of the active metal in the catalyst compared with the fresh catalyst.

Direct transformation of 5-hydroxymethylfurfural (HMF) to 1,6-hexanediol (1,6-HDO) via hydrogenation/hydrogenolysis by a monometallic Pt-NPs and a series of bimetallic catalysts (PtPd, PtCo, PtRu and PtRe) on different support was also investigated. All the catalysts were prepared using the wet impregnation method. The nature of the support and the second metal in the bimetallic catalysts were found to be essential for furan ring opening. It was found that Pt catalysts supported on acidic supports such as Pt/HAP, Pt/SZ and Pt/WZ displayed better selectivity towards 1,6-HDO than those on basic support. Equally, synergistic effect between

metals was found to be crucial to the selective C-O bond scission leading to ring opening products. The selectivity of 1,6-HDO with PtRu bimetallic catalyst was found to be the best (57%) relative to the corresponding monometallic Pt catalysts and bimetallic catalysts such as PtCo, PtPd and PtRe.

To improve the selectivity of the desired product, 1,6-HDO, the reaction conditions of the PtRu/HAP was optimized by varying the temperature, H₂ pressure, reaction time and solvent. The optimum reaction conditions for the ring opening of HMF using 5% PtRu/HAP catalyst was found to be 2 MPa of H₂ gas at 140°C for 5 h, with methanol as solvent of choice. Reaction temperature was found to have strong influence on 1,6-HDO selectivity while at pressures below 2 MPa, 1,6-HDO selectivity decreases due to competing side reactions.

The PtRu/HAP bimetallic catalyst has been characterised using XPS and TEM. From the TEM images, the catalyst displayed uniform dispersion on the surface of HAP support with a small particle size (2.5 nm). In addition, XPS analysis confirms electron modification in the PtRu/HAP catalyst and this in turn has a positive impact on the catalyst activity and selectivity. Also, the ratio between Ca/ P is found to be 1.5 and this confirms the presence of acid sites on the catalyst. The PtRu/HAP catalyst was found to be stable over 3 cycles without losing its activity. Characterisation of the spent catalyst using TEM confirmed the particle size to be stable after 3 catalytic cycles. Relative to fresh catalyst, analysis of results from ICP-AES showed there was no leaching of the catalyst over 3 cycles.

6.2 Future work.

The research reported in this thesis will be a beneficial guide in developing catalysts for the selective hydrogenation of the carbonyl group in α, β -unsaturated molecules with high-activity and selectivity. In particular, it can serve as a guide to further advance the development of heterogeneous catalyst beyond the state-of-the-art for the hydrogenation of FF to FFA, and hydrogenation/hydrogenolysis of HMF to polyols with high activity and selectivity. I have been able to establish that post-synthesis thermal treatment that involves calcination followed by reduction helps preserve the active metal (Pt⁰) on the surface of the catalyst. This heat treatment protocols will be useful for the development of highly active and selective catalysts with exceptional stability. In addition, It is essential to expand the substrate scope of the 0.6%

Pt/TiO₂ (Calc + Red) catalyst for the hydrogenation of the carbonyl group in other α,β -unsaturated molecules. Also, due to the unstable nature of the 0.6% Pt/TiO₂ (Calc + Red) catalyst, other methods of preparation could be used to improve the catalyst stability for the hydrogenation of FF to FFA.

Platinum catalyst supported on Nb₂O₅ support presented promising results, and from an industry perspective, other metals and combination of metals on a variety of supports could be explored for the hydrogenation of furfural and furfuryl alcohol to methyl furan or ring-opening products. Other preparation methods should be explored and it is equally essential to investigate the effects of the various components after characterization in order to understand the reaction pathways and factors responsible for the activity and selectivity.

Lastly, it has been found that water can significantly promote the ring-opening process of HMF on supported Pt catalysts.¹ It is essential to explore the roles of other polar protic solvents and their influence on the catalyst's activity and selectivity. In addition, Diffused Reflectance Infrared Fourier Transform Spectra (DRIFTS) could be employed to study the influence of the nature of the support and to determine which of the functional groups in HMF interact with the catalyst surface and its mode of adsorption on the active sites of the catalyst.²

6.3 References

1. R. Ma, X.-P. Wu, T. Tong, Z.-J. Shao, Y. Wang, X. Liu, Q. Xia and X.-Q. Gong, *ACS Catal.*, 2016, **7**, 333-337.
2. J. Wang, J. Zhao, J. Fu, C. Miao, S. Jia, P. Yan and J. Huang, *Appl. Catal. A: Gen.*, 2022, **643**.